

# UC San Diego

## UC San Diego Electronic Theses and Dissertations

### Title

The importance of metal binding in metalloprotein inhibitors

### Permalink

<https://escholarship.org/uc/item/14d6d15m>

### Author

Agrawal, Arpita

### Publication Date

2011

Peer reviewed|Thesis/dissertation

UNIVERSITY OF CALIFORNIA, SAN DIEGO

**The Importance of Metal Binding in Metalloprotein Inhibitors**

A Dissertation submitted in partial satisfaction of the requirements for the degree  
Doctor of Philosophy

in

Chemistry

by

Arpita Agrawal

Committee in charge:

Professor Seth M. Cohen, Chair  
Professor Gourisankar Ghosh  
Professor Alexander Hoffmann  
Professor Geert Schmid-Schoenbein  
Professor F. Akif Tezcan

2011



The Dissertation of Arpita Agrawal is approved, and it is acceptable in quality and form for publication on microfilm and electronically:

---

---

---

---

---

Chair

University of California, San Diego

2011

## **DEDICATION**

I dedicate this chapter of my life to my family for their unconditional love and support  
over the years

## TABLE OF CONTENTS

|   |       |
|---|-------|
| Signature Page .....  | iii   |
| Dedication.....   | iv    |
| Table of Contents .....   | v     |
| List of Symbols and Abbreviations .....                           | x     |
| List of Figures.....  | xv    |
| List of Schemes .....   | xxii  |
| List of Tables .....  | xxiii |
| Acknowledgements .....  | xxiv  |
| Vita and Publications.....  | xxvii |
| Abstract of the Dissertation .....                                | xxix  |
| <u>Chapter 1. Zinc metalloenzymes in health and disease</u> ..... | 1     |
| 1.A Introduction .....  | 2     |
| 1.B Catalytic zinc sites as medicinal targets .....               | 6     |
| 1.I.A Matrix metalloproteinases (MMPs) .....                      | 8     |
| 1.I.B Structure of MMPs .....                                     | 11    |
| 1.I.C Regulation of MMPs and Endogenous Inhibitors.....           | 16    |
| 1.I.D Synthetic Inhibitors of MMPs .....                          | 18    |
| 1.II.A Anthrax lethal factor (LF) .....                           | 25    |
| 1.II.B Structure of anthrax lethal factor .....                   | 28    |
| 1.II.C Anthrax lethal factor inhibitors (LFi) .....               | 31    |
| 1.C References.....   | 35    |

|  |     |
|--|-----|
| <u>Chapter 2. Zinc-Binding Groups (ZBGs) Modulate Selective Inhibition of MMPs</u> .....   | 40  |
| 2.A Introduction .....   | 41  |
| 2.B Synthesis of MMPi .....  | 45  |
| 2.C Activity of MMPi in <i>in vitro</i> assays.....  | 48  |
| 2.D Kinetic studies on 1,2-HOPO-2.....   | 51  |
| 2.E Cell viability assays .....  | 54  |
| 2.F <i>Ex vivo</i> efficacy of inhibitors .....  | 55  |
| 2.G Discussion .....   | 58  |
| 2.G.i Selectivity beyond the backbone .....  | 58  |
| 2.G.ii Possible origin of ZBG based selectivity .....  | 64  |
| 2.G.iii <i>Ex vivo</i> effects of the ZBG .....  | 65  |
| 2.G.iv Expanding derivatives of 1,2-HOPO-2 .....   | 66  |
| 2.G.v Synthesis of 1,2-HOPO-2 derivatives .....  | 66  |
| 2.G.vi Activity of 1,2-HOPO-2 derivatives.....   | 72  |
| 2.H Conclusions .....  | 73  |
| 2.I Experimental .....   | 74  |
| 2.I.i Synthesis of MMPi in Schemes 2-1 to 2-3 .....  | 74  |
| 2.I.ii Synthesis of backbones in Schemes 2-4 and 2-5 .....   | 80  |
| 2.I.ii Synthesis of 1,2-HOPO-2 derivatives in Scheme 2-6.....  | 88  |
| 2.J Acknowledgements.....  | 98  |
| 2.K References .....   | 99  |
| <u>Chapter 3. Thioamide Hydroxypyrothiones Supersede Amide Hydroxypyrothiones in Potency against Anthrax Lethal Factor</u> ..... | 102 |

|  |            |
|--|------------|
| 3.A Introduction .....   | 103        |
| 3.B Synthesis of a series of lethal factor inhibitors (LFi).....                     | 106        |
| 3.C Single-crystal X-ray structure of <b>5c</b> .....                                | 112        |
| 3.D <i>In vitro</i> potency of synthesized LFi .....                                 | 113        |
| 3.E Computational Modeling .....   | 116        |
| 3.F Discussion .....   | 121        |
| 3.G Conclusions .....  | 126        |
| 3.H Experimental.....  | 127        |
| 3.H.i Synthesis of LF inhibitors .....   | 127        |
| 3.H.ii Recombinant fluorescence-based LF assays .....                                | 142        |
| 3.H.iii Single-crystal X-ray diffraction .....                                       | 143        |
| 4.H.iv.a Construction of an Inhibitor/Anthrax LF Complex Model .....                 | 143        |
| 4.H.iv.b QM/MM Minimization Calculations.....  | 144        |
| 3.I Appendix .....   | 146        |
| 3.J Acknowledgements.....  | 147        |
| 3.K References .....   | 148        |
| <u>Chapter 4. Chelator Fragment Libraries for Targeting Metalloproteinases .....</u> | <u>152</u> |
| 4.A Introduction .....   | 153        |
| 4.B Chelator Fragment Library (CFL-1) .....  | 159        |
| 4.C. Expanded Chelator Fragment Library (eCFL-1) .....                               | 163        |
| 4.D <i>In vitro</i> screening of eCFL-1 against MMPs and LF.....                     | 165        |
| 4.E Discussion.....  | 169        |



|   |   |     |
|---|---|-----|
| 4.F   | Fragment Evolution.....   | 172 |
| 4.F.i   | <i>In vitro</i> potency of fragment evolution .....                                       | 175 |
| 4.G   | Conclusions .....   | 177 |
| 4.H   | Experimental.....   | 178 |
| 4.H.i   | Synthesis of eCFL-1 .....   | 178 |
| 4.H.ii  | Synthesis of fragment evolution.....  | 196 |
| 4.H.iii   | eCFL-1 Screening against MMP-2, -3, -9 and LF .....                                       | 198 |
| 4.H.iii.a   | MMP Inhibition Assays.....  | 199 |
| 4.H.iii.b   | LF Inhibition Assays .....  | 200 |
| 4.H.iii.c   | Enzyme Kinetic Assays .....   | 200 |
| 4.I   | Acknowledgements .....  | 202 |
| 4.J   | References.....   | 203 |
| <u>Chapter 5. Beyond mononuclear Zn<sup>2+</sup> endopeptidases .....</u> |   | 206 |
| 5.A.i   | HIV integrase (HIV-IN), a dinuclear endonuclease target.....                              | 207 |
| 5.A.ii  | HIV is the causative agent of AIDS .....  | 209 |
| 5.B   | Anti-retroviral therapy .....   | 212 |
| 5.C.i   | HIV-1 integrase (HIV-IN) – belongs to the family of<br>polynucleotidyl transferases ..... | 215 |
| 5.C.ii  | Structural and Functional Domains of HIV-IN .....   | 218 |
| 5.D   | HIV-IN inhibitors: the historical synopsis.....   | 222 |
| 5.E.  | PFV-IN active site with cognate DNA and bound HIV-IN<br>inhibitors.....                   | 225 |
| 5.F   | Synthesis of HIV-IN inhibitors .....  | 228 |
| 5.G   | <i>In vitro</i> potency of HIV-IN inhibitors .....  | 231 |

|                            |     |
|----------------------------|-----|
| 5.H Discussion.....        | 235 |
| 5.I Conclusions .....      | 240 |
| 5.J Experimental.....      | 241 |
| 5.K Acknowledgements ..... | 250 |
| 5.L References.....        | 251 |

## LIST OF SYMBOLS AND ABBREVIATIONS

|          |  |
|----------|--|
| Å        | Ångström; $10^{-10}$ m                 |
| AHA      | Acetohydroxamic acid                   |
| APMA     | <i>p</i> -Aminophenylmercuric acetate  |
| Ar       | Aryl peak (NMR)                        |
| Bn       | Benzyl                                 |
| °C       | Degree Celsius                         |
| CA       | Carbonic anhydrase                     |
| Calc.    | Calculated                             |
| CA-MMP   | Cysteine array MMP                     |
| CCD      | Catalytic Core Domain                  |
| CCDC     | Cambridge Crystallographic Data Center |
| CF       | Neonatal rat cardiac fibroblast        |
| CFL      | Chelator Fragment Library              |
| Cou      | 7-Hydroxy-4-methyl-3-acetylcoumarinyl  |
| CPCA     | Consensus principal component analysis |
| CTD      | C-terminal Domain                      |
| $\delta$ | Chemical shift; ppm                    |
| $\Delta$ | Difference                             |
| d        | Doublet (NMR)                          |
| DKA      | Diketo Acid                            |
| DMF      | Dimethylformamide                      |
| DMSO     | Dimethyl sulfoxide                     |

|                   |   |
|-------------------|---|
| Dpa               | N-3-(2,4-dinitrophenyl)-L- $\alpha$ - $\beta$ -diaminopropionyl |
| DPA               | Dipyridylamine  |
| DTNB              | 5,5'-dithiobis(2-nitrobenzoic acid)                             |
| eCFL              | Expanded Chelator Fragment Library                              |
| ECM               | Extracellular matrix  |
| EDTA              | Ethylenediaminetetraacetic acid                                 |
| EF                | Edema factor  |
| ESI-MS            | Electrospray ionization mass spectrometry                       |
| Et <sub>3</sub> N | Triethylamine   |
| EXAFS             | Extended X-ray absorption fine structure                        |
| FAB               | Fast atom bombardment   |
| FBLD              | Fragment-based lead design                                      |
| FGF               | Fibroblast growth factor  |
| FT-IR             | Fourier transform infrared spectroscopy                         |
| GNFI              | Global no flow ischemia   |
| GPI               | Glycosylphosphatidylinositol                                    |
| HDAC              | Histone deacetylase   |
| HIV               | Human immunodeficiency virus                                    |
| HIV-IN            | Human immunodeficiency virus integrase                          |
| HMDO              | Hexamethyldisiloxane  |
| HOPO              | Hydroxypyridinone   |
| HOPTO             | Hydroxypyridinethione   |
| HRMS              | High resolution mass spectrometry                               |

|           |   |
|-----------|---|
| HTS       | High Throughput Screening                       |
| Hz        | Hertz   |
| <i>I</i>  | Ionic strength                                  |
| IgG       | Immunoglobulin G                                |
| IN        | Integrase                                       |
| <i>J</i>  | Coupling constant                               |
| <i>K</i>  | Kelvin  |
| $\lambda$ | Wavelength; nm                                  |
| LE        | Ligand Efficiency                               |
| LF        | Lethal factor                                   |
| LFi       | Lethal factor inhibitor                         |
| MALDI-TOF | Matrix-assisted laser desorption time-of-flight |
| MAPKK     | Mitogen-activated protein kinase kinase         |
| MBG       | Metal Binding Group                             |
| Mca       | (7-Methoxycoumarin-4-yl)-acetyl                 |
| MCP       | Monocyte chemoattractant protein                |
| MeOH      | Methanol  |
| MES       | 2-( <i>N</i> -morpholino)ethanesulfonic acid    |
| MI        | Myocardial infarction                           |
| MIFR      | MMP in the female reproductive tract            |
| MLCT      | Metal-to-ligand charge transfer                 |
| MMP       | Matrix metalloproteinase                        |
| MMPi      | Matrix metalloproteinase inhibitor              |

|                |  |
|----------------|--|
| MS             | Mass spectrometry  |
| MS             | Molecular surface (computational modeling)                   |
| MT-MMP         | Membrane-type MMP  |
| MTT            | 3-(4,5-Dimethylthiazol-2-yl)-2,5-diphenyltetrazolium bromide |
| $\nu$          | Wavenumber; $\text{cm}^{-1}$                                 |
| <i>N</i> -MMA  | <i>N</i> -methylmercaptoacetamide                            |
| NMR            | Nuclear magnetic resonance spectroscopy                      |
| NTD            | N-terminal Domain  |
| OAc            | Acetate, $[\text{C}_2\text{H}_3\text{O}_2]^-$                |
| $\alpha_1$ -PI | $\alpha_1$ -Proteinase inhibitor                             |
| 3'-P           | 3'-processing  |
| PA             | Protective antigen   |
| PDB            | Protein Data Bank  |
| PEG            | Polyethylene glycol  |
| PFV-IN         | Prototype Foamy Virus Integrase                              |
| $pK_a$         | Acid dissociation constant                                   |
| QSAR           | Quantitative structure-activity relationship                 |
| QSY-35         | N-(4-((7-nitro-2,1,3-benzoxziazol-4-yl)amino) phenyl)acetyl  |
| RAL            | Raltegravir  |
| RASI           | Rheumatoid arthritis synovial inflammation                   |
| RCD            | Raltegravir-like Chelator Derivative                         |
| RFU            | Relative fluorescence units                                  |
| RT             | Room temperature   |

|               |  |
|---------------|--|
| S             | Singlet (NMR)                          |
| SAHA          | Suberoylanilide hydroxamic acid        |
| SAR           | Structure-activity relationship        |
| ST            | Strand Transfer                        |
| STi           | Strand Transfer Inhibitors             |
| <i>T</i>      | Temperature                            |
| TGF- $\beta$  | Transforming growth factor- $\beta$    |
| THF           | Tetrahydrofuran                        |
| TIMP          | Tissue inhibitor of metalloproteinases |
| TNF- $\alpha$ | Tumor necrosis factor- $\alpha$        |
| vdWS          | van der Waals surface                  |
| <i>V</i>      | Volume                                 |
| VEGF          | Vascular endothelial growth factor     |
| ZBG           | Zinc-binding group                     |

## LIST OF FIGURES

**Figure 1-1.** a) Ribbon representation of MMP-3 structural Zn<sup>2+</sup> site. Coordinating residues His151, Asp153, His166 and His179 are shown as color-coded sticks. PDB:1CQR.<sup>6</sup> b) Ribbon representation of HIV-IN structural Zn<sup>2+</sup> site. Coordinating residues His12, His16, Cys40 and Cys43 are shown as color-coded sticks. Zn<sup>2+</sup> ions are shown as magenta spheres. (carbon = green, nitrogen = blue, oxygen = red, sulfur = yellow). PDB:1K6Y.<sup>7</sup> .....5

**Figure 1-2.** a) Ribbon representation of MMP-3 catalytic Zn<sup>2+</sup> site. Coordinating residues His201, His205 and His211 are shown as color-coded sticks. PDB:1CQR.<sup>6</sup> b) Ribbon representation of anthrax LF catalytic Zn<sup>2+</sup> site. Coordinating residues His686, His690, and Glu735 are shown as color-coded sticks. Zn<sup>2+</sup> ions are shown as magenta spheres. (carbon = green, nitrogen = blue, oxygen = red). PDB:1YQY.<sup>8</sup> .....5

**Figure 1-3.** Basic domain structures of MMPs. MMPs consist of: a propeptide (grey); a catalytic domain (blue) with the active site and the catalytic zinc (Zn<sup>2+</sup>) (red); and, with the exception of the matrilysins, a COOH-terminal domain (C) (yellow) with homology to the serum protein hemopexin. The latter two domains are connected by a linker peptide. Gelatinases have an insert of three fibronectin type II repeats (turquoise) in the catalytic domain. Membrane-type MMPs contain a transmembrane domain (black) and a cytoplasmic tail (green) at the COOH terminus, which anchors these enzymes in the cell membrane.<sup>36</sup> ..... 11

**Figure 1-4.** Reaction mechanism for proteolysis by MMPs.<sup>18</sup> ..... 12

**Figure 1-5.** Ribbon representation of the catalytic domain of MMP-3 showing the spherical topology consisting of five β-sheets and three α-helices. Coordinating residues of structural site (upper left) and catalytic site (center) are shown as sticks in color code. Zn<sup>2+</sup> ions are shown as magenta spheres and Ca<sup>2+</sup> ions are shown as orange spheres. (carbon = green, nitrogen = blue, oxygen = red). PDB: 1CQR.<sup>6</sup> ..... 14

**Figure 1-6.** Surface representation of the catalytic domain of MMP-3 shown in Figure 1-4, highlighting the positions of the subsite pockets – S3', S2', S1', S1, S2, S3. Zn<sup>2+</sup> ion is shown as a magenta sphere. PDB: 1CQR.<sup>6</sup> Shown below is a linearized cartoon schematic of the active site of MMPs with a generalized peptide substrate depicted in green. The scissile peptide bond is shown in sticks ..... 15



|  |    |
|--|----|
| <b>Figure 1-7.</b> Endogenous MMP inhibition. a) In the ribbon representation of pro-MMP-2, the catalytic Zn <sup>2+</sup> is inactivated via coordination of the “cysteine switch” thiol/sulfhydryl group. Coordinating His residues and pro-domain Cys are shown as color-coded sticks in a tetrahedral coordination environment around the Zn <sup>2+</sup> .PDB:1GXD. <sup>42</sup> b) In TIMP-2 inhibition of MT1-MMP, the catalytic Zn <sup>2+</sup> is coordinated in a bidentate fashion by the backbone of the N-terminal Cys residue to form a five-coordinate highly distorted square-pyramidal with the protein active site. PDB: 1BUV. <sup>43</sup> (carbon = green, nitrogen = blue, oxygen = blue, sulfur = yellow; Zn <sup>2+</sup> ions are shown as magenta spheres). ..... | 17 |
| <b>Figure 1-8.</b> FDA approved MMPi .....   | 18 |
| <b>Figure 1-9.</b> Generalized representation of early generation hydroxamate based MMPi in the MMP active site. The ZBG binds to the Zn <sup>2+</sup> in a bidentate fashion. The P substituents represent substrate -mimic backbone substituents that interact with the primed subsites in the MMP active site.....  | 19 |
| <b>Figure 1-10.</b> First and second generation hydroxamate-based MMPi.....  | 19 |
| <b>Figure 1-11.</b> Examples of second-generation MMPi with alternative ZBGs (highlighted in red). .....   | 21 |
| <b>Figure 1-12.</b> The structures of various ZBGs used in different MMPi. <sup>45</sup> .....   | 23 |
| <b>Figure 1-13.</b> Pathogenesis of anthrax toxin. <sup>57</sup> .....   | 27 |
| <b>Figure 1-14.</b> Ribbon representation of LF color coded by domain: I, PA binding domain (blue); II, VIP2-like domain (red); III, helix bundle domain (green); IV, catalytic domain (purple). PDB:1JKY. <sup>71</sup> .....   | 28 |
| <b>Figure 1-15.</b> Ribbon representation of LF catalytic domain. His686, His690 and Glu735 shown as sticks (carbon = green, nitrogen = blue, oxygen = blue). On the right is a zoomed in picture of the active site also showing second sphere coordination residues Glu687 and Tyr728 as sticks in cyan. PDB: 1YQY. <sup>8</sup> .....   | 30 |
| <b>Figure 1-16.</b> Some previously described LFi with their IC <sub>50</sub> values .....   | 32 |
| <b>Figure 1-17.</b> Ribbon representation of LF catalytic site in the presence of LFi, with coordinating residues His686, His690, Glu735 shown as sticks (carbon = green, nitrogen = blue, oxygen = red). <b>a.</b> NSC 12155 in sticks (carbon = yellow, nitrogen = blue, oxygen = red) bound within the active site. PDB: 1PWP. <sup>77</sup> <b>b.</b> Merck LFi in sticks (carbon = yellow, nitrogen = blue, oxygen = red) bound within the active site.PDB: 1YQY. <sup>8</sup> .....  | 33 |

|  |    |
|--|----|
| <b>Figure 2-1.</b> Early generation peptidic (top) and non-peptidic (bottom) MMP inhibitors. Catalytic Zn <sup>2+</sup> coordination and S1' pocket substituent is shown for Batimastat. ....  | 42 |
| <b>Figure 2-2.</b> Structures of MMPi examined in this study (1-7). Compounds 6 and 7 are negative controls, as they do not contain a high affinity ZBG. The numbering scheme used for the pyrone ring system found in inhibitors 2 and 3 is shown on the left.....  | 44 |
| <b>Figure 2-3.</b> A graph representing the linear relationship between substrate fluorescence and MMP activity. Relative fluorescence units (RFU) are plotted on the y-axis and time (in min) on the x-axis. Slope of each equation represents MMP activity. Blue diamonds show MMP activity without inhibitor and red squares show MMP activity in the presence of compound 2 (PY-2).....  | 49 |
| <b>Figure 2-4.</b> Dixon plot of MMP-12 with different substrate concentrations (10 μM = filled circles, 5 μM = open squares, 2.5 μM = open diamonds, 1.67 μM = crosses, 1 μM = plus signs) against varying concentrations of MMPi 1 in nM. The reciprocal of the activity (1/v) in mmol <sup>-1</sup> min mg is plotted on the y-axis.....  | 53 |
| <b>Figure 2-5.</b> Cytotoxicity assays of 1,2-HOPO-2, PY-2 and PICO-2 in comparison to broad spectrum inhibitors CGS 27023A and PD 166793.....   | 54 |
| <b>Figure 2-6.</b> Effects of 5 μM (A) PY-2, (B) PICO-2, (C) CGS27023A, (D) PD 166793, (E) 1,2-HOPO-2 on isolated, perfused rat hearts subjected to 20 minutes of GNFI and 30-minute reperfusion. (F) 5 μM 1,2-HOPO-2 subjected to 30 minutes of GNFI and 30-minute reperfusion. ....  | 57 |
| <b>Figure 2-7.</b> Three different views comparing the binding of MMPi 3 (left) and 5 (right) in the MMP-3 active site. Zn <sup>2+</sup> ions are shown as magenta spheres, the MMPi in ball and stick colored by atom, and the protein in gray. The three views highlight the steric clash of the N-methyl group on compound 5 with the protein. Val163 (shown as sticks in the bottom views) is the residue that conflicts with the N-methyl substituent.....                    | 62 |
| <b>Figure 2-8.</b> MMP active sites (gray surface) with different ZBGs. ZBGs are colored by atom: carbon (green), oxygen (red), nitrogen (blue). The Zn <sup>2+</sup> ion is shown as a magenta sphere. Each row is representative of a different MMP (shown to the right) and each column of a different ZBG (shown above each column). Active site residues are colored as follows:<br>MMP-2: Gly162 (cyan), Leu163 (light orange), Leu164 (red), Ala165 (pink), His166 (yellow) |    |

MMP-3: Asn162 (blue), Val163 (olive), Leu164 (red), Ala165 (pink), His166 (yellow)  
MMP-8: Gly158 (cyan), Ile159 (orange), Leu160 (red), Ala161 (pink), His162 (yellow)  
MMP-12: Gly179 (cyan), Ile180 (orange), Leu181 (red), Ala182 (pink), His183 (yellow)..... 63

**Figure 3-1.** ZBGs and linkers used in the LFi reported here. Abbreviations for each subset of compounds are shown in parentheses. The heteroatom terminology used throughout this study is highlighted in the top three structures by the use of a numbering scheme and bold and italics atom labels. Shown in the bottom right is the complete LFi **11b** which was previously reported..... 105

**Figure 3-2.** Structures of the inhibitors tested in the study. The heteroatom terminology used throughout is highlighted in the top three structures by the use of bold and italics atom labels. Shown in the box is the complete (O,O,O) LFi **1a** (for clarity). Other inhibitors are hydroxypyrones with an amide linker (**1a** – **8a**), hydroxypyrothiones with an amide linker (**1b** – **8b**), hydroxypyrothiones with a thioamide linker (**1c** – **8c**). Shown below the thick line are *N*-hydroxypyridinones with an amide linker (**9a**, **10a**) and *N*-hydroxypyridinethiones with an amide linker (**9b**, **10b**)..... 109

**Figure 3-3.** Structural diagram of **5c** with 50% probability ellipsoids. Hydrogen atoms have been omitted for clarity. .... 112

**Figure 3-4.** QM/MM optimized structures of the complex between anthrax LF (ribbons) and inhibitors **1b**, **1c**, **3b**, **3c**, **4b** and **4c** (ball and stick). Some active site residues (ball and stick) and catalytic Zn<sup>2+</sup> ion (gray sphere) are also shown. .... 118

**Figure 3-5.** QM/MM optimized structures of the complex between anthrax LF (ribbons) and inhibitors **7c**, **2c** and **8c** (ball and stick) from top to bottom. Some active site residues (ball and stick) and catalytic Zn<sup>2+</sup> ion (gray sphere) are also shown ..... 119

**Figure 3-6.** Correlation between log (IC<sub>50</sub>) and calculated Free energy of binding (ΔG). .... 120

**Figure 4-1. Schematic representation of HTS vs fragment hit.** **a)** The HTS hit is large and makes surface contacts with the receptor without forming high quality interactions in key pockets. The affinity is spread throughout the entire molecule **b)** The fragment is much smaller and makes high-quality contacts with the receptor despite the weak affinity..... 154

|   |     |
|---|-----|
| <b>Figure 4-2.</b> Fragment 1 binds to the receptor at one site and the lead molecule is evolved by building away from the starting fragment and making good contact with the upper surface and then by growing into a second pocket..  | 156 |
| <b>Figure 4-3.</b> Fragments 1 and 2 bind to the receptor at different sites from the various fragments screened, and are joined together by a linking group that allows the lead molecule to span both sites.  | 156 |
| <b>Figure 4-4.</b> A summary of the SAR by NMR fragment based method as applied to discovery of stromelysin inhibitors  | 158 |
| <b>Figure 4-5.</b> Chelator fragment library (CFL-1). The library consists of 96 compounds grouped into several classes including picolinic acids, hydroxyquinolones, pyrimidines, hydroxypyrones, hydroxypyridinones, salicylic acids, hydroxamic acids and sulphonamides.                                       | 160 |
| <b>Figure 4-6.</b> Thermoplot representing the percent inhibition of MMP-2 by the various fragments of the chelator fragment library (CFL-1). Those in black were not tested due to interference with the assay readout and/or solubility issues. Structures of each 96-well plate label are shown in Figure 4-5. | 162 |
| <b>Figure 4-7.</b> 3,4-HOPO and 3,4-HOPTO components (87 total) of extended chelator fragment library (eCFL-1).   | 164 |
| <b>Figure 4-8.</b> Lead hits identified against Zn <sup>2+</sup> -dependent metalloenzymes from a expanded library (eCFL-1) of 3,4-HOPO (blue chelating groups) and 3,4-HOPTO (green chelating groups) fragments.   | 166 |
| <b>Figure 4-9.</b> Mechanism of amine insertion in a pyrone/pyrothione ring system. <sup>40</sup> The numbering scheme used for the pyrone ring system is shown above.  | 173 |
| <b>Figure 4-10.</b> Structures of the five different fragments ( <b>94G5.1-94G5.5</b> ) evolved from <b>94G5</b> (shown boxed above)  | 174 |
| <b>Figure 4-11.</b> Non-linear dose response curve of the % inhibition versus the log of the inhibitor concentration using GraphPad Prism 5.  | 199 |
| <b>Figure 4-12.</b> Lineweaver-burk plot of MMP-9 to determine enzyme kinetic parameters.   | 201 |

**Figure 5-1.** Raltegravir (left) shows a striking similarity to metalloenzyme inhibitors that have been reported in our lab.<sup>3,4</sup> The three compounds shown have the same *p*-fluorophenyl backbone, but employ different metal-binding groups (MBGs). From left to right (including RAL), the MBGs are a N-methylhydroxypyridinone, N-hydroxypyridin(one/thione), hydroxypyr(one/thione). The metal binding atoms are highlighted in bold red. Shown below in the box is the proposed metal binding of RAL to the dinuclear Mg<sup>2+</sup> active site of HIV-IN, compared to the proposed binding of our inhibitors against mononuclear Zn<sup>2+</sup> endopeptidases MMPs and LF. .... 208

**Figure 5-2. Life cycle of HIV-1 replication.** (a-e) represents the different stages and/or proteins that can be targeted for inhibition in the replication cycle.<sup>12</sup> ..... 211

**Figure 5-3. Integrase catalytic reactions: 3'-processing and Strand transfer.** a, b) 3'-processing of conserved CAGT viral DNA ends by Mg<sup>2+</sup> bound H<sub>2</sub>O (green arrows) mediated endonucleolytic cleavage. Open circles represent recessed 3'-CpA-OH ends. c, d) Strand transfer of nicked, reactive 3'-OH DNA ends of viral DNA into a host-cell chromosome. e) Gap filling of integrated viral DNA by cellular repair enzymes. Adapted from reference.<sup>12</sup> ..... 216

**Figure 5-4. The two-metal dependent catalytic mechanism.** Schematic representation of catalytic triad (DDE) involved in integration reactions. a, b) 3'-processing of viral DNA by attack of Mg<sup>2+</sup> (yellow spheres) coordinated H<sub>2</sub>O on phosphodiester bond. c, d) Strand transfer of viral DNA by nucleophilic attack of 3'-OH of viral DNA on phosphodiester bond of host DNA. Adapted from reference.<sup>28</sup> ..... 217

**Figure 5-5.** The various domains of HIV-IN with structural features highlighted in bullet points below each domain. Adapted from reference.<sup>12</sup> ..... 218

**Figure 5-6. The three domains of HIV-IN.** Shown above from left to right are the N-terminal domain (NTD) in ribbon representation, HHCC site in sticks and the Zn<sup>2+</sup> ion as a magenta sphere, PDB code: 1K6Y;<sup>32</sup> Catalytic core domain (CCD) in ribbon representation with the catalytic triad DDE shown in sticks and one of two Mg<sup>2+</sup> ions as an orange sphere, PDB code: 1QS4;<sup>33</sup> C-terminal domain (CTD) in ribbon representation highlighting the β barrel SH3 fold, PDB code: 1EX4.<sup>34</sup> (carbon = green, nitrogen = blue, oxygen = red, sulfur = yellow) ..... 220

**Figure 5-7.** Structures of second generation and “me-too” HIV-IN inhibitors ..... 223

|   |     |
|---|-----|
| <b>Figure 5-8. Crystal structure of PFV-IN (PDB: 3OYA) with RAL.</b> The protein is represented by a gray ribbon, RAL and the active site coordinating residues are shown as sticks and are color-coded (carbon = green, nitrogen = blue, oxygen = red, fluorine = cyan) and the Mg <sup>2+</sup> ions are represented by orange spheres. ....  | 225 |
| <b>Figure 5-9. Crystal structure of PFV-IN (PDB: 3L2U) with GS-3197 and viral DNA.</b> The protein is represented by a gray ribbon, GS-3197 and the active site coordinating residues are shown as sticks and color-coded (carbon = green, nitrogen = blue, oxygen = red, fluorine = cyan) and the Mg <sup>2+</sup> ions are represented by orange spheres. The viral DNA is shown in rainbow colors and the invariant base A17 of the 3'-OH end of viral DNA is shown as sticks in cyan..... | 226 |
| <b>Figure 5-10.</b> A representation of the metal-binding mode of Raltegravir (left) and Elvitegravir (right) in the active site of HIV-IN/PFV-IN. ....   | 227 |
| <b>Figure 5-11. Raltegravir-Chelator Derivatives (RCD).</b> Derivatives of RAL based off the simplified scaffold RCD-1. Each RCD employs a different MBG to bind the active site metal ions. ....   | 229 |
| <b>Figure 5-12.</b> Numbering scheme of the hydroxyquinoline ring (left) and hydroxypyridone(thione) (center) and hydroxypyridinone (right).....  | 231 |
| <b>Figure 5-13.</b> Docking studies of select RCD compounds in the active site of PFV-IN (PDB:3OYA). Selective RCD compounds are shown with their IC <sub>50</sub> values .....   | 239 |

## LIST OF SCHEMES

|   |     |
|---|-----|
| <b>Scheme 2-1.</b> Synthesis of 1,2-HOPO-2 .....  | 46  |
| <b>Scheme 2-2.</b> Synthesis of PY-2.....   | 46  |
| <b>Scheme 2-3.</b> Synthesis of PY-NMe-2, AM-NMe-2.....   | 47  |
| <b>Scheme 2-4.</b> Synthesis of Suzuki-Miyaura coupled biphenyl backbones .....                           | 68  |
| <b>Scheme 2-5.</b> Synthesis of pyridinyl and miscellaneous biphenyl backbones .....                      | 69  |
| <b>Scheme 2-6.</b> Synthesis of 1,2-HOPO-2 derivatives .....  | 70  |
| <b>Scheme 3-1.</b> Synthesis of Hydroxypyrrone (O,O,O) Inhibitors ( <b>1a</b> – <b>8a</b> ) .....         | 110 |
| <b>Scheme 3-2.</b> Synthesis of Hydroxypyrothione Analogues <b>1b</b> (O,S,O) and (O,S,S) Compounds ..... | 110 |
| <b>Scheme 3-3.</b> Synthesis of <i>N</i> -Hydroxypyridinone <b>10a</b> .....                              | 111 |
| <b>Scheme 3-4.</b> Synthesis of <i>N</i> -Hydroxypyridinethione Inhibitors <b>9b</b> and <b>10b</b> ..... | 111 |
| <b>Scheme 4-1.</b> Synthesis of 3,4-HOPO and 3,4-HOPTO derivatives of eCFL-1 .....                        | 164 |
| <b>Scheme 4-2.</b> Synthesis of fragments evolved from <b>94G5</b> .....                                  | 174 |
| <b>Scheme 5-1.</b> Synthesis of RCD-11 .....  | 229 |
| <b>Scheme 5-2.</b> Synthesis of RCD-12 .....  | 230 |
| <b>Scheme 5-3.</b> Synthesis of RCD-19 .....  | 230 |
| <b>Scheme 5-4.</b> Synthesis of RCD-20 .....  | 230 |

## LIST OF TABLES

|   |     |
|---|-----|
| <b>Table 1-1.</b> General summary of zinc metalloproteins that have been examined as medicinal targets. <sup>4</sup> .....  | 7   |
| <b>Table 1-2.</b> Classification of MMPs. <sup>34</sup> .....   | 10  |
| <b>Table 1-3.</b> A list of IC <sub>50</sub> values (μM) for ZBGs against MP-1,-2,-3 and LF, from Figure 1-12. N.D. = Not determined due to fluorescence or solubility issues. <sup>47-49</sup> .....   | 24  |
| <b>Table 2-1.</b> IC <sub>50</sub> values (in μM) for MMPi <b>1-7</b> (rows) against eight different MMPs (columns) using a fluorescence-based assay .....  | 50  |
| <b>Table 2-2.</b> IC <sub>50</sub> values (in μM) of the different 1,2-HOPO-2 derivatives against different MMPs. Values are the average of two independent experiments performed in duplicate. For comparison, the IC <sub>50</sub> values of 1,2-HOPO-2 are also listed in the top row.....   | 71  |
| <b>Table 3-1.</b> IC <sub>50</sub> values of LFi using a Fluorescence-Based Assay.....  | 114 |
| <b>Table 3-2.</b> Crystallographic data collection and structural parameters of crystal structure of (O,S,S) inhibitor <b>5c</b> .....  | 146 |
| <b>Table 4-1.</b> IC <sub>50</sub> values (μM) of lead fragments against metalloenzyme targets. IC <sub>50</sub> values of non-hits (>50 μM) are designated with an ×. Standard deviations from triplicate measurements for all values listed are <10%. <sup>a</sup> Ligand efficiency for some fragments are provided against MMP-9 only ..... | 168 |
| <b>Table 4-2.</b> Comparison of leads identified by chelator-based FBLD (this work) versus large library (≥ 10,000 compounds) HTS findings.....   | 171 |
| <b>Table 4-3.</b> IC <sub>50</sub> values (in μM) of <b>94G5</b> derivatives synthesized above. (n.d. = not determined) .....   | 176 |
| <b>Table 5-1.</b> A current and comprehensive list of FDA approved anti-AIDS drugs. <sup>1</sup> .....  | 213 |
| <b>Table 5-2.</b> Evolution of DKAs as metal binding groups towards the discovery of Raltegravir.....   | 224 |
| <b>Table 5-3.</b> Screening results of select RCD compounds from Figure 8 against both the 3'-processing (3'-P) reaction and the strand transfer (ST) reaction of HIV-IN .....  | 234 |



## ACKNOWLEDGEMENTS

I want to thank my Ph.D. advisor Prof. Seth M. Cohen and my committee, Prof. Alexander Hoffmann, Prof. F. Akif Tezcan and Prof. Gourisankar Ghosh for your continued support and advice throughout my Ph.D. career. I am grateful to you for your endless advice and insightful discussions. Your door has always been open to me as both a mentor and a friend, for which I am extremely grateful.

I would like to especially thank my advisor, Prof. Seth M. Cohen to whom I am also extremely indebted. Seth, you agreed to take me on in your lab, though I was a synthetic novice and looking back, I cannot fathom the amount I have learned under your guidance. You have not only been a great mentor but also a great friend. Even though we have had our difficult moments, I will always respect you for pushing me to the limit. It has truly been a pleasure working in your lab and I sincerely thank you for a wonderful graduate experience. Also, I am one of the few students to have witnessed your transition from Associate to full Professor and along the way, have encountered many a generation of talented graduate and post-doctoral students.

I am grateful to all my lab mates both past and present for truly making lab an enjoyable experience, to David, Jana and Misha for your mentorship and setting the stage for my research; to Tanabe, Sergio, Rick and Jen for riding most of this journey along with me; to Joe, Jody and Christophe for your help and advice during my graduate career; to Kevin, Aniline, Jamie, Dave and Jess for keeping it hip. I am especially thankful to my dear friend and Organic GURU – Dr. Matthieu Rouffet. You are a great scientist and a genuine person. You have taught me all that is organic chemistry and synthesis. You have been a great friend and my backbone in the lab.

You let me come to you with all my problems both personal and professional and to you, I am forever indebted.

I would also like to especially thank Dr. Cesar Oliveira from Prof. Andrew McCammon's lab who is my Computational MAESTRO. I am extremely grateful to you for playing an important role in my research throughout my Ph.D. career and always being there whenever I turned to you for computational help. You never once refused to help me for which I will always be thankful.

Finally, I would like to thank my family for being by my side all these years and supporting me through all my decisions. My parents especially, have instilled a great deal of dedication and patience in me that carried me through and to them I am forever grateful. My siblings for always being there and hearing me out. I dedicate this chapter of my life to my family with love, because I could not have done it without you.

The text, schemes, and figures of Chapter 2 are in part reprints of the materials published in the following papers: Agrawal, Arpita; Romero-Perez, Diego; Jacobsen, Jennifer, A.; Villarreal, Francisco, J.; Cohen, Seth, M. "Zinc-Binding Groups Modulate Selective Inhibition of MMPs" *ChemMedChem* **2008**, *3*, 812-820; Romero-Perez, Diego; Agrawal, Arpita; Jacobsen, Jennifer, A.; Yan, Yi-long; Thomas, Robert; Cohen, Seth, M.; Villarreal, Francisco, J. "Effects of Novel Semi-selective MMP Inhibitors on Ex vivo cardiac Structure/Function" *J. Cardiovasc. Pharmacol.* **2009**, *53*, 452-461.

The text, schemes, and figures of Chapter 3 are in part reprints of the materials published in the following paper: Agrawal, Arpita; De Oliveira, Cesar, A.F.; Cheng,

Yuhui; Jacobsen, Jennifer, A.; McCammon, J. Andrew; Cohen, Seth, M. “Thioamide Hydroxypyrothiones Supersede Amide Hydroxypyrothiones in Potency against Anthrax Lethal Factor” *J. Med. Chem.* **2009**, *52*, 1063-1074.

The text, schemes, and figures of Chapter 4 are in part reprints of the materials published in the following paper: Agrawal, Arpita; Johnson, Sherida, L.; Jacobsen, Jennifer, A.; Miller, Melissa, T.; Chen, Li, H.; Pellecchia, Maurizio; Cohen, Seth, M. “Chelator Fragment Libraries for Targeting Metalloproteinases” *ChemMedChem* **2010**, *5*, 195-109. The dissertation author was the primary researcher for the data presented and was either the primary author or a co-author on the papers included. The co-authors listed in these publications also participated in the research.

## VITA AND PUBLICATIONS

### Education

- 2011 Doctor of Philosophy, Chemistry, University of California, San Diego, La Jolla, CA
- 2001 Bachelor of Arts, Chemistry, Rutgers University, New Brunswick, NJ

### Awards and Professional Affiliations

- 2000 Excellence in Organic Chemistry Award, Rutgers University, New Brunswick, NJ
- 2005 – Present ACS Member, Division of Inorganic Chemistry

### Publications

1. Christianson, C.; Shim, J.H.; Agrawal, A.; Cohen, S.M.; Hua, X.Y. and Yaksh, T. “Spinal Matrix Metalloproteinase 3: A paracrine role in spinally mediated inflammatory hyperalgesia via a glial-TNF dependent mechanism”, Submitted for publication
2. Schulze, W.J.; Innocenti, A.; Vullo, D.; Agrawal, A.; Cohen, S.M.; Heine, A.; Supuran, C.T. and Klebe, G. “Bidentate Zinc Chelators for alpha-Carbonic Anhydrases that Produce a Trigonal Bipyramidal Coordination Geometry” *ChemMedChem* **2010**, *5*, 1609-1615.
3. Agrawal, A.; Johnson, S.L.; Jacobsen, J.A.; Miller, M.T.; Chen, L.H.; Pellecchia, M. and Cohen, S.M. “Chelator Fragment Libraries for Targeting Metalloproteinases” *ChemMedChem* **2010**, *5*, 195-109.
4. Rouffet, M.; De Oliveira, C.A.F.; Udi, Y.; Agrawal, A.; Sagi, I.; McCammon, J.A. and Cohen, S.M. “From sensors to silencers: quinoline- and benzimidazole-sulfonamides as inhibitors for zinc proteases” *J. Am. Chem. Soc.* **2010**, *132*, 8232-8233.
5. Romero-Perez, D.; Agrawal, A.; Jacobsen, J.A.; Yan, Y.; Thomas, R.; Cohen, S.M. and Villarreal, F.J. “Effects of Novel Semi-selective MMP Inhibitors on Ex vivo cardiac Structure/Function” *J. Cardiovasc. Pharmacol.* **2009**, *53*, 452-461

6. Agrawal, A.; De Oliveira, C.A.F.; Cheng, Y.; Jacobsen, J.A.; McCammon, J.A. and Cohen, S.M. “Thioamide Hydroxypyrothiones Supersede Amide Hydroxypyrothiones in Potency against Anthrax Lethal Factor” *J. Med. Chem.* **2009**, *52*, 1063-1074.
7. Agrawal, A.; Romero-Perez, D.; Jacobsen, J.A.; Villarreal, F.J. and Cohen, S.M. “Zinc-Binding Groups Modulate Selective Inhibition of MMPs” *ChemMedChem* **2008**, *3*, 812-820.
8. O'Donnell, L.A.; Agrawal, A.; Sabnekar, P.; Dichter, M.A.; Lynch, D.R. and Kolson, D.L. “Apelin, an endogenous neuronal peptide, protects hippocampal neurons against excitotoxic injury” *J. Neurochem.* **2007**, *102*, 1905-17.
9. O'Donnell, L.A.; Agrawal, A.; Jordan-Sciutto, K.L.; Dichter, M.A.; Lynch, D.R. and Kolson, D.L. “Human Immunodeficiency Virus (HIV) – Induced Neurotoxicity: Roles for the NMDA Receptor Subtypes 2A and 2B and the Calcium-Activated Protease Calpain by a CSF-derived HIV-1 Strain” *J. Neurosci.* **2006**, *26*, 981-990.

## **ABSTRACT OF THE DISSERTATION**

### **The Importance of Metal Binding in Metalloprotein Inhibitors**

by

Arpita Agrawal

Doctor of Philosophy in Chemistry

University of California, San Diego, 2011

Professor Seth M. Cohen, Chair

The development of novel and selective full-length inhibitors against medicinally relevant zinc metalloenzymes has been described. The diversity of zinc metalloenzymes described, range from those present in humans to bacteria to viruses. The dissertation will first focus on the development of selective inhibitors against matrix metalloproteinases (MMPs). MMPs are  $\text{Zn}^{2+}$  hydrolytic enzymes that are present in vertebrates, invertebrates and even plants. They are responsible for the cleavage of the extracellular matrix, and this study demonstrates the importance the zinc-binding group (ZBG) plays in developing inhibitors that are selective against different MMP isoforms. The selectivity obtained from the (O,O) chelating MMP inhibitors (MMPi) was very interesting; considering the active site of MMPs are highly homologous with a conserved  $\text{Zn}^{2+}$  metal cofactor bound by three histidine residues within a conserved HEXGHXXGXXH metal binding motif.

In Chapter 3, the development of full length metalloprotein inhibitors is expanded beyond MMP isoform selectivity to selectivity against another  $Zn^{2+}$  endopeptidase, Anthrax lethal factor (LF). This study shows that the potent (O,O) containing MMPi show no inhibition against LF. The bis-histidine and glutamate coordinated catalytic  $Zn^{2+}$  in LF favors the softer (O,S) donor ligands. In addition a backbone and linker SAR study shows that a thioamide linkage instead of the traditional amide linkage for backbone attachment introduces a hydrogen bond within the LF active site to enhance potency of the studied inhibitors.

Chapter 4 introduces the relatively novel approach of fragment-based lead design (FBLD) in the lab toward the microwave assisted rapid synthesis of a 87-component chelator fragment library that showed potent hits with good ligand efficiencies (LEs) against both MMPs and LF.

The final chapter culminates with the study of an entirely new metalloenzyme Human Immunodeficiency Virus Integrase (HIV-IN). As opposed to the mononuclear  $Zn^{2+}$  endopeptidases MMPs and LF, HIV-IN is a dinuclear  $Mg^{2+}$  endonuclease and preliminary studies show that inhibitors developed against MMPs and LF show submicromolar potencies against this structurally different metalloenzyme. Based on these results, novel HIV-IN inhibitors (HIV-INi) were generated to study the effects of different tris-chelating metal binding groups (MBGs) on this enzyme, while maintaining a constant backbone.

## **Chapter 1. Zinc metalloenzymes in health and disease**



## 1.A Introduction

Zinc metalloenzymes are ubiquitous enzymes that are present in various biological systems including microorganisms, plants and animals. Zinc is the second most abundant metal in biological systems and is present in over 300 metalloenzymes.<sup>1,2</sup> Zinc is also the only metal that is found across all six classes of enzymes (as established by the International Union of Biochemistry) – oxidoreductases (E.C.1), transferases (E.C.2), hydrolases (E.C.3), lyases (E.C.4), isomerases (E.C.5) and ligases (E.C.6).<sup>2</sup> Therefore, zinc has multifarious biological functions, and in humans, 10% of the proteome is comprised of zinc metalloproteins.<sup>3</sup> In proteins, zinc is only found as a divalent cation ( $\text{Zn}^{2+}$ ) and the closed  $d^{10}$  electron configuration of  $\text{Zn}^{2+}$  makes it redox stable under physiological conditions.<sup>4</sup> The intermediate polarizability of the zinc cation attracts both hard and soft donor ligands of oxygen, nitrogen, and sulfur. In proteins, zinc is found bound by different combinations of histidine (His), cysteine (Cys), aspartic acid (Asp), and glutamic acid (Glu) in a tetrahedral, trigonal bipyramidal or octahedral geometry.<sup>1</sup> The coordination geometry adopted by zinc in proteins is a good indicator of the classification of the zinc site as (i) structural, (ii) catalytic or (iii) co-catalytic.<sup>5</sup>

- (i) Structural zinc sites are typically characterized by an inner sphere tetrahedral coordination by four amino acid residues. The  $\text{Zn}^{2+}$  ion is coordinatively saturated to maintain the secondary and/or tertiary structure of the protein. Structural sites are best represented by zinc fingers which are also the most abundant zinc protein present in the human proteome.<sup>3</sup> In zinc fingers the metal ion is tetrahedrally coordinated by two His and two Cys residues. Of the

aforementioned zinc-coordinating amino acids, Cys is the most common residue present in structural zinc sites, though there are exceptions to this rule. For example, matrix metalloproteinases (MMPs) discussed later in this chapter and in Chapter 2, contain a structural  $\text{Zn}^{2+}$  site that is coordinated by three His residues and one Asp residue (Figure 1-1a). Conversely, HIV integrase, the focus of Chapter 5, contains a structural  $\text{Zn}^{2+}$  site coordinated by two His and two Cys residues (Figure 1-1b) that resembles a zinc finger motif. Cys is commonly found in structural sites due to its ability to transfer the most charge, in relation to other amino acids, to the  $\text{Zn}^{2+}$  ion making it less acidic. Additionally, the bulkiness of the thiol group shields the zinc and prevents the coordination of a fifth ligand. Therefore the presence of Cys in structural zinc sites enhances the structural integrity of the metal center and the protein.<sup>5</sup>

- (ii) Catalytic zinc sites are most commonly distinguished by the coordination of a labile water molecule in the place of a fourth amino acid residue. Catalytic zinc sites exhibit coordination numbers (CN) for zinc from 4 to 6, although a tetrahedral geometry (CN = 4) is most common. As opposed to the bulky, negatively charged Cys ligands in structural zinc sites, the neutral imidazole ligand of His is the most common residue present in catalytic zinc sites. For example, the catalytic  $\text{Zn}^{2+}$  in MMPs (mentioned above) is coordinated by three His residues and a water molecule when active (Figure 1-2a). A similar catalytic site is observed for anthrax lethal factor (LF, discussed later and in Chapter 3) in which the catalytic  $\text{Zn}^{2+}$  is coordinated by two His residues, one Glu residue and a water molecule (Figure 1-2b). The presence of water and His

lowers the charge transfer to  $Zn^{2+}$  (compared to Cys) resulting in a higher positive charge on the metal making  $Zn^{2+}$  a good Lewis acid and enabling it to play a catalytic role. The charge imparted by the coordinating residues on the catalytic  $Zn^{2+}$  also plays an important role in metal binding selectivity of inhibitors of the different zinc metalloproteases discussed in Chapters 2-4.

- (iii) Cocatalytic zinc sites are distinguished by the presence of more than one zinc and/or other metal ion in the active site. Amino acids commonly found in these sites are Asp and His that bridge neighboring metal ions. An example is that of Cu-Zn superoxide dismutase (SOD) which contains a Cu and Zn ion bridged by a His residue.

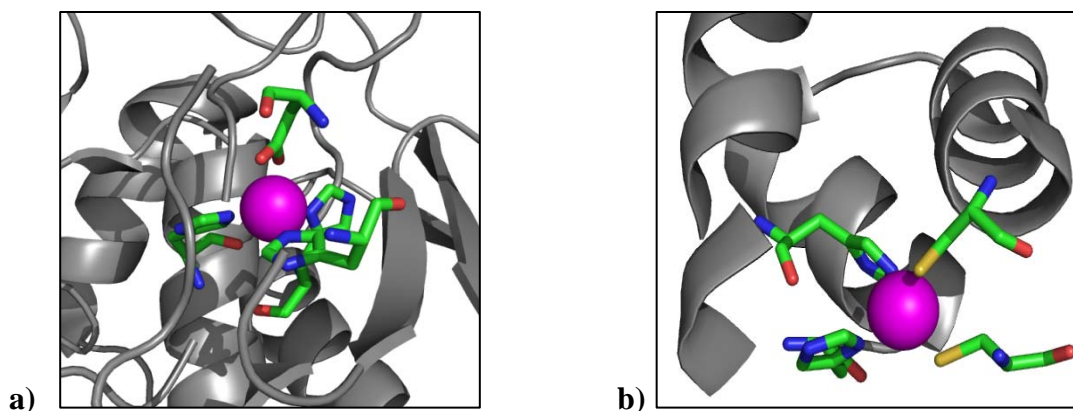


**Figure 1-1.** a) Ribbon representation of MMP-3 structural  $Zn^{2+}$  site. Coordinating residues His151, Asp153, His166 and His179 are shown as color-coded sticks. PDB:1CQR.<sup>6</sup> b) Ribbon representation of HIV-IN structural  $Zn^{2+}$  site. Coordinating residues His12, His16, Cys40 and Cys43 are shown as color-coded sticks.  $Zn^{2+}$  ions are shown as magenta spheres. (carbon = green, nitrogen = blue, oxygen = red, sulfur = yellow). PDB:1K6Y.<sup>7</sup>

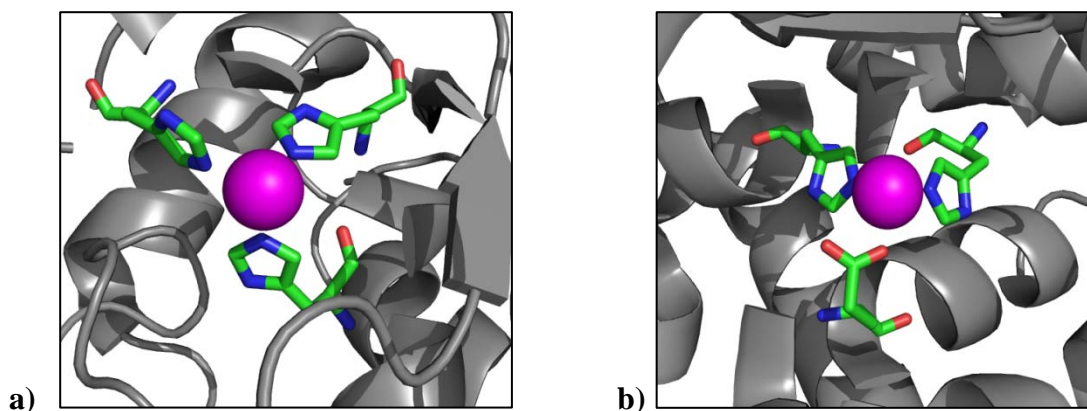


**Figure 1-2.** a) Ribbon representation of MMP-3 catalytic  $Zn^{2+}$  site. Coordinating residues His201, His205 and His211 are shown as color-coded sticks. PDB:1CQR.<sup>6</sup> b) Ribbon representation of anthrax LF catalytic  $Zn^{2+}$  site. Coordinating residues His686, His690, and Glu735 are shown as color-coded sticks.  $Zn^{2+}$  ions are shown as magenta spheres. (carbon = green, nitrogen = blue, oxygen = red). PDB:1YQY.<sup>8</sup>

## 1.B Catalytic zinc sites as medicinal targets

A unique feature for a catalytic zinc site is the existence of a labile ligand in the coordination sphere.<sup>2,5</sup> The  $Zn^{2+}$  in a catalytic site contains at least one water molecule in addition to three or four protein ligands. The  $Zn^{2+}$  bound water is critical for a catalytic site because it can be either ionized to a hydroxide ion (as in carbonic anhydrase, CA), polarized by a general base to generate a nucleophile for catalysis (as in MMPs and LF), or be displaced by a substrate.<sup>2</sup> This labile site provides an opportunity for the binding of small molecules that can act as inhibitors. The unique active site of each protein discussed dictates the preference for different metal-binding groups (MBGs) and will be discussed in more detail throughout the following chapters.

Zinc metalloproteases were first discovered with carbonic anhydrases (CAs) in 1940, which were the first enzymes shown to be dependent on the  $Zn^{2+}$  ion.<sup>1,9</sup> CAs are ubiquitous metalloenzymes responsible for the physiologically important, reversible hydration of carbon dioxide.<sup>2,9,10</sup> The various isoforms of CAs are also implicated in pathological conditions such as glaucoma, epilepsy, obesity, and cancer. This makes CAs an attractive therapeutic target for metalloprotein inhibition.<sup>11</sup> The catalytic  $Zn^{2+}$  site is tetrahedrally coordinated by three His residues and a water molecule. An enormous number of CA inhibitors (CAi) have been developed, with the vast majority relying on  $Zn^{2+}$ -coordinating groups to bind the active site metal ion.

Other catalytic  $Zn^{2+}$  medical targets include MMPs, Histone deacetylases (HDACs), bacterial toxins such as anthrax LF and botulinum neurotoxin (BoNT). Table 1-1 lists different metalloproteins containing a  $Zn^{2+}$  catalytic active site and

their medical relevance. The table also highlights the different first coordination spheres for the various  $Zn^{2+}$  metalloproteases. The coordination sphere of  $Zn^{2+}$  is very important in that it dictates the nature of the metal ion, i.e. the charge and acidity of the catalytic  $Zn^{2+}$ ; and thereby dictates the preference for various metal chelating groups by the  $Zn^{2+}$  ion, in inhibitors designed against these metalloproteins. The primary focus of this thesis is the design of inhibitors against mononuclear zinc endopeptidases such as matrix metalloproteinases (MMPs) and anthrax lethal factor (LF).

**Table 1-1.** General summary of zinc metalloproteins that have been examined as medicinal targets.<sup>4</sup>

| Enzyme              | Function   | Zn coordination sphere                                 | Medical relevance  |
|---------------------|--|--|--|
| Catalytic Zinc MMPs | Degradation of extracellular matrix proteins                 | HisHisHis H <sub>2</sub> O                             | Cancer, diabetes, neurodegenerative disorders, arthritis, infectious diseases          |
| HDACs               | Deacetylation of lysine residues in histone N-terminal tails | HisAspAsp H <sub>2</sub> O                             | Cancer, diabetes, neurodegenerative disorders, inflammatory related diseases, diabetes |
| PTs                 | Prenylation of proteins involved in signal transduction      | CysHisAsp H <sub>2</sub> O                             | Cancer, rheumatoid arthritis, parasitic infections, multiple sclerosis                 |
| SOD                 | Disproportionation of superoxide ion                         | HisHisAspHis   | Familial Amyotrophic Lateral Sclerosis (fALS)  |
| MβLs                | Hydrolysis of β-lactam ring in antibiotics                   | HisHisHis HisHisAsn (Zn1)<br>AspCysHis AspHisHis (Zn2) | Bacterial resistance to antibiotics  |
| Structural Zinc ZFs | Structural DNA RNA protein recognition                       | CysCysHisHis   | Applications in human gene therapy, cancer, inflammatory conditions, antiviral therapy |
| P53                 | Tumor suppressor protein                                     | CysCysCysHis<br>CysCysCysCys<br>CysCysCysHis           | Cancer, neurodegenerative disorders  |

### 1.I.A Matrix Metalloproteinases (MMPs)

Matrix metalloproteinases (MMPs) are a family of  $Zn^{2+}$  and  $Ca^{2+}$ -dependent endopeptidases involved in the breakdown of the extracellular matrix (ECM) and basement membrane components such as aggrecan, collagen, elastin, fibronectin, gelatin, and laminin.<sup>12-15</sup> In normal physiology, MMPs are responsible for ECM homeostasis, embryonic development, tissue remodeling, wound healing, angiogenesis, and apoptosis amongst other important processes.<sup>16-18</sup> However, MMPs can also participate in the pathophysiology of diseases such as arthritis, multiple sclerosis, periodontal disease, cancer metastasis, atherosclerosis, and cardiac injury and remodeling.<sup>19-24</sup> MMPs have therefore been an important therapeutic target for over three decades, with growing interest towards the design of inhibitors that are highly specific against different MMP isoforms and possess a high therapeutic index over older generation compounds.<sup>25-31</sup>

MMPs were first discovered in vertebrates in 1962 by Charles Lapiere and Jerome Gross while studying the degradation of triple-helical collagen during the metamorphosis of a tadpole tail.<sup>32</sup> Therefore, the enzyme was named interstitial collagenase; now known as MMP-1. The enzyme was first isolated from human skin in its inactive form, proMMP (or as a zymogen) in 1968.<sup>33</sup> Since then, 23 different MMP isoforms have been identified in humans and Table 1-2 lists the various isoforms along with the substrates they cleave and the different substrate classes they belong to. The fact that MMPs are involved in the degradation of the extracellular matrix may explain the evolutionary redundancy seen in this enzyme class (Table 1-2). For example, even though MMP-7 is classified as a matrilysin, it still cleaves

collagens IV and V, as does MMP-9 which is a gelatinase. Despite the extensive overlap in substrate cleavage, MMPs can be broadly classified based on their substrate specificity into collagenases, gelatinases, stromelysins, matrilysins, membrane type, and unclassified.<sup>16,26,29</sup>



**Table 1-2.** Classification of MMPs.<sup>34</sup>

| MMP     | Metalloproteinase                  | kDa | EC classification | Locus         | Substrates   |
|---------|------------------------------------|-----|-------------------|---------------|--|
| MMP-1   | Collagenase (type I, interstitial) | 43  | EC3.4.24.7        | 11q22-q23     | Collagens (I,II,III,VIII and X); gelatin; aggrecan; L-selectin; IL-1 $\beta$ proteoglycans; entactin; ovostatin; MMP-2; MMP-9  |
| MMP-2   | Gelatinase A 72 kDa                | 66  | EC3.4.24.24       | 16q13         | Collagens (I,IV,V,VII,X,XI and XIV); gelatin; elastin; fibronectin;aggrecan, MBP; osteonectin; laminin-1; MMP-1; MMP-9; MMP-13   |
|         | Gelatinase type IV collagenase     |     |                   |               |  |
| MMP-3   | Stromelysin-1                      | 46  | EC3.4.24.17       | 11q23         | Collagens (III,IV,V, and IX); gelatin; aggrecan; perlecan; decorin; laminin; elastin; casein; osteonectin; ovostatin; antactin; plasminogen; MBP; IL-1 $\beta$ ; MMP-2/TIMP-2; MMP-7; MMP-8; MMP-9; MMP-13 |
|         | Proteoglykanase                    |     |                   |               |  |
| MMP-7   | Matrilysin                         | 20  | EC3.4.24.23       | 11q21-q22     | Collagens (IV and X); gelatin; aggrecan; decorin; fibronectin; laminin; entactin; elastin; casein; transferrin; plasminogen; MBP; $\beta$ 4-integrin; MMP-1; MMP-2; MMP-9; MMP-9/TIMP-1                    |
| MMP-8   | Neutrophil collagenase             | 58  | EC3.4.24.34       | 11q21-q22     | Collagens (I,II,III,V,VII,VIII and X); gelatin; aggrecan; fibronectin  |
| MMP-9   | Gelatinase B                       | 92  | EC3.4.24.35       | 20q11.2-q13.1 | Collagens (IV,V,VII,X and XIV); gelatin; entactin; aggrecan; elastin; fibronectin; osteonectin; plasminogen; MBP; IL-1b  |
| MMP-10  | Stromelysin-2                      | 46  | EC3.4.2.22        | 11q22.3-q23   | Collagens ( III-V); gelatin; casein; aggrecan; elastin; MMP-1; MMP-8   |
| MMP-11  | Stromelysin-3                      | 44  | no match          | 22q11.2       | Unknown (the most likely casein)   |
| MMP-12  | Macrophage metalloelastase         | 45  | EC3.4.24.65       | 11q22.2-q22.3 | Collagen IV; gelatin; elastin; casein; fibronectin; vitronectin; laminin; entactin; MBP; fibrinogen; fibrin; plasminogen   |
| MMP-13  | Collagenase-3                      | 55  | no match          | 11q22.3       | Collagens (I,II,III,IV,IX,X and XIV); gelatin; plasminogen; aggrecan; perlecan; fibronectin; osteonectin; MMP-9  |
| MMP-14  | MT1-MMP                            | 54  | no match          | 14q11-q12     | Collagens (I-III); gelatin; casein; fibronectin; laminin; vitronectin; entactin; proteoglycans; MMP-2; MMP-13  |
| MMP-15  | MT2-MMP                            | 61  | no match          | 16q12.2-q21   | Fibronectin; entactin; laminin; perlecan; MMP-2  |
| MMP-16  | MT3-MMP                            | 55  | no match          | 8q21          | Collagen III; gelatin; casein; fibronectin; MMP-2  |
| MMP-17  | MT4-MMP                            | 54  | no match          | 12q24         | Unknown  |
| MMP-18  | Collagenase-4                      |     | no match          | unknown       | Collagens (I,II,III,VIII a X); gelatin; aggrecan   |
| MMP-19  | RASI-1                             |     | no match          | 12q14         | Gelatin; aggrecan; fibronectin   |
| MMP-20  | Enamelysin                         |     | no match          | unknown       | Amelogreinein; aggrecan  |
| MMP-21* |                                    |     | no match          | 1p36.3        | Unknown  |
| MMP-22* |                                    |     | no match          | 1p36.3        | Unknown  |
| MMP-23* |                                    |     | no match          | unknown       | Unknown  |
| MMP-24  | MT5-MMP                            |     | no match          | 20q11.2       | Unknown  |
| MMP-25  | Leukolysin/MT6-MMP                 |     | no match          | 16p/3.3       | Pro-gelatinase A; fibrin; fibronectin; collagen IV; gelatin  |
| MMP-26  | Endometase, matrilysin-2           |     | no match          | unknown       | Gelatin I $\alpha$ ; P1; fibrinogen; fibronectin; vitronectin  |
| MMP-28  | Epilysin                           |     | no match          | 17q11.2       | Casein   |

\*... MMP genes were found on chromosomes, but their function and structure have not been identified yet.

### 1.I.B Structure of MMPs

Since the publication of the crystal structure of the catalytic domain of human collagenase in 1994,<sup>35</sup> numerous X-ray crystallography structures and NMR solution structures have followed to unravel the architecture of these multi-domain proteases. The general MMP structure includes a signal peptide domain, a propeptide domain, a catalytic domain, the hinge region or linker peptide, and a C-terminal hemopexin-like domain (Figure 1-3). The membrane domain serves to anchor trans-membrane MMPs to cellular membranes.<sup>40</sup>

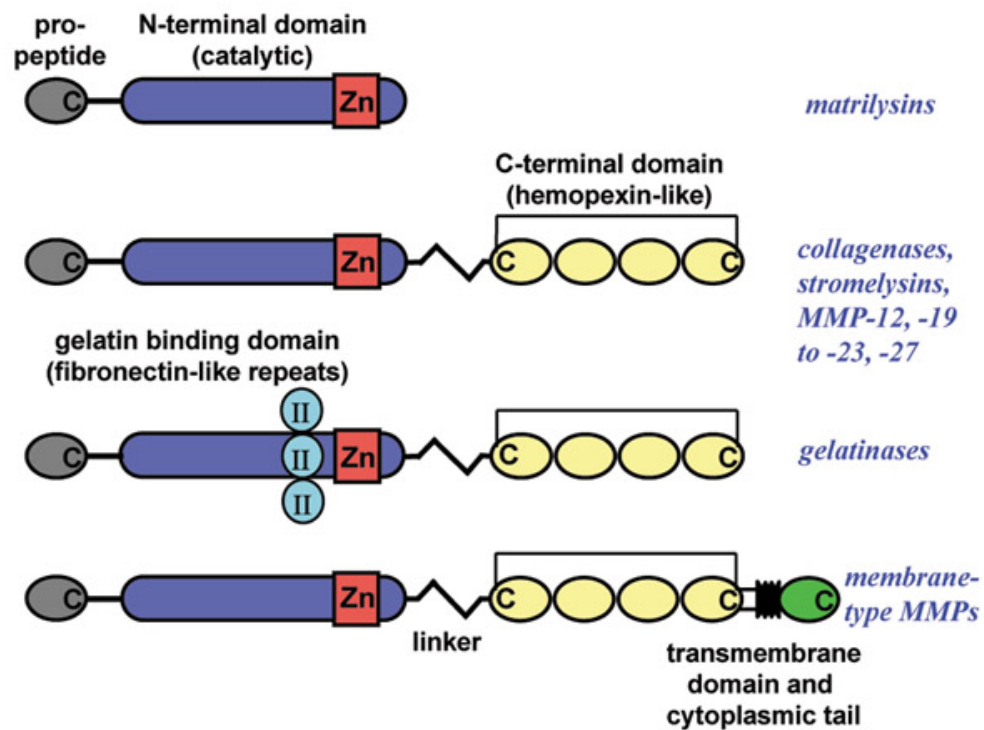


**Figure 1-3.** Basic domain structures of MMPs. MMPs consist of: a propeptide (grey); a catalytic domain (blue) with the active site and the catalytic zinc ( $Zn^{2+}$ ) (red); and, with the exception of the matrilysins, a COOH-terminal domain (C) (yellow) with homology to the serum protein hemopexin. The latter two domains are connected by a linker peptide. Gelatinases have an insert of three fibronectin type II repeats (turquoise) in the catalytic domain. Membrane-type MMPs contain a transmembrane domain (black) and a cytoplasmic tail (green) at the COOH terminus, which anchors these enzymes in the cell membrane.<sup>36</sup>

The propeptide domain consists of three  $\alpha$ -chains and connecting loops, and contains a “cysteine switch” PRCGXPD consensus sequence.<sup>37,38</sup> The sulfhydryl group of the conserved cysteine residue in this sequence coordinates to the catalytic  $\text{Zn}^{2+}$  to maintain enzyme latency. Thus, the MMP activity is suppressed as a result of the sulfhydryl coordinated pro-peptide to the enzyme active site. Upon activation of pro-MMPs, the Cys- $\text{Zn}^{2+}$  interaction is disrupted (vide infra), which exposes the active site, and enables  $\text{Zn}^{2+}$  to bind to  $\text{H}_2\text{O}$  for peptide hydrolysis as shown in Figure 1-4. Figure 1-4 shows the mechanism of MMP catalysis. The Glu residue (present in the second coordination sphere of the catalytic  $\text{Zn}^{2+}$ ) of the conserved HEXGHXXGXXH MMP sequence acts as a general base to activate the zinc-bound water for catalysis.

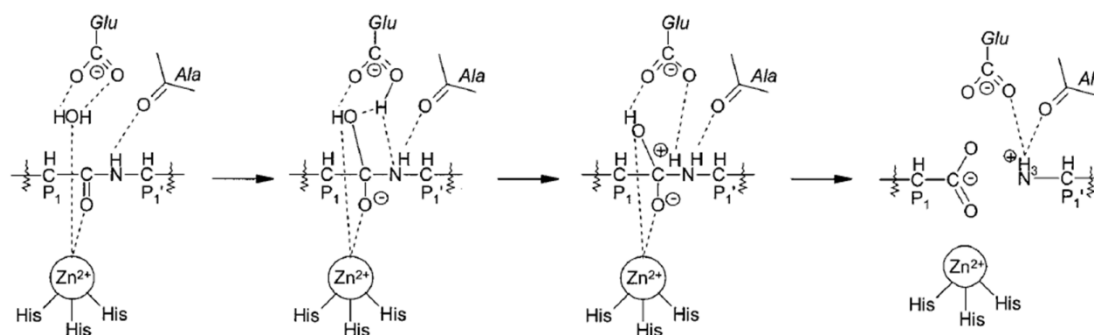


**Figure 1-4.** Reaction mechanism for proteolysis by MMPs.<sup>18</sup>

The catalytic domain consists of a five-stranded  $\beta$  sheet and three  $\alpha$ -helices to form an overall spherical topology that is conserved among MMP family members (Figure 1-5). This domain also has two  $\text{Zn}^{2+}$  ions and three  $\text{Ca}^{2+}$  ions. One of the  $\text{Zn}^{2+}$  ions is catalytic and one is structural. The structural  $\text{Zn}^{2+}$  is tetrahedrally coordinated by three His residues and one Asp residue. The catalytic  $\text{Zn}^{2+}$  is coordinated in a tetrahedral geometry by three histidine residues of the conserved HEXGHXXGXXH sequence found in all MMPs. The catalytic  $\text{Zn}^{2+}$  is flanked by loosely defined

specificity pockets labeled “primed” subsite pockets - S1', S2' and S3' to one side of the Zn<sup>2+</sup> and unprimed subsite pockets – S1, S2 and S3, to the other side of the Zn<sup>2+</sup> ion.<sup>27</sup> The labeling of the pockets is based on the Schechter-Berger nomenclature of the scissile peptide bond of the protein substrate accommodated in the active site of proteases.<sup>39</sup>

A surface representation of MMP-3 catalytic domain displaying the pockets, and a linearized cartoon schematic of the active site is shown in Figure 1-6. As seen in Figure 1-6, the substrate binding groove narrows into a well-defined pocket and variations in the residues that form this pocket can distinguish one MMP from another. The most variable pocket is that formed by the loop that defines the S<sub>1</sub>' pocket. This pocket not only varies in the makeup of amino acids, but also in the depth of the pocket. MMPs can be very broadly classified based on the depth of their S<sub>1</sub>' pockets into shallow, medium, and deep pocket MMPs.<sup>27,29</sup> The variable depth of this pocket allows for the accommodation of large inhibitor backbones that do not fit in shallow S<sub>1</sub>' pocket MMPs. The specificity of MMPs for different substrates is not only dependent on the catalytic domain and the specificity pockets but also on the C-terminal hemopexin-like domain and additionally for gelatinases (MMP-2,-9) on the fibronectin domain.

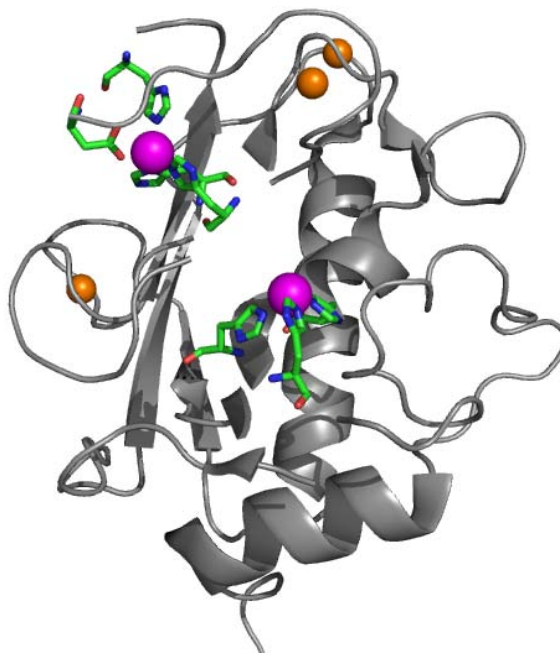


**Figure 1-5.** Ribbon representation of the catalytic domain of MMP-3 showing the spherical topology consisting of five  $\beta$ -sheets and three  $\alpha$ -helices. Coordinating residues of structural site (upper left) and catalytic site (center) are shown as sticks in color code.  $\text{Zn}^{2+}$  ions are shown as magenta spheres and  $\text{Ca}^{2+}$  ions are shown as orange spheres. (carbon = green, nitrogen = blue, oxygen = red). PDB: 1CQR.<sup>6</sup>

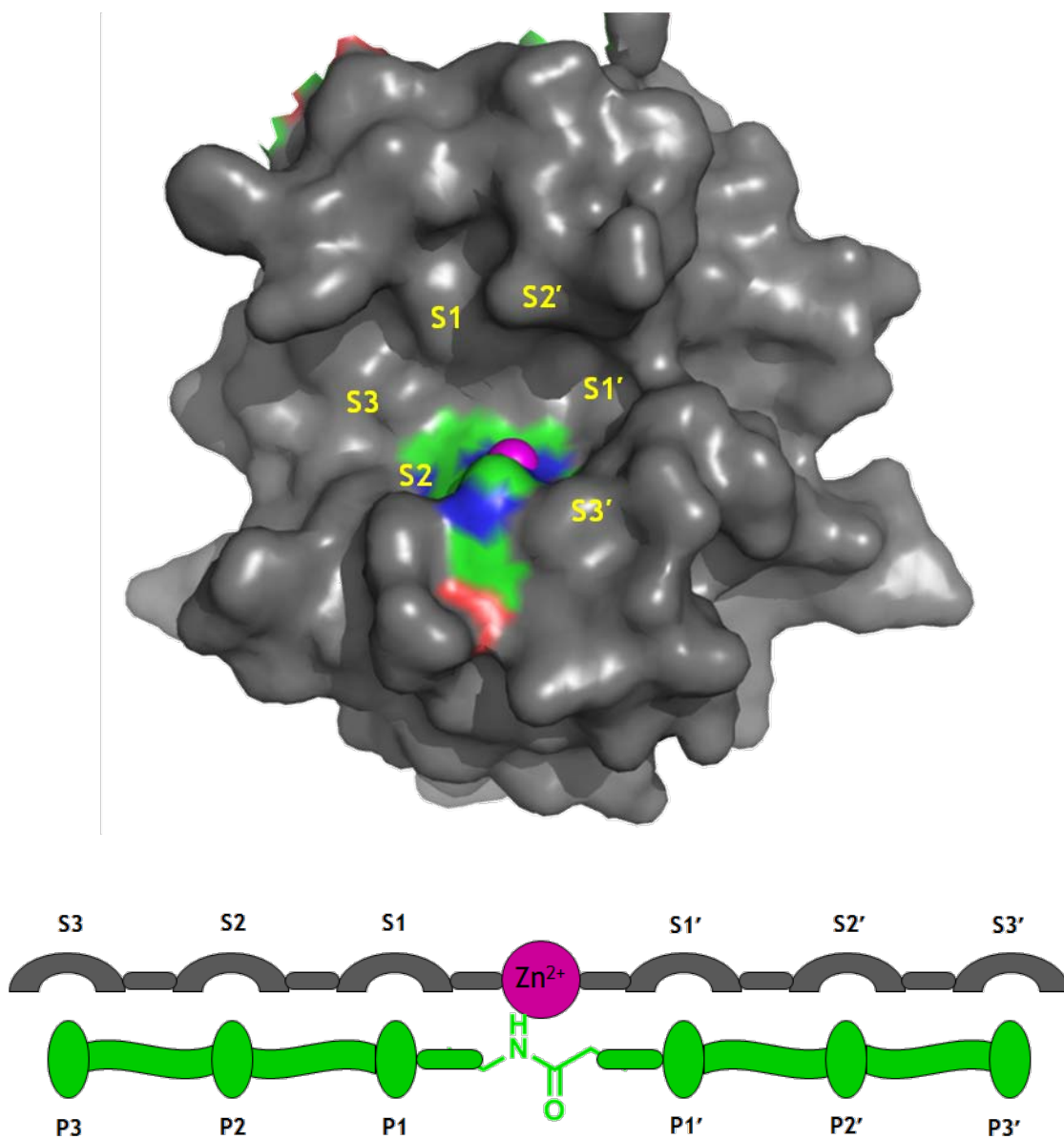


**Figure 1-6.** Surface representation of the catalytic domain of MMP-3 shown in Figure 1-4, highlighting the positions of the subsite pockets – S3', S2', S1', S1, S2, S3.  $Zn^{2+}$  ion is shown as a magenta sphere. PDB: 1CQR.<sup>6</sup> Shown below is a linearized cartoon schematic of the active site of MMPs with a generalized peptide substrate depicted in green. The scissile peptide bond is shown in sticks.

### 1.I.C Regulation of MMPs and Endogenous Inhibitors

MMPs are primarily responsible for the turnover and degradation of the extracellular matrix. However, MMPs also act on a variety of non-matrix proteins including antimicrobial peptides, cytokines, chemokines and receptors.<sup>41</sup> In order to maintain normal expression levels, MMPs are regulated at four points – gene expression, compartmentalization (*i.e.* pericellular accumulation of enzyme), proenzyme activation, and enzyme inactivation. MMP zymogens or pro-MMPs are activated *in vivo* by proteases such as trypsin, kallikrein, and other MMPs. MMPs can be activated *in vitro* by chemical agents such as aminophenyl mercuric acetate (or other heavy metal containing reagents), sulfur-reactive agents, reactive oxygen species (ROS), and even detergents such as SDS. The common underlying mechanism for activation of these zymogens involves the dissociation of the cysteine atom from the catalytic Zn<sup>2+</sup> and its replacement by water, followed by proteolytic removal of the propeptide.<sup>41</sup>

The *in vivo* proteolytic activity of MMPs is regulated by four endogenous inhibitors called tissue inhibitors of metalloproteinases TIMPs (TIMP-1, -2, -3, -4) and also by  $\alpha$ 2-macroglobulin. Wedge shaped TIMPs fit into the catalytic cleft of MMPs and use their N-terminal cysteine residue to coordinate to the MMP active site Zn<sup>2+</sup> ion. Unlike the monodentate coordination of the cysteine thiol in prodomain inhibition (Figure 1-7a), in the TIMP-MMP complex, the cysteine residue binds to the Zn<sup>2+</sup> in a bidentate fashion through the cysteine backbone amino and carbonyl groups (Figure 1-7b). The disruption of this delicate balance between proMMPs and/or MMP-TIMPs

can lead to various pathologies discussed earlier prompting the need for synthetic MMPi.

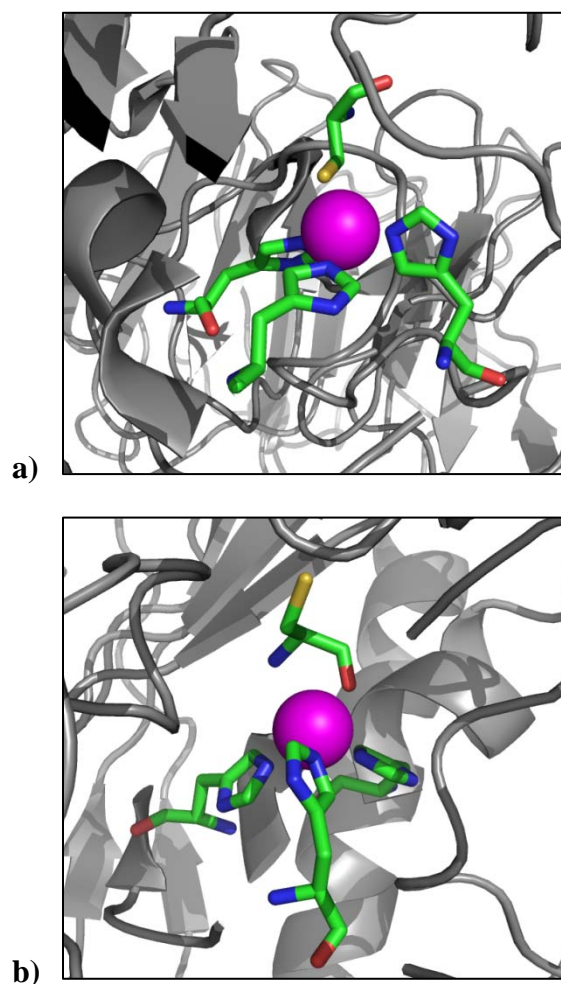


**Figure 1-7.** Endogenous MMP inhibition. a) In the ribbon representation of pro-MMP-2, the catalytic Zn<sup>2+</sup> is inactivated via coordination of the “cysteine switch” thiol/sulfhydryl group. Coordinating His residues and pro-domain Cys are shown as color-coded sticks in a tetrahedral coordination environment around the Zn<sup>2+</sup>. PDB:1GXD.<sup>42</sup> b) In TIMP-2 inhibition of MT1-MMP, the catalytic Zn<sup>2+</sup> is coordinated in a bidentate fashion by the backbone of the N-terminal Cys residue to form a five-coordinate highly distorted square-pyramidal geometry with the protein active site. PDB: 1BUV.<sup>43</sup> (carbon = green, nitrogen = blue, oxygen = blue, sulfur = yellow; Zn<sup>2+</sup> ions are shown as magenta spheres).



### 1.I.D Synthetic Inhibitors of MMPs

Inhibition of MMPs has been widely sought as an intervention to many disease states. Despite more than twenty-five years of MMPi development, there is only one FDA approved drug – Periostat, a tetracycline used for periodontal disease (Figure 1-8).<sup>44</sup> Several reviews have outlined the development and low success rate of various MMPi over the past two decades, which generally stems from non-specific targeting of other proteases, low bioavailability, and the onset of musculoskeletal syndrome (MSS). MSS manifests itself as musculoskeletal pain and inflammation and was commonly observed in clinical trials of several first-generation MMPi.

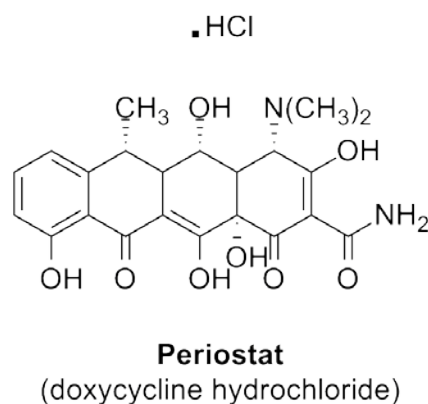
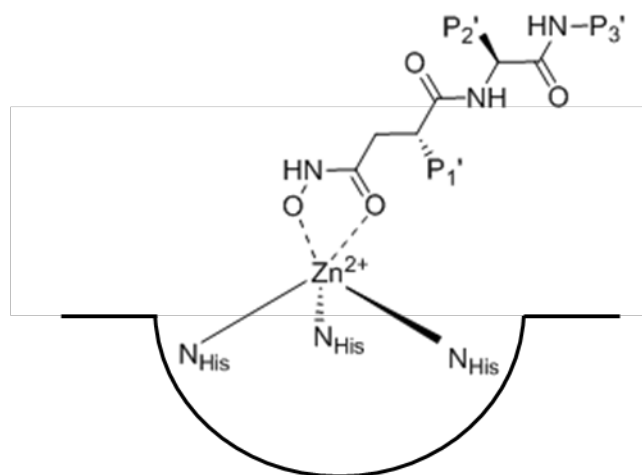


**Figure 1-8.** The FDA approved MMPi Periostat.

First-generation MMPi generally combined a hydroxamate ZBG attached to a peptide backbone derived from the cleavage sites of MMP substrates (Figure 1-9). These early MMPi were generally broad-based and were therefore not specific against any one or group of MMPs. Batimastat and Marimastat (Figure 1-10) are two of the

first peptidic hydroxamate MMPi reported to enter clinical trials; only to be later withdrawn due to the adverse side effects.



MMP active site

**Figure 1-9.** Generalized representation of first generation hydroxamate based MMPi in the MMP active site. The ZBG binds to the Zn<sup>2+</sup> in a bidentate fashion. The 'P' substituents represent substrate-mimic backbone substituents that interact with the primed subsites in the MMP active site.

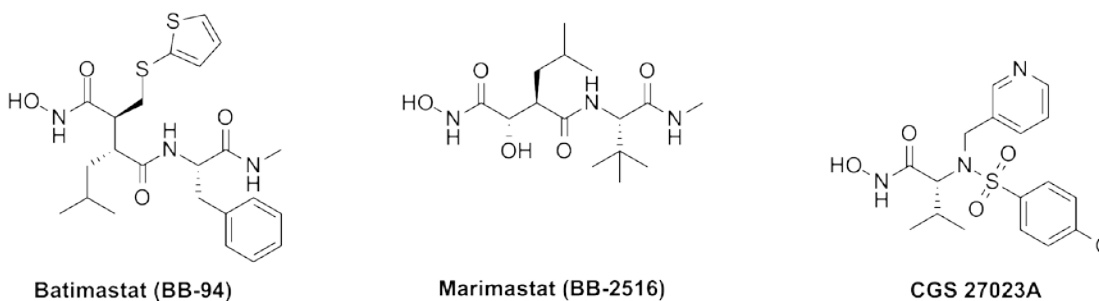
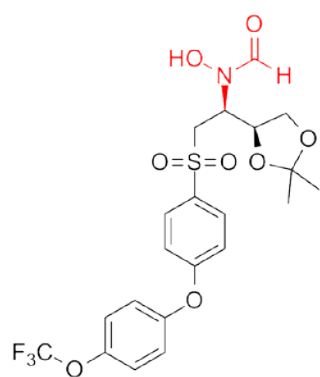


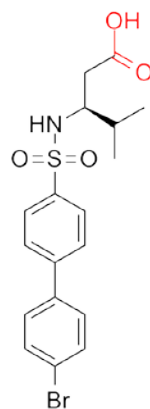
**Figure 1-10.** First and second generation hydroxamate-based MMPi.

The second generation of MMP inhibitors emerged from structure based drug design. After the emergence of crystal structures with the first generation MMPi and their clinical failure, second generation MMPi were designed with alternative backbones. These MMPi contained non-peptidic backbones to avoid the broad

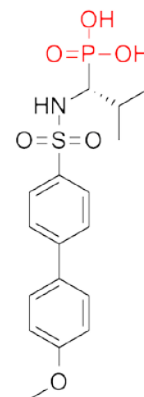
spectrum inhibition witnessed with MMP substrate mimetic backbones. CGS 27023 (Figure 1-10), containing a hydroxamic acid ZBG was the first non-peptidic MMPi to enter clinical trials. Despite good in vitro activity, none of the first- and second-generation hydroxamate MMPi successfully completed clinical trials. Hydroxamic acids are highly unstable as they have been shown to readily hydrolyze in vivo to the corresponding carboxylic acid, resulting in poor pharmacokinetics. As a result, other second-generation inhibitors were developed with novel ZBGs, some of which are shown in Figure 1-11.



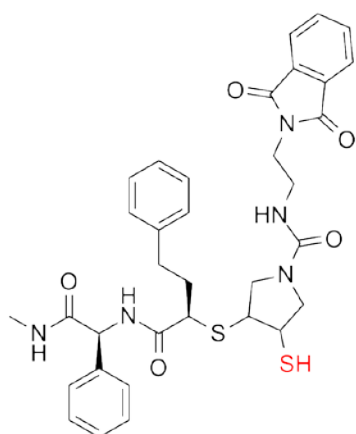
Retrohydroxamate  
**ABT-518**



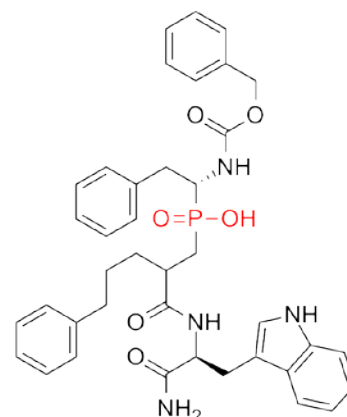
Carboxylic acid  
**PD 166793**



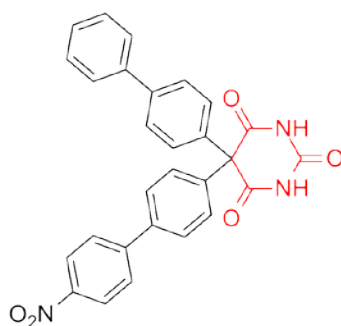
Phosphonate acid



Thiolate  
**YHJ-223**



Phosphinate acid  
**RXP-03**



Pyrimidinetrione  
**Ro 28-2653**

**Figure 1-11.** Examples of second-generation MMPi with alternative ZBGs (highlighted in red).

Our lab has been actively investigating alternative ZBGs towards metalloprotein inhibition to be developed into full-length potent and selective MMPi. A recent review highlights the various ZBGs that have been explored in MMPi.<sup>45</sup> Figure 1-12 displays a comprehensive list of ZBGs used in various MMPi. A large number of these ZBGs (18 out of 34) were developed in the Cohen group. These include ZBGs **10-16** and ZBGs **20-30** which capture various bidentate donor atom sets including (O,O), (O,N), (N,N), (O,S), tris-chelate donor atoms such as (O,N,O) and (N,N,N), and also four donor ligand sets such as (N,N,N,N). A compilation of the activity of several ZBGs is listed in Table 1-3. Even though some of the potent ZBGs do not show selectivity for one MMP isoform over another, development of these ZBGs into full-length inhibitors has led to several isoform-specific MMPi. The hydroxypyronone **ZBG24** was the first ZBG from the lab developed into a highly selective MMP-3 inhibitor.<sup>46</sup>

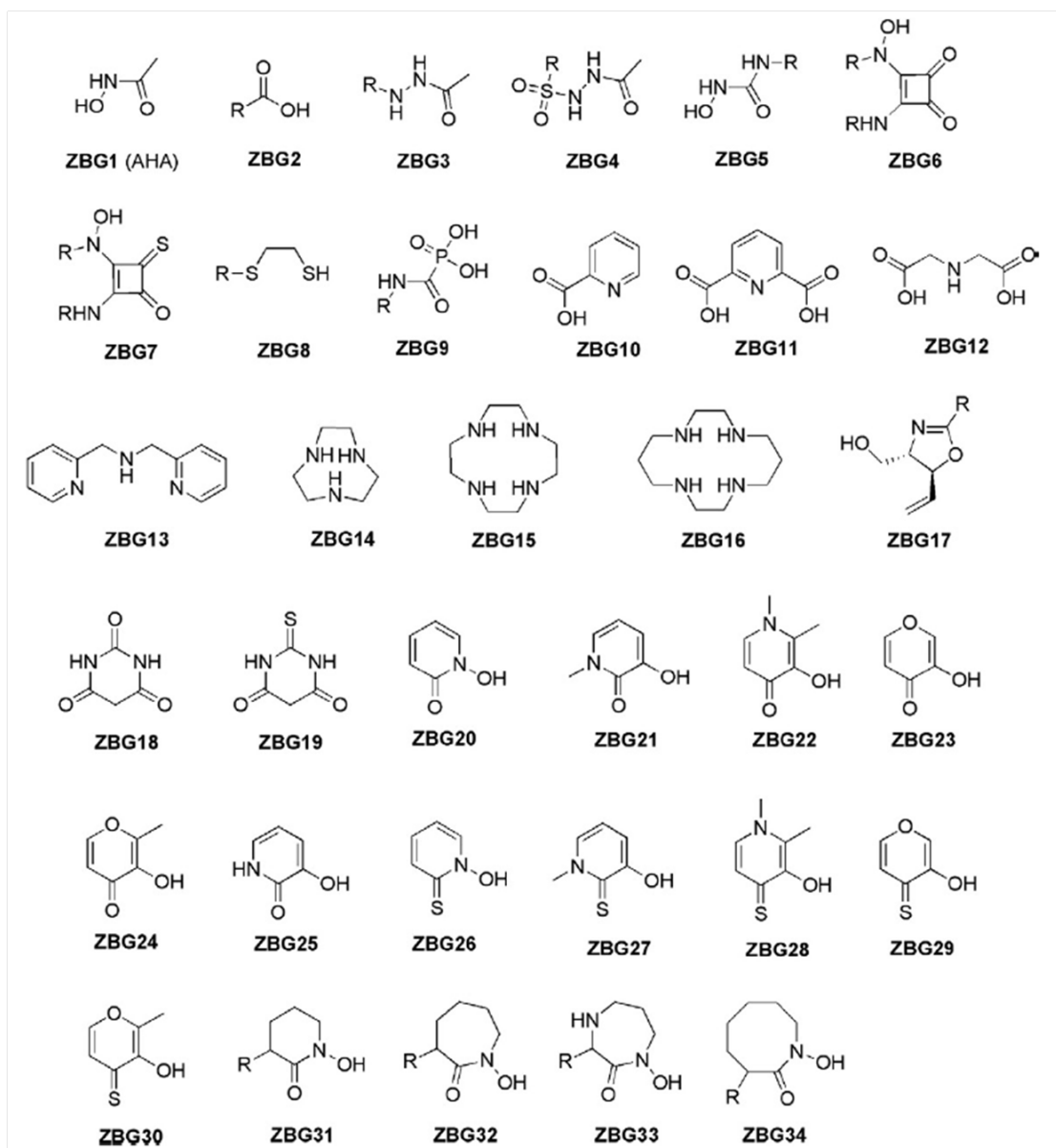


**Figure 1-12.** The structures of various ZBGs used in different MMPi.<sup>45</sup>

**Table 1-3.** A list of IC<sub>50</sub> values (μM) for ZBGs against MP-1,-2,-3 and LF, from Figure 1-12. N.D. = Not determined due to fluorescence or solubility issues.<sup>47-49</sup>

| <b>ZBG</b> | <b>MMP-1</b> | <b>MMP-2</b>   | <b>MMP-3</b>  | <b>LF</b>     |
|------------|--------------|----------------|---------------|---------------|
| AHA        | 41600 (±400) | 15000 (±3,000) | 25100 (±4000) | 11400 (±1000) |
| 10         | N.D.         | N.D.           | 181 (±10)     | 3500 (±300)   |
| 11         | N.D.         | N.D.           | 1350 (±160)   | 1275 (±7)     |
| 12         | N.D.         | N.D.           | 6100 (±200)   | 2690 (±80)    |
| 13         | N.D.         | N.D.           | 154 (±13)     | 5700 (±700)   |
| 14         | N.D.         | N.D.           | 136 (±9)      | 370 (±40)     |
| 15         | N.D.         | N.D.           | 180 (±30)     | 930 (±30)     |
| 16         | N.D.         | N.D.           | 1330 (±140)   | 2920 (±80)    |
| 20         | 5960 (±40)   | 5600 (±100)    | 1600 (±100)   | 6570 (±160)   |
| 21         | 4200 (±300)  | 2600 (±400)    | 5100 (±200)   | 32000 (±3000) |
| 22         | N.D.         | N.D.           | N.D.          | N.D.          |
| 23         | N.D.         | N.D.           | 7200 (±1200)  | 27000 (±3000) |
| 24         | 4200 (±300)  | 2600 (±100)    | 5700 (±100)   | N.D.          |
| 25         | N.D.         | N.D.           | 5700 (±200)   | 6100 (±500)   |
| 26         | 490 (±10)    | 100 (±40)      | 35 (±3)       | 3900 (±200)   |
| 27         | 680 (±20)    | 380 (±10)      | 362 (±3)      | 690 (±70)     |
| 28         | 150 (±10)    | 60 (±10)       | 140 (±200)    | 1,460 (±60)   |
| 29         | N.D.         | 76 (±1)        | 120 (±40)     | 204 (±16)     |
| 30         | 400 (±10)    | 140 (±10)      | 210 (±20)     | 260 (±30)     |

### 1.II.A Anthrax Lethal Factor

Anthrax is one of the oldest documented diseases on record known to infect animals, and to this day poses a serious threat to both animals and humans.<sup>50</sup> Anthrax is caused by the Gram-positive, rod-shaped bacterium *Bacillus anthracis* that is notorious for its ability to form endospores. The bacteria adopt a dormant spore structure when threatened by external factors and can survive for decades in this state before entering a host. *B. anthracis* spores are mostly soil-borne and their dormant longevity in the soil significantly contributes to their lethality. Anthrax spores are hence amongst the most worrisome biological weapons used, with recent attacks in the US in 2001 sparking significant concern.<sup>51-53</sup>

Anthrax infection can occur via three routes: inhalational, gastrointestinal, and subcutaneous, with inhalational being the most fatal. When *B. anthracis* spores are inhaled they bind to alveolar macrophages, which phagocytose the spores and traffic them to regional lymph nodes. En route the spores germinate to pathogenic bacteria that release a potent anthrax toxin.<sup>54</sup> Anthrax toxin is composed of three proteins: protective antigen (PA, 83 kDa), edema factor (EF, 89 kDa) and lethal factor (LF, 90 kDa). Independently the proteins are non-toxic, but in concert can induce cell death. PA first binds to one of two ubiquitous receptors, ANTXR1 (tumor endothelium marker 8) or ANTXR2 (capillary morphogenesis protein 2).<sup>55,56</sup> Once bound, PA is activated by the cleavage of a 20 kDa N-terminal fragment by membrane bound furin-like proteases (Figure 1-13). Upon activation, the 63 kDa PA oligomerizes to form a heptameric pre-pore to which three molecules of LF and/or EF can bind.<sup>57</sup> The complex then undergoes receptor mediated endocytosis and the low pH in the



endosome triggers a conformational change that converts the pre-pore to a mature cation-specific pore. LF and EF are translocated across the mature pore to the cytosol of the cell where they exert their toxicity.<sup>58-63</sup> EF is a calcium and calmodulin dependent adenylate cyclase that causes elevated levels of cAMP in the cytosol of infected cells and also plays a role in impairment of the immune system. Together with PA, EF forms the Edema Toxin (ETx).<sup>12,64</sup>

LF is a zinc-dependent hydrolytic metalloenzyme that cleaves the N-terminus of mitogen activated protein kinase kinases (MAPKKs) to disrupt downstream signaling pathways and cause macrophage apoptosis. In combination with PA, LF forms the lethal toxin (LeTx).<sup>12,65-67</sup> There are several published reviews describing the pathogenesis of anthrax via its toxins and despite extensive research in the field, the exact pathway via which LF imparts toxicity is still somewhat unclear; nevertheless, this protein is an important target for inhibition.<sup>67-70</sup> Inactivation of the LF gene in *B. anthracis* leads to a 1000-fold reduction in its virulence, which suggests that anthrax pathology is largely dictated by LF.<sup>70</sup> However, current therapies against *B. anthracis* include FDA approved antibiotics such as ciproflaxin that target the bacteria but are ineffective towards the toxins secreted by the bacterium including LF.

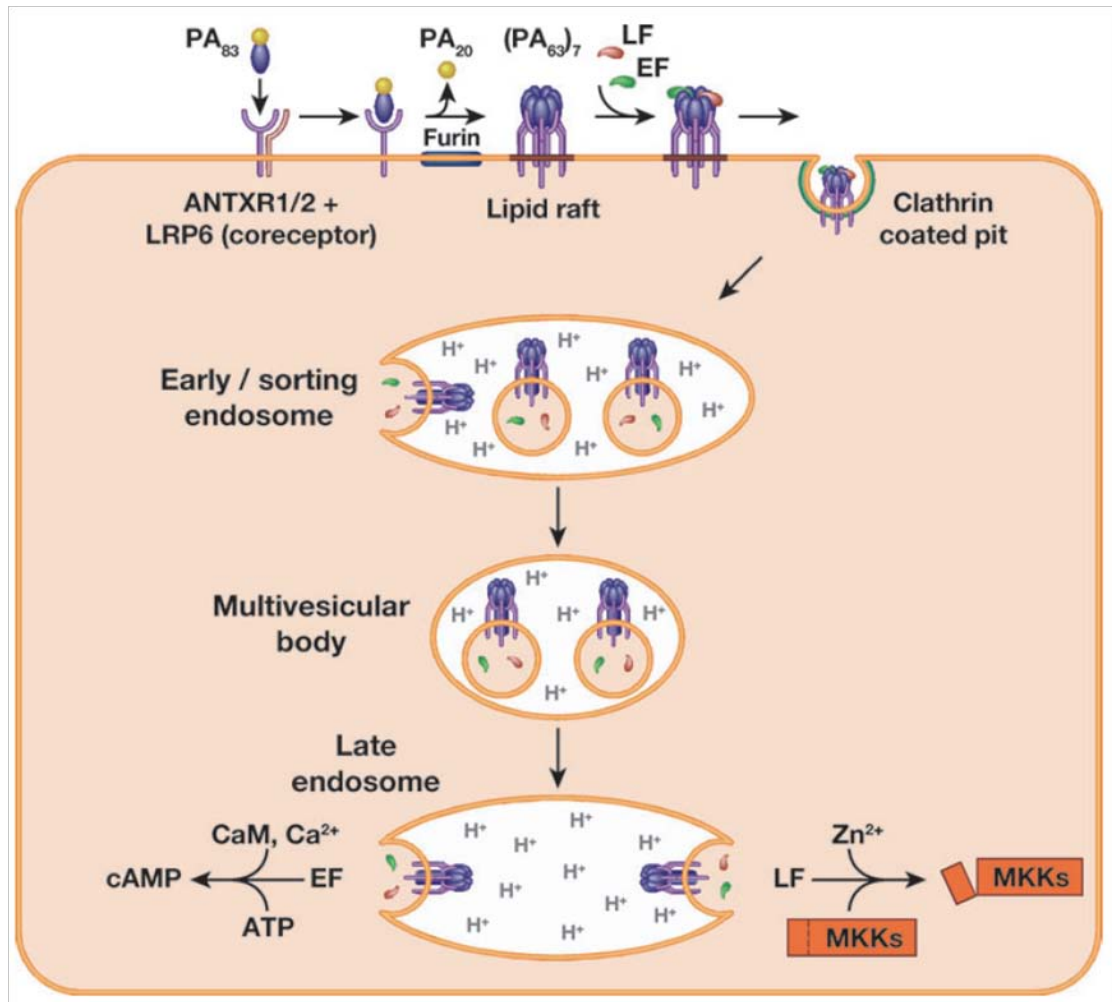


**Figure 1-13.** Pathogenesis of anthrax toxin.<sup>57</sup>

### 1.II.B Structure of Anthrax Lethal Factor

Anthrax lethal factor is a 90 kDa protein composed of four domains: a protective antigen binding domain, a VIP2-like domain, a helix bundle domain and a catalytic domain (Figure 1-14). The details and significance of each domain is listed below.

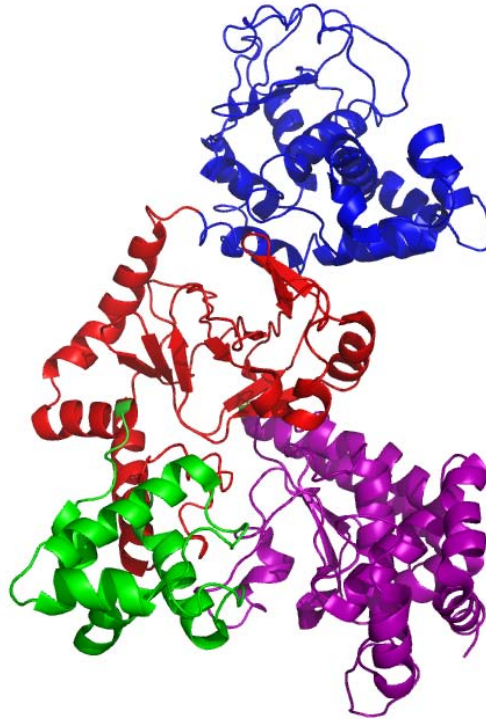


**Figure 1-14.** Ribbon representation of LF color coded by domain: I, PA binding domain (blue); II, VIP2-like domain (red); III, helix bundle domain (green); IV, catalytic domain (purple). PDB:1JKY.<sup>71</sup>

- I. The PA binding domain (residues 1-262) consists of a 12-helix bundle and four beta sheets; and as the name suggests is involved in binding of LF to the heptameric pore of PA. Specifically, the acidic residues Glu135 and Asp182 of this LF domain form electrostatic interactions with Lys197 on adjacent subunits of oligomeric PA.<sup>72</sup>

- II. The VIP2 like domain (residues 263-297 and 385-550) resembles the ADP-ribosylating toxin VIP2 from *Bacillus cereus* and is composed of five alpha helices and eight beta sheets. This domain is involved in substrate recognition.
- III. Helix bundle domain (residues 303-382) is a small four  $\alpha$ -helical bundle with a hydrophobic core that is inserted at a turn between the second and third helices of domain II. This domain is important for LF activity because mutations in this domain abrogate LF activity. It shares a hydrophobic surface with the catalytic domain; and contributes to substrate specificity by restricting access to the active site.

Catalytic domain (residues 552-776) consists of a nine helix bundle packed against a four-stranded  $\beta$  sheet and contains the active site catalytic  $Zn^{2+}$  ion. The active site contains the HExxH motif which contains the catalytic  $Zn^{2+}$  coordinated in a tetrahedral geometry by the two histidine residues - His686 and His690, one distal glutamate residue Glu735 (Figure 1-15) and a water molecule/hydroxide ion, which is the nucleophile acting on the scissile peptide bond. The HExxH motif is a characteristic zinc binding motif found in other zinc metalloenzymes such as thermolysin. The glutamate of HExxH Glu687 is present in the second coordination sphere and is positioned to act as a general base to activate the zinc-bound water for catalysis. Additionally, a tyrosine residue Tyr728 is also present in the second shell to stabilize the negative charge on the scissile bond carbonyl oxygen in the transition state, through its OH moiety.<sup>73</sup> The presence of a catalytic metal ion ( $Zn^{2+}$ ) in the LF

active site is exploited toward the design and synthesis of LF small molecule inhibitors as discussed below.

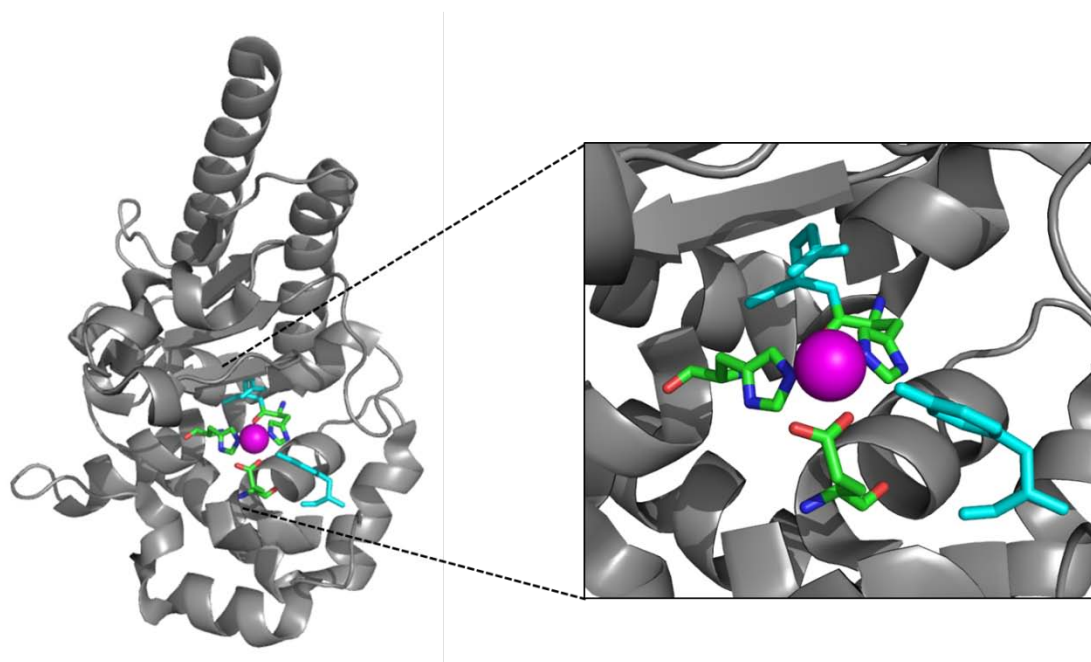


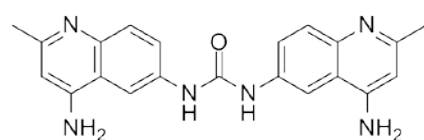
**Figure 1-15.** Ribbon representation of LF catalytic domain. His686, His690 and Glu735 shown as sticks (carbon = green, nitrogen = blue, oxygen = blue). The Zn<sup>2+</sup> ion is shown as a magenta sphere. On the right is a zoomed in picture of the active site also showing second sphere coordination residues Glu687 and Tyr728 as sticks in cyan. PDB: 1YQY.<sup>8</sup>

### 1.II.C Anthrax lethal factor inhibitors

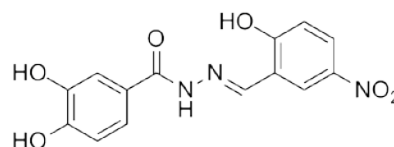
The limited success of antibiotic therapy for anthrax infection has motivated investigation into synthetic inhibitors against the bacteria's secreted toxin. The zinc-dependent metalloprotease, LF has emerged as an important drug target in the past few years for synthetic small molecule inhibitors. Several groups have been successful in developing potent LF inhibitors (LFI), some of which include known MMPi.<sup>74,75</sup> To date, some of the most potent LFI carry a chelating hydroxamic acid ZBG similar to other zinc metalloprotease inhibitors.

Some of the first generation compounds designed against LF used the traditional metalloprotease inhibitor approach. This involved the biomolecular assay screening of various substrate like peptidic backbones linked to a traditional hydroxamic acid ZBG.<sup>76</sup> Even though the peptidic hydroxamate based LFI generated potent compounds *in vitro*, both in cell-free and cell-based assays, LFI were later pursued by alternative approaches. In 2004, Panchal, *et. al.* identified inhibitors of LF in the 0.5-5  $\mu\text{M}$   $K_i$  range from the screening of a National Cancer Institute (NCI) repository. The lead compounds however did not possess any ZBG and the most potent compound identified was NSC 12155 (Figure 1-16). A co-crystal of NSC 12155 with LF was also obtained in which the inhibitor was shown to sit laterally above the metal ion in the active site, and interact with the  $\text{Zn}^{2+}$  via its urea moiety (Figure 1-17a).<sup>77</sup> The Mrksich's group at the University of Chicago utilized matrix-assisted laser-desorption ionization (MALDI) time of flight (TOF) mass spectrometry to evaluate large libraries of low molecular weight compounds for activity against LF.

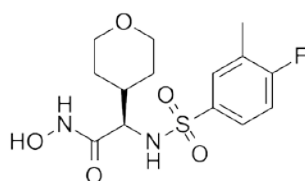
The screening generated LF inhibitors containing polyhydroxylated groups such as Mrksich LFi with potencies in the 100 nM – 4.3  $\mu$ M range (Figure 1-16).<sup>78</sup>



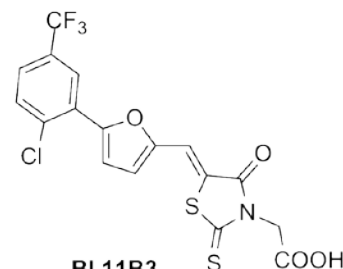
**NSC 12155**  
 $IC_{50} = 0.5 \mu M$



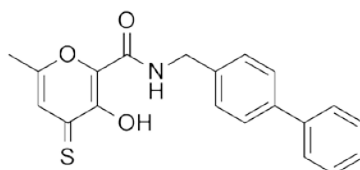
**Mrksich LFi**  
 $IC_{50} = 1.1 \mu M$



**Merck LFi**  
 $IC_{50} = 60 \text{ nM}$



**BI 11B3**  
 $IC_{50} = 60 \text{ nM}$



**AM-2S**  
 $IC_{50} = 13.9 \mu M$

**Figure 1-16.** Some previously described LFi with their  $IC_{50}$  values.

One of the most potent LF inhibitors generated to date came from a group at Merck who screened their in house sample collection of compounds to identify several weak hydroxamate leads. These hydroxamates were further guided by medicinal chemistry efforts to identify (2*R*)-2-[(4-fluoro-3-methylphenyl)sulfonylamino]-*N*-hydroxy-2-(tetrahydro-2*H*-pyran-4-yl)acetamide as a potent LFi with an  $IC_{50}$  value of 60 nM (Figure 1-16). This LFi was also co-crystallized within the LF active site and as

expected shows chelation of the  $Zn^{2+}$  ion via its hydroxamic acid ZBG (1-17b). The potency imparted by  $Zn^{2+}$  chelation is not only observed in vitro in both cell-free and macrophage based cell assays, but also showed extremely promising results in vivo. The LFi showed 100% protection in a lethal mouse model that was injected with recombinant LF and PA, up to 50% survival by mice challenged with a lethal dose of *B. anthracis* spores and up to 100% protection when administered with ciproflaxin in *B. anthracis* spore challenged mice.<sup>8</sup>

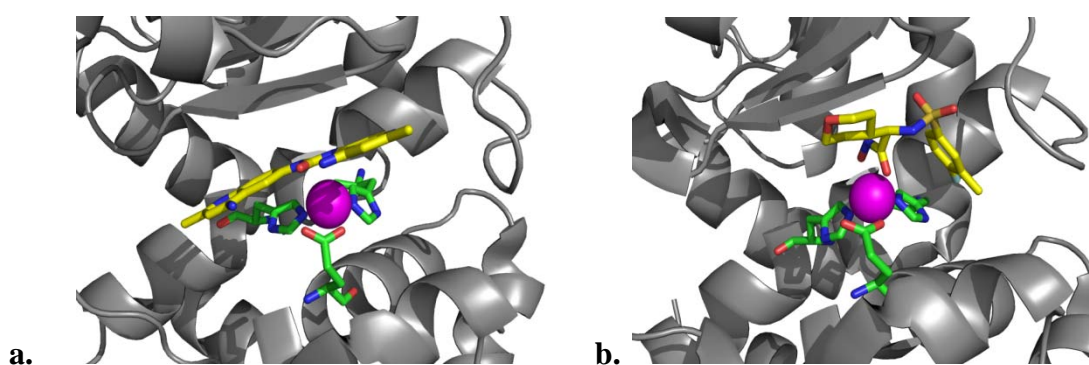


**Figure 1-17.** Ribbon representation of LF catalytic site in the presence of LFi, with coordinating residues His686, His690, Glu735 shown as sticks (carbon = green, nitrogen = blue, oxygen = red). **a.** NSC 12155 in sticks (carbon = yellow, nitrogen = blue, oxygen = red) bound within the active site. PDB: 1PWP.<sup>77</sup> **b.** Merck LFi in sticks (carbon = yellow, nitrogen = blue, oxygen = red) bound within the active site. PDB: 1YQY.<sup>8</sup>

Fragment based-lead design (FBLD) has also been used to develop novel LFi. FBLD which is the focus of Chapter 4, utilizes libraries consisting of modest collections (100-1000 compounds) of small molecular fragments (MW < 300 amu). Screening for protein binding using low molecular mass molecules is the essence of the fragment approach.<sup>79</sup> Even though Fesik and co-workers introduced the concept of fragment screening to metalloproteins,<sup>80</sup> Pellecchia and co-workers have pioneered the field of FBLD toward identifying fragment leads against anthrax lethal factor.<sup>81</sup>



Several potent LFi were developed as a result of this approach, including **BI 11B3** (Figure 1-16). As opposed to the commonly used hydroxamic acid chelating ZBG, **BI 11B3** is shown to coordinate the  $Zn^{2+}$  catalytic ion via a monodentate coordination through the thiazolidine ring.<sup>81</sup>

The field of metal chelating LFi still remains mostly unexplored. As previously discussed, our lab is extensively involved in the identification of novel metal binding groups against various metalloproteins. Some of the ZBGs listed in Figure 1-12 were tested against anthrax LF. The results are listed in Table 1-3 in the form of  $IC_{50}$  values and shows that the active site  $Zn^{2+}$  ion of LF favors the softer (O,S) chelating ZBGs. Based on these initial ZBG results, Dr. Jana Lewis developed the first full length LFi in the lab, AM-2S which laid the groundwork for the study presented in Chapter 3 (Figure 1-16).

## 1.C References

- (1) Parkin, G. *Chem. Comm.* **2000**, 2000, 1971.
- (2) McCall, K. A.; Huang, C. C.; Fierke, C. A. *J Nutr.* **2000**, 130, 1437S.
- (3) Bertini, I.; Decaria, L.; Rosato, A. *J. Biol. Inorg. Chem.* **2010**, 15, 1071.
- (4) Anzellotti, A. I.; Farrell, N. P. *Chem. Soc. Rev.* **2008**, 37, 1629.
- (5) Lee, Y.; Lim, C. *J. Mol. Biol.* **2008**, 379, 545.
- (6) Chen, L.; Rydel, T. J.; Gu, F.; Dunaway, C. M.; Pikul, S.; Dunham, K. M.; Barnett, B. L. *J. Mol. Biol.* **1999**, 293, 545.
- (7) Wang, J. Y.; Ling, H.; Yang, W.; Craigie, R. *EMBO J.* **2001**, 20, 7333.
- (8) Shoop, W. L.; Xiong, Y.; Wiltsie, J.; Woods, A.; Guo, J.; Pivnichny, J. V.; Felcetto, T.; Michael, B. F.; Bansal, A. C., R.T.; Cunningham, B. R.; Friedlander, A. M.; Douglas, C. M.; Patel, S. B.; Wisniewski, D.; Scapin, G.; Salowe, S. P.; Zaller, D. M.; Chapman, K. T.; Scolnick, E. M.; Schmatz, D. M.; Bartizal, K.; MacCoss, M. *Proc. Natl. Acad. Sci., USA* **2005**, 102, 7958.
- (9) Krishnamurthy, V. M.; Kaufman, G. K.; Urbach, A. R.; Gitlin, I.; Gudiksen, K. L.; Weibel, D. B.; Whitesides, G. M. *Chem. Rev.* **2008**, 108, 946.
- (10) Supuran, C. T. *Nat. Rev. Drug Discov.* **2008**, 7, 168.
- (11) Supuran, C. T. *Bioorg. Med. Chem. Lett.* **2010**, 20, 3467.
- (12) Agrawal, A.; Pulendran, B. *Cell. Mol. Life Sci* **2004**, 61, 2859.
- (13) Murphy, G. J. P.; Murphy, G.; Reynolds, J. J. *FEBS Lett.* **1991**, 289, 4.
- (14) Nagase, H.; Woessner, J. J. *J. Biol. Chem.* **1999**, 274, 21491.
- (15) Page-McCaw, A.; Ewald, A. J.; Werb, Z. *Nat. Rev. Mol. Cell Biol.* **2007**, 8, 221.
- (16) Nelson, A.; Fingleton, B.; Rothenberg, M.; Matrisian, L. *J. Clin. Oncol.* **2000**.
- (17) Skiles, J. W.; Gonnella, N. C.; Jeng, A. Y. *Curr. Med. Chem.* **2004**, 11, 2911.
- (18) Whittaker, M. F.; Floyd, C. D.; Brown, P.; Gearing, A. J. H. *Chem. Rev.* **1999**, 99, 2735.

- (19) Basset, P.; Bellocq, J. P.; Wolf, C.; Stoll, I.; Hutin, P.; Limacher, J. M.; Podhajcer, O. L.; Chenard, M. P.; Rio, M. C.; Chambon, P. *Nature* **1990**, *348*, 699.
- (20) Coussens, L. M.; Fingleton, B.; Matrisian, L. M. *Science* **2002**, *295*, 23872392.
- (21) Creemers, E. E.; Cleutjens, J. P.; Smits, J. F.; Daemen, M. J. *Circ Res* **2001**, *89*, 201.
- (22) Lindsey, M. L. *Heart Failure Rev.* **2004**, *9*, 7.
- (23) Maeda, A.; Sobel, R. A. *J. Neuropathol. Exp. Neurol.* **1996**, *55*, 300.
- (24) Reynolds, J. J.; Hembry, R. M.; Meikle, M. C. *Adv. Dent. Res.* **1994**, *8*, 312.
- (25) Beckett, R. P.; Whittaker, M. *Exp Opin Ther Patents* **1998**, *8*, 259.
- (26) Fisher, J. F.; Mobashery, S. *Cancer Metastasis Rev* **2006**, *25*, 115.
- (27) Jacobsen, F. E.; Lewis, J. A.; Cohen, S. M. *ChemMedChem* **2007**, *2*, 152.
- (28) Lukacova, V.; Zhang, Y.; Mackov, M.; Baricic, P.; Raha, S.; Calvo, J. A.; Balaz, S. *J. Biol. Chem.* **2004**, *279*, 14194.
- (29) Overall, C. M.; Kleinfeld, O. *Br. J. Cancer* **2006**, *94*, 941.
- (30) Puerta, D. T.; Cohen, S. M. *Curr. Top. Med. Chem.* **2004**, *4*, 1551.
- (31) Rush III, T. S.; Powers, R. *Curr. Top. Med. Chem.* **2004**, *4*, 1311.
- (32) Gross, J.; Lapiere, C. M. *Proc. Natl. Acad. Sci., USA* **1962**, *48*, 1014.
- (33) Eisen, A. Z.; Jeffrey, J.; Gross, J. *Biochim. Biophys. Acta* **1986**, *151*, 637.
- (34) Zitka, O.; Kuckacka, J.; Krizkova, S.; Huska, D.; Adam, V.; Masarik, M.; Prusa, R.; Kizek, R. *Curr. Med. Chem.* **2010**, *17*, 3751.
- (35) Lovejoy, B.; Cleasby, A.; Hassell, A. M.; Longley, K.; Luther, M. A.; Weigi, D.; McGeehan, G.; McElroy, A. B.; Drewry, D.; Lambert, M. H.; Jordan, S. R. *Science* **1994**, *263*, 375.
- (36) Murphy, G.; Knäuper, V.; Atkinson, S.; Butler, G.; English, W.; Hutton, M.; Stracke, J.; Clark, I. *Arthritis Res.* **2002**, *4*, S39.
- (37) Gomis-Ruth, F. X. *Mol. Biotechnol.* **2003**, *24*, 157.

- (38) Gomis-Ruth, F. X. *J. Biol. Chem.* **2009**, *284*, 15353.
- (39) Schecter, I.; Berger, A. *Biochem. Biophys. Res. Commun.* **1967**, *27*, 157.
- (40) Brinckerhoff, C. E.; Matrisian, L. M. *Nat. Rev. Mol. Cell Biol.* **2002**, *3*, 207.
- (41) Ra, H.-J.; Parks, W. C. *Matrix Biol.* **2007**, *26*, 587.
- (42) Morgunova, E.; Tuuttila, A.; Bergmann, U.; Tryggvason, K. *Proc. Natl. Acad. Sci. USA* **2002**, *99*, 7414.
- (43) Fernandez-Catalan, C.; Bode, W.; Huber, R.; Turk, D.; Calvete, J. J.; Lichte, A.; Tschesche, H.; Maskos, K. *EMBO J.* **1998**, *17*, 5238.
- (44) Golub, L. M.; Lee, H.-M.; Ryan, M. E.; Giannobile, W. V.; Payne, J.; Sorsa, T. *Adv. Dent. Res.* **1998**, *12*, 12.
- (45) Jacobsen, J. A.; Jourden, J. L. M.; Miller, M. T.; Cohen, S. M. *Biochim. Biophys. Acta.* **2010**, *1803*, 72.
- (46) Puerta, D. T.; Mongan, J.; Tran, B. L.; McCammon, J. A.; Cohen, S. M. *J. Am. Chem. Soc.* **2005**, *127*, 14148.
- (47) Jacobsen, F. E.; Lewis, J. A.; Cohen, S. M. *J. Am. Chem. Soc.* **2006**, *10*, 3156.
- (48) Lewis, J. A.; Mongan, J.; McCammon, J. A.; Cohen, S. M. *ChemMedChem* **2006**, *7*, 694.
- (49) Puerta, D. T.; Griffin, M. O.; Lewis, J. A.; Romero-Perez, D.; Garcia, R.; Villarreal, F. J.; Cohen, S. M. *J. Biol. Inorg. Chem.* **2006**, *11*, 131.
- (50) Pile, J. C.; Malone, J. D.; Eitzen, E. M.; Friedlander, A. M. *Arch. Intern. Med.* **1998**, *158*, 429.
- (51) Collier, R. J.; Young, J. A. T. *Annu. Rev. Cell Dev. Biol.* **2003**, *19*, 45.
- (52) Smith, H.; Keppie, J. *Nature* **1954**, *173*, 869.
- (53) Tournier, J. N.; Quesnel-Hellmann, A.; Cleret, A.; Vidal, D. R. *Cell. Microbiol.* **2007**, *9*, 555.
- (54) Bradley, K. A.; Mogridge, J.; Mourez, M.; Collier, R. J.; Young, J. A. T. *Nature* **2001**, *414*, 225.
- (55) Miller, C. J.; Elliot, J. L.; Collier, R. J. *Biochemistry* **1999**, *38*, 10432.

- (56) Scobie, H. M.; Rainey, J. A.; Bradley, K. A.; Young, J. A. T. *Proc. Natl. Acad. Sci., USA* **2003**, *100*, 5170.
- (57) Young, J. A.; Collier, R. J. *Annu. Rev. Biochem.* **2007**, *76*, 243.
- (58) Krantz, B. A.; Finkelstein, A.; Collier, R. J. *J. Mol. Biol.* **2006**, *355*, 968.
- (59) Leppla, S. H. *Proc. Natl. Acad. Sci., USA* **1982**, *79*, 3162.
- (60) Paccani, S. R.; Tonello, F.; Patrussi, L.; Capitani, N.; Simonato, M.; Montecucco, C.; Baldari, C. T. *Cell. Microbiol.* **2007**, *9*, 924.
- (61) Scobie, H. M.; Marlett, J. M.; Rainey, G. J. A.; Lacy, D. B.; Collier, R. J.; Young, J. A. T. *PLoS ONE* **2007**, *2*, e329.
- (62) Sun, J.; Lang, A. E.; Aktories, K.; Collier, R. J. *Proc. Natl. Acad. Sci., USA* **2008**, *105*, 4346.
- (63) Wimalasena, D. S.; Cramer, J. C.; Janowiak, B. E.; Julius, S. J.; Melnyk, R. A.; Anderson, D. E.; Kirk, K. L.; Collier, R. J.; Bann, J. G. *Biochemistry* **2007**, *46*, 14928.
- (64) Park, J. M.; Greten, F. R.; Li, Z. W.; Karin, M. *Science* **2002**, *297*, 2048.
- (65) Chopra, A. P.; Boone, S. A.; Liang, X.; Duesbery, N. S. *J. Biol. Chem.* **2003**, *278*, 9402.
- (66) Puhar, A.; Montecucco, C. *TRENDS in Microbiol.* **2007**, *15*, 477.
- (67) Tonello, F.; Ascenzi, P.; Montecucco, C. *J. Biol. Chem.* **2003**, *278*, 40075.
- (68) Ascenzi, P.; Visca, P.; Ippolito, G.; Spallarossa, A.; Bolognesi, M.; Montecucco, C. *FEBS Lett.* **2002**, *531*, 384.
- (69) Hanna, P. C.; Acosta, D.; Collier, R. J. *Proc. Natl. Acad. Sci., USA* **1993**, *90*, 10198.
- (70) Pezard, C.; Berche, P.; Mock, M. *Infect. Immun.* **1991**, *59*, 3472.
- (71) Pannifer, A. D.; Wong, T. Y.; Schwarzenbacher, R.; Renatus, M.; Petosa, C.; Bienkowska, J.; Lacy, D. B.; Collier, R. J.; Park, S.; Leppla, S. H.; Hanna, P. C.; Liddington, R. C. *Nature* **2001**, *414*, 229.
- (72) Melnyk, R. A.; Hewitt, K. M.; Lacy, D. B.; Lin, H. C.; Gessner, C. R.; Li, S.; Woods, V. L.; Collier, R. J. *J. Biol. Chem.* **2006**, *281*, 1630.

- (73) Tonello, F.; Naletto, L.; Romanello, V.; Dal Molin, F.; Montecucco, C. *Biochem. Biophys. Res. Commun.* **2004**, *313*, 496.
- (74) Forino, M.; Johnson, S. L.; Wong, T. Y.; Rozanov, D. V.; Savinov, A. Y.; Li, W.; Fattorusso, R.; Becattini, B.; Orry, A. J.; Jung, D.; Abagyan, R. A.; Smith, J. W.; Alibek, K.; Liddington, R. C.; Strongin, A. Y.; Pellecchia, M. *Proc. Natl. Acad. Sci., USA* **2005**, *2005*, 9499.
- (75) Gaddis, B. D.; Avramova, L. V.; Chmielewski, J. *Bioorg. Med. Chem. Lett.* **2007**, *17*, 4575.
- (76) Tonello, F.; Seveso, M.; Marin, O.; Mock, M.; Montecucco, C. *Nature* **2002**, *418*, 386.
- (77) Panchal, R. G.; Hermone, A. R.; Nguyen, T. L.; Wong, T. Y.; Schwarzenbacher, R.; Schmidt, J.; Lane, D.; McGrath, C.; Turk, B. E.; Burnett, J.; Aman, M. J.; Little, S.; Sausville, E. A.; Zaharevitz, D. W.; Cantley, L. C.; Liddington, R. C.; Gussio, R.; Bavari, S. *Nat. Struct. Mol. Biol.* **2004**, *11*, 67.
- (78) Min, D. H.; Tang, W. J.; Mrksich, M. *Nat. Biotechnol.* **2004**, *22*, 717.
- (79) Rees, D. C.; Congreve, M.; Murray, C. W.; Carr, R. *Nat. Rev. Drug Discov.* **2004**, *3*, 660.
- (80) Hajduk, P. J.; Sheppard, G.; Nettlesheim, D. G.; Olejniczak, E. T.; Shuker, S. B.; Meadows, R. P.; Steinman, D. H.; Carrera Jr, G. M.; Marcotte, P. A.; Severin, J.; Walter, K.; Smith, H.; Gubbins, E.; Simmer, R.; Holzman, T. F.; Morgan, D. W.; Davidsen, S. K.; Summers, J. B.; Fesik, S. W. *J. Am. Chem. Soc.* **1997**, *119*, 5818.
- (81) Johnson, S. L.; Jung, D.; Forino, M.; Chen, Y.; Satterhwait, A.; Rozanov, D. V.; Strongin, A. Y.; Pellecchia, M. *J. Med. Chem.* **2006**, *49*, 27.

## **Chapter 2. Zinc-Binding Groups Modulate Selective Inhibition of MMPs**

## 2.A Introduction

In response to the elevated levels of matrix metalloproteinase activity in several disease states, numerous MMP inhibitors (MMPi) have been synthesized in the past 20 years.<sup>1-3</sup> Some of the diseases associated with MMPs are rheumatoid arthritis and cancer metastases. In fact, rheumatoid arthritis was the first disease targeted by early MMPi.<sup>4</sup> These first-generation inhibitors mostly contained a peptide group (that interacted with the primed subsite pockets of MMPs) attached to a zinc-binding group (ZBG) to chelate the active site  $Zn^{2+}$  ion (Figure 2-1). The most common ZBG used in these early MMPi was the hydroxamic acid moiety; which is present in both Batimastat and Marimastat (Figure 2-1), two of the first peptidic inhibitors to enter clinical trials.<sup>3</sup> CGS 27023A (which also contains a hydroxamic acid ZBG) was the first non-peptidic MMPi to enter clinical trials.<sup>3</sup> Unfortunately, all three MMPi showed no clinical success and were later withdrawn. Numerous MMPi have been prepared and investigated, but most show little efficacy against human diseases; and very limited success in clinical trials. In addition, some inhibitors caused side effects including musculoskeletal pain, tendonitis, and in some cases, mild anemia. These adverse effects may be attributed to the lack of selectivity of the inhibitors. In addition, many hydroxamate-based MMPi suffer from poor pharmacokinetics and poor oral bioavailability. Consequently, some efforts have been made to identify alternative ZBGs as a means to identifying MMPi with improved performance.



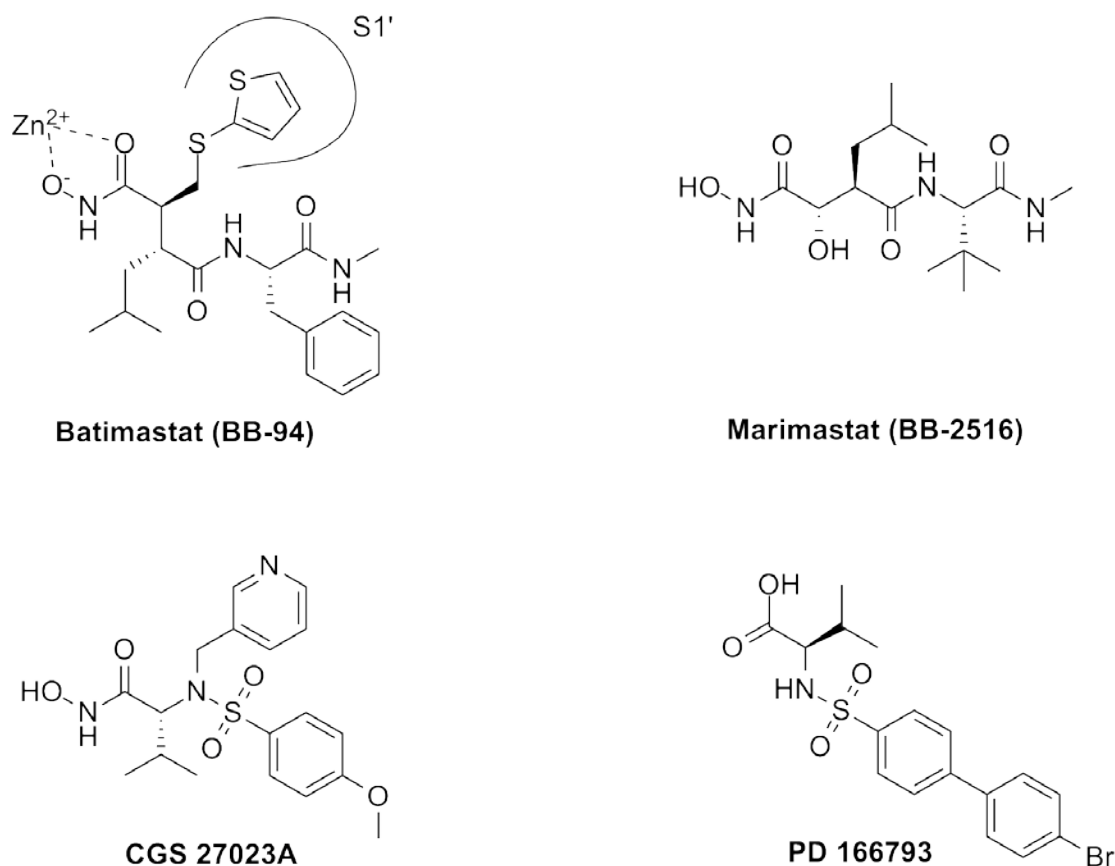


**Figure 2-1.** Early generation peptidic (top) and non-peptidic (bottom) MMP inhibitors. Catalytic  $Zn^{2+}$  coordination and  $S1'$  pocket substituent is shown for Batimastat.

Carboxylic acids (the synthetic precursor to most hydroxamic acids) have been used as ZBGs, but generally result in a loss of potency,<sup>1,5</sup> likely due to the change in binding mode and diminished donor ability of the carboxylate ligand;<sup>6</sup> PD 166793 is an example of a carboxylic acid MMPi (Figure 2-1). Castelhana and co-workers reported the selectivity and potency of MMPi with several different ZBGs (for example, hydroxamates, ‘reverse’ hydroxamates, carboxylates, thiols, phosphinates) on a common indolactam/isobutyl backbone moiety.<sup>7</sup> The results of this study showed that the use of ZBGs other than a hydroxamate resulted in a 10- to 250-fold loss in

potency. Although several MMPs were tested, no extensive study of isoform selectivity was performed; and the data generated generally showed no changes in selectivity based on the nature of the ZBG. Fesik and co-workers used structure–activity relationship by nuclear magnetic resonance (SAR-by-NMR) to screen several molecular fragments to identify new ZBGs, only to find a naphthyl-substituted hydroxamic acid to be the most potent among the compounds examined.<sup>8</sup>

In an effort to obtain more promising compounds as alternative ZBGs, and counteract the broad spectrum effects of hydroxamic acid-based MMPi, our lab investigated several zinc binding groups (ZBGs) as discussed in Chapter 1. These ZBGs include a variety of (O,O) and (O,S) donor atom chelators such as hydroxypyridinones and pyridinethiones, hydroxypyrones and pyrothiones, and also mixed nitrogen/oxygen donor-atom chelators such as pyridine and aza-macrocyclic based ligands.<sup>6,9-13</sup> Based on the results of these studies, a series of hydroxypyron MMPi, effective against deep pocket MMPs, were developed.<sup>13</sup>

In the present study, a series of hydroxypyron and hydroxypyridinone inhibitors have been synthesized and demonstrate that the isoform selectivity of an MMPi can be influenced by the choice of ZBG (Figure 2-2). By linking different ZBGs to a common biphenyl backbone, we demonstrate that small changes in the ZBG modulate the selectivity against deep SI pocket MMPs. These observations are particularly notable, because the ZBGs employed in this study all use two oxygen donor atoms to bind the  $Zn^{2+}$  ion, and only possess subtle differences in electrostatics, hydrophobicity, and acidity. While studies have previously investigated the design of the backbone, leaving the hydroxamate ZBG unvaried, this study represents the first

example where variation of the ZBG leads to selective MMP inhibition.<sup>14-16</sup> Furthermore, to demonstrate the importance of the ZBG in a relevant pathophysiological model, some of these MMPi were tested in an isolated perfused rat heart (Langendorff) system. Taken together, the in vitro, computational, and ex vivo results described herein show that MMPi can display different isoform selectivity and hence show variable ex vivo activity depending on the ZBG employed.

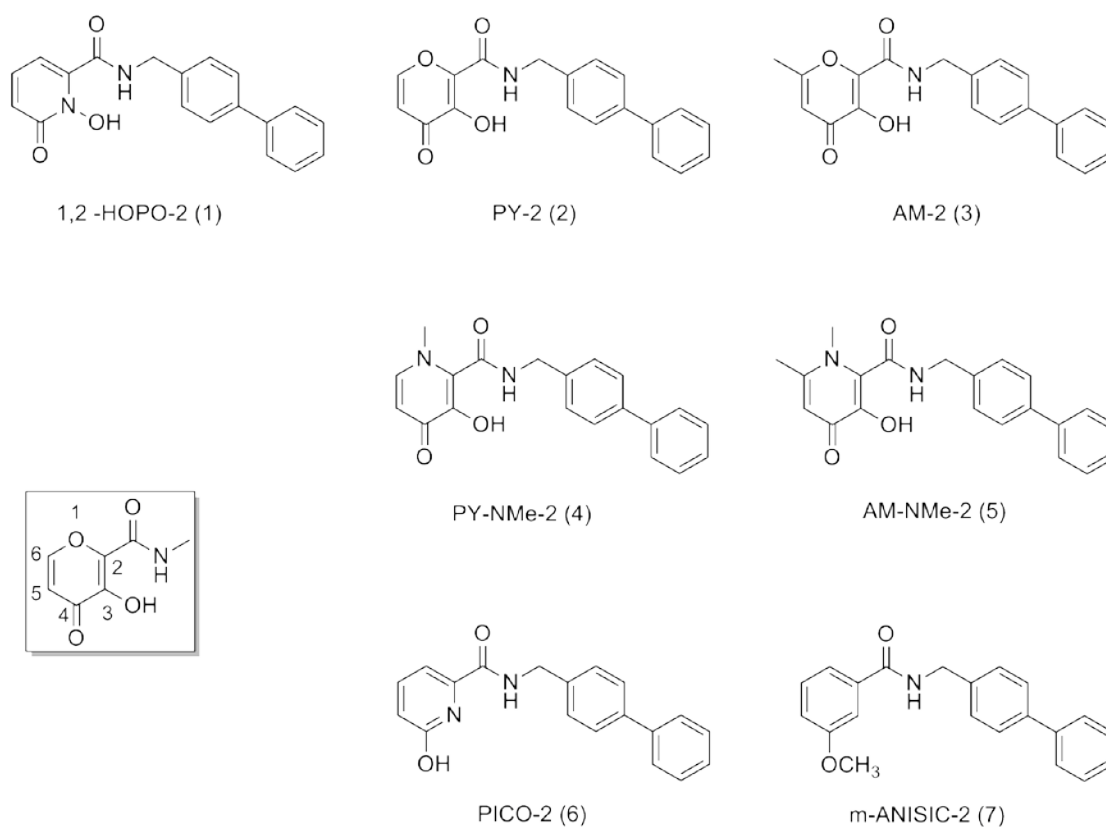


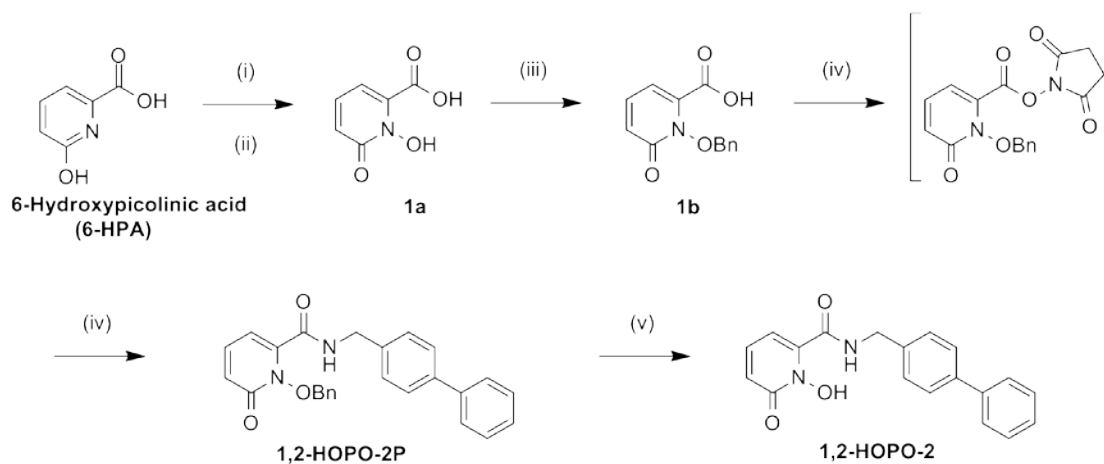
**Figure 2-2.** Structures of MMPi examined in this study (1-7). Compounds 6 and 7 are negative controls, as they do not contain a high affinity ZBG. The numbering scheme used for the pyrone ring system found in inhibitors 2 and 3 is shown on the left.

## 2.B Synthesis of MMPi

Previous work from our laboratory showed that several hydroxypyronone and hydroxypyridinone ZBGs had improved potency against MMPs when compared to a standard hydroxamate compound, acetohydroxamic acid (AHA).<sup>10,12</sup> A novel, full-length inhibitor AM-2 (compound **3**, Figure 2-2), based on a hydroxypyronone ZBG, was shown to be a potent inhibitor of MMP-2 and MMP-3 but not MMP-1.<sup>13</sup> These results showed that potent, non-hydroxamate MMPi could be devised, and AM-2 was selected as the basis for the design and synthesis of the MMPi examined here (Figure 2-2). Each inhibitor contains a chelating, heterocyclic ZBG attached to the same biphenyl backbone as in AM-2 (Figure 2-2).

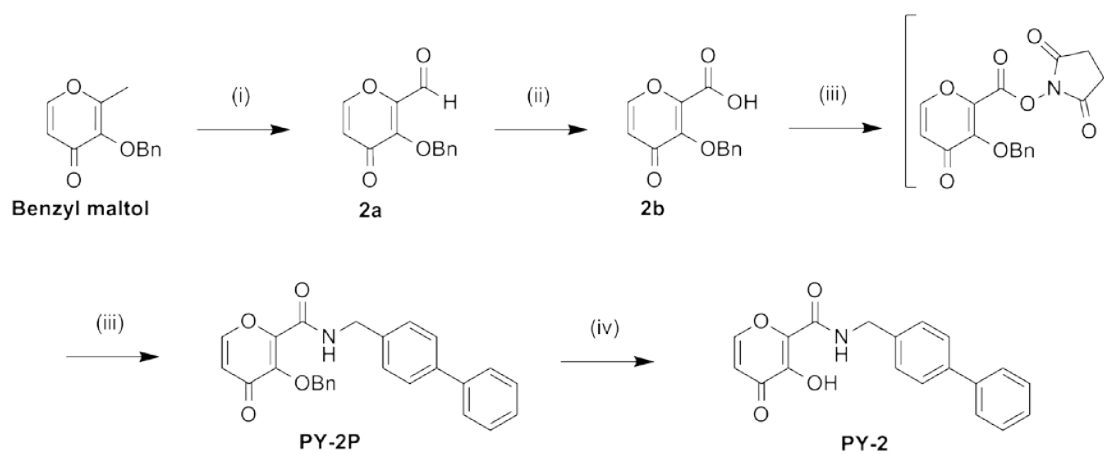
As outlined in Schemes 2-1 to 2-3, the inhibitors were generally prepared by benzyl protection of the hydroxyl group of each ZBG, followed by conversion of each benzyl-protected ZBG from a carboxylic acid to an activated ester. The esters were then coupled with phenylbenzylamine, and finally deprotected to obtain the compounds shown in Figure 2-2. The MMPi in Figure 2-2 are relatively facile to prepare and readily allow for their preparation on multigram scales. As negative controls, compounds **6** and **7** were synthesized; both contain the same biphenyl backbone as the other inhibitors, but use an isosteric (**6**) or nearly isosteric (**7**) ring that is not an effective Zn<sup>2+</sup> chelator. Interestingly, the ZBG (6-hydroxypicolinic acid)<sup>17</sup> of compound **6** is the synthetic precursor to the chelating ZBG used in compound **1**.

**Scheme 2-1.** Synthesis of 1,2-HOPO-2<sup>a</sup>

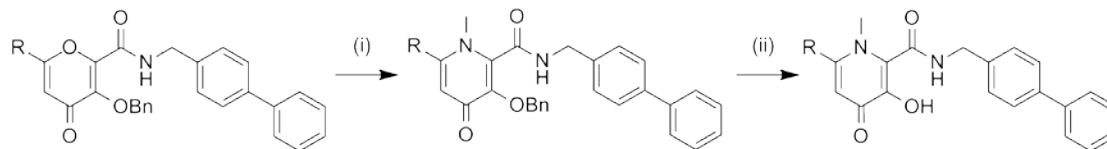


<sup>a</sup>Reagents and conditions: (i) 30% H<sub>2</sub>O<sub>2</sub>, acetic anhydride, TFA, 0 °C (ii) MeOH, 10% KOH, 80 °C, HCl, 48% (iii) BnCl, K<sub>2</sub>CO<sub>3</sub>, MeOH, 75 °C, 6 N HCl, 92% (iv) NHS, DCC, 4-phenylbenzylamine, dry THF, 82%. (v) 1:1 HCl/glacial HOAc, 98%.

**Scheme 2-2.** Synthesis of PY-2<sup>b</sup>



<sup>b</sup>Reagents and conditions: (i) SeO<sub>2</sub>, bromobenzene, 150 °C (ii) sulfamic acid, 80% NaClO<sub>2</sub>, 1:1 acetone:H<sub>2</sub>O, 59% (iii) NHS, DCC, 4-phenylbenzylamine, dry THF, 62% (iv) 1:1 HCl/glacial HOAc, 94%.

**Scheme 2-3.** Synthesis of PY-NMe-2, AM-NMe-2<sup>c</sup>

R = H, PY-NMe-2  
R = CH<sub>3</sub>, AM-NMe-2

<sup>c</sup>Reagents and conditions: (i) 1:4 40% CH<sub>3</sub>NH<sub>2</sub>:H<sub>2</sub>O, 1:1 EtOH:H<sub>2</sub>O, R = H, 75%, R = CH<sub>3</sub>, 64% (ii) 1:1 HCl/glacial HOAc, R = H, 67%, R = CH<sub>3</sub>, 82%.

## 2.C Activity of MMPi in in vitro MMP Assays

The ability of the compounds listed in Figure 2-2 to inhibit the hydrolytic activity of eight different MMP isoforms (MMP-1, -2, -3, -7, -8, -9, -12, -13) was measured using an established assay that utilizes a fluorescent peptide substrate cleaved by all MMPs.<sup>18</sup> A self-quenching fluorogenic peptide (Mca-Pro-Leu-Gly-Leu-Dpa-Ala-Arg-NH<sub>2</sub>): Mca = (7-methoxycoumarin-4-yl)-acetyl, Dpa = N-3-(2,4-dinitrophenyl)-L- $\alpha$ - $\beta$ -diaminopropionyl) from Enzo Life Sciences (formerly BIOMOL) is used in the assay. When this peptide is cleaved by MMPs at the Gly-Leu bond, the resulting Mca fluorescence ( $\lambda_{\text{ex}} = 335 \text{ nm}$ ,  $\lambda_{\text{em}} = 405 \text{ nm}$ ) can be monitored. The increase in fluorescence over time is positively correlated with enzyme activity (Figure 2-3). The enzyme activity is therefore measured as the relative fluorescence units (RFU) over time (which is equivalent to the slope of the linear equation). The assays utilize a positive control supplied with the kit to establish a benchmark against which the potencies of the compounds are determined.

The activities of compounds **1-7** were evaluated and IC<sub>50</sub> values were determined (Table 2-1). The IC<sub>50</sub> value is a measure of the inhibitor concentration required for 50% inhibition of enzyme activity compared to uninhibited enzyme activity. As shown in Figure 2-3, the raw data of inhibited enzyme activity of compound **2** (PY-2) is compared to the uninhibited enzyme activity (represented by the DMSO control). IC<sub>50</sub> values were determined (Table 2-1) as previously described.<sup>10,11,19</sup>

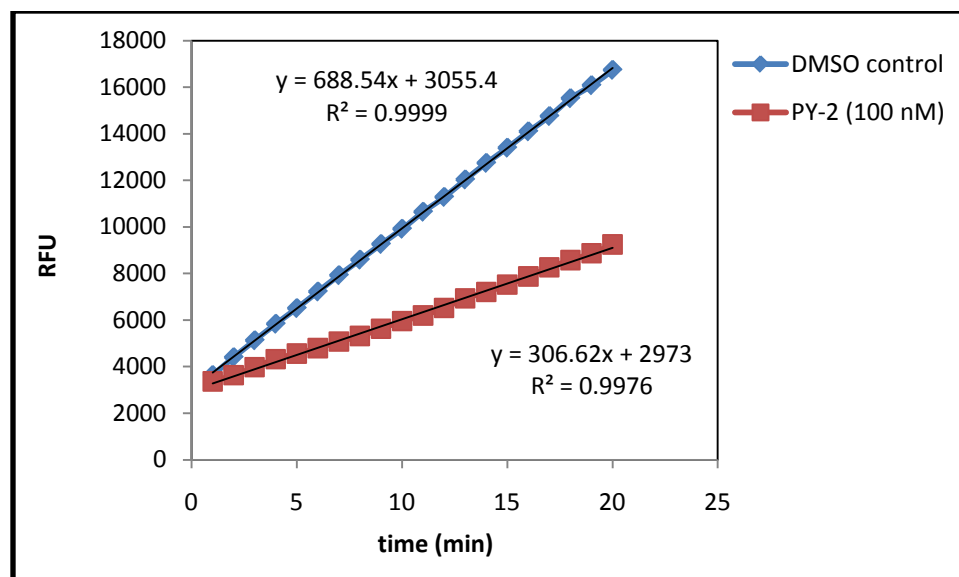


**Figure 2-3.** A graph representing the linear relationship between substrate fluorescence and MMP activity. Relative fluorescence units (RFU) are plotted on the y-axis and time (in min) on the x-axis. Slope of each equation represents MMP activity. Blue diamonds show MMP activity without inhibitor and red squares show MMP activity in the presence of compound **2** (PY-2).

As expected, MMPi **1–5** are poor inhibitors of shallow S1' pocket MMPs (MMP-1 and MMP-7) with  $IC_{50}$  values greater than 50  $\mu$ M. The MMPi also show poor inhibition against MMP-9 with  $IC_{50}$  values greater than 25  $\mu$ M. MMP-13 is inhibited with  $IC_{50}$  values of  $\sim$  4–20  $\mu$ M by MMPi **1–5** with no notable differences in potency based upon the different ZBGs. MMP-2 is inhibited by compound **1** with a nanomolar  $IC_{50}$ , but compounds **2–5** display low micromolar activity. MMP-8 and MMP-12 are strongly inhibited by compounds **1–3** with  $IC_{50}$  values ranging from 0.018–0.248  $\mu$ M, but are inhibited less effectively by **4** and **5** (1.2–5  $\mu$ M). Similarly, inhibitors **1–3** show good activity against MMP-3 with  $IC_{50}$  values of 0.56, 0.077, and 0.24  $\mu$ M respectively. In contrast to MMPi **2** and **3**, the corresponding hydroxypyridinone analogues **4** and **5** were more than two orders of magnitude less



potent against MMP-3. As a control, compounds **6** and **7** were also tested against MMP-8 and MMP-12 and showed no or negligible inhibition at concentrations up to 100  $\mu$ M. The weak activity of compounds **6** and **7** clearly demonstrates that a tight-binding ZBG is required for potent inhibition and that the biphenyl backbone alone is not sufficient for efficacy. Collectively, the results show that the nature of the ZBG has a pronounced effect on the scope and potency of the resulting MMPi.

**Table 2-1.** IC<sub>50</sub> values (in  $\mu$ M) for MMPi **1-7** (rows) against eight different MMPs (columns) using a fluorescence-based assay<sup>a</sup>

| MMP      | -1  | -2        | -3          | -7  | -8          | -9       | -12         | -13          |
|----------|-----|-----------|-------------|-----|-------------|----------|-------------|--------------|
| <b>1</b> | >50 | 0.92±0.04 | 0.56±0.04   | >50 | 0.086±0.01  | 27.1±5.3 | 0.018±0.001 | 4.1±0.<br>6  |
| <b>2</b> | >50 | 4.4±1.4   | 0.077±0.005 | >50 | 0.248±0.005 | 32.3±2.5 | 0.085±0.004 | 6.6±0.<br>1  |
| <b>3</b> | >50 | 9.3±0.5   | 0.24±0.01   | >50 | 0.064±0.008 | >50      | 0.022±0.002 | 20.6±3<br>.0 |
| <b>4</b> | >50 | 16.5±2.8  | 41.7±4.8    | >50 | 3.8±0.1     | >50      | 1.2±0.4     | 16.5±3<br>.0 |
| <b>5</b> | >50 | 7.6±0.2   | >50         | >50 | 5.0±0.4     | >50      | 6.7±1.5     | 6.7±0.<br>2  |
| <b>6</b> | ND  | ND        | ND          | ND  | >100        | ND       | >100        | ND           |
| <b>7</b> | ND  | ND        | ND          | ND  | >100        | ND       | >100        | ND           |

Compounds **6** and **7** showed no inhibition at concentrations up to 100  $\mu$ M. Values in the table include standard deviations of at least four independent measurements. ND = Not determined.

## 2.D Kinetic studies on 1,2-HOPO-2

Kinetic studies were performed using the same fluorescence-based assay kit used for IC<sub>50</sub> measurements with identical ratios of enzyme, substrate, and inhibitor. Assuming a Michaelis–Menten mechanism, estimations of  $K_m$  were obtained from plots of reaction velocity versus substrate concentration, using substrate concentrations ranging from 0 to 80  $\mu$ M.  $K_i$  was then calculated from the Michaelis-Menten equation (equation 1):

$$K_i = \frac{[I]}{1 + \frac{[S]}{K_m}} \quad (\text{equation 1})$$

where [I] = inhibitor concentration at the IC<sub>50</sub> value and [S] = initial substrate concentration used to determine the IC<sub>50</sub> value. To confirm the calculated value of  $K_i$  experimentally, a Dixon plot (Figure 2-4) was generated. To generate the Dixon plot, the reciprocal of the initial velocities for the enzyme at different substrate concentrations were calculated from equation 2, and plotted against different inhibitor concentrations.<sup>20</sup> The x-coordinate value corresponding to the intersection of the lines for different substrate concentrations is equal to  $-K_i$ .

$$V_o = \frac{V_{max} [S]}{K_m + [S]} \quad (\text{equation 2})$$

As a representative example, compound **1** was selected for further kinetic studies against MMP-12 (the isoform against which **1** is most potent). The  $V_{max}$  and  $K_m$

for MMP-12 were determined to be  $829 \text{ mmol min}^{-1} \text{ mg}^{-1}$  and  $4 \text{ }\mu\text{M}$ , respectively. The value of  $K_i$  for **1** against MMP-12 was calculated from equation 1 to be  $9 \text{ nM}$ .<sup>20</sup> A Dixon plot was generated with concentrations of inhibitor ranging from 0 to  $40 \text{ nM}$  to determine the mode of inhibition and confirm the calculated  $K_i$  value. The Dixon plot shown in Figure 2-4 is indicative of a mixed competitive mode of inhibition with an experimental  $K_i$  value of approximately  $18 \text{ nM}$ ,<sup>20,21</sup> which is consistent with the observed  $\text{IC}_{50}$  value.

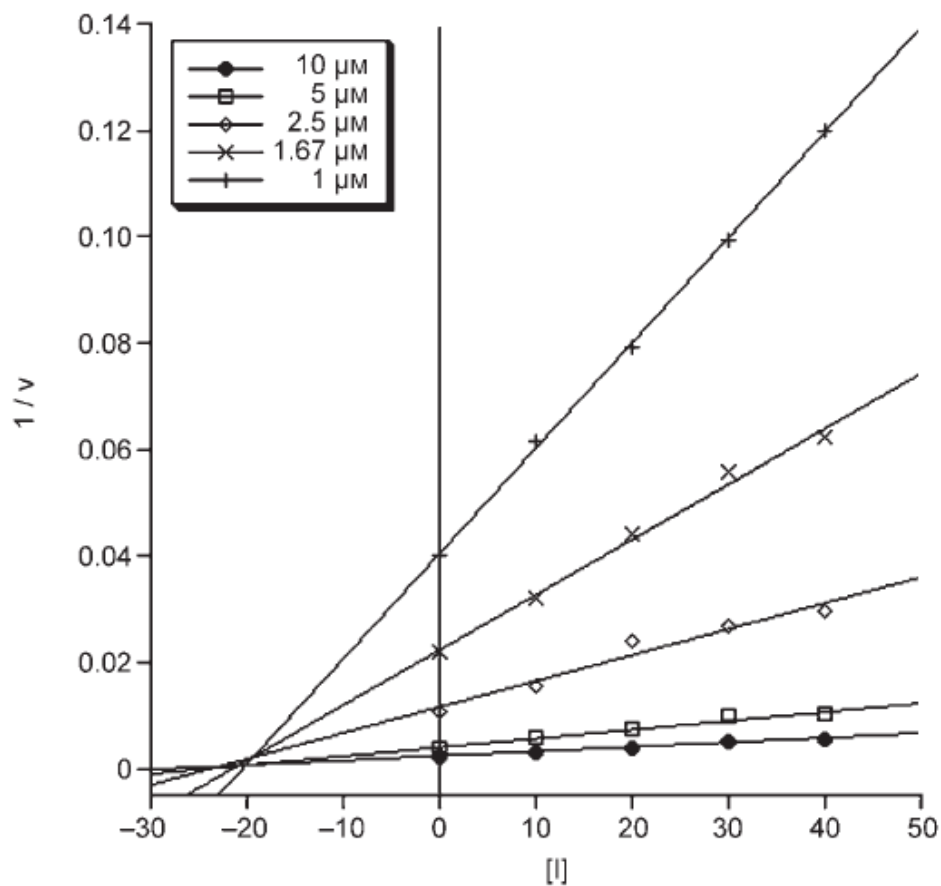


**Figure 2-4.** Dixon plot of MMP-12 with different substrate concentrations (10  $\mu\text{M}$  = filled circles, 5  $\mu\text{M}$  = open squares, 2.5  $\mu\text{M}$  = open diamonds, 1.67  $\mu\text{M}$  = crosses, 1  $\mu\text{M}$  = plus signs) against varying concentrations of MMPi 1 in nM. The reciprocal of the activity ( $1/v$ ) in  $\text{mmol}^{-1} \text{min mg}$  is plotted on the y-axis.

## 2.E Cell viability assays

Neonatal rat ventricular fibroblasts and myocytes were prepared in the laboratory of Dr. Francisco Villarreal at the School of Medicine, University of California, San Diego. The cell-based studies were performed by Dr. Diego Romero-Perez and the results are briefly discussed here. The cytotoxicity of two potent and semi-selective inhibitors, 1,2-HOPO-2 (compound **1**) and PY-2 (compound **2**), was compared to one of the negative controls (PICO-2, **6**) and two broad-spectrum inhibitors, CGS 27023A and PD 166793.<sup>22,23</sup> As shown in Figure 2-5, compounds **1**, **2**, and **6** are generally less toxic than the broad spectrum inhibitor PD 166793 and comparable to that of CGS 27023A. It is important to note that 1,2-HOPO-2 and PY-2 display good cellular viability up to concentrations as high as 1  $\mu$ M and 10  $\mu$ M, respectively.

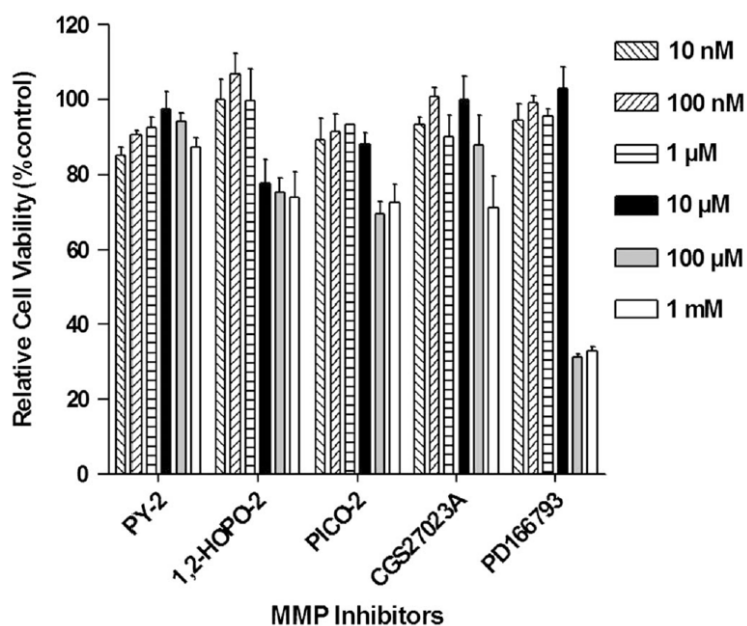


**Figure 2-5.** Cytotoxicity assays of 1,2-HOPO-2(**1**), PY-2 (**2**) and PICO-2 (**6**) in comparison to broad spectrum inhibitors CGS 27023A and PD 166793.<sup>24</sup>

## 2.F Ex vivo efficacy of inhibitors

Cardiac myocytes and other myocardial cells express multiple MMPs which are involved in organ ECM homeostasis.<sup>25-27</sup> Ischemia-reperfusion (IR) injury in ex vivo heart preparations is known to activate MMPs that mediate myocardial damage, and as a consequence, loss of contractile function.<sup>28</sup> Measurements of the recovery of contractile performance with different MMPi after a period of global IR demonstrate that the ZBG significantly impacts the magnitude of recovery of function.

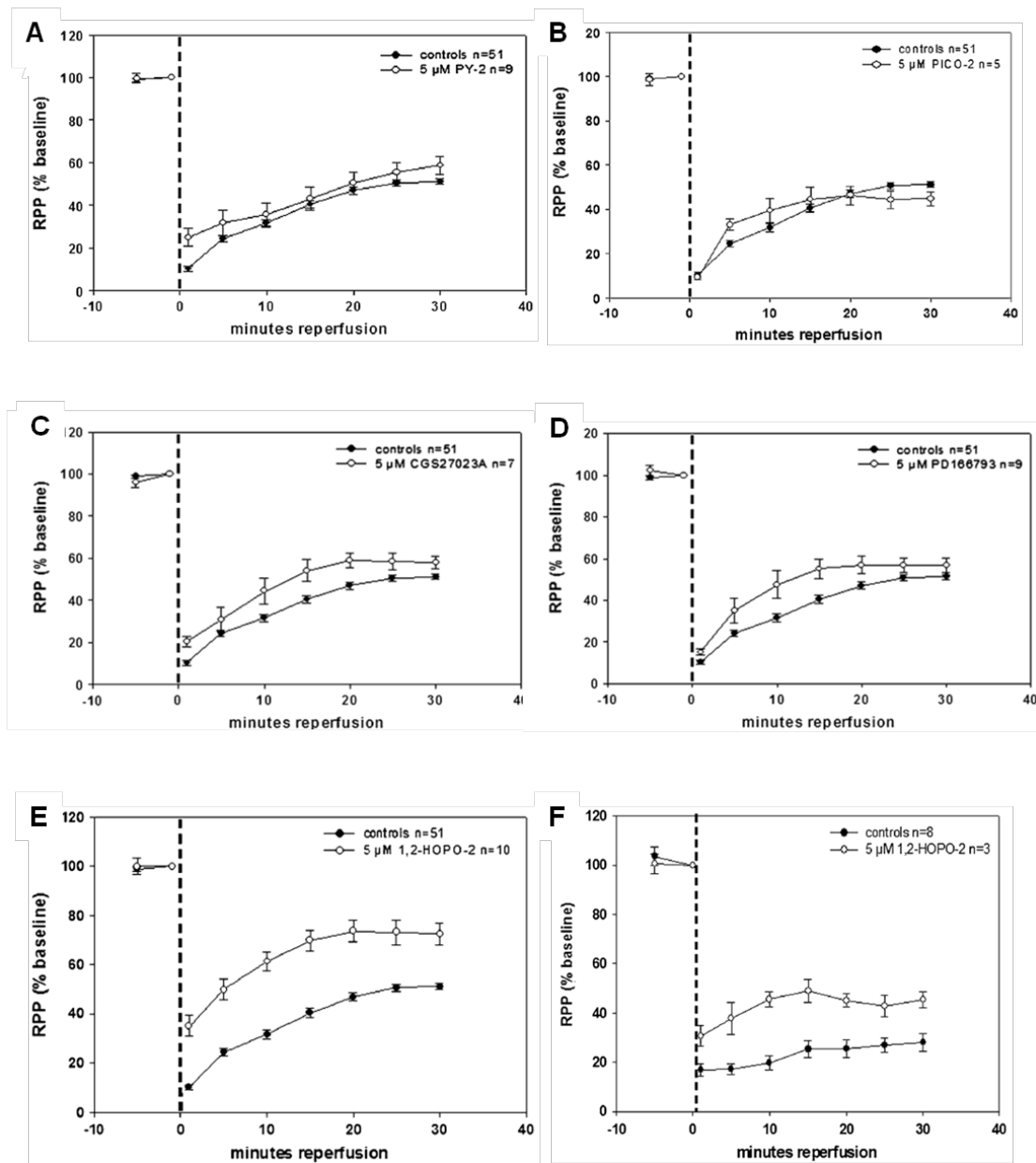
The MMPi chosen for the cell toxicity studies above were also studied for their physiological relevance in an ex vivo rat heart model. Several MMPi were examined, each of which contains a different ZBG to further investigate the importance of the ZBG in a biologically relevant context. The results from these studies are shown in Figure 2-6. Isolated hearts were subjected to 20-30 min of global no-flow ischemia (GNFI) and 30 min reperfusion. Myocardial performance was assessed as the product of the heart rate and left ventricular developed pressure (rate-pressure product, RPP). After implementation of a 20-30 min GNFI, untreated hearts led to a progressive recovery of contractile function of ~50% of the work index rate-pressure product (RPP) after 30 min reperfusion. This ~50% recovery provided a benchmark to which hearts treated with an MMPi could be compared.

Figure 2-6 directly compares the values for the recovery of contractile function between hearts treated with the five different MMPi. The MMPi tested conferred different levels of recovery and preservation of contractile function as indicated by the cardiac work index, RPP. Addition of 5  $\mu$ M of MMPi 2 (PY-2) to the model system yielded ~9% improvement (from 50% in controls to 59% in treated) in RPP versus

controls at 30 min reperfusion (Figure 2-6, A). As expected, 5  $\mu$ M of negative control PICO-2 (Figure 2-6, B) led to essentially no improvement in the recovery of contractile function when compared with the untreated controls. Broad spectrum MMPi CGS 27023A and PD 166793 (Figure 2-6, C and D) conferred a modest but insignificant recovery in RPP with ~8% improvement in RPP compared to controls.

More significantly, the use of 5  $\mu$ M of MMPi **1** (1,2-HOPO-2) led to a notable and persistent improvement in the recovery of contractile function (RPP) at all time points after reperfusion (Figure 2-6, E). Because 5  $\mu$ M 1,2-HOPO-2 conferred higher levels of improved recovery (23% versus controls), additional approaches were pursued to test this compound. In the isolated rat heart, the time of ischemia was increased to 30 min in order to stimulate infarction conditions and still yielded ~17% recovery in RPP versus controls (Figure 2-6, F).

It is important to note that compounds **1** and **2** are entirely isosteric, have nearly identical solubilities, and only differ in the nature of the heterocyclic ZBG (Figure 2-2). Testing with compound **6** and the broad spectrum MMPi showed minimal recovery. These results show that compounds lacking a potent ZBG (**6**) or conversely, containing a broad spectrum ZBG (CGS 27023A and PD 166793), show none or negligible recovery effects in this model. The data obtained therefore highlight the importance of the ZBG in MMPi isoform selectivity, and clearly demonstrate the potency of 1,2-HOPO-2 both *in vitro* and *ex vivo* in cardioprotection.



**Figure 2-6.** Effects of 5  $\mu$ M A. PY-2 (2), B. PICO-2 (6), C. CGS27023A, D. PD 166793, E. 1,2-HOPO-2 (1) on isolated, perfused rat hearts subjected to 20 minutes of GNFI and 30-minute reperfusion. F. 5  $\mu$ M 1,2-HOPO-2 (1) subjected to 30 minutes of GNFI and 30-minute reperfusion.



## 2.G Discussion

### 2.G.i Selectivity beyond the backbone

The MMP active site is mostly solvent exposed and is characterized by six subsite pockets as mentioned in Chapter 1. Apart from substrate classification, MMPs can also generally be described as being shallow, intermediate, or deep pocket enzymes based on the size of their S1' pocket.<sup>32</sup> MMP-1 and MMP-7 are considered shallow pocket MMPs; MMP-2, MMP-9, and MMP-13 are classified as intermediate pocket MMPs; MMP-3, MMP-8, and MMP-12 are designated deep pocket MMPs.<sup>32</sup> Table 2-1 provides a summary of the selectivity for MMPi **1-7** against the aforementioned MMPs. The poor IC<sub>50</sub> values of all the inhibitors against MMP-1 and MMP-7 are consistent with the description of these enzymes as shallow S1' pocket MMPs. All the inhibitors tested use a large biphenyl backbone that is incompatible with the small S1' subsite in these MMPs.<sup>13</sup> The poor inhibition of the compounds against MMP-9 may also be a result of its relatively shallow S1' subsite being unable to accommodate the bulky biphenyl moiety. These findings are consistent with the known structural data for the MMPs examined, and show the typical selectivity expected based on incorporation of a large S1'-directed backbone substituent.<sup>16</sup>

Looking beyond the S1' pocket, examination of the data in Table 2-1 reveals that in addition to the selectivity obtained by the backbone, a second level of selectivity (“fine tuning”) was observed based on differences in the ZBGs. When inspecting the inhibition of each compound against MMP-2, we see that **1** shows nanomolar potency, and is almost an order of magnitude better than the other MMPi. The remaining MMPi (**2-5**) inhibit MMP-2 with IC<sub>50</sub> values in the low micromolar

range. With an invariant backbone among these inhibitors, the enhanced potency of **1** against MMP-2 can be attributed to its unique 1-hydroxypyridin-2(1*H*)-one ZBG. When examining only the subset of MMPs for which compound **1** displays some potency, a >50-fold selectivity for MMP-12 over MMP-2 is observed. Further, compound **1** is at least 2500-fold more potent against MMP-12 over MMP-1 or MMP-7. By comparison, the first generation hydroxamic acid MMPi Batimastat (BB-94) inhibits MMP-1, -2, -3, -8, -9, and -13 with little selectivity, inhibiting all these isoforms within a narrow range of IC<sub>50</sub> values (~1–20 nm).<sup>3</sup>

The effect of the ZBG becomes more pronounced in the deep pocket MMPs, MMP-8, and MMP-12. Table 2-1 shows that both MMP-8 and MMP-12 are strongly inhibited by MMPi **1–3** with IC<sub>50</sub> values in the nanomolar range, but to a much lesser extent by MMPi **4** and **5** with IC<sub>50</sub> values in the low-micromolar range. The only structural difference in the ZBGs from **4** and **5** when compared with MMPi **1–3** is an additional methylated nitrogen atom in the heterocyclic ring system (Figure 2-2). As expected, MMP-8 and MMP-12 show negligible inhibition by negative controls **6** and **7** (Table 2-1).

The attenuated potency of the inhibition profiles of **4** and **5** is most prominent against the deep S1' pocket MMP-3. The *N*-methyl substituent on MMPi **4** and **5** decreases MMP-3 inhibition by three orders of magnitude compared to their pyrone analogues **2** and **3**. Based on computational modeling, the decrease in inhibition caused by the methyl substituent can be attributed to a steric clash within the active site of MMP-3 as shown in Figure 2-7. The region responsible for the steric conflict lies directly above the catalytic Zn<sup>2+</sup> ion. The *N*-methyl group on MMPi **4** and **5**

collides with a methyl group on the isopropyl side chain of Val163 in MMP-3, as confirmed by performing a 'bump' analysis using Insight II (Accelrys). Interestingly, residue 163 is also a significant residue in the S1 subsite of different MMP isoforms, where it is frequently found to interact with inhibitors targeting the S1 subsite. The variability in residue 163 has been exploited in the design of inhibitors to confer selectivity against different MMPs.<sup>16,33</sup> In contrast, Figure 2-7 also shows that methyl substituents in the 6-position of the pyrone ring (for example, compound **3**, Figure 2-1) do not lead to any steric conflicts within the MMP-3 active site. Indeed, this methyl group appears to contribute to the isoform selectivity observed for MMPi **3**.

The protein residues present in the immediate vicinity of the Zn<sup>2+</sup> ion in different MMP isoforms are generally conserved. The residues surrounding the Zn<sup>2+</sup> ion in MMP-8 and MMP-12 are identical, which would explain the similar inhibition trends portrayed by the compounds against these MMPs. In contrast, MMP-3 has a polar Asn162 residue in place of Gly162, Gly158, and Gly179 found in MMP-2, MMP-8, and MMP-12, respectively (Figure 2-8). This may contribute to the reduced potency of compound **3** relative to compound **2** against MMP-3. The 6-methyl substituent on the pyrone ring of **3** makes the ZBG more hydrophobic relative to **2**. The more polar active site environment generated by Asn162 in MMP-3 may disfavor binding of inhibitors with more hydrophobic ZBGs, hence, the difference in potency observed between compounds **2** and **3**. This may also explain the observation of MMPi **1** and **3** being more potent than **2** in the hydrophobic active sites of MMP-8 and MMP-12 versus the more polar active site of MMP-3.

Variation in active site polarity has been previously invoked to explain differences in the potency of a thirane-based inhibitor on two structurally homologous zinc metalloproteinases, TACE and MMP-2.<sup>34</sup> Together these results highlight the importance of the ZBG and the interactions they make within the MMP active site.

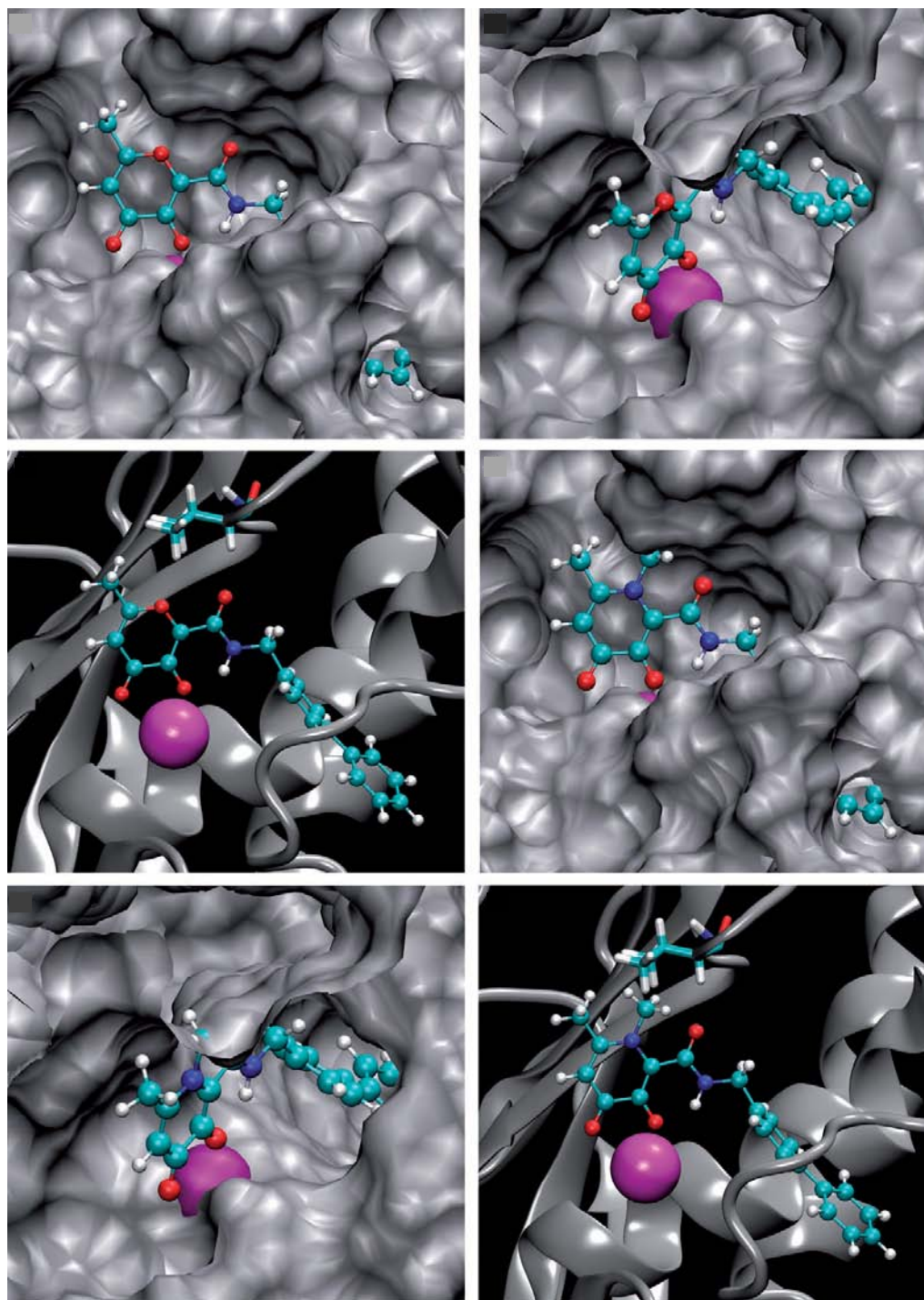


**Figure 2-7.** Three different views comparing the binding of MMPi **3** (left) and **5** (right) in the MMP-3 active site.  $\text{Zn}^{2+}$  ions are shown as magenta spheres, the MMPi in ball and stick colored by atom, and the protein in gray. The three views highlight the steric clash of the N-methyl group on compound **5** with the protein. Val163 (shown as sticks in the bottom views) is the residue that conflicts with the N-methyl substituent.

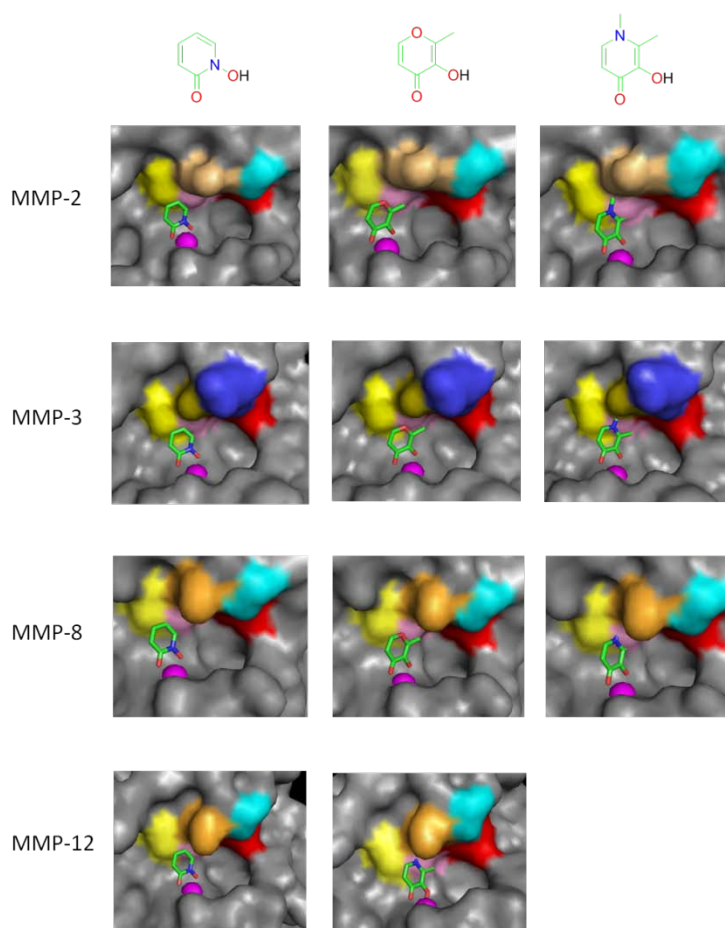


**Figure 2-8.** MMP active sites (gray surface) with different ZBGs. ZBGs are colored by atom: carbon (green), oxygen (red), nitrogen (blue). The  $Zn^{2+}$  ion is shown as a magenta sphere. Each row is representative of a different MMP (shown to the right) and each column of a different ZBG (shown above each column). Active site residues are colored as follows:

MMP-2: Gly162 (cyan), Leu163 (light orange), Leu164 (red), Ala165 (pink), His166 (yellow)

MMP-3: Asn162 (blue), Val163 (olive), Leu164 (red), Ala165 (pink), His166 (yellow)

MMP-8: Gly158 (cyan), Ile159 (orange), Leu160 (red), Ala161 (pink), His162 (yellow)

MMP-12: Gly179 (cyan), Ile180 (orange), Leu181 (red), Ala182 (pink), His183 (yellow)

## 2.G.ii Possible origin of ZBG-based selectivity

Based on the observations reported here, several factors may play a role in ZBG-generated selectivity in MMPi. First, ring sterics can affect inhibitor binding. As described above, compounds **4** and **5** are poor MMPi, as the addition of a methyl group at the 1-position on the ring is not well accommodated by the MMP active sites. In contrast, substitution at the 6-position of the ring, as in inhibitor **3**, is tolerated by several MMPs, and can be used as a means to select against MMP-2. This suggests a second ZBG effect that may be important, which is hydrophobicity. In general the MMP active site immediately surrounding the  $\text{Zn}^{2+}$  ion is relatively hydrophobic (Figure 2-8), but small differences in active site polarity can be exploited by changing the hydrophobicity and dipole of the ZBG. A third possible parameter in modulating ZBG-mediated selectivity is the  $\text{pK}_a$  of the chelating ZBG. In hydroxamic acid ZBGs, as well as all of the ZBGs examined here, there is a labile hydroxy proton that likely dissociates upon  $\text{Zn}^{2+}$  binding. It is known that different MMP isoforms operate at different optimal pH values,<sup>35-37</sup> and it has been shown that the protonation state of an MMPi can have a significant impact on inhibition.<sup>36</sup> Therefore, the differences in  $\text{pK}_a$  of different ZBGs may play a role in the inhibition and, thereby, the selectivity of a given inhibitor. The ZBGs examined in this study have  $\text{pK}_a$  values that span more than three log units.<sup>38</sup> All of the aforementioned factors will have an influence on the overall, preferred binding orientation of a ZBG in the MMP active site. The overall conformation of the bound ZBG will have consequences on the strength of the  $\text{Zn}^{2+}$ -inhibitor interaction, as well as on the positioning of the backbone toward the subsite(s). The synergism/interplay between the ZBG and backbone may also give rise

to new patterns of isoform selectivity, which could not be observed by only examining hydroxamic acid based MMPi. Ongoing computational and structural studies with even more inhibitors will be required to elucidate which of the aforementioned features is most important for tuning MMPi selectivity.

### **2.G.iii Ex vivo effects of the ZBG**

Perhaps the most significant effect of ZBG-modulated selectivity was observed in an ex vivo physiological model (Figure 2-6). Isolated perfused rat hearts were subjected to a temporary interruption of coronary flow and reflow to mimic the damage caused by IR. The isolated perfused rat heart system allows the examination of cardiac performance in the absence of influence from the nervous system or blood-borne cells.<sup>39,40</sup> This system has made it possible to identify factors which can mediate IR injury such as oxidative stress, protease activation, and apoptosis.<sup>27,28,41,42</sup> The system can also allow investigators to characterize compounds which may be able to confer cardioprotection upon an ischemic insult such as tetracyclines, antioxidants, or MMPi.<sup>27,41,43,44</sup> It has been demonstrated that MMPs play a role in mediating ischemia-reperfusion cardiac injury and that inhibition of MMP-2 by either broad-spectrum MMPi or neutralizing antibodies significantly protects from this injury.<sup>28</sup> In a study by Cheung et al, use of high concentrations (100  $\mu$ M) of the nonspecific MMPi *o*-phenanthroline or doxycycline resulted in substantial cardioprotective effects.<sup>28</sup> In our experimental model, 5  $\mu$ M of **2** yielded essentially no improvement in the recovery of contractile function. On the other hand, 5  $\mu$ M of **1** displayed an overall constant and progressive recovery after ischemia (average >80% versus controls



throughout reperfusion). Finally, negative control **6**, a compound that shows no substantial inhibition of MMPs, generally did not confer improvement versus the control group. As the difference in the molecular structure of the three compounds tested resides only in the ZBG, it is possible to establish for this study that the ZBG, rather than the peptidomimetic backbone, modulates the *ex vivo* efficacy as indicated by the recovery of cardiac contractile function.

#### **2.G.iv Expanding derivatives of 1,2-HOPO-2**

The aforementioned studies focused on various ZBGs appended to a constant biphenyl backbone and successfully showed the importance of the ZBG on selectivity against different MMP isoforms. From the *in vitro* and *ex vivo* studies performed, 1,2-HOPO-2 was shown to be one of the more potent MMP inhibitors synthesized. 1,2-HOPO-2 contains the metal chelating group 1-hydroxypyridin-2(1*H*)-one and as an extension to the ZBG study, was appended to different substituted biphenyl and pyridinyl backbones to achieve enhanced selectivity against different MMP isoforms.

#### **2.G.v Synthesis of 1,2-HOPO-2 derivatives**

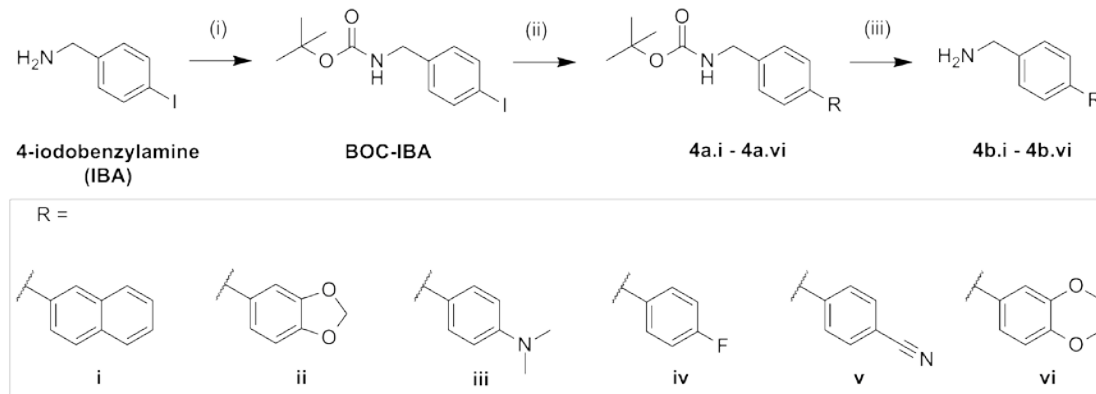
The choice of chemical additions to the biphenyl ring was arbitrary and new substitutions were chosen based on their synthetic accessibility. Due to the lack of commercially-available substituted phenylbenzylamines, new biphenyl amines were synthesized using Suzuki-Miyaura coupling conditions as outlined in Scheme 2-4. Aryl boronic acids were reacted with BOC (di-*tert*-butyl-dicarbonate) protected 4-iodo-benzylamine (**BOC-IBA**) and a palladium catalyst in the presence of a base to

produce various BOC-protected biphenyl amines. The BOC amines were then acid deprotected in TFA and  $\text{CH}_2\text{Cl}_2$  to yield the corresponding amines or triflate salts of the amines shown in Scheme 2-4.

A second set of biphenyl derivatives were synthesized using the Buchwald-Hartwig<sup>29</sup> coupling reaction and are summarized in Scheme 2-5. In general, different aryl halides were coupled with either 5-aminopicolonitrile or 4-aminobenzonitrile in the presence of cesium carbonate, palladium acetate, and Xantphos to form new nitrile backbones. These nitriles were then reduced to their corresponding amines in the presence of lithium aluminum hydride.

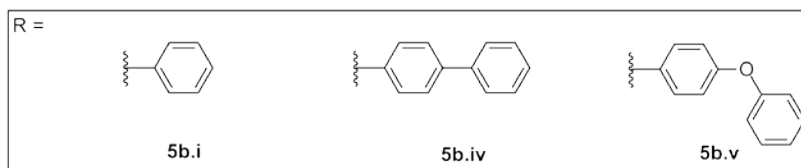
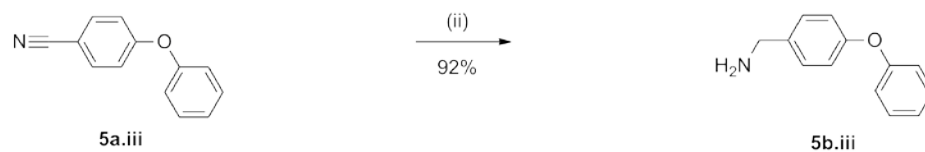
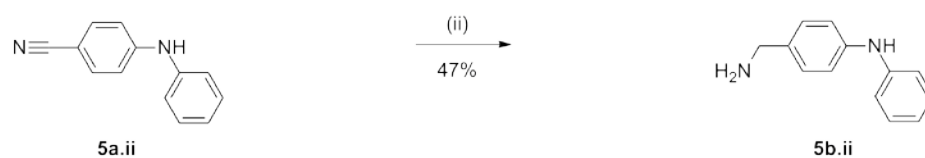
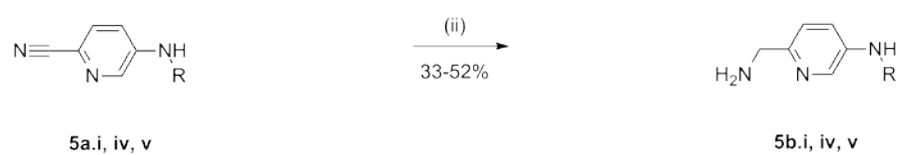
The amines generated through the Suzuki-Miyaura (**4b.i** – **4b.ii**) and Buchwald-Hartwig (**5b.i** – **5b.v**) reactions were then coupled to 1,2-HOPO acid (**1b** from Scheme 1) as outlined in Scheme 2-6 using EDCI (1-ethyl-3-(3-dimethylaminopropyl) carbodiimide) and HOBt (*N*-Hydroxybenzotriazole) peptide coupling reagents to generate novel 1,2-HOPO-2 derivatives. The derivatives were tested against different MMP isoforms as previously described and the  $\text{IC}_{50}$  values are listed in Table 2-2.

**Scheme 2-4.** Synthesis of Suzuki-Miyaura coupled biphenyl backbones<sup>d</sup>



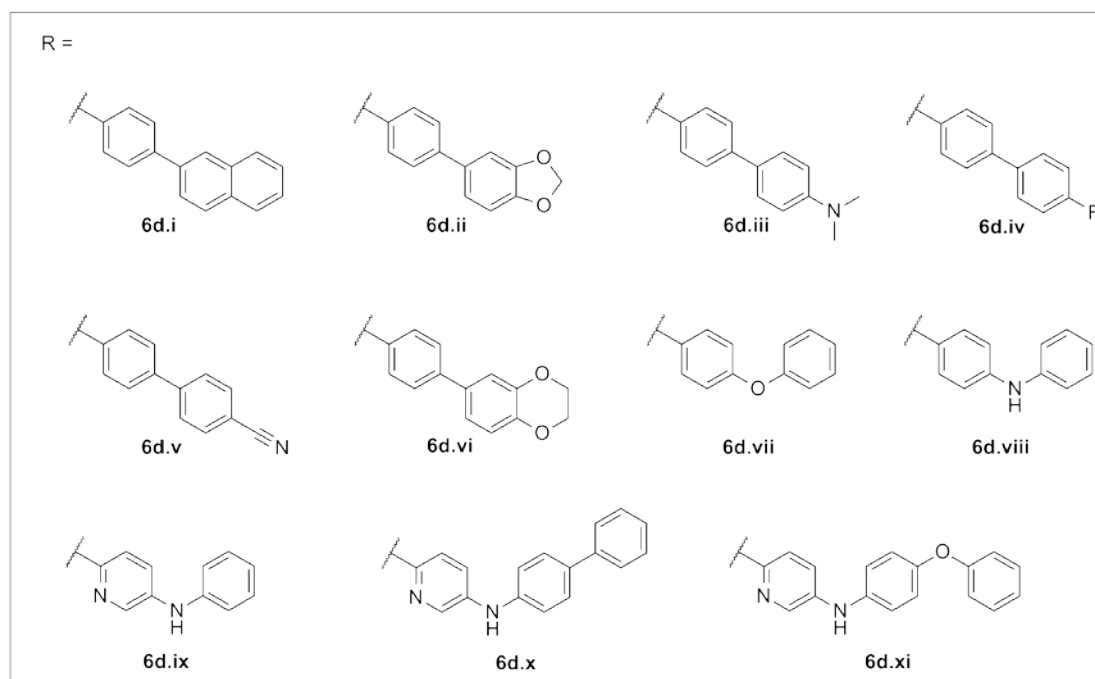
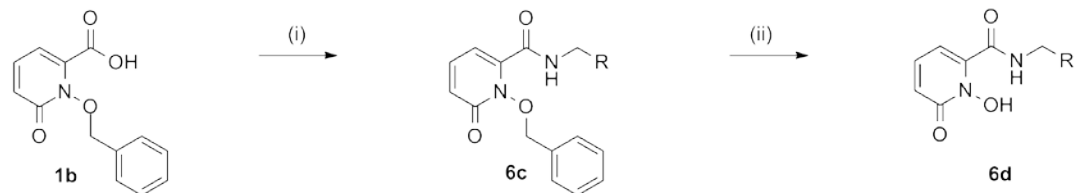
<sup>d</sup>Reagents and conditions: (i) di-*tert*-butyl dicarbonate (BOC), CH<sub>2</sub>Cl<sub>2</sub>, 75% (ii) boronic acid, Pd(C<sub>2</sub>H<sub>3</sub>O<sub>2</sub>)<sub>2</sub>, PPh<sub>3</sub>, 1:1 2 M K<sub>2</sub>CO<sub>3</sub>/toluene, 115 °C OR boronic acid, Pd(PPh<sub>3</sub>)<sub>4</sub>, 1:1 THF/H<sub>2</sub>O, excess Cs<sub>2</sub>CO<sub>3</sub>, MW synthesizer, 160 °C, 20 min OR boronic acid, Pd(PPh<sub>3</sub>)<sub>4</sub>, 1:1 THF/H<sub>2</sub>O, excess Cs<sub>2</sub>CO<sub>3</sub>, 115 °C OR boronic acid, Pd(PPh<sub>3</sub>)<sub>4</sub>, 1:1 2 M K<sub>2</sub>CO<sub>3</sub>/toluene, 115 °C (iii) 1:1 TFA/CH<sub>2</sub>Cl<sub>2</sub>, N<sub>2</sub>, 59-96%.

**Scheme 2-5.** Synthesis of pyridinyl and miscellaneous biphenyl backbones<sup>e</sup>



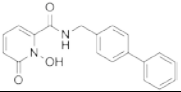
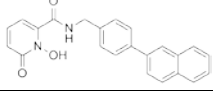
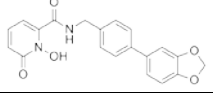
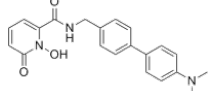
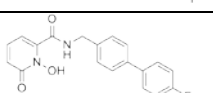
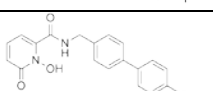
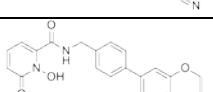
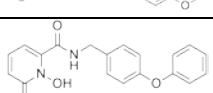
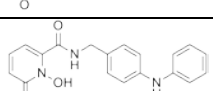
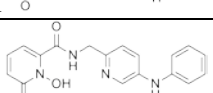
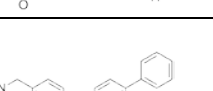
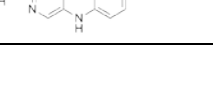
<sup>e</sup>Reagents and conditions: (i) Pd(C<sub>2</sub>H<sub>3</sub>O<sub>2</sub>)<sub>2</sub>, Xantphos, Cs<sub>2</sub>CO<sub>3</sub>, dioxane, 110 °C, N<sub>2</sub> (ii) LiAlH<sub>4</sub>, dry THF, 0 °C - room temperature, N<sub>2</sub>.

**Scheme 2-6.** Synthesis of 1,2-HOPO-2 derivatives<sup>f</sup>



<sup>f</sup>Reagents and conditions: (i) EDCI, HOBT, R-NH<sub>2</sub>, dry CH<sub>2</sub>Cl<sub>2</sub>, 19-97%. (ii) 1:1 HCl/glacial HOAc, 78-100%.

**Table 2-2.** IC<sub>50</sub> values (in  $\mu\text{M}$ ) of the different 1,2-HOPO-2 derivatives against different MMPs. Values are the average of two independent experiments performed in duplicate. For comparison, the IC<sub>50</sub> values of 1,2-HOPO-2 are also listed in the top row.

| MMP   | -2   | -3    | -8   | -9   | -12  | -14   |
|---|------|-------|------|------|------|-------|
| 1,2-HOPO-2<br> | 0.92 | 0.56  | 0.09 | 27.0 | 0.02 | n.d.  |
| 6d.i<br>       | >50  | 0.49  | >50  | >50  | 0.40 | n.d.  |
| 6d.ii<br>      | 0.28 | 0.17  | 0.11 | 3.6  | 0.07 | n.d.  |
| 6d.iii<br>     | 0.08 | 0.07  | 0.30 | 1.1  | 0.02 | n.d.  |
| 6d.iv<br>      | 0.35 | 0.08  | 0.03 | 1.3  | 0.04 | 1.75  |
| 6d.v<br>       | 0.04 | 0.001 | 0.03 | 1.3  | 0.03 | n.d.  |
| 6d.vi<br>     | 0.62 | 0.05  | 0.19 | 2.6  | 0.04 | 15-50 |
| 6d.vii<br>   | 2.0  | 0.03  | 4.4  | 16.0 | 3.7  | n.d.  |
| 6d.viii<br>  | 0.31 | 0.03  | 0.17 | 2.1  | 0.14 | n.d.  |
| 6d.ix<br>    | 0.60 | 0.003 | 0.84 | 4.6  | 0.56 | n.d.  |
| 6d.x<br>     | 7.9  | 0.16  | 2.5  | 43.0 | 5.5  | n.d.  |
| 6d.xi<br>    | 3.8  | 0.23  | 3.6  | 82.0 | 2.4  | n.d.  |

### 2.G.vi Activity of 1,2-HOPO-2 derivatives

Table 2-2 compares the IC<sub>50</sub> values calculated for the various derivatives relative to 1,2-HOPO-2. Compound **6d.i**, which has a naphthyl group on the backbone, completely abrogates activity against MMP-2, -8, and -9 while maintaining potency for MMP-3 and MMP-12, making **6d.i** a more selective inhibitor for MMP-8 and MMP-12 than 1,2-HOPO-2. The substituents of compounds **6d.ii-vi** results in compounds displaying broad-spectrum inhibition. Compound **6d.viii** is unstable and the values shown in Table 2-2 are unreliable. Compound **6d.viii** is isolated as a green solid and appears pure as gauged by <sup>1</sup>H and <sup>13</sup>C NMR, but the compound turns into a dark green residue when left at room temperature. Compounds **6d.vii** and **6d.ix** are two of the first MMP-3 selective inhibitors to be generated from our lab, and show selectivity over the other MMP isoforms by at least 60-fold and 180-fold respectively. The backbone utilized in **6d.vii** is very commonly used in gelatinase specific (MMP-2 and -9) inhibitors;<sup>30,31</sup> which indirectly lends credence once again to the role the ZBG plays in MMP targeted specificity. Compound **6d.ix** is by far the most potent MMP-3 inhibitor to date from our lab and is over 180-fold more potent over the other MMP isoforms. In summary, the current backbone study proved to be very fruitful in transforming a MMP-8 and MMP-12 selective inhibitor (1,2-HOPO-2) into a MMP-3 specific inhibitor. Overall, the compounds in Table 2-2 show both broad and selective inhibitory action that can hopefully be used in future studies of these interesting MMPi.

## 2.H Conclusions

The results presented here are the first to demonstrate that a change in ZBG can modulate, as opposed to simply abrogate, the potency and selectivity observed for MMPi against different MMP isoforms. It is proposed that the backbone substituent can be used to obtain an initial degree of selectivity (for example, shallow versus deep pocket S1' MMPs), whereas the ZBG can then be optimized to fine tune inhibition to obtain further specificity. Furthermore, results from an *ex vivo* rat heart system demonstrate that the choice of ZBG can also have a substantial impact on inhibitor efficacy in a biological model. This latter finding indicates that to discover MMPi with better clinical prospects, molecular platforms other than hydroxamic acids should be explored. Recent work in the literature has suggested that ZBGs with weaker binding constants may be one route to obtaining more selective MMPi.<sup>45</sup> In contrast, the unique findings reported herein strongly suggest that high affinity ZBGs can be used as the basis for new patterns of selective inhibition against MMPs. Ongoing studies using *in vitro*, as well as relevant preclinical systems, will be required to fully exploit this new discovery and to wholly understand the origin of the observed trends in selectivity.



## 2.I Experimental

Unless otherwise noted, all chemicals were purchased from commercial suppliers and used as received. Flash silica gel chromatography was performed using Merck silica gel 40-63  $\mu\text{m}$  mesh. Inert reactions were carried out under a dinitrogen atmosphere.  $^1\text{H}/^{13}\text{C}$  NMR spectra were recorded at ambient temperature on a 300, 400 or 500 MHz Varian FT-NMR instrument at the Department of Chemistry and Biochemistry, University of California San Diego. Mass spectra were obtained at the Small Molecule Mass Spectrometry Facility in the Department of Chemistry and Biochemistry at the University of California, San Diego. Elemental Analysis was performed by NuMega Resonance Labs, San Diego.

### 2.I.i Synthesis of MMPi in Schemes 2-1 to 2-3

**1-Hydroxy-6-oxo-1,6-dihydropyridine-2-carboxylic acid (1a):** The synthesis is based on a literature procedure.<sup>46</sup> 80 mL of acetic anhydride and 20 mL of 30% hydrogen peroxide were combined and stirred under  $\text{N}_2$  for 4 h in an ice-bath to form a peracetic acid solution. 120 mL of trifluoroacetic acid (TFA) and 80 mL of glacial acetic acid were added to 20 g (144 mmol) of 6-hydroxypicolinic acid (6-HPA) in a separate flask and turned a dark brown solution. The peracetic acid solution was added drop wise to the dark brown solution and the mixture was stirred under  $\text{N}_2$  for 1 h. A suspension formed that fully dissolved after 1 h to a clear orange solution that was heated to reflux at 80  $^\circ\text{C}$  for 10 h under  $\text{N}_2$  giving an off-white precipitate. The reaction was cooled to room temperature and then cooled to 4  $^\circ\text{C}$  for 5-6 h to allow more precipitate to crash out. The precipitate was vacuum filtered, washed with cold MeOH, and dried in a vacuum oven overnight. The dried precipitate was dissolved in

40 mL of 10% KOH and refluxed at 80 °C under N<sub>2</sub> for 6 h to yield an off-white precipitate in a clear orange solution. Concentrated HCl was added to the orange solution, which was cooled to 4 °C overnight to generate more precipitate. The combined precipitates were vacuum filtered, washed with water, and dried to yield 10.8 g (70 mmol) of an off-white solid. Yield = 48%. <sup>1</sup>H NMR (400 MHz, DMSO-*d*<sub>6</sub>): δ 6.64 (dd, *J* = 6.8, 1.2 Hz, 1H; ArH), 6.72 (dd, *J* = 9.2, 1.2 Hz, 1H; ArH), 7.43 (dd, *J* = 9.0, 7.2 Hz, 1H; ArH). ESI-MS(-): *m/z* 153.93 [M-H]<sup>-</sup>.

**1-(Benzyloxy)-6-oxo-1,6-dihydropyridine-2-carboxylic acid (1b):** The synthesis is based on a literature procedure.<sup>46</sup> 7.2 g (46.4 mmol) of compound **1a**, 10.6 mL (11.7 g, 92.8 mmol) of benzyl chloride, and 12.8 g (92.8 mmol) of K<sub>2</sub>CO<sub>3</sub> were mixed in 115 mL of MeOH. The mixture was heated to reflux for 16 h at 75 °C under N<sub>2</sub>, vacuum filtered, and the filtrate was evaporated to dryness. The resulting light brown residue was dissolved in water with heat. The solution was acidified to pH 2 with 6 N HCl and the resulting precipitate was vacuum filtered, washed with cold water, and oven-dried to yield 10.5 g (42.8 mmol) of an off-white solid. Yield = 92%. <sup>1</sup>H NMR (400 MHz, DMSO-*d*<sub>6</sub>): δ 5.27 (s, 2H; CH<sub>2</sub>), 6.56 (dd, *J* = 7, 1.2 Hz, 1H; ArH), 6.74 (dd, *J* = 9.4, 1.8 Hz, 1H; ArH), 7.40-7.51 (m, 6H; ArH).

***N*-([1,1'-Biphenyl]-4-ylmethyl)-1-(benzyloxy)-6-oxo-1,6-dihydropyridine-2-carboxamide (1,2-HOPO-2P):** 10.5 g (42.8 mmol) of compound **1b** was dissolved in 150 mL of dry THF. 4.9 g (42.8 mmol) of *N*-hydroxysuccinimide (NHS) was added to the flask and the mixture was stirred for 30 min under N<sub>2</sub> to a clear yellow solution. 8.8 g (42.8 mmol) of *N,N'*-dicyclohexylcarbodiimide (DCC) was added to the solution and stirred for 3 h under N<sub>2</sub> to yield the activated ester shown in the scheme above.

The solution was vacuum filtered to remove the precipitated dicyclohexylurea DCU. 7.8 g (42.8 mmol) of 4-phenylbenzylamine was added to the clear amber filtrate and the mixture was stirred for 40 h at room temperature under N<sub>2</sub>. The solution was evaporated to an off-white residue, dissolved in a minimal amount of CH<sub>2</sub>Cl<sub>2</sub>, extracted (3×) with saturated NaHCO<sub>3</sub>, and the organic layer was dried over anhydrous MgSO<sub>4</sub>. MgSO<sub>4</sub> was filtered off and the filtrate was evaporated to an off-white residue. The residue was sonicated in a minimal amount of MeOH to remove any remaining DCU. The solution was vacuum filtered and the precipitate was oven-dried to yield 14.4 g (35 mmol) of a white solid of **1,2-HOPO-2P**. Yield = 82%. <sup>1</sup>H NMR (400 MHz, DMSO-*d*<sub>6</sub>): δ 4.48 (d, *J* = 6 Hz, 2H; CH<sub>2</sub>), 5.24 (s, 2H; OCH<sub>2</sub>), 6.38 (dd, *J* = 6.4, 1.6 Hz, 1H; ArH), 6.68 (dd, *J* = 9.4, 1.4 Hz, 1H; ArH), 7.36-7.62 (m, 15H; ArH), 9.46 (t, *J* = 5.8 Hz, 1H; CONHCH<sub>2</sub>). APCI-MS(+): *m/z* 410.85 [M+H]<sup>+</sup>.

***N*-([1,1'-Biphenyl]-4-ylmethyl)-1-hydroxy-6-oxo-1,6-dihydropyridine-2-carboxamide (1,2-HOPO-2)**: To 6.2 g (15.1 mmol) of **1,2-HOPO-2P** was added 180 mL of a 1:1 solution of concentrated HCl and glacial acetic acid. The solution was stirred at room temperature for 5 d to obtain a white milky solution. The solution was evaporated to dryness to yield a white residue which was further co-evaporated with methanol (3×) and the solid was dried in a vacuum oven overnight to yield 4.8 g (14.8 mmol) of a white solid of **1,2-HOPO-2**. Yield = 98%. <sup>1</sup>H NMR (400 MHz, DMSO-*d*<sub>6</sub>): δ 4.47 (d, *J* = 6 Hz, 2H; CH<sub>2</sub>), 6.35 (dd, *J* = 6.8, 1.6 Hz, 1H; ArH), 6.59 (dd, *J* = 9, 1.4 Hz, 1H; ArH), 7.32-7.65 (m, 10H; ArH), 9.35 (t, *J* = 5.8 Hz, 1H; CONHCH<sub>2</sub>). APCI-MS(-): *m/z* 319.11 [M-H]<sup>-</sup>. HR-EI-MS Calculated for C<sub>19</sub>H<sub>16</sub>N<sub>2</sub>O<sub>3</sub>: 320.1155.

Expected: 320.1158. Anal. Calcd for C<sub>19</sub>H<sub>16</sub>N<sub>2</sub>O<sub>3</sub>: C, 71.24; H, 5.03; N, 8.74. Found: C, 70.95; H, 5.15; N, 8.70.

**3-(Benzyloxy)-4-oxo-4H-pyran-2-carbaldehyde (2a):** 4.39 mL (5 g, 23 mmol) of benzyl maltol and 62 mL of fresh bromobenzene were heated to 105 °C and stirred for 5 min. To the solution was added 7.65 g (69 mmol) of selenium dioxide and the mixture was refluxed at 150 °C for 40 h under N<sub>2</sub>. The solution turned dark brown with a black residue on the bottom. The solution was vacuum filtered over a layer of sand to remove the selenium dioxide. The filtrate was diluted with diethyl ether, filtered to remove insoluble impurities, and then evaporated to dryness to yield 2.4 g (10.4 mmol) of a brown oil. Yield = 45%. <sup>1</sup>H NMR (400 MHz, DMSO-*d*<sub>6</sub>): δ 5.34 (s, 2H; CH<sub>2</sub>), 6.61 (d, *J* = 4.8 Hz, 1H; ArH), 7.32-7.39 (m, 5H; ArH), 8.23 (d, *J* = 5.6 Hz, 1H; ArH), 9.82 (s, 1H; COH).

**3-(Benzyloxy)-4-oxo-4H-pyran-2-carboxylic acid (2b):** To a flask containing 2.4 g (10.4 mmol) of compound **2a** was added 50 mL of a 1:1 solution of acetone and water. 1.4 g (14.6 mmol) of sulfamic acid and 988 mg (10.9 mmol) of 80% sodium chlorite were added to the clear orange solution which turned yellow. The solution was stirred at room temperature for 6 h, evaporated to dryness, and dried in a vacuum oven to yield 1.5 g (6.1 mmol) of an off-white solid. Yield = 59%. <sup>1</sup>H NMR (400 MHz, DMSO-*d*<sub>6</sub>): δ 5.10 (s, 2H; CH<sub>2</sub>), 6.54 (d, *J* = 6 Hz, 1H; ArH), 7.31-7.43 (m, 5H; ArH), 8.20 (d, *J* = 6 Hz, 1H; ArH).

**N-([1,1'-Biphenyl]-4-ylmethyl)-3-(benzyloxy)-4-oxo-4H-pyran-2-carboxamide (PY-2P):** 500 mg (2 mmol) of compound **2b** was dissolved in 30 mL of dry THF to give clear yellow solution. 4-Phenylbenzylamine was coupled to **2b** in an

identical fashion to that reported above for compound **1b**. 520 mg (1.3 mmol) of a white solid was obtained. Yield = 62%. <sup>1</sup>H NMR (400 MHz, DMSO-*d*<sub>6</sub>): δ 4.45 (d, *J* = 6 Hz, 2H; CH<sub>2</sub>), 5.16 (s, 2H; OCH<sub>2</sub>), 6.54 (d, *J* = 5.6 Hz, 1H; ArH), 7.29-7.64 (m, 14H; ArH), 8.22 (d, *J* = 5.6 Hz, 1H; ArH), 9.19 (t, *J* = 2.8 Hz, 1H; CONHCH<sub>2</sub>). ESI-MS(+): *m/z* 410.95 [M+H]<sup>+</sup>. HR-EI-MS Calculated for C<sub>26</sub>H<sub>21</sub>NO<sub>4</sub>: 411.1472. Expected 411.1465.

***N*-([1,1'-Biphenyl]-4-ylmethyl)-3-hydroxy-4-oxo-4*H*-pyran-2-carboxamide (PY-2)**: Deprotection of **PY-2P** was identical to that of **1,2-HOPO-2P** described above. 500 mg (1.3 mmol) of **PY-2P** was treated with acid to yield 365 mg (1.1 mmol) of a white solid. Yield = 94%. <sup>1</sup>H NMR (400 MHz, DMSO-*d*<sub>6</sub>): δ 4.53 (d, *J* = 7.6 Hz, 2H; CH<sub>2</sub>), 6.48 (d, *J* = 7.2 Hz, 1H; ArH), 7.39-7.65 (m, 9H; ArH), 8.18 (d, *J* = 7.2 Hz, 1H; ArH), 9.36 (s, 1H; CONHCH<sub>2</sub>). APCI-MS(-): *m/z* 320.06 [M-H]<sup>-</sup>. HR-EI-MS Calculated for C<sub>19</sub>H<sub>15</sub>NO<sub>4</sub>: 321.0993. Expected 321.0996. Anal. Calcd for C<sub>19</sub>H<sub>15</sub>NO<sub>4</sub>: C, 71.02; H, 4.71; N, 4.36. Found: C, 71.15; H, 5.04; N, 4.43.

***N*-([1,1'-Biphenyl]-4-ylmethyl)-3-hydroxy-6-methyl-4-oxo-4*H*-pyran-2-carboxamide (AM-2)**: This compound was prepared as previously reported.<sup>13</sup> <sup>1</sup>H NMR (400 MHz, DMSO-*d*<sub>6</sub>): δ 2.30 (s, 3H; CH<sub>3</sub>), 4.52 (d, *J* = 6.4 Hz, 2H; CH<sub>2</sub>), 6.32 (s, 1H; ArH), 7.32-7.64 (m, 9H; ArH), 9.34 (t, *J* = 6 Hz, 1H; CONHCH<sub>2</sub>). ESI-MS(+): *m/z* 335.95 [M+H]<sup>+</sup>. Anal. Calcd for C<sub>20</sub>H<sub>17</sub>NO<sub>4</sub>: C, 71.63; H, 5.11; N, 4.18. Found: C, 71.44; H, 5.42; N, 4.04.

***N*-([1,1'-Biphenyl]-4-ylmethyl)-3-(benzyloxy)-1-methyl-4-oxo-1,4-dihydropyridine-2-carboxamide (PY-NMe-2P)**: Synthesis of this compound was based on a procedure by Robert Hider *et al.*<sup>47,48</sup> To 100 mg (0.24 mmol) of **PY-2P** was

added 5 mL of a 1:1 solution of EtOH and H<sub>2</sub>O to produce a white suspension. The suspension was heated to 80 °C. To the suspension was added 5 mL of a 1:4 solution of 40% methylamine and H<sub>2</sub>O in a drop wise fashion. The solution turned yellow after 15 min. The reaction was stirred for 17 h and a cream colored precipitate settled on the bottom. The reaction was cooled to room temperature, the precipitate was vacuum filtered and oven-dried to yield 75 mg (0.18 mmol) of a white solid. Yield = 75%. <sup>1</sup>H NMR (400 MHz, DMSO-*d*<sub>6</sub>): δ 3.56 (s, 3H; NCH<sub>3</sub>), 4.48 (d, *J* = 10 Hz, 2H; CH<sub>2</sub>), 5.08 (s, 2H; OCH<sub>2</sub>), 6.26 (d, *J* = 7.2 Hz, 1H; ArH), 7.48-7.60 (m, 14H; ArH), 7.67 (d, *J* = 7.2 Hz, 1H; ArH), 9.44 (t, *J* = 6.2 Hz, 1H; CONHCH<sub>2</sub>). ESI-MS(+): *m/z* 425.02 [M+H]<sup>+</sup>.

***N*-([1,1'-Biphenyl]-4-ylmethyl)-3-hydroxy-1-methyl-4-oxo-1,4-dihydropyridine-2-carboxamide (PY-NMe-2):** Deprotection of **PY-NMe-2P** was similar to that of **1,2-HOPO-2P** described above. 50 mg (0.12 mmol) of **PY-NMe-2P** was deprotected to yield 26 mg (0.08 mmol) of a white solid. Yield = 67%. <sup>1</sup>H NMR (400 MHz, DMSO-*d*<sub>6</sub>): δ 3.81 (s, 3H; NCH<sub>3</sub>), 4.54 (d, *J* = 6 Hz, 2H; CH<sub>2</sub>), 6.84 (d, *J* = 6 Hz, 1H; ArH), 7.34-7.67 (m, 9H; arH), 8.00 (d, *J* = 7.2 Hz, 1H; ArH), 9.50 (t, *J* = 5.8 Hz, 1H; CONHCH<sub>2</sub>). APCI-MS(-): *m/z* 333.08 [M-H]<sup>-</sup>. Anal. Calcd for C<sub>20</sub>H<sub>18</sub>N<sub>2</sub>O<sub>3</sub>•0.4H<sub>2</sub>O: C, 70.33; H, 5.55; N, 8.20. Found: C, 70.20; H, 5.79; N, 8.44.

***N*-([1,1'-Biphenyl]-4-ylmethyl)-3-(benzyloxy)-1,6-dimethyl-4-oxo-1,4-dihydropyridine-2-carboxamide (AM-NMe-2P):** Synthesis of **AM-NMe-2P** was identical to that described above for **PY-NMe-2P**. 100 mg (0.24 mmol) of **AM-2P** was used to yield 67 mg (0.15 mmol) of a yellow solid of **AM-NMe-2P**. Yield = 64%. <sup>1</sup>H NMR (400 MHz, DMSO-*d*<sub>6</sub>): δ 2.31 (s, 3H; CH<sub>3</sub>), 3.45 (s, 3H; NCH<sub>3</sub>), 4.48 (d, *J* =

7.2 Hz, 2H;  $CH_2$ ), 5.05 (s, 2H;  $OCH_2$ ), 6.24 (s, 1H; ArH), 7.31-7.65 (m, 14H; ArH), 9.43 (t,  $J = 6.8$  Hz, 1H;  $CONHCH_2$ ). ESI-MS(+):  $m/z$  439.06  $[M+H]^+$ .

***N*-([1,1'-Biphenyl]-4-ylmethyl)-3-hydroxy-1,6-dimethyl-4-oxo-1,4-dihydropyridine-2-carboxamide (AM-NMe-2):** Deprotection of **AM-NMe-2P** was similar to that of **1,2-HOPO-2P** described above 50 mg (0.11 mmol) of **AM-NMe-2P** was treated with acid to yield 32 mg (0.09 mmol) of a white solid of **AM-NMe-2**. Yield = 82%.  $^1H$  NMR (400 MHz,  $DMSO-d_6$ ):  $\delta$  2.50 (s, 3H;  $CH_3$ ), 3.70 (s, 3H;  $NCH_3$ ), 4.56 (d,  $J = 6$  Hz, 2H;  $CH_2$ ), 6.93 (s, 1H; ArH), 7.33-7.68 (m, 9H; ArH), 9.54 (t,  $J = 5.8$  Hz, 1H;  $CONHCH_2$ ). APCI-MS(-):  $m/z$  347.05  $[M-H]^-$ . HR-EI-MS Calculated for  $C_{21}H_{20}N_2O_3$ : 348.1470. Expected 348.1468. Anal. Calcd for  $C_{21}H_{20}N_2O_3 \cdot 0.5H_2O$ : C, 70.57; H, 5.92; N, 7.84. Found: C, 70.40; H, 6.00; N, 8.21.

Compounds PICO-2 and *m*-ANISIC-2 were synthesized by Jennifer Jacobsen in the lab.

## 2I.ii Synthesis of backbones in Schemes 2-4 and 2-5

***tert*-Butyl 4-iodobenzylcarbamate (BOC-IBA):** Combined 2.74 g (11.8 mmol) of 4-iodobenzylamine, 2.58 g (11.8 mmol, 1 eq) of di-*tert*-butyldicarbonate and 50 ml of methylene chloride in a 100 ml RB flask. The solution was milky white. Stirred solution overnight at RT under  $N_2$  and turned a clear yellow. Added 50 ml more of methylene chloride to dilute while stirring. Washed solution 3 times with 5% citric acid and 3 times with brine. Extracted organic layer, dried over anhydrous magnesium sulfate and vacuum filtered. Rotovaped filtrate to a cream residue. Sonicated residue in 50 ml of hexanes to remove impurities, vacuum filtered and put filtrate in fridge to allow more precipitate to crash out. Vacuum filtered precipitate,

and oven dried to yield 2.98 g (0.9 mmol) of an off-white solid. Yield = 75%.  $^1\text{H}$  NMR (400 MHz,  $\text{CDCl}_3$ - $d_1$ ):  $\delta$  1.450 (s, 10 H), 4.247 (d,  $J = 8$  Hz, 2H), 4.838 (brs, 1H, NH), 7.028 (d,  $J = 11.2$  Hz, 1H), 7.646 (d,  $J = 11.2$  Hz, 1H). ESI-MS(+):  $m/z$  355.85  $[\text{M}+\text{Na}]^+$ .

***tert*-Butyl 4-(naphthalen-2-yl)benzylcarbamate (4a.i):** BOC-IBA (500 mg, 1.50 mmol), naphthaleneboronic acid (1.5 equiv., 2.25 mmol, 387 mg), tetrakis(triphenylphosphine)palladium (0.1 equiv., 0.15 mmol, 173 mg) and 2 mL of 1 M  $\text{Cs}_2\text{CO}_3$  were reacted in 30 mL of a 1:1 solution of THF and  $\text{H}_2\text{O}$  and heated to reflux at 110 °C for 16 h under  $\text{N}_2$ . The reaction mixture was filtered over a bed of celite to efficiently remove the palladium catalyst and the filtrate was extracted with  $\text{CH}_2\text{Cl}_2$ . The organic phase was dried over anhydrous  $\text{MgSO}_4$ , and the crude product was evaporated in vacuo and purified via column chromatography in 40-60%  $\text{CH}_2\text{Cl}_2$ /hexanes to yield 290 mg (0.87 mmol) of product. Yield = 58%.  $^1\text{H}$  NMR (500 MHz,  $\text{CDCl}_3$ , 25 °C):  $\delta = 1.56$  (s, 9H;  $\text{C}(\text{CH}_3)_3$ ), 4.38 (d,  $J = 5.2$  Hz, 2H;  $\text{NHCH}_2$ ), 7.39 (d,  $J = 8.0$  Hz, 2H; ArH), 7.46 (p,  $J = 6.9$  Hz, 2H; ArH), 7.68 (d,  $J = 8.0$  Hz, 2H; ArH), 7.72 (d,  $J = 8.6$  Hz, 1H; ArH), 7.85 (m, 3H; ArH), 8.02 (s, 1H; ArH). ESI-MS(+)  $m/z$  356.09  $[\text{M}+\text{Na}]^+$ .

**(4-(Naphthalen-2-yl)phenyl)methanamine (4b.i):** 234 mg (0.70 mmol) of **4a.i** was deprotected in 30 mL of a 1:1 solution of TFA and  $\text{CH}_2\text{Cl}_2$  which stirred overnight at room temperature. Both solvents were evacuated with  $\text{N}_2$ ; and diethyl ether was added to the flask to induce precipitation of 144 mg (0.41 mmol) a tan solid of the triflate salt. Yield = 59%.  $^1\text{H}$  NMR (400 MHz,  $\text{CDCl}_3$ , 25 °C):  $\delta = 4.07$  (s, 2H;



NHCH<sub>2</sub>), 7.46 (m, 4H; ArH), 7.66 (dd, *J* = 1.6, 7.2 Hz, 1H; ArH), 7.72 (d, *J* = 8.0 Hz, 2H; ArH), 7.83 (m, 3H; ArH), 7.97 (s, 1H; ArH). ESI-MS(+) *m/z* 233.82 [M+H]<sup>+</sup>.

***tert*-Butyl 4-(benzo[d][1,3]dioxol-5-yl)benzylcarbamate (4a.ii):** This compound was prepared from **BOC-IBA** according to the procedure outlined for **4a.i**. **BOC-IBA** (1.0 g, 3.00 mmol), 3,4-(methylenedioxy)-phenylboronic acid (4.50 mmol, 746 mg) and tetrakis(triphenylphosphine)palladium (0.30 mmol, 346 mg) were reacted in 50 mL of a 1:1 solution of toluene and 2 M K<sub>2</sub>CO<sub>3</sub> for 16 h under N<sub>2</sub>. The crude product was purified via column chromatography in CH<sub>2</sub>Cl<sub>2</sub> to yield 661 mg (2.02 mmol) of a white solid. Yield = 67%. <sup>1</sup>H NMR (400 MHz, CDCl<sub>3</sub>, 25 °C): δ = 1.47 (s, 9H), 4.34 (d, *J* = 6.0 Hz, 2H), 4.86 (brs, 1H), 6.00 (s, 2H), 6.86 (d, *J* = 8.8 Hz, 1H; ArH), 7.03 (m, 2H; ArH), 7.31 (d, *J* = 8.0 Hz, 2H; ArH), 7.46 (d, *J* = 8.0 Hz, 2H; ArH). ESI-MS(+) *m/z* 327.82 [M+H]<sup>+</sup>.

**(4-(Benzo[d][1,3]dioxol-5-yl)phenyl)methanamine (4b.ii):** This compound was prepared from **4a.ii** according to the procedure outlined for **4a.i**. **4a.ii** (623 mg, 1.90 mmol) was deprotected and upon evaporation of TFA, the resulting residue was extracted with 1 N NaOH and CH<sub>2</sub>Cl<sub>2</sub>. The organic phase was dried over anhydrous MgSO<sub>4</sub> and evaporated in vacuo to yield 360 mg (1.58 mmol) of an off-white solid. Yield = 83%. <sup>1</sup>H NMR (500 MHz, CDCl<sub>3</sub>, 25 °C): δ = 3.89 (s, 2H), 5.99 (s, 2H), 6.86 (d, *J* = 7.4 Hz, 1H; ArH), 7.04 (d, *J* = 9.1 Hz, 2H; ArH), 7.34 (d, *J* = 8.0 Hz, 2H; ArH), 7.47 (d, *J* = 8.0 Hz, 2H; ArH). ESI-MS(+) *m/z* 227.82 [M+H]<sup>+</sup>.

***tert*-Butyl (4'-(dimethylamino)biphenyl-4-yl)methylcarbamate (4a.iii):** This compound was prepared from **BOC-IBA** according to the procedure outlined for **4a.i**. **BOC-IBA** (1.0 g, 3.00 mmol), 4-(dimethylamino)phenylboronic acid (1.4 equiv., 4.20

mmol, 695 mg) and tetrakis(triphenylphosphine)palladium (0.30 mmol, 346 mg) were reacted in 50 mL of a 1:1 solution of toluene and 2 M K<sub>2</sub>CO<sub>3</sub>. The crude product was purified via column chromatography in 0-1% MeOH/CH<sub>2</sub>Cl<sub>2</sub> to yield 657 mg (2.01 mmol) of a cream solid. Yield = 67%. <sup>1</sup>H NMR (500 MHz, CDCl<sub>3</sub>, 25 °C): δ = 1.46 (s, 9H), 2.99 (s, 6H), 4.32 (d, *J* = 5.7 Hz, 2H), 4.82 (brs, 1H), 6.79 (d, *J* = 8.6 Hz, 2H; ArH), 7.29 (d, *J* = 8.0 Hz, 2H; ArH), 7.47 (d, *J* = 8.6 Hz, 2H; ArH), 7.50 (d, *J* = 8.0 Hz, 2H; ArH). ESI-MS(+) *m/z* 327.23 [M+H]<sup>+</sup>.

**4'-(Aminomethyl)-*N,N*-dimethylbiphenyl-4-amine (4b.iii):** This compound was prepared from **4a.iii** according to the procedure outlined for **4a.i**. **4a.iii** (657 mg, 2.01 mmol) was de-protected to yield 527 mg (1.54 mmol) of a grey solid. Yield = 77%. <sup>1</sup>H NMR (500 MHz, CD<sub>3</sub>OD, 25 °C): δ = 2.96 (s, 6H), 4.09 (s, 2H), 6.84 (d, *J* = 8.6 Hz, 2H; ArH), 7.43 (d, *J* = 8.0 Hz, 2H; ArH), 7.50 (d, *J* = 8.6 Hz, 2H; ArH), 7.61 (d, *J* = 8.0 Hz, 2H; ArH). ESI-MS(+) *m/z* 227.22 [M+H]<sup>+</sup>.

**tert-Butyl (4'-fluorobiphenyl-4-yl)methylcarbamate (4a.iv):** This compound was prepared from **BOC-IBA** according to the procedure outlined for **4a.i**. **BOC-IBA** (1.0 g, 3.00 mmol), 4-fluoroboronic acid (1.5 equiv., 4.50 mmol, 629 mg) and tetrakis(triphenylphosphine)palladium (0.1 equiv., 0.30 mmol, 346 mg) were reacted in 60 mL of a 1:1 solution of toluene and 2 M K<sub>2</sub>CO<sub>3</sub> and heated to reflux at 115 °C for 16 h under N<sub>2</sub>. The crude product was purified via column chromatography in CH<sub>2</sub>Cl<sub>2</sub> to yield 687 mg (2.28 mmol) of a white solid. Yield = 76%. <sup>1</sup>H NMR (500 MHz, CDCl<sub>3</sub>, 25 °C): δ = 1.46 (s, 9H), 4.35 (d, *J* = 5.7 Hz, 2H), 4.87 (brs, 1H), 7.10 (t, *J* = 8.9 Hz, 2H; ArH), 7.33 (d, *J* = 8.0 Hz, 1H; ArH), 7.49 (d, *J* = 8.0 Hz, 3H; ArH), 7.50 (m, 2H; ArH). ESI-MS(+) *m/z* 301.75 [M+H]<sup>+</sup>.

**(4'-Fluorobiphenyl-4-yl)methanamine (4b.iv):** This compound was prepared from **4a.iv** according to the procedure outlined for **4a.i**. **4a.iv** (687 mg, 2.28 mmol) was de-protected to yield 366 mg (1.53 mmol) of a silvery white triflate salt. Yield = 67%. <sup>1</sup>H NMR (500 MHz, CDCl<sub>3</sub>, 25 °C): δ = 4.13 (s, 2H), 7.15 (td, *J* = 8.6, 1.7 Hz, 2H; ArH), 7.50 (d, *J* = 6.3 Hz, 2H; ArH), 7.62 (m, 4H; ArH). ESI-MS(+) *m/z* 201.88 [M+H]<sup>+</sup>.

**tert-Butyl (4'-cyanobiphenyl-4-yl)methylcarbamate (4a.v):** This compound was prepared from **BOC-IBA** according to the procedure outlined for **4a.i**. **BOC-IBA** (1.0 g, 3.00 mmol), 4-cyanophenylboronic acid (4.50 mmol, 661 mg) and tetrakis(triphenylphosphine)palladium (0.30 mmol, 346 mg) were reacted in 60 mL of a 1:1 solution of toluene and 2 M K<sub>2</sub>CO<sub>3</sub>. The crude product was purified via column chromatography in 0-3% MeOH/CH<sub>2</sub>Cl<sub>2</sub> to yield 703 mg (2.28 mmol) of a yellow solid. Yield = 76%. <sup>1</sup>H NMR (500 MHz, CDCl<sub>3</sub>, 25 °C): δ = 1.47 (s, 9H), 4.37 (d, *J* = 5.7 Hz, 2H), 4.90 (brs, 1H), 7.38 (d, *J* = 8.0 Hz, 2H; ArH), 7.54 (d, *J* = 8.0 Hz, 2H; ArH), 7.65 (d, *J* = 8.0 Hz, 2H; ArH), 7.71 (d, *J* = 8.5 Hz, 2H; ArH). ESI-MS(+) *m/z* 308.86 [M+H]<sup>+</sup>.

**4'-(Aminomethyl)biphenyl-4-carbonitrile (4b.v):** This compound was prepared from **4a.v** according to the procedure outlined for **4b.i**. **4a.v** (703 mg, 2.28 mmol) was de-protected to yield 573 mg (1.78 mmol) of a yellow solid. Yield = 78%. <sup>1</sup>H NMR (500 MHz, CD<sub>3</sub>OD, 25 °C): δ = 4.08 (s, 2H), 7.59 (d, *J* = 8.0 Hz, 2H; ArH), 7.82 (d, *J* = 7.4 Hz, 2H; ArH), 7.91 (d, *J* = 8.0 Hz, 2H; ArH), 7.94 (d, *J* = 8.5 Hz, 2H; ArH). ESI-MS(+) *m/z* 208.94 [M+H]<sup>+</sup>.

***tert*-Butyl-4-(2,3-dihydrobenzo[*b*][1,4]dioxin-6-yl)benzylcarbamate (4a.vi):**

This compound was prepared from **BOC-IBA** according to the procedure outlined for **4a.i**. **BOC-IBA** (1.0 g, 3.00 mmol), 1,4-benzodioxane-6-boronic acid (1.3 equiv., 3.90 mmol, 702 mg) and tetrakis(triphenylphosphine)palladium (0.30 mmol, 346 mg) were reacted in 50 mL of a 1:1 solution of toluene and 2 M K<sub>2</sub>CO<sub>3</sub>. The crude product was purified via column chromatography in CH<sub>2</sub>Cl<sub>2</sub> to yield 782 mg (2.29 mmol) of product. Yield = 76%. <sup>1</sup>H NMR (500 MHz, CDCl<sub>3</sub>, 25 °C): δ = 1.47 (s, 9H), 4.27 (s, 4H), 4.32 (d, *J* = 5.7 Hz, 2H), 4.94 (brs, 1H), 6.91 (d, *J* = 8.0 Hz, 1H; ArH), 7.05 (dd, *J* = 8.6, 2.3, 1H; ArH), 7.09 (d, *J* = 2.3 Hz, 1H; ArH), 7.30 (d, *J* = 8.0 Hz, 2H; ArH), 7.47 (d, *J* = 8.0 Hz, 2H; ArH). ESI-MS(+) *m/z* 363.97 [M+Na]<sup>+</sup>.

**(4-(2,3-Dihydrobenzo[*b*][1,4]dioxin-6-yl)phenyl)methanamine (4b.vi):** This compound was prepared from **4a.vi** according to the procedure outlined for **4b.i**. **4a.vi** (718 mg, 2.10 mmol) was de-protected to yield 584 mg (1.64 mmol) of a white solid of the triflate salt. Yield = 78%. <sup>1</sup>H NMR (500 MHz, CD<sub>3</sub>OD, 25 °C): δ = 4.11 (s, 2H), 4.24 (s, 4H), 6.87 (d, *J* = 8.6 Hz, 1H; ArH), 7.06 (m, 2H), 7.45 (d, *J* = 8.0 Hz, 2H; ArH), 7.59 (d, *J* = 8.0 Hz, 2H; ArH). ESI-MS(+) *m/z* 241.66 [M+H]<sup>+</sup>.

**5-(Phenylamino)picolinonitrile (5a.i):** 500 mg (4.20 mmol) of 5-aminopicolinonitrile, 486 μL (4.62 mmol) of bromobenzene, 170 mg (0.29 mmol) of Xantphos, 2.47 g (7.56 mmol) of Cs<sub>2</sub>CO<sub>3</sub> were combined in an oven-dried flask. To this was added 57 mg (0.25 mmol) of Pd(OAc)<sub>2</sub> and 20 mL of dry dioxane, and the resulting solution was heated to reflux under N<sub>2</sub> for 3 h. The reaction mixture was extracted 2× with CHCl<sub>3</sub> and H<sub>2</sub>O and the organic phase was dried over anhydrous magnesium sulfate and vacuum filtered. The filtrate was evaporated in vacuo and the

crude product was purified via column chromatography in 0-1% MeOH/CH<sub>2</sub>Cl<sub>2</sub> to yield 639 mg (3.27 mmol) of an off-white solid. Yield = 71%. <sup>1</sup>H NMR (500 MHz, CDCl<sub>3</sub>, 25 °C): δ = 6.17 (s, 1H), 7.17 (t, *J* = 7.4 Hz, 3H; ArH), 7.06 (dd, *J* = 8.6, 2.9 Hz, 1H; ArH), 7.38 (d, *J* = 7.4 Hz, 2H; ArH), 7.50 (d, *J* = 8.6 Hz, 1H; ArH), 8.32 (d, *J* = 2.8 Hz, 1H; ArH). ESI-MS(+) *m/z* 196.20 [M+H]<sup>+</sup>.

**6-(Aminomethyl)-*N*-phenylpyridin-3-amine (5b.i):** 639 mg (3.27 mmol) of **5a.i** was dissolved in 10 ml of dry THF under N<sub>2</sub> with a syringe. In a separate flask, 620 mg (16.35 mmol) of LiAlH<sub>4</sub> was dissolved in 5 ml of dry THF. The LiAlH<sub>4</sub> solution was added drop-wise to the **5a.i** solution at 0 °C, and the reaction mixture was stirred overnight under N<sub>2</sub> at room temperature. To the reaction was added drop wise 800 μl of water (100 μl/100 mg of LiAlH<sub>4</sub>), then 800 μl of 1 M NaOH followed by 2.4 ml of water. The reaction mixture was allowed to stir for 20 min after which an excess of anhydrous potassium carbonate was added. The reaction was vacuum filtered and the filtrate was evaporated to a yellow oil. The crude oil was purified via flash silica column chromatography in 1% NH<sub>4</sub>OH/10% MeOH/CH<sub>2</sub>Cl<sub>2</sub> to yield 214 mg (1.07 mmol) of product. Yield = 33%. <sup>1</sup>H NMR (500 MHz, CDCl<sub>3</sub>, 25 °C): δ = 3.88 (s, 2H), 6.03 (s, 1H), 6.92 (t, *J* = 7.4 Hz, 1H; ArH), 7.01 (d, *J* = 8.0 Hz, 2H; ArH), 7.11 (d, *J* = 8.6 Hz, 1H; ArH), 7.23 (t, *J* = 7.4 Hz, 2H; ArH), 7.36 (dd, *J* = 8.6, 2.8 Hz, 1H; ArH), 8.30 (d, *J* = 2.3 Hz, 1H; ArH). ESI-MS(+) *m/z* 199.95 [M+H]<sup>+</sup>.

**4-(Phenylamino)benzotrile (5a.ii):** This compound was synthesized according to the same procedure outlined for **5a.i**. 500 mg (4.23 mmol) of 4-aminobenzotrile, 489 μl (1.1 equiv., 4.65 mmol) of bromobenzene, 170 mg (7 mol%, 0.29 mmol) of Xantphos, 2.5 g (1.8 equiv., 7.6 mmol) of Cs<sub>2</sub>CO<sub>3</sub> and 57 mg (6

mol%, 0.25 mmol) of Pd(OAc)<sub>2</sub> were reacted in dry dioxane. The crude product was recrystallized from diethyl ether to yield 785 mg (4.04 mmol) of product. Yield = 95%. <sup>1</sup>H NMR (500 MHz, CDCl<sub>3</sub>, 25 °C): δ = 6.46 (brs, 1H), 6.95 (d, *J* = 8.6 Hz, 2H), 7.07 (t, *J* = 6.8 Hz, 1H; ArH), 7.14 (d, *J* = 8.0 Hz, 2H; ArH), 7.31 (t, *J* = 8.0 Hz, 2H; ArH), 7.42 (d, *J* = 8.6 Hz, 2H; ArH). ESI-MS(+) *m/z* 195.13 [M+H]<sup>+</sup>.

**4-(Aminomethyl)-*N*-phenylaniline (5b.ii):** This compound was synthesized according to the same procedure outlined for **5b.i**. 822 mg (4.23 mmol) of **5a.ii** and 803 mg (21.15 mmol) of LiAlH<sub>4</sub> were reacted in THF. The crude product was purified via column chromatography in 1% NH<sub>4</sub>OH/10% MeOH/CH<sub>2</sub>Cl<sub>2</sub> to yield 398 mg (2.00 mmol) of product. Yield = 47%. <sup>1</sup>H NMR (400 MHz, CDCl<sub>3</sub>, 25 °C): δ = 3.81 (s, 2H), 5.88 (brs, 1H), 6.91 (t, *J* = 7.6 Hz, 1H), 7.04 (d, *J* = 8.0 Hz, 4H; ArH), 7.20 (d, *J* = 8.0 Hz, 2H; ArH), 7.25 (dd, *J* = 8.8, 7.6 Hz, 2H; ArH). ESI-MS(+) *m/z* 182.34 [fragment+H]<sup>+</sup>.

**4-Phenoxyphenylmethanamine (5b.iii):** This compound was synthesized according to the same procedure outlined for **5b.i**. 500 mg (4.20 mmol) of **5a.iii** and 486 mg (12.8 mmol) of LiAlH<sub>4</sub> were reacted in THF. The crude product was purified via column chromatography in 1% NH<sub>4</sub>OH/10% MeOH/CH<sub>2</sub>Cl<sub>2</sub> to yield 486 mg (2.35 mmol) of product. Yield = 92%. <sup>1</sup>H NMR (500 MHz, CDCl<sub>3</sub>, 25 °C): δ = 3.82 (s, 2H), 7.96 (t, *J* = 7.7 Hz, 4H; ArH), 7.06 (t, *J* = 7.2 Hz, 1H; ArH), 7.25 (d, *J* = 8.5 Hz, 2H; ArH), 7.29 (td, *J* = 7.3, 1.1 Hz, 2H; ArH). ESI-MS(+) *m/z* 199.65 [M+H]<sup>+</sup>.

**5-(Biphenyl-4-ylamino)picolinonitrile (5a.iv)** was kindly provided by Dr. Matthieu Rouffet in the laboratory.

**6-(Aminomethyl)-N-(biphenyl-4-yl)pyridin-3-amine (5b.iv):** This compound was synthesized according to the same procedure outlined for **5b.i**. 75 mg (0.28 mmol) of **5a.iv** and 53 mg (1.40 mmol) of LiAlH<sub>4</sub> were reacted in THF. The crude product was purified via column chromatography in 1% NH<sub>4</sub>OH/10% MeOH/CH<sub>2</sub>Cl<sub>2</sub> to yield 40 mg (0.14 mmol) of product. Yield = 52%. <sup>1</sup>H NMR (500 MHz, CDCl<sub>3</sub>, 25 °C): δ = 3.92 (brs, 2H), 5.86 (brs, 1H), 7.09 (d, *J* = 8.0 Hz, 2H), 7.18 (d, *J* = 8.5 Hz, 1H; ArH), 7.29 (d, *J* = 7.4 Hz, 1H; ArH), 7.40 (m, 3H; ArH), 7.51 (dd, *J* = 20.0, 7.4 Hz, 4H; ArH), 8.37 (s, 1H; ArH). ESI-MS(+) *m/z* 275.96 [M+H]<sup>+</sup>.

**5-(4-Phenoxyphenylamino)picolinonitrile (5a.v)** was kindly provided by Dr. Matthieu Rouffet in the laboratory.

**6-(Aminomethyl)-N-(4-phenoxyphenyl)pyridin-3-amine (5b.v):** This compound was synthesized according to the same procedure outlined for **5b.i**. 186 mg (0.65 mmol) of **5a.v** and 123 mg (3.24 mmol) of LiAlH<sub>4</sub> were reacted in THF. The crude product was purified via column chromatography in 1% NH<sub>4</sub>OH/10% MeOH/CH<sub>2</sub>Cl<sub>2</sub> to yield 93 mg (0.32 mmol) of product. Yield = 49%. <sup>1</sup>H NMR (400 MHz, CDCl<sub>3</sub>, 25 °C): δ = 3.91 (s, 2H), 5.59 (brs, 1H), 6.97 (m, 4H, ArH), 7.04 (m, 3H; ArH), 7.14 (d, *J* = 7.6 Hz, 1H; ArH), 7.30 (t, *J* = 8.0 Hz, 3H; ArH), 8.29 (d, *J* = 2.4 Hz, 1H; ArH). ESI-MS(+) *m/z* 291.95 [M+H]<sup>+</sup>.

### 2I.iii Synthesis of 1,2-HOPO-2 derivatives in Scheme 2-6

**1-(Benzyloxy)-N-(4-(naphthalen-2-yl)benzyl)-6-oxo-1,6-dihydropyridine-2-carboxamide (6c.i):** To 80 mg (0.33 mmol) of **1b** in 20 mL of dry CH<sub>2</sub>Cl<sub>2</sub> was added 69 mg (0.36 mmol) of EDC, 49 mg (0.36 mmol) of HOBt and 125 mg (0.36 mmol) of the triflate salt of **4b.i**, and an excess of TEA. The resulting reaction mixture was

reacted overnight under N<sub>2</sub>. The reaction mixture was evaporated in vacuo and the crude product was extracted with 1 M HCl and CH<sub>2</sub>Cl<sub>2</sub>. The organic phase was dried over anhydrous MgSO<sub>4</sub>, evaporated in vacuo and purified via column chromatography to yield 50 mg (0.11 mmol) of pure product. Yield = 33%. <sup>1</sup>H NMR (500 MHz, CDCl<sub>3</sub>, 25 °C): δ = 4.57 (d, *J* = 5.7 Hz, 2H), 5.27 (s, 2H), 6.57 (dd, *J* = 6.9, 1.7 Hz, 1H; ArH), 6.68 (dd, *J* = 9.2, 1.1 Hz, 1H; ArH), 7.28 (t, *J* = 2.0 Hz, 1H; CONHCH<sub>2</sub>), 7.30 (d, *J* = 7.4 Hz, 2H; ArH), 7.34-7.37 (m, 5H; ArH), 7.43-7.55 (m, 3H; ArH), 7.60-7.66 (m, 4H; ArH), 7.68 (dd, *J* = 8.6, 1.7, 1H; ArH), 7.85-7.92 (m, 2H; ArH). ESI-MS(+) *m/z* 461.10 [M+H]<sup>+</sup>, 483.19 [M+Na]<sup>+</sup>, 484.20 [M+K]<sup>+</sup>.

**1-Hydroxy-*N*-(4-(naphthalen-2-yl)benzyl)-6-oxo-1,6-dihydropyridine-2-carboxamide (6d.i):** 45 mg (0.1 mmol) of **6c.i** was acid deprotected to yield 30 mg (0.08 mmol) of **6d.i**. Yield = 81%, <sup>1</sup>H NMR (500 MHz, CDCl<sub>3</sub>, 25 °C): δ = 5.28 (s, 2H), 5.94, 7.41-7.48 (m, 5H; ArH), 7.52-7.55 (m, 2H; ArH), 7.65-7.70 (m, 3H; ArH), 7.81-7.89 (m, 3H; ArH), 7.92 (s, 1H; ArH). APCI-MS(+) *m/z* 370.99 [M+H]<sup>+</sup>. Anal. Calcd for C<sub>23</sub>H<sub>18</sub>N<sub>2</sub>O<sub>3</sub>•0.65 HCl: C, 70.39; H, 4.50; N, 7.17. Found: C, 70.11; H, 4.89; N, 7.11.

***N*-(4-(Benzo[d][1,3]dioxol-5-yl)benzyl)-1-(benzyloxy)-6-oxo-1,6-dihydropyridine-2-carboxamide (6c.ii):** **6c.ii** was synthesized according to the procedure outlined for **6c.i**. 147 mg (0.60 mmol) of **1b**, 115 mg (0.66 mmol) of EDC, 81 mg (0.66 mmol) of HOBT, 225 mg (0.66 mmol) of the triflate salt of **4b.ii** and an excess of TEA were reacted overnight. The crude product was purified column chromatography in 0-1% MeOH/CH<sub>2</sub>Cl<sub>2</sub> to yield 117 mg (0.26 mmol) of product. Yield = 43 %. <sup>1</sup>H NMR (500 MHz, CDCl<sub>3</sub>, 25 °C): δ = 4.42 (d, *J* = 5.7 Hz, 2H), 5.21



(s, 2H), 6.33 (dd,  $J = 6.9, 1.7$  Hz, 1H; ArH), 6.63 (dd,  $J = 9.7, 1.7$  Hz, 1H; ArH), 6.96 (d,  $J = 8.0$  Hz, 1H; ArH), 7.05 (dd,  $J = 8.0, 1.7$  Hz, 1H; ArH), 7.15 (d,  $J = 1.7$  Hz, 1H; ArH), 7.29 (m, 8H; ArH), 7.41 (d,  $J = 8.0, 2$ H; ArH), 7.45 (dd,  $J = 9.7, 6.8$  Hz, 1H; ArH), 9.39 (brt,  $J = 5.7$  Hz, 1H). ESI-MS(+)  $m/z$  455.05 [M+H]<sup>+</sup>.

***N*-(4-(Benzo[d][1,3]dioxol-5-yl)benzyl)-1-hydroxy-6-oxo-1,6-dihydropyridine-2-carboxamide (6d.ii):** 117 mg (0.26 mmol) of **6c.ii** was acid deprotected to yield 92 mg (0.25 mmol) of product. Yield = 97%. <sup>1</sup>H NMR (500 MHz, CDCl<sub>3</sub>, 25 °C):  $\delta = 4.63$  (s, 2H), 5.94 (s, 2H), 6.81 (d,  $J = 8.5$  Hz, 1H; ArH), 6.95 (m, 3H; ArH), 7.34 (d,  $J = 8.0$  Hz, 2H; ArH), 7.43 (d,  $J = 8.0$  Hz, 4H; ArH). APCI-MS(-)  $m/z$  363.17 [M-H]<sup>-</sup>. Anal. Calcd for C<sub>20</sub>H<sub>16</sub>N<sub>2</sub>O<sub>5</sub>•0.3 HCl: C, 64.01; H, 4.38; N, 7.46. Found: C, 63.90; H, 4.27; N, 7.45.

**1-(Benzyloxy)-*N*-((4'-(dimethylamino)biphenyl-4-yl)methyl)-6-oxo-1,6-dihydropyridine-2-carboxamide (6c.iii):** **6c.iii** was synthesized according to the procedure outlined for **6c.i**. 196 mg (0.80 mmol) of **1b**, 169 mg (0.88 mmol) of EDC, 119 mg (0.88 mmol) of HOBt, 300 mg (0.88 mmol) of the triflate salt of **4b.iii** and an excess of TEA were reacted overnight. The crude product was recrystallized from THF to yield 19 mg (0.15 mmol) of product. Yield = 19%. <sup>1</sup>H NMR (500 MHz, CDCl<sub>3</sub>, 25 °C):  $\delta = 3.00$  (s, 6H), 4.52 (d,  $J = 5.7$  Hz, 2H), 5.26 (s, 2H), 6.30 (dd,  $J = 6.3, 1.7$  Hz, 1H; ArH), 6.76 (dd,  $J = 9.1, 1.7$  Hz, 1H; ArH), 6.79 (d,  $J = 9.2$  Hz, 2H; ArH), 7.02 (brt,  $J = 5.1$ Hz, 1H; ArH), 7.24 (m, 8H; ArH), 7.46 (dd,  $J = 8.5, 1.7$  Hz, 4H; ArH). ESI-MS(+)  $m/z$  454.09 [M+H]<sup>+</sup>.

***N*-((4'-(Dimethylamino)biphenyl-4-yl)methyl)-1-hydroxy-6-oxo-1,6-dihydropyridine-2-carboxamide (6d.iii):** 57 mg (0.13 mmol) of **6c.iii** was acid

deprotected to yield 46 mg (0.13 mmol) of an oily residue. Yield = 100%.  $^1\text{H}$  NMR (400 MHz,  $\text{CDCl}_3$ , 25 °C):  $\delta$  = 3.20 (s, 6H), 4.69 (d,  $J$  = 5.2 Hz, 2H), 7.10 (dd,  $J$  = 8.0, 1.6 Hz, 1H; ArH), 7.45 (m, 5H; ArH), 7.68 (d,  $J$  = 8.4 Hz, 2H; ArH), 7.76 (dd,  $J$  = 8.0, 2.4 Hz, 1H; ArH), 7.83 (d,  $J$  = 8.8 Hz, 2H; ArH). ESI-MS(+)  $m/z$  364.14  $[\text{M}+\text{H}]^+$ . HRMS calcd for  $\text{C}_{21}\text{H}_{21}\text{N}_3\text{O}_3$ : 364.1656. Found: 364.1660. Anal. Calcd for  $\text{C}_{21}\text{H}_{21}\text{N}_3\text{O}_3 \cdot 1.8 \text{HCl}$ : C, 58.79; H, 5.38; N, 9.79. Found: C, 58.49; H, 5.67; N, 9.86.

**1-(Benzyloxy)-*N*-((4'-fluorobiphenyl-4-yl)methyl)-6-oxo-1,6-**

**dihydropyridine-2-carboxamide (6c.iv):** **6c.iv** was synthesized according to the procedure outlined for **6c.i**. 283 mg (1.15 mmol) of **1b**, 243 mg (1.27 mmol) of EDC, 172 mg (1.27 mmol) of HOBt, 400 mg (1.27 mmol) of the triflate salt of **4b.iv** and an excess of TEA were reacted overnight. The crude product was purified via flash silica column chromatography in 0-3% MeOH/  $\text{CH}_2\text{Cl}_2$  to yield 186 mg (0.43 mmol) of an off-white solid. Yield = 38%.  $^1\text{H}$  NMR (400 MHz,  $\text{DMSO}-d_6$ , 25 °C):  $\delta$  = 4.52 (d,  $J$  = 8.4 Hz, 2H), 5.23 (s, 2H), 6.33 (dd,  $J$  = 6.8, 1.7 Hz, 1H; ArH), 6.63 (dd,  $J$  = 9.7, 1.7 Hz, 1H; ArH), 7.24 (t,  $J$  = 8.6 Hz, 2H; ArH), 7.31 (m, 8H; ArH), 7.45 (m, 2H; ArH), 7.60 (dd,  $J$  = 8.5, 5.1 Hz, 2H; ArH), 9.41 (t,  $J$  = 6.3 Hz, 1H). ESI-MS(+)  $m/z$  429.01  $[\text{M}+\text{H}]^+$ .

***N*-((4'-Fluorobiphenyl-4-yl)methyl)-1-hydroxy-6-oxo-1,6-dihydropyridine-**

**2-carboxamide (6d.iv):** 182 mg (0.42 mmol) of **6c.iv** was deprotected in 10 mL of a 1:1 solution of HCl and HOAc as previously described to yield 142 mg (0.42 mmol) of a white solid. Yield = 100%.  $^1\text{H}$  NMR (500 MHz,  $\text{CDCl}_3$ , 25 °C):  $\delta$  = 4.69 (s, 2H), 7.04 (dd,  $J$  = 8.5, 1.7 Hz, 1H; ArH), 7.07 (t,  $J$  = 8.9 Hz, 2H; ArH), 7.40 (d,  $J$  = 8.6 Hz, 2H; ArH), 7.46 (m, 5H; ArH), 7.62 (dd,  $J$  = 8.0, 1.7 Hz, 1H; ArH). APCI-MS(-)

$m/z$  337.14 [M-H]<sup>-</sup>. Anal. Calcd for C<sub>19</sub>H<sub>15</sub>FN<sub>2</sub>O<sub>3</sub>: C, 67.45; H, 4.47; N, 8.28. Found: C, 67.25; H, 4.50; N, 8.40.

**1-(Benzyloxy)-N-((4'-cyanobiphenyl-4-yl)methyl)-6-oxo-1,6-dihydropyridine-2-carboxamide (6c.v):** **6c.v** was synthesized according to the procedure outlined for **6c.i**. 108 mg (0.44 mmol) of **1b**, 92 mg (0.48 mmol) of EDC, 65 mg (0.48 mmol) of HOBt, 100 mg (0.48 mmol) of **5b** were reacted overnight. The crude product was purified via column chromatography in 0-1% MeOH/CH<sub>2</sub>Cl<sub>2</sub> to yield 109 mg (0.25 mmol) of product. Yield = 52%. <sup>1</sup>H NMR (500 MHz, CDCl<sub>3</sub>, 25 °C): δ = 4.56 (d, *J* = 6.3 Hz, 2H), 5.25 (s, 2H), 6.56 (dd, *J* = 6.8, 1.7 Hz, 1H; ArH), 6.67 (dd, *J* = 9.1, 1.7 Hz, 1H; ArH), 7.27 (m, 2H; ArH), 7.33 (m, 6H; ArH), 7.45 (d, *J* = 8.0 Hz, 2H; ArH), 7.62 (d, *J* = 8.6, 2H; ArH), 7.71 (d, *J* = 8.6, 2H; ArH). ESI-MS(+)  $m/z$  436.11 [M+H]<sup>+</sup>.

**N-((4'-Cyanobiphenyl-4-yl)methyl)-1-hydroxy-6-oxo-1,6-dihydropyridine-2-carboxamide (6d.v):** 100 mg (0.23 mmol) of **6c.v** was acid deprotected to yield 79 mg (0.23 mmol) of product. Yield = 100%. <sup>1</sup>H NMR (500 MHz, CDCl<sub>3</sub>, 25 °C): δ = 4.65 (s, 2H), 7.01 (dd, *J* = 8.5, 1.7 Hz, 1H; ArH), 7.42 (d, *J* = 8.6 Hz, 3H; ArH), 7.51 (m, 3H; ArH), 7.60 (d, *J* = 8.6 Hz, 2H; ArH), 7.65 (d, *J* = 8.0 Hz, 2H; ArH). APCI-MS(-)  $m/z$  344.21 [M-H]<sup>-</sup>. Anal. Calcd for C<sub>20</sub>H<sub>15</sub>N<sub>3</sub>O<sub>3</sub>• 1.2 CH<sub>3</sub>OH: C, 66.34; H, 5.20; N, 10.95. Found: C, 66.72; H, 4.88; N, 10.64.

**1-(Benzyloxy)-N-(4-(2,3-dihydrobenzo[b][1,4]dioxin-6-yl)benzyl)-6-oxo-1,6-dihydropyridine-2-carboxamide (6c.vi):** **6c.vi** was synthesized according to the procedure outlined for **6c.i**. 251 mg (1.02 mmol) of **1b**, 215 mg (1.12 mmol) of EDC, 151 mg (1.12 mmol) of HOBt, 400 mg (1.12 mmol) of the triflate salt of **4b.vi** and an

excess of TEA were reacted overnight. The crude product was purified via column chromatography in 0-1% MeOH/CH<sub>2</sub>Cl<sub>2</sub> to yield 276 mg (0.59 mmol) of product. Yield = 58 %. <sup>1</sup>H NMR (400 MHz, CDCl<sub>3</sub>, 25 °C): δ = 4.28 (s, 4H; ArH), 4.50 (d, *J* = 6.0 Hz, 2H), 5.18 (s, 2H), 6.42 (m, 2H; ArH), 6.90 (d, *J* = 8.8, 1H; ArH), 7.00 (td, *J* = 11.2, 2.4 Hz, 1H; ArH), 7.13 (dd, *J* = 9.2, 7.6 Hz, 1H; ArH), 7.25 (m, 7H; ArH), 7.36 (d, *J* = 8.0 Hz, 2H; ArH), 7.71 (brt, *J* = 5.2 Hz, 1H). ESI-MS(+) *m/z* 468.89 [M+H]<sup>+</sup>.

***N*-(4-(2,3-Dihydrobenzo[*b*][1,4]dioxin-6-yl)benzyl)-1-hydroxy-6-oxo-1,6-dihydropyridine-2-carboxamide (6d.vi):** 203 mg (0.43 mmol) of **6c.vi** was acid deprotected to yield 144 mg (0.38 mmol) of a cream solid. Yield = 88%. <sup>1</sup>H NMR (500 MHz, CDCl<sub>3</sub>, 25 °C): δ = 4.29 (s, 4H), 4.71 (d, *J* = 5.7 Hz, 2H), 6.91 (d, *J* = 8.6 Hz, 1H; ArH), 7.05 (dd, *J* = 8.2, 2.0 Hz, 1H; ArH), 7.07 (dd, *J* = 6.6, 2.0 Hz, 2H; ArH), 7.40 (d, *J* = 8.0 Hz, 2H; ArH), 7.47 (m, 3H; ArH), 7.73 (dd, *J* = 8.0, 1.7 Hz, 1H; ArH), 10.18 (brs, NH). APCI-MS(+) *m/z* 378.80 [M+H]<sup>+</sup>. Anal. Calcd for C<sub>21</sub>H<sub>18</sub>N<sub>2</sub>O<sub>5</sub>: C, 66.66; H, 4.79; N, 7.40. Found: C, 66.26; H, 4.84; N, 7.34.

**1-(Benzyloxy)-6-oxo-*N*-(4-phenoxybenzyl)-1,6-dihydropyridine-2-carboxamide (6c.vii):** **6c.vii** was synthesized according to the procedure outlined for **6c.i**. 480 mg (1.96 mmol) of **1b**, 450 mg (2.35 mmol) of EDC, 317 mg (2.35 mmol) of HOBt and 468 mg (2.35 mmol) of **5b.iii** were reacted overnight. The crude product was purified via column chromatography in 0-1% MeOH/CH<sub>2</sub>Cl<sub>2</sub> to yield 690 mg (1.62 mmol) of product. Yield = 82 %. <sup>1</sup>H NMR (400 MHz, CDCl<sub>3</sub>, 25 °C): δ = 4.48 (d, *J* = 6.0 Hz, 2H), 5.26 (s, 2H), 6.59 (dd, *J* = 7.2, 1.2 Hz, 1H; ArH), 6.74 (dd, *J* = 9.2, 1.6 Hz, 1H; ArH), 6.88 (d, *J* = 8.8 Hz, 2H; ArH), 6.97 (d, *J* = 8.8 Hz, 2H; ArH),

7.06 (brt,  $J = 4.8$  Hz, 1H), 7.10 (t,  $J = 6.8$  Hz, 1H; ArH), 7.17 (d,  $J = 7.6$  Hz, 2H; ArH), 7.30 (m, 8H; ArH). ESI-MS(+)  $m/z$  426.85  $[M+H]^+$ .

**1-Hydroxy-6-oxo-*N*-(4-phenoxybenzyl)-1,6-dihydropyridine-2-carboxamide (6d.vii):** 602 mg (1.41 mmol) of **6c.vii** was acid deprotected to yield 460 mg (1.37 mmol) of a cream solid. Yield = 97%.  $^1\text{H}$  NMR (500 MHz,  $\text{CDCl}_3$ , 25 °C):  $\delta = 4.61$  (s, 2H), 6.94 (m, 4H; ArH), 7.01 (dd,  $J = 8.6, 1.7$  Hz, 1H; ArH), 7.05 (t,  $J = 7.4$  Hz, 1H; ArH), 7.28 (m, 4H; ArH), 7.46 (t,  $J = 8.0$ , 1H; ArH), 7.55 (dd,  $J = 8.0, 1.7$  Hz, 1H; ArH). APCI-MS(+)  $m/z$  336.84  $[M+H]^+$ . Anal. Calcd for  $\text{C}_{19}\text{H}_{16}\text{N}_2\text{O}_4$ : C, 67.85; H, 4.79; N, 8.33. Found: C, 67.46; H, 5.12; N, 8.73.

**1-(Benzyloxy)-6-oxo-*N*-(4-(phenylamino)benzyl)-1,6-dihydropyridine-2-carboxamide (6c.viii):** **6c.viii** was synthesized according to the procedure outlined for **1c**. 359 mg (1.46 mmol) of **1b**, 309 mg (1.61 mmol) of EDC, 217 mg (1.61 mmol) of HOBT and 319 mg (1.61 mmol) of **5b.ii** were reacted overnight. The crude product was recrystallized from a concentrated solution of  $\text{CH}_2\text{Cl}_2$  to yield 273 mg (0.64 mmol) of an off-white solid. Yield = 44 %.  $^1\text{H}$  NMR (400 MHz,  $\text{CDCl}_3$ , 25 °C):  $\delta = 4.43$  (d,  $J = 6.0$  Hz, 2H), 5.23 (s, 2H), 6.52 (dd,  $J = 6.8, 1.6$  Hz, 1H; ArH), 6.63 (dd,  $J = 8.8, 1.2$  Hz, 1H; ArH), 6.93 (m, 3H; ArH), 7.03 (d,  $J = 8.8$  Hz, 2H; ArH), 7.10 (d,  $J = 8.8$  Hz, 1H), 7.23 (m, 5H; ArH), 7.31 (m, 5H; ArH). ESI-MS(+)  $m/z$  426.05  $[M+H]^+$ .

**1-Hydroxy-6-oxo-*N*-(4-(phenylamino)benzyl)-1,6-dihydropyridine-2-carboxamide (6d.viii):** 273 mg (0.64 mmol) of **6c.viii** was acid deprotected to yield 82 mg (0.24 mmol) of a green solid. Yield = 38%.  $^1\text{H}$  NMR (400 MHz,  $\text{DMSO-}d_6$ , 25 °C):  $\delta = 4.33$  (d,  $J = 4.8$  Hz, 2H), 6.30 (dd,  $J = 5.6, 1.2$  Hz, 1H; ArH), 6.56 (dd,  $J$

= 7.2, 1.2 Hz, 1H; ArH), 6.77 (t,  $J = 5.6$  Hz, 1H; ArH), 7.02 (m, 4H; ArH), 7.18 (m, 4H; ArH), 7.38 (dd,  $J = 7.2, 5.6$  Hz, 1H; ArH), 9.21 (brt,  $J = 4.8$  Hz, 1H).  $^{13}\text{C}$  NMR (75 MHz, DMSO- $d_6$ , 25 °C):  $\delta$  21.5 (CH<sub>2</sub>), 104.1 (ArC), 116.9 (ArC), 117.2 (ArC), 119.8 (ArC), 119.9 (ArC), 128.7 (ArC), 129.6 (ArC), 130.0 (ArC), 137.8 (ArC), 142.7 (ArC), 143.9 (ArC), 157.9 (ArC), 160.6 (C=O), 172.5 (C=O). APCI-MS(+)  $m/z$  190.87 [fragment+Na]<sup>+</sup>.

**1-(Benzyloxy)-6-oxo-*N*-((5-(phenylamino)pyridin-2-yl)methyl)-1,6-dihydropyridine-2-carboxamide (6c.ix):** **6c.ix** was synthesized according to the procedure outlined for **6c.i**. 238 mg (0.97 mmol) of **1b**, 205 mg (1.07 mmol) of EDC, 145 mg (1.07 mmol) of HOBT and 214 mg (1.07 mmol) of **5b.i** were reacted overnight. The crude product was recrystallized from a concentrated solution of CH<sub>2</sub>Cl<sub>2</sub> to yield 125 mg (0.29 mmol) of an off-white solid. Yield = 30 %.  $^1\text{H}$  NMR (500 MHz, DMSO- $d_6$ , 25 °C):  $\delta$  = 4.53 (d,  $J = 5.7$  Hz, 2H), 5.20 (s, 2H), 6.41 (dd,  $J = 6.9, 1.7$  Hz, 1H; ArH), 6.65 (dd,  $J = 9.1, 1.7$  Hz, 1H; ArH), 6.98 (t,  $J = 7.4$  Hz, 1H; ArH), 7.10 (d,  $J = 7.4$  Hz, 2H; ArH), 7.29 (m, 7H; ArH), 7.40 (d,  $J = 8.5$  Hz, 1H; ArH), 7.47 (dd,  $J = 9.1, 6.3$  Hz, 1H; ArH), 7.57 (brd,  $J = 8.0$  Hz, 1H; ArH), 8.24 (d,  $J = 2.3$  Hz, 1H; ArH), 8.91 (brs, 1H), 9.55 (brt,  $J = 5.7$  Hz; 1H). ESI-MS(+)  $m/z$  427.00 [M+H]<sup>+</sup>.

**1-Hydroxy-6-oxo-*N*-((5-(phenylamino)pyridin-2-yl)methyl)-1,6-dihydropyridine-2-carboxamide (6d.ix):** 125 mg (0.29 mmol) of **6c.ix** was acid deprotected to yield 76 mg (0.23 mmol) of a yellow solid. Yield = 78%.  $^1\text{H}$  NMR (500 MHz, DMSO- $d_6$ , 25 °C):  $\delta$  = 4.57 (d,  $J = 5.7$  Hz, 2H), 6.41 (dd,  $J = 6.8, 1.7$  Hz, 1H; ArH), 6.58 (dd,  $J = 9.2, 1.7$  Hz, 1H; ArH), 6.99 (t,  $J = 7.4$  Hz, 1H; ArH), 7.15 (d,  $J = 7.4$  Hz, 2H; ArH), 7.30 (t,  $J = 8.0, 2\text{H}$ ; ArH), 7.38 (dd,  $J = 9.3, 7.4$  Hz, 1H; ArH),

7.59 (d,  $J = 8.6$  Hz, 1H; ArH), 7.87 (brd,  $J = 8.3$  Hz, 1H; ArH), 8.27 (d,  $J = 2.9$  Hz, 1H; ArH), 9.04 (brs, 1H), 9.50 (t,  $J = 5.7$  Hz, 1H). APCI-MS(-)  $m/z$  335.06 [M-H]<sup>-</sup>. Anal. Calcd for C<sub>18</sub>H<sub>16</sub>N<sub>4</sub>O<sub>3</sub>•2 HCl: C, 53.78; H, 4.46; N, 13.94. Found: C, 53.85; H, 4.99; N, 13.67.

**1-(Benzyloxy)-N-((5-(biphenyl-4-ylamino)pyridin-2-yl)methyl)-6-oxo-1,6-dihydropyridine-2-carboxamide (6c.x):** **6c.x** was synthesized according to the procedure outlined for **6c.i**. 32 mg (0.13 mmol) of **1b**, 27 mg (0.14 mmol) of EDC, 20 mg (0.14 mmol) of HOBt and 40 mg (0.14 mmol) of **5b.iv** were reacted overnight. The crude product was recrystallized from a concentrated solution of CH<sub>2</sub>Cl<sub>2</sub> to yield 51 mg (0.10 mmol) of an orange solid. Yield = 77 %. <sup>1</sup>H NMR (500 MHz, CDCl<sub>3</sub>, 25 °C):  $\delta = 4.58$  (d,  $J = 5.1$  Hz, 2H), 5.34 (s, 2H), 6.32 (brs, 1H), 6.54 (dd,  $J = 6.9, 1.7$  Hz, 1H; ArH), 6.76 (dd,  $J = 9.1, 1.7$  Hz, 1H; ArH), 7.11 (d,  $J = 8.6$  Hz, 2H; ArH), 7.17 (d,  $J = 8.5$  Hz, 1H; ArH), 7.27 (t,  $J = 6.6$  Hz, 3H; ArH), 7.31 (m, 3H; ArH), 7.39 (m, 6H; ArH), 7.53 (m, 4H; ArH), 8.10 (brt,  $J = 4.3$  Hz, 1H; ArH), 8.21 (d,  $J = 2.2$  Hz, 1H; ArH). ESI-MS(+)  $m/z$  503.02 [M+H]<sup>+</sup>.

**N-((5-(Biphenyl-4-ylamino)pyridin-2-yl)methyl)-1-hydroxy-6-oxo-1,6-dihydropyridine-2-carboxamide (6d.x):** 51 mg (0.10 mmol) of **6c.x** was acid deprotected to yield 47 mg (0.10 mmol) of a yellow solid. Yield = 100%. <sup>1</sup>H NMR (400 MHz, DMSO-*d*<sub>6</sub>, 25 °C):  $\delta = 4.57$  (d,  $J = 5.6$  Hz, 2H), 6.41 (dd,  $J = 6.4, 1.6$  Hz, 1H; ArH), 6.60 (dd,  $J = 8.8, 1.6$  Hz, 1H; ArH), 7.22 (d,  $J = 9.2$  Hz, 2H; ArH), 7.28 (t,  $J = 7.2$  Hz, 1H; ArH), 7.40 (m, 3H; ArH), 7.53 (d,  $J = 8.8$  Hz, 1H; ArH), 7.62 (m, 5H; ArH), 7.83 (brd,  $J = 7.2$  Hz, 1H; ArH), 8.35 (d,  $J = 2.4$  Hz, 1H; ArH), 8.98 (brs, 1H), 9.51 (t,  $J = 6.0$  Hz, 1H). APCI-MS(-)  $m/z$  335.06 [M-H]<sup>-</sup>.

**1-(Benzyloxy)-6-oxo-N-((5-(4-phenoxyphenylamino)pyridin-2-yl)methyl)-1,6-dihydropyridine-2-carboxamide (6c.xi):** **6c.xi** was synthesized according to the procedure outlined for **6c.i**. 74 mg (0.30 mmol) of **1b**, 63 mg (0.33 mmol) of EDC, 45 mg (0.33 mmol) of HOBt and 97 mg (0.33 mmol) of **5b.v** were reacted overnight. The crude product was extracted with dilute HCl and saturated NaHCO<sub>3</sub> to yield 149 mg (0.29 mmol) of an orange solid. Yield = 97 %. <sup>1</sup>H NMR (500 MHz, CDCl<sub>3</sub>, 25 °C): δ = 4.55 (d, *J* = 5.1 Hz, 2H), 5.34 (s, 2H), 5.62 (brs, 1H), 6.59 (dd, *J* = 6.8, 1.7 Hz, 1H; ArH), 6.78 (dd, *J* = 9.2, 1.7 Hz, 1H; ArH), 6.98 (m, 4H, ArH), 7.05 (d, *J* = 9.2 Hz, 2H; ArH), 7.08 (t, *J* = 8.6 Hz, 1H; ArH), 7.27 (m, 8H; ArH), 7.40 (dd, *J* = 8.0, 1.7 Hz, 2H; ArH), 7.85 (brt, *J* = 4.6 Hz, 1H), 8.13 (d, *J* = 2.8 Hz, 1H; ArH). ESI-MS(+) *m/z* 519.06 [M+H]<sup>+</sup>.

**1-Hydroxy-6-oxo-N-((5-((4-phenoxyphenyl)amino)pyridin-2-yl)methyl)-1,6-dihydropyridine-2-carboxamide (6d.xi):** 137 mg (0.26 mmol) of **6c.xi** was acid deprotected to yield 113 mg (0.26 mmol) of a yellow solid. Yield = 100%. <sup>1</sup>H NMR (500 MHz, DMSO-*d*<sub>6</sub>, 25 °C): δ = 4.50 (d, *J* = 5.1 Hz, 2H), 6.38 (d, *J* = 6.3 Hz, 1H; ArH), 6.57 (d, *J* = 9.1 Hz, 1H; ArH), 6.94 (d, *J* = 8.0 Hz, 2H; ArH), 6.97 (d, *J* = 8.5 Hz, 2H; ArH), 7.05 (t, *J* = 7.4, 1H; ArH), 7.15 (d, *J* = 8.6 Hz, 2H; ArH), 7.32 (t, *J* = 7.4 Hz, 3H; ArH), 7.37 (t, *J* = 8.5 Hz, 1H; ArH), 7.45 (brd, *J* = 8.0 Hz, 1H; ArH), 7.67 (brs, 1H), 8.22 (d, *J* = 2.3 Hz, 1H; ArH), 9.45 (brs, 1H; ArH). APCI-MS(+) *m/z* 429.05 [M+H]<sup>+</sup>. Anal. Calcd for C<sub>18</sub>H<sub>16</sub>N<sub>4</sub>O<sub>3</sub>•2 HCl: C, 53.78; H, 4.46; N, 13.94. Found: C, 53.85; H, 4.99; N, 13.67.

## 2.J Acknowledgements



Text, schemes, and figures in this chapter, in part, are reprints of materials published in the following papers: Agrawal, Arpita; Romero-Perez, Diego; Jacobsen, Jennifer A.; Villarreal, Francisco J.; Cohen, Seth M. “Zinc-Binding Groups Modulate Selective Inhibition of MMPs” *ChemMedChem* **2008**, *3*, 812-820; Romero-Perez, Diego; Agrawal, Arpita; Jacobsen, Jennifer A.; Yan, Yilong; Thomas, Robert; Cohen, Seth M.; Villarreal, Francisco J. “Effects of Novel Semiselective Matrix Metalloproteinase Inhibitors on Ex Vivo Cardiac Structure-Function” *J. Cardiovasc. Pharmacol.* **2009**, *53*, 452-461. The dissertation author was the primary researcher for the data presented and was either the primary or a co-author on the papers included. The co-authors listed in these publications also participated in the research. The author would also like to thank Dr. Faith E. Jacobsen and Dr. Cesar A.F. De Oliveira for assistance with computational studies. The permissions to reproduce these papers were granted by Wiley-VCH Verlag GmbH & Co. KGaA, Weinham, copyright 2008; Lippincott Williams & Wilkins, Inc. copyright 2009.

**2.K References**

- (1) Skiles, J. W.; Gonnella, N. C.; Jeng, A. Y. *Curr. Med. Chem.* **2001**, *8*, 425.
- (2) Overall, C. M.; Kleinfeld, O. *Nat. Rev. Cancer* **2007**, *6*, 227.
- (3) Skiles, J. W.; Gonnella, N. C.; Jeng, A. Y. *Curr. Med. Chem.* **2004**, *11*, 2911.
- (4) *Matrix Metalloproteinases*; Parks, W. C.; Mecham, R. P., Eds.; Academic Press: San Diego, 1998.
- (5) O'Brien, P. M.; Ortwine, D. F.; Pavlovsky, A. G.; Picard, J. A.; Sliskovic, D. R.; Roth, B. D.; Dyer, R. D.; Johnson, L. L.; Man, C. F.; Hallak, H. *J. Med. Chem.* **2000**, *43*, 156.
- (6) Puerta, D. T.; Cohen, S. M. *Curr. Top. Med. Chem.* **2004**, *4*, 1551.
- (7) Castelhana, A. L.; Billedeau, R.; Dewdney, N.; Donnelly, S.; Horne, S.; Kurz, L. J.; Liak, T. J.; Martin, R.; Uppington, R.; Yuan, Z.; Krantz, A. *Bioorg. Med. Chem. Lett.* **1995**, *5*, 1415.
- (8) Hajduk, P. J.; Shuker, S. B.; Nettlesheim, D. G.; Craig, R.; Augeri, D. J.; Betebenner, D.; Albert, D. H.; Guo, Y.; Meadows, R. P.; Xu, L.; Michaelides, M.; Davidsen, S. K.; Fesik, S. W. *J. Med. Chem.* **2002**, *45*, 5628.
- (9) Jacobsen, F. E.; Lewis, J. A.; Cohen, S. M. *J. Am. Chem. Soc.* **2006**, *128*, 3156.
- (10) Puerta, D. T.; Cohen, S. M. *Inorg. Chem.* **2003**, *42*, 3423.
- (11) Puerta, D. T.; Griffin, M. O.; Lewis, J. A.; Romero-Perez, D.; Garcia, R.; Villarreal, F. J.; Cohen, S. M. *J. Biol. Inorg. Chem.* **2006**, *11*, 131.
- (12) Puerta, D. T.; Lewis, J. A.; Cohen, S. M. *J. Am. Chem. Soc.* **2004**, *126*, 8388.
- (13) Puerta, D. T.; Mongan, J.; Tran, B. L.; McCammon, J. A.; Cohen, S. M. *J. Am. Chem. Soc.* **2005**, *127*, 14148.
- (14) Johnson, L. L.; Bornemeier, D. A.; Janowicz, J. A.; Chen, J.; Pavlovsky, A. G.; Ortwine, D. F. *J. Biol. Chem.* **1999**, *274*, 24881.
- (15) Overall, C. M.; Kleinfeld, O. *Br. J. Cancer* **2006**, *94*, 941.
- (16) Rao, B. G. *Curr. Pharm. Des.* **2005**, *11*, 295.
- (17) Hayashi, R.; Jin, X.; Cook, G. *Bioorg. Med. Chem. Lett.* **2007**, *17*, 6864.

- (18) Knight, C. G.; Willenbrock, F.; Murphy, G. *FEBS Lett.* **1992**, 296, 263.
- (19) Lim, N. C.; Schuster, J. V.; Porto, M. C.; Tanudra, M. A.; Yao, L.; Freake, H. C.; Bruckner, C. *Inorg. Chem.* **2005**, 44, 2018.
- (20) Segel, I. H. *Enzyme Kinetics - Behavior and Analysis of Rapid Equilibrium and Steady-State Enzyme Systems*; Wiley Classics Library: New York, 1993.
- (21) Cortés, A.; Cascante, M.; Cárdenas, M. L.; Cornish-Bowden, A. *Biochem. J.* **2001**, 357, 263.
- (22) Kaludercic, N.; Lindsey, M. L.; Tavazzi, B.; Lazzarino, G.; Paolocci, N. *Cardiovasc. Ther.* **2008**, 26, 24.
- (23) MacPherson, L. J.; Bayburt, E. K.; Capparelli, M. P.; Carroll, B. J.; Goldstein, R.; Justice, M. R.; Zhu, L.; Hu, S. I.; Melton, R. A.; Fryer, L.; Goldberg, R. L.; Doughty, J. R.; Spirito, S.; Blancuzzi, V.; Wilson, D.; O'Byrne, E. M.; Ganu, V.; Parker, D. T. *J. Med. Chem.* **1997**, 40, 2525.
- (24) Romero-Perez, D.; Agrawal, A.; Jacobsen, J. A.; Yan, Y.; Thomas, R.; Cohen, S. M.; Villarreal, F. J. *J. Cardiovasc. Pharmacol.* **2009**, 53, 452.
- (25) Creemers, E. E.; Cleutjens, J. P.; Smits, J. F.; Daemen, M. J. *Circ. Res.* **2001**, 89, 201.
- (26) Lindsey, M. L. *Heart Failure Rev.* **2004**, 9, 7.
- (27) Schulz, R. *Annu. Rev. Pharmacol. Toxicol.* **2007**, 47, 211.
- (28) Cheung, P. Y.; Sawicki, G.; Wozniak, M.; Wang, W.; Radomski, M. W.; Schulz, R. *Circulation* **2000**, 101, 1833.
- (29) Queiroz, M. R. P.; Ferreira, I. C. F. R.; Calhelha, R. C.; Estevinho, L. M. *Bioorg. Med. Chem.* **2007**, 15, 1788.
- (30) Zhang, Y. M.; Fan, X.; Chakaravarty, D.; Xiang, B.; Scannevin, R. H.; Huang, Z.; Ma, J.; Burke, S. L.; Karnachi, P.; Rhodes, K. J.; Jackson, P. F. *Bioorg. Med. Chem. Lett.* **2008**, 18, 409.
- (31) Zhang, Y. M.; Fan, X.; Yang, S. M.; Scannevin, R. H.; Burke, S. L.; Rhodes, K. J.; Jackson, P. F. *Bioorg. Med. Chem. Lett.* **2008**, 18, 405.
- (32) Park, H. I.; Jin, Y.; Hurst, D. R.; Monroe, C. A.; Lee, S.; Schwartz, M. A.; Sang, Q. A. *J. Biol. Chem.* **2003**, 278, 51646.

- (33) Hanessian, S.; MacKay, D. B.; Moitessier, N. *J. Med. Chem.* **2001**, *44*, 3074.
- (34) Solomon, A.; Rosenblum, G.; Gonzales, P. E.; Leonard, J. D.; Mobashery, S.; Milla, M. E.; Sagi, I. *J. Biol. Chem.* **2004**, *279*, 31646.
- (35) Cha, J.; Pedersen, M. V.; Auld, D. S. *Biochemistry* **1996**, *35*, 15831.
- (36) Johnson, L. L.; Pavlovsky, A. G.; Johnsoni, A. R.; Janowiczi, J. A.; Mani, C. F.; Ortwine, D. F.; Purchase, C. F.; White, A. D.; Hupei, D. J. *J Biol Chem* **2000**, *275*, 11026.
- (37) Fasciglione, G. F.; Marini, S.; D'Alessio, S.; Politi, V.; Coletta, M. *Biophy. J.* **2000**, *79*, 2138..
- (38) Gorden, A. E. V.; Xu, J.; Raymond, K. N.; Durbin, P. *Chem. Rev.* **2003**, *103*, 4207.
- (39) Sutherland, F. J.; Hearse, D. J. *Pharmacol. Res.* **2000**, *41*, 613.
- (40) Ytrehus, K. *Pharmacol. Res.* **2000**, *42*, 193.
- (41) Ferrari, R.; Guardigli, G.; Mele, D.; Percoco, G. F.; Ceconi, C.; Curello, S. *Curr Pharm Des* **2004**, *10*, 1699.
- (42) Kang, P. M.; Izumo, S. *Trends Mol Med* **2003**, *9*, 177.
- (43) Griffin, M. O.; Jinno, M.; Miles, L. A.; Villarreal, F. J. *Mol Cell Biochem* **2005**, *270*, 1.
- (44) Scarabelli, T. M.; Stephanou, A.; Pasini, E.; Gitti, G.; Townsend, P.; Lawrence, K.; Chen-Scarabelli, C.; Saravolatz, L.; Latchman, D.; Knight, R.; Gardin, J. *J Am Coll Cardiol* **2004**, *43*, 865.
- (45) Tochowicz, A.; Maskos, K.; Huber, R.; Oltenfreiter, R.; Dive, V.; Yiotakis, A.; Zanda, M.; Pourmotabbed, T.; Bode, W.; Goettig, P. *J. Mol. Biol.* **2007**, *371*, 989.
- (46) Scarrow, R. C.; Riley, P. E.; Abu-Dari, K.; White, D. L.; Raymond, K. N. *Inorg. Chem.* **1985**, *24*.
- (47) Dehkordi, L. S.; Liu, Z. D.; Hider, R. C. *Eur. J. Med. Chem.* **2008**, *43*, 1035.
- (48) Dobbin, P. S.; Hider, R. C.; Hall, A. D.; Taylor, P. D.; Sarping, P.; Porter, J. B.; Xiao, G.; Van der Helm, D. *J. Med. Chem.* **1993**, *36*, 2448.

**Chapter 3. Thioamide Hydroxypyrothiones Supersede Amide Hydroxypyrothiones in Potency against Anthrax Lethal Factor**

### 3.A Introduction

Anthrax lethal factor (LF) is one of three toxins secreted by *Bacillus anthracis*. LF is a zinc-dependent hydrolytic metalloenzyme that cleaves the N-terminus of mitogen activated protein kinase kinases (MAPKKs) to disrupt downstream signaling pathways and cause macrophage apoptosis. As discussed in Chapter 1, in combination with PA, LF forms the lethal toxin (LeTx).<sup>1-4</sup> There are several published reviews describing the pathogenesis of anthrax via its toxins but despite extensive research in the field, the exact pathway by which LF imparts toxicity is still somewhat unclear; nevertheless, anthrax lethal factor is an important target for inhibition.<sup>4-7</sup>

Current therapies against *B. anthracis* include FDA approved antibiotics such as ciproflaxin, doxycyclin, and penicillin that target the bacteria but are ineffective against the toxins secreted by the bacterium. The limited success of antibiotic therapy against anthrax infections has motivated investigation of complementary therapeutic strategies that target the bacteria's secreted toxins. Inactivation of the LF gene alone in *B.anthraxis* leads to a 1000-fold reduction in its virulence, which suggests that anthrax pathology is largely dictated by LF.<sup>7</sup>

In the past few years, several groups have been successful in developing potent lethal factor inhibitors (LFi), some of which include known matrix metalloproteinase inhibitors (MMPi).<sup>8,9</sup> To date, some of the most potent LFi carry a hydroxamic acid zinc-binding group (ZBG) similar to other zinc metalloprotease inhibitors. Hydroxamic acids are known to be limited by poor pharmacokinetics and oral availability, as well as a lack of selectivity for  $Zn^{2+}$ .<sup>10,11</sup> To overcome the limitations

of hydroxamic acids, the design of LFi that incorporate alternative ZBGs merits investigation.

In this study we have focused on a three-component strategy to the design of a LFi: (i) a ZBG to chelate and inactivate the catalytic  $\text{Zn}^{2+}$  ion, (ii) a backbone to interact non-covalently with the LF active site, and (iii) a linker to connect the backbone to the ZBG. A similar overall scheme has been used in the development of MMP and histone deacetylase (HDAC) inhibitors.<sup>12,13</sup> In the work presented below, the specific ZBGs employed are derivatives of 3-hydroxy-2-methyl-4-pyrone (maltol), 3-hydroxy-2-methyl-4-pyrothione (thiomaltol), 1-hydroxypyridin-2(1*H*)-one (1,2-HOPO), and 1-hydroxypyridine-2(1*H*)-thione (1,2-HOPTO) (Figure 3-1). We have previously shown that these are effective ZBGs for inhibiting LF and other metalloproteinases.<sup>14-18</sup>

The study presented here is focused on the synthesis and structure-activity relationship (SAR) of the hydroxypyronone and hydroxypyrothione-based LFi. Different aromatic backbones were attached to the ZBGs via an amide or a thioamide linkage (Figure 3-1). The results presented elucidate the contribution of each component to the potency of the different LFi, which was tested in vitro using a fluorescence-based assay that has been previously reported.<sup>15,19</sup> The activity of each LFi is reflected in calculated kinetic parameters such as  $\text{IC}_{50}$ ,  $K_i$ , and ligand efficiency (LE). LE is a metric that provides an estimate of the binding free energy per heavy atom in the molecule and is calculated from equation 1, shown below:<sup>20,21</sup>

$$\text{LE} = \Delta G / \# \text{ of heavy atoms (HA)} \quad \text{equation (1)}$$

$$= \frac{-RT \ln (K_i/IC_{50})}{\text{HA}}$$

In order to better understand the importance of the linker and backbone in protein-inhibitor interactions, computational studies were performed to build models of the inhibitors bound to the LF active site. Our computational models are in agreement with the experimental results and suggest a key role of the thioamide group in stabilizing the protein-inhibitor complex.

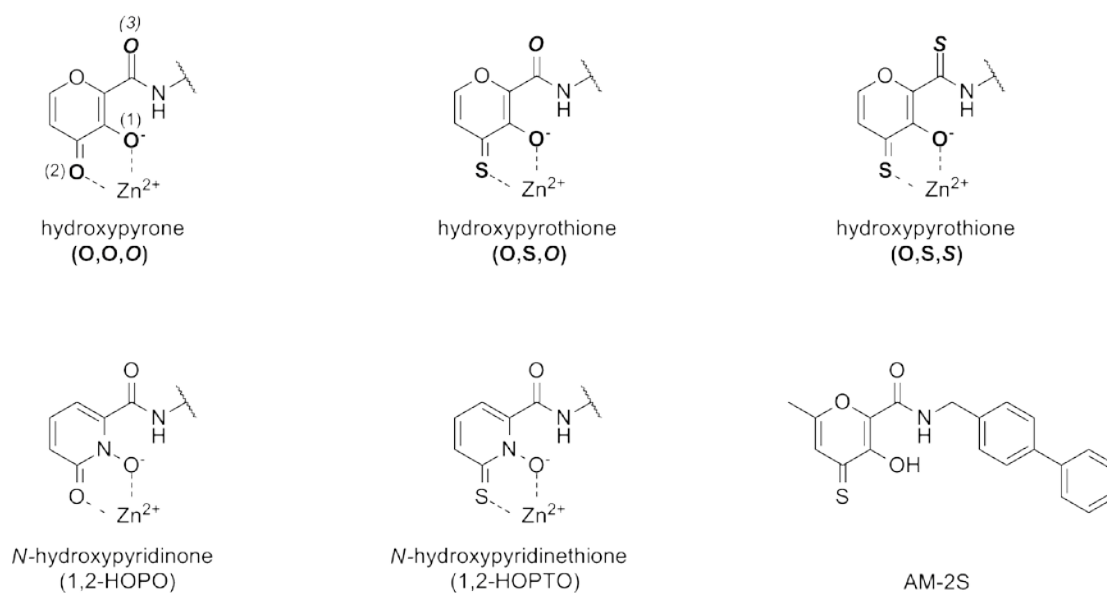


**Figure 3-1.** ZBGs and linkers used in the LFi reported. Abbreviations for each subset of compounds are shown in parentheses. The heteroatom terminology used throughout this study is highlighted in the top three structures by the use of a numbering scheme and bold and italicized atom labels. Shown in the bottom right is the complete LFi **11b** which was previously reported.<sup>15</sup>



### 3.B Synthesis of a series of lethal factor inhibitors (LFI)

As discussed in Chapter 1, our group has previously identified alternative ZBGs that are more potent than simple hydroxamic acids against LF.<sup>14,15</sup> On the basis of these earlier findings, a novel hydroxypyrothione-based (O,S metal-binding donor atom set) LFI (AM-2S, **11b**, Figure 3-1) was designed, synthesized, and found to be moderately potent against LF ( $IC_{50} = 13.9 \mu\text{M}$ ).<sup>15</sup> **11b** thereby inspired the design of additional hydroxypyrene, hydroxypyrothione, *N*-hydroxypyridinone, and *N*-hydroxypyridinethione LFI shown in Figures 1 and 2. Compounds **1a** (PY-2) and **9a** (1,2-HOPO-2) were previously synthesized and identified as nanomolar inhibitors against deep pocket MMPs.<sup>22</sup> Several similar compounds containing hydroxypyrene ZBGs (O,O metal-binding donor atom set), amide linking groups, and a series of different backbone substituents were synthesized (Scheme 3-1, Figure 3-2, **1a-10a**). Compounds **1a-10a** were universally found to be ineffective as LFI (*vide supra*).

Because compounds **1a-10a** were not potent LFI and our previously reported inhibitor (**11b**) used a hydroxypyrothione ZBG, compounds **1a-10a** were similarly converted to their O,S donor hydroxypyrothione analogues. Reaction of the hydroxypyrene compounds **1a-10a** with phosphorus pentasulfide ( $\text{P}_4\text{S}_{10}$ ) and hexamethyldisiloxane (HMDO) in benzene generates two products as shown in Scheme 3-2. One major product contains a single sulfur atom, designated (O,S,O) compounds, at the pyrene carbonyl group thereby converting it to a thionyl group. The second major product contains two sulfur atoms, designated (O,S,S) compounds, with one sulfur atom at the pyrene carbonyl group and the other at the amide carbonyl linker group, now converting it to a thioamide linkage. This structural assignment was

based on the spectroscopic characterization of the compounds ( $^1\text{H}$  NMR and  $^{13}\text{C}$  NMR) and was unambiguously confirmed by the X-ray crystal structure of compound **5c** (vide infra).

Upon thionation of the hydroxypyrrone (O,O,O) compounds, the (O,S,O) compounds are produced first followed by production of the (O,S,S) compounds. The pyrrone carbonyl oxygen of each compound reacts prior to conversion of the amide to a thioamide linker, and therefore, the percentage of each major product can be modulated by the reaction time. The reactivity of each compound however was found to also depend on the backbone substituent. When **1a**, with a biphenyl backbone, was treated with  $\text{P}_4\text{S}_{10}$  and HMDO for 3 h, the reaction yielded **1b** (O,S,O) in 16% and **1c** (O,S,S) in 43%, respectively. When **1a** was treated for about 1 h, **1b** and **1c** were obtained in 69% and 2% yields, respectively. When **8a**, with a simple ethyl backbone was treated for only 30 min, the isolated products consisted of 55% **8b** (O,S,O) and 20% **8c** (O,S,S). Similarly, when the reaction time was extended to 1 h, **8b** was obtained in 25% yield, whereas **8c** was isolated in a 43% yield. The results obtained show that optimal reaction times have to be considered for each compound of interest. An additional point of interest is that the  $R_f$  values for the (O,S,O) and (O,S,S) compounds tend to be very similar and chromatographic separation can be challenging, resulting in poor yields.

As for the *N*-hydroxypyridinone-based (1,2-HOPO) inhibitors, synthesis of **9a** was previously reported;<sup>22</sup> the synthesis of **10a** parallels the synthetic procedure for **9a** (Scheme 3-3). Unlike the hydroxypyrrones described above, the syntheses of the *N*-hydroxypyridinethione-based (1,2-HOPTO) inhibitors are not derived from their O,O

chelate analogues. The synthesis of 1-hydroxy-6-thioxo-1,6-dihydropyridine-2-carboxylic acid (**HTDCA**) in Scheme 3-4 is based on literature procedures with slight modifications (see Experimental Section).<sup>23,24</sup> Syntheses of **9b** and **10b** from **HTDCA** are outlined in Scheme 3-4. The 4-phenylbenzylamine and 4-fluorobenzylamine backbones are appended to **HTDCA** under standard amide coupling conditions. EDCI (1-ethyl-3-(3-dimethylaminopropyl) carbodiimide) and NHS (*N*-hydroxysuccinimide) were used as the coupling reagents for **9b**, whereas EDCI and HOBt (*N*-hydroxybenzotriazole) were the coupling reagents used in the production of **10b**.

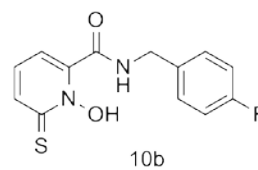
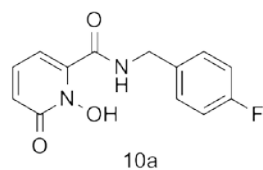
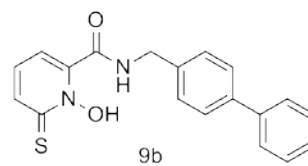
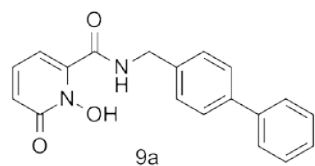
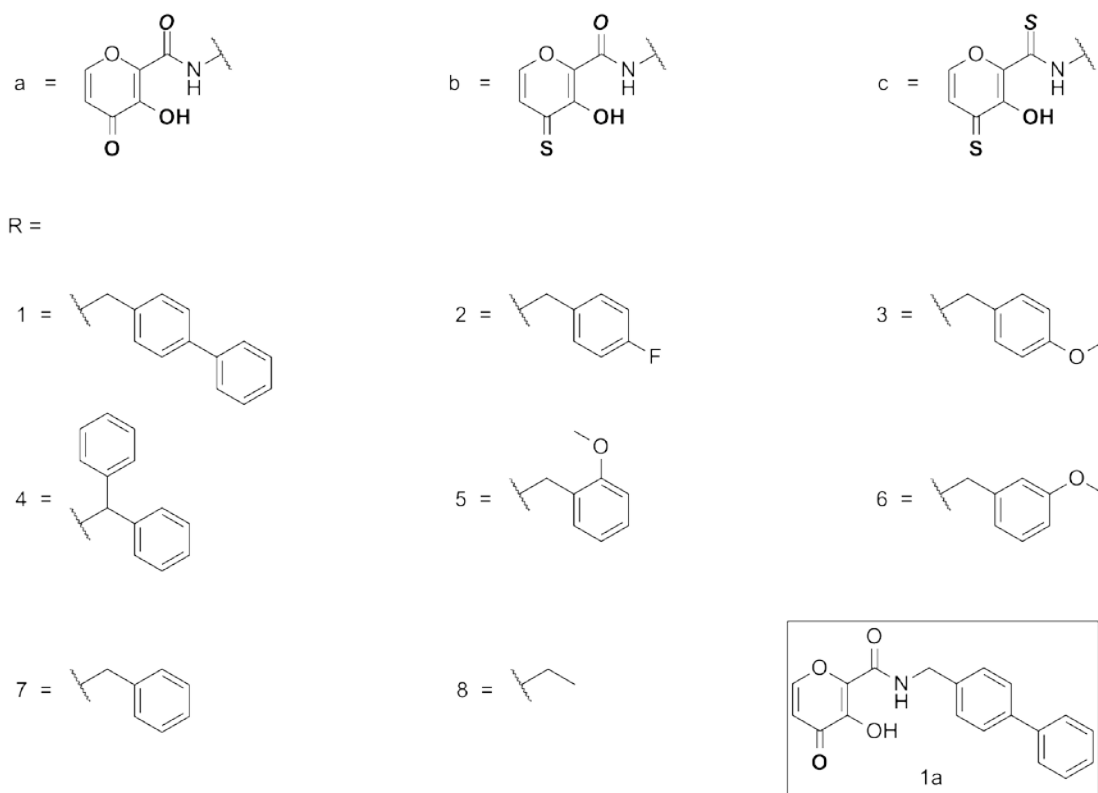
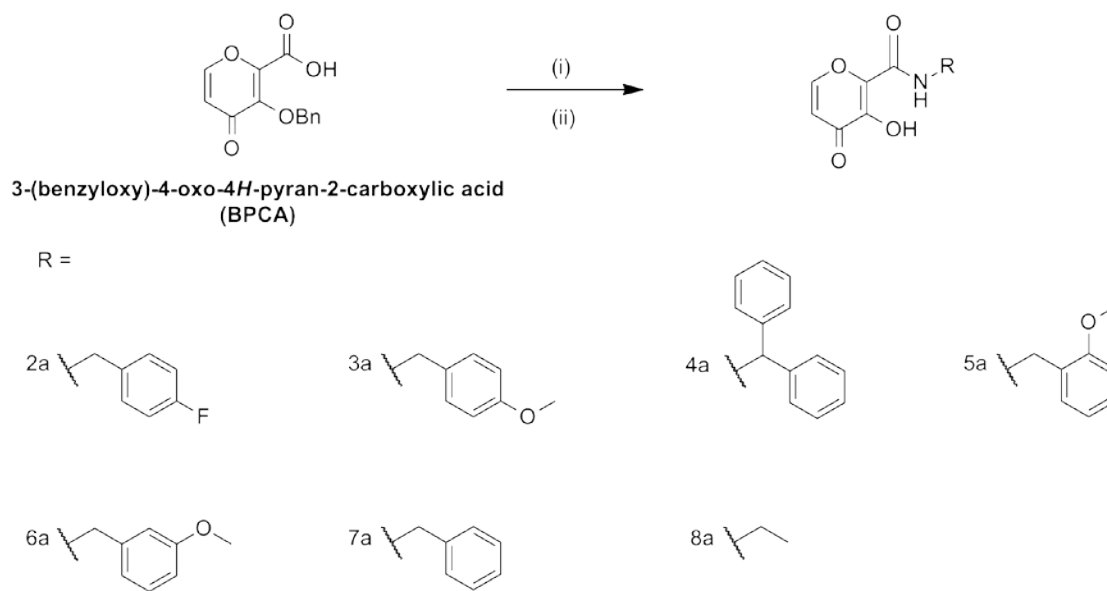


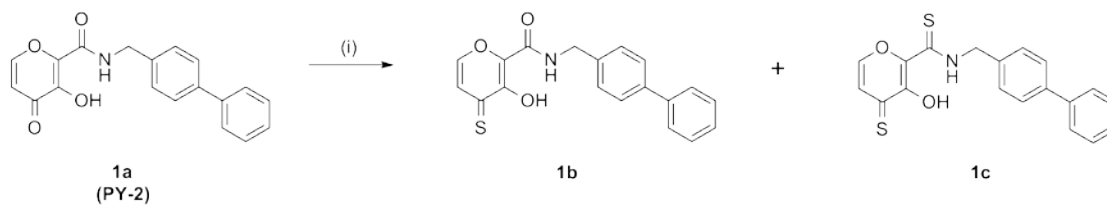
**Figure 3-2.** Structures of the inhibitors tested in the study. The heteroatom terminology used throughout is highlighted in the top three structures by the use of bold and italics atom labels. Shown in the box is the complete (O,O,O) LFi **1a** (for clarity). Other inhibitors are hydroxypyronones with an amide linker (**1a – 8a**), hydroxypyrothiones with an amide linker (**1b – 8b**), hydroxypyrothiones with a thioamide linker (**1c – 8c**). Shown below the thick line are *N*-hydroxypyridinones with an amide linker (**9a, 10a**) and *N*-hydroxypyridinethiones with an amide linker (**9b, 10b**).

**Scheme 3-1.** Synthesis of Hydroxypyrrone (O,O,O) Inhibitors (**1a – 8a**)<sup>a</sup>



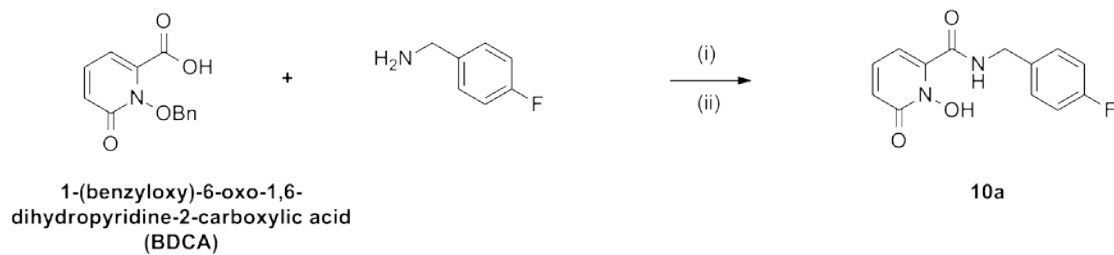
<sup>a</sup>Reagents and conditions: (i) RNH<sub>2</sub>, EDCI, HOBT, CH<sub>2</sub>Cl<sub>2</sub>, N<sub>2</sub> (ii) 1:1 HCl/CH<sub>3</sub>COOH.

**Scheme 3-2.** Synthesis of Hydroxypyrothione Analogues **1b** (O,S,O) and (O,S,S) Compounds<sup>b</sup>



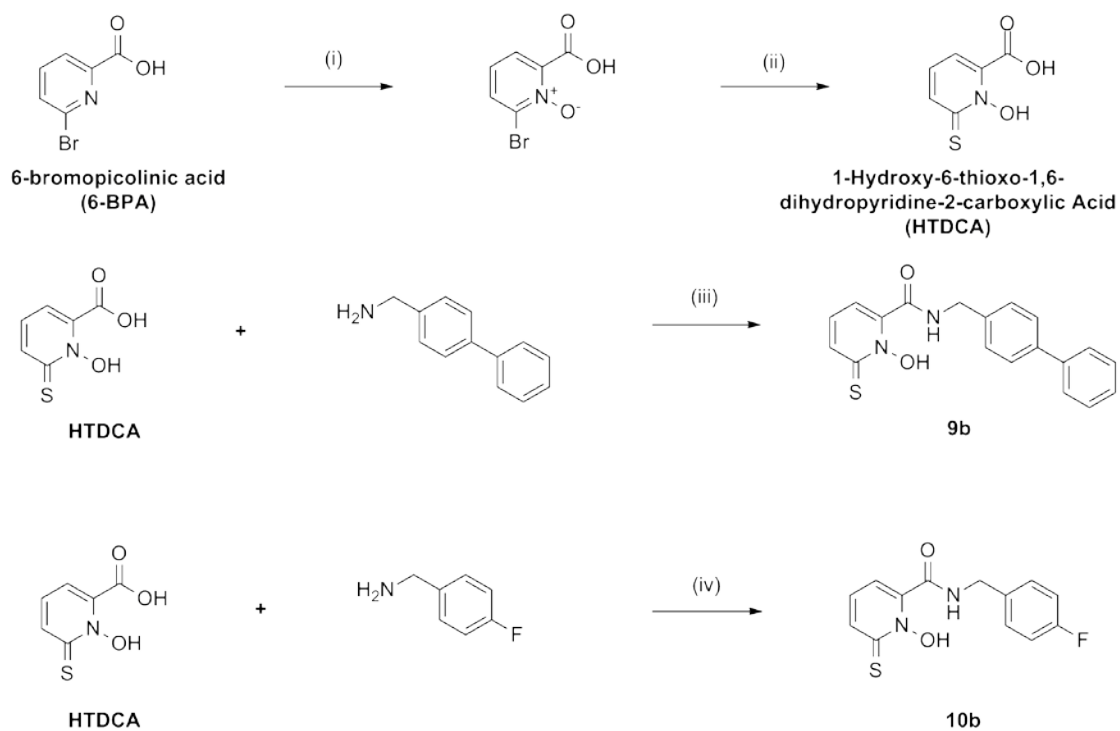
<sup>b</sup>Reagents and conditions: (i) P<sub>4</sub>S<sub>10</sub>, HMDO, benzene, 110 °C.

**Scheme 3-3.** Synthesis of *N*-Hydroxypyridinone **10a**<sup>c</sup>



<sup>c</sup>Reagents and conditions: (i) EDCI, HOBt,  $\text{CH}_2\text{Cl}_2$ ,  $\text{N}_2$  (ii) 1:1  $\text{HCl}/\text{CH}_3\text{COOH}$ , 32%.

**Scheme 3-4.** Synthesis of *N*-Hydroxypyridinethione Inhibitors **9b** and **10b**<sup>d</sup>



<sup>d</sup>Reagents and conditions: (i) TFA, 30%  $\text{H}_2\text{O}_2$ , 80 °C, 94% (ii)  $\text{Na}^+\text{HS}^-$ ,  $\text{H}^+\text{Cl}^-$ , 95 °C, 89% (iii) EDCI, NHS,  $\text{CH}_2\text{Cl}_2$ , 46% (iv) EDCI, HOBt,  $\text{CH}_2\text{Cl}_2$ , 95%.

### 3.C Single-Crystal X-ray Structure of 5c

To provide further evidence for the conversion of both carbonyl oxygen atoms to sulfur atoms, an X-ray diffraction study was performed on inhibitor **5c**. Large red plates of **5c** were obtained by slow evaporation from a concentrated solution of the compound in chloroform. The crystal structure (Figure 3-3 and Table 3-2 in the Appendix) confirms the presence of the two expected sulfur atoms. In addition to the measured electron density, the C-S bond lengths confirm the correct identity of the sulfur atoms. The thionyl C(4)-S(4) bond distance of 1.66 Å lies within the range of C-S bonds from other hydroxypyrothiones (1.65 - 1.68 Å).<sup>16</sup> The thioamide C(1)-S(1) bond distance of 1.68 Å is similar to the average thioamide bond distance (1.67 Å) predicted from the Cambridge Crystallographic Data Center (CCDC) and is too long to be an amide C-O bond (~1.22 Å).

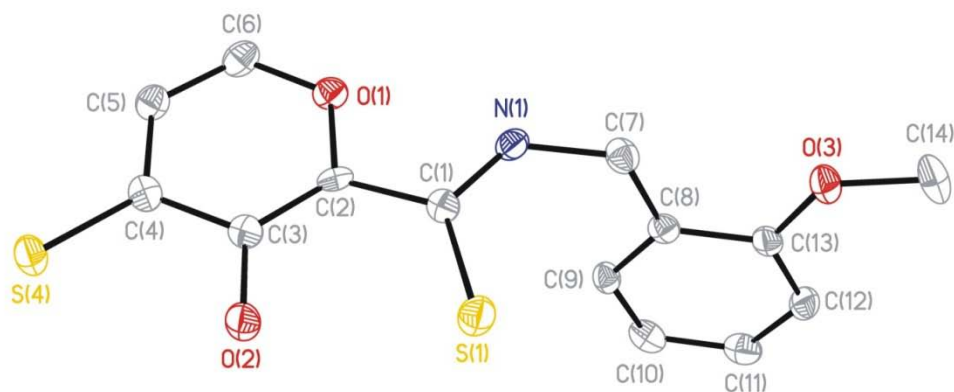


**Figure 3-3.** Structural diagram of **5c** with 50% probability ellipsoids. Hydrogen atoms have been omitted for clarity.

### 3.D In Vitro Potency of synthesized LFi

The in vitro potency of each inhibitor was evaluated against LF using an established procedure with a quenched fluorogenic substrate, where observed fluorescence is directly proportional to LF activity.<sup>19</sup> The  $IC_{50}$  values (Table 3-1) were calculated for each synthesized inhibitor as described under the Experimental Section. Kinetic parameters ( $V_{max}$ ,  $K_m$ ,  $K_i$ ) were also calculated using the same fluorogenic assay. Additionally, LE values of most inhibitors were calculated from the respective  $K_i$  values (vide infra).<sup>20,21,25</sup> Compounds **1a-8a** (Table 3-1, column “a”), which consist of a hydroxypyronone ZBG and amide linker (O,O,O), are ineffective against LF having  $IC_{50}$  values greater than 100  $\mu$ M. Compounds **1b-8b** (Table 3-1, column “b”), which consist of a hydroxypyrothione ZBG and amide linker (O,S,O), show moderate potency against LF with  $IC_{50}$  values ranging from 13 to >100  $\mu$ M. Surprisingly, compounds **1c-8c** (Table 3-1, column “c”), which consist of a hydroxypyrothione ZBG and thioamide linker (O,S,S), are uniformly the most potent compounds with  $IC_{50}$  values in the range of 5-11  $\mu$ M.

Together these data show that (i) a hydroxypyronone ZBG when coupled via an amide linker (O,O,O) is ineffective against LF regardless of the backbone used, (ii) a hydroxypyrothione ZBG when coupled via an amide linker (O,S,O) can have moderate potency against LF depending on the backbone substituent, and (iii) a hydroxypyrothione ZBG when coupled via a thioamide linker (O,S,S) provides consistent potency against LF with little influence from the backbone group.



**Table 3-1.** IC<sub>50</sub> values of LFi using a Fluorescence-Based Assay<sup>a</sup>

| Compound  | IC <sub>50</sub> (μM) |                  |             |
|-----------|-----------------------|------------------|-------------|
|           | a (O,O,O)             | b (O,S,O)        | c (O,S,S)   |
| <b>1</b>  | >100                  | 13.2 (±0.9)      | 8.3 (±0.1)  |
| <b>2</b>  | >100                  | 29.2 (±1.4)      | 9.2 (±0.2)  |
| <b>3</b>  | >100                  | 50.4 (±2.4)      | 10.6 (±0.6) |
| <b>4</b>  | >100                  | 14.1 (±2.0)      | 5.0 (±0.2)  |
| <b>5</b>  | >100                  | 33.5 (±2.3)      | 8.7 (±0.8)  |
| <b>6</b>  | >100                  | 37.4 (±3.1)      | 6.6 (±0.8)  |
| <b>7</b>  | >100                  | >100             | 7.9 (±0.6)  |
| <b>8</b>  | >100                  | 72.5 (±5.4)      | 11.4 (±0.7) |
| <b>9</b>  | >100                  | >50 <sup>b</sup> |             |
| <b>10</b> | >100                  | >100             |             |

<sup>a</sup>All values represent the average and standard deviation from at least three independent experiments. <sup>b</sup>Determination of a more accurate IC<sub>50</sub> value was precluded by the limited solubility of this compound.

The minimal effect of the backbone in compounds **1c-8c** is highlighted by inhibitor **8c**, which utilizes only a simple ethyl backbone and yet has a similar IC<sub>50</sub> value compared to the rest of the series that employ a variety of aromatic backbones. These findings underline the importance of all three components: the ZBG, linker, and backbone. Each of these components therefore, must be considered when optimizing LFi.

In order to confirm the importance of the ZBG and linker in generating effective LFi, we synthesized four additional inhibitors, based on *N*-

hydroxypyridinone (**9a**, **10a**) and *N*-hydroxypyridinethione (**9b**, **10b**) chelators. Compounds **9a** and **9b** contain the same biphenyl backbone and amide linker found in **1a**. Compounds **10a** and **10b** have the same fluorobenzyl backbone and amide linker as compound **2a**. Therefore, on the basis of our earlier classification, **9a** and **10a** are (O,O,O) inhibitors like **1a** and **2a**; **9b** and **10b** are (O,S,O) inhibitors similar to **1b** and **2b**. Notably, the only difference between these inhibitors lies in the use of a *N*-hydroxypyridinone (1,2-HOPO) versus hydroxypyrrone, or *N*-hydroxypyridinethione (1,2-HOPTO) versus hydroxypyrothione ZBG. These heterocyclic ZBGs are essentially isosteric and very similar in overall composition. With that in mind, it was surprising to find that whereas the (O,O,O) hydroxypyrones (**1a**, **2a**) are less effective than the (O,S,O) hydroxypyrothiones (**1b**, **2b**), no substantial differences are seen between the 1,2-HOPO (**9a**, **10a**) and 1,2-HOPTO (**9b**, **10b**) compounds, with the latter inhibitors showing very poor potency ( $>100 \mu\text{M}$ ). The lack of potency of the 1,2-HOPO and 1,2-HOPTO chelators may be due to (a) a significantly different binding mode of these chelators to the active site  $\text{Zn}^{2+}$  ion or (b) the significantly greater acidity of these chelators relative to the hydroxypyrones and hydroxypyrothiones. In either case, these data show that the nature of the ZBG is critical and that even small changes in ZBG structure can result in large differences in efficacy.

### 3.E Computational Modeling

In order to verify the structural and energetic factors that are relevant for the differences in observed potency, we built QM/MM optimized structures for the complex between the LF active site and several of the hydroxypyrothione inhibitors. Figure 3-4 displays the models for the bound structures of inhibitors **1b**, **1c**, **3b**, **3c**, **4b**, and **4c** in the active site of LF. Figure 3-5 displays the models for the (O,S,S) inhibitors **2c**, **7c** and **8c** in the active site. Interestingly, optimized structures of molecules **1b** and **1c** in the active site of LF presented very similar configurations and no significant difference was observed in the orientation of the backbone fragment or the amide and thioamide linker groups. This is consistent with the observations that **1b** and **1c** have similar IC<sub>50</sub> values against LF. In contrast, even though the backbone fragments of **3b** and **3c** adopt similar configurations, the ZBG shows distinct orientations relative to the amide/thioamide linker groups. By comparing the structures of **1c** and **3c**, we observed that the sulfur atom of the thioamide group acts as a hydrogen bond acceptor, interacting with the backbone amide *N*-H group of residues Lys392 and Gly393. Similar hydrogen bonding was also observed in the optimized structures of thioamide containing LFi: **2c**, **7c**, and **8c** (Figure 3-5). Figure 3-4 shows that although the two hydrogen bonds were observed in the complexes of LF with **1b**, **1c**, and **3c**, they were not found with compound **3b**. The distance between the amide oxygen of **3b** and the backbone *N*-H groups was greater than 4.0 Å (Figure 3-4). These observations are consistent with the IC<sub>50</sub> values obtained for these compounds (Table 3-1), where **3b** is clearly the least effective of these inhibitors (50.4 μM). Similar interactions involving either Lys392 or Gly393 have already been characterized in

crystal structures of anthrax lethal factor bound to small molecule inhibitors, which indicates that these residues may play an important role in the inhibitor binding.<sup>26,27</sup>

Previous work has suggested that the plasticity and flexibility of the S1 binding pocket allow the receptor to accommodate small and large hydrophobic residues at the P1' position.<sup>27</sup> These studies also indicate that the design of compounds with greater complementarity to the S1' pocket would lead to potent and selective inhibition of LF. In order to explore interactions with the S1 binding pocket, inhibitors **4b** and **4c** were designed. In fact, **4c** shows a modest ~2-fold improvement in LF potency when compared to **1c**.

To further investigate the quality of our models, all optimized structures were submitted to energy calculation procedures by using the program Autodock 4.0.<sup>28</sup> Because there is a good agreement between the calculated structures and the experimentally determined IC<sub>50</sub> values, the calculated models were used to obtain a rough estimation of the binding free energy of molecules **1b**, **1c**, **2b**, **2c**, **3b**, **3c**, **4b**, and **4c**. Figure 3-6 shows the plot of log(IC<sub>50</sub>) value against the estimated free energy of binding ( $\Delta G$ ), which demonstrates that the trend in potency is captured reasonably well by the calculated models.

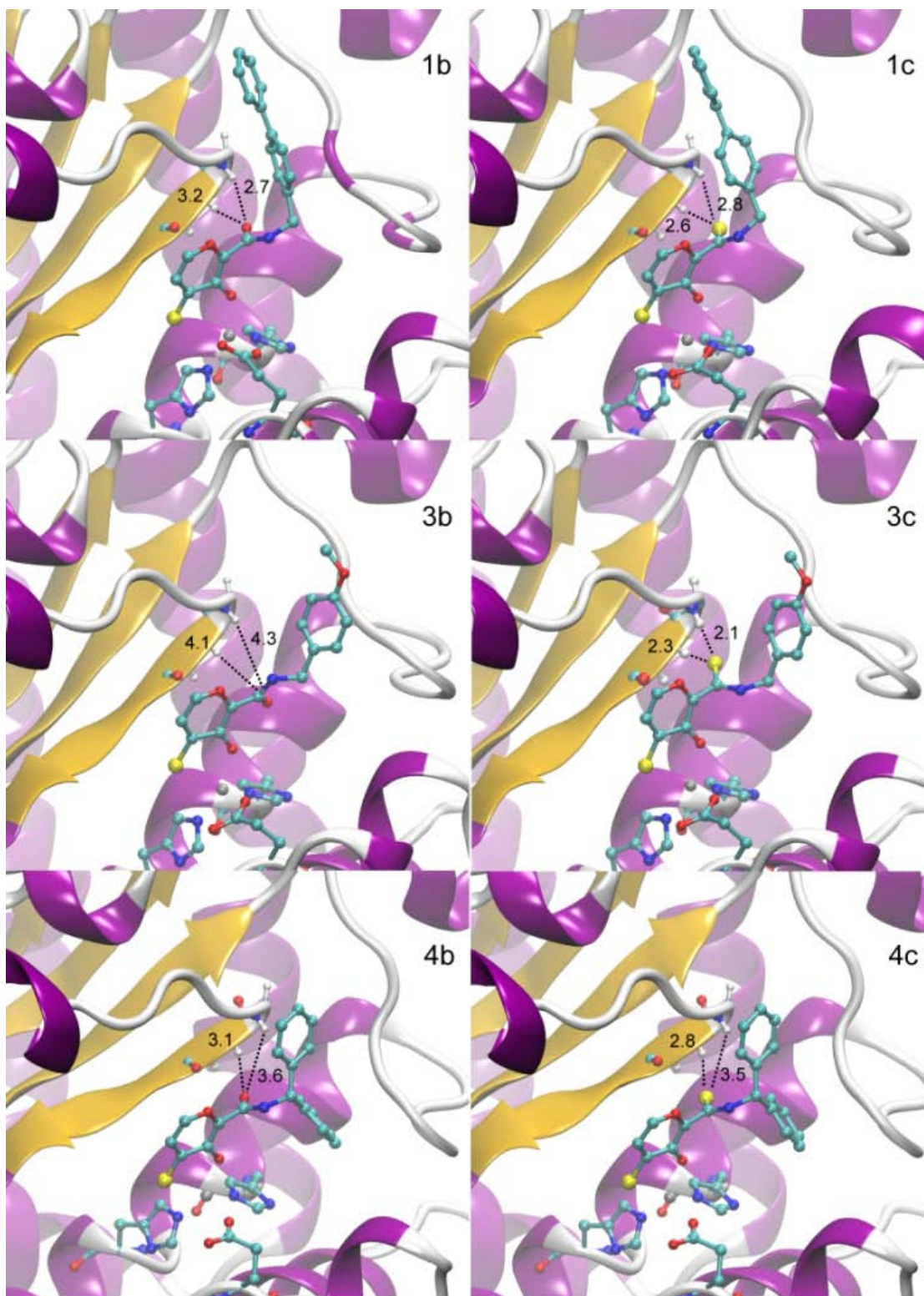


**Figure 3-4.** QM/MM optimized structures of the complex between anthrax LF (ribbons) and inhibitors **1b**, **1c**, **3b**, **3c**, **4b** and **4c** (ball and stick). Some active site residues (ball and stick) and catalytic  $\text{Zn}^{2+}$  ion (gray sphere) are also shown.

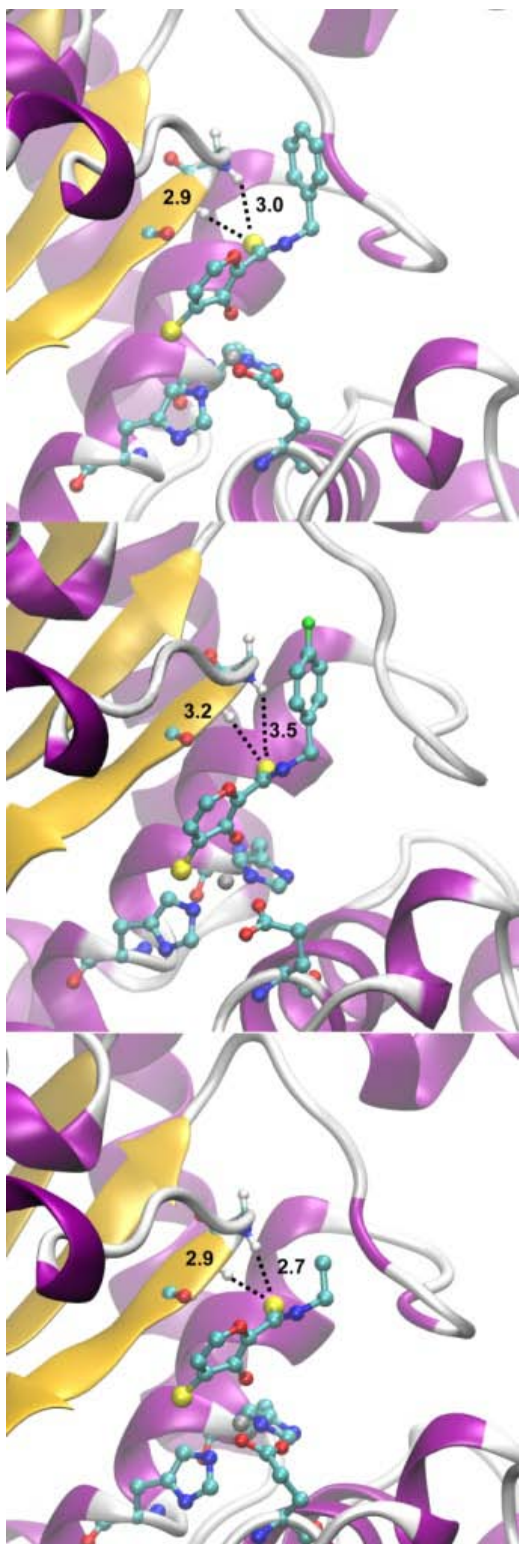


**Figure 3-5.** QM/MM optimized structures of the complex between anthrax LF (ribbons) and inhibitors **7c**, **2c** and **8c** (ball and stick) from top to bottom. Some active site residues (ball and stick) and catalytic Zn<sup>2+</sup> ion (gray sphere) are also shown.

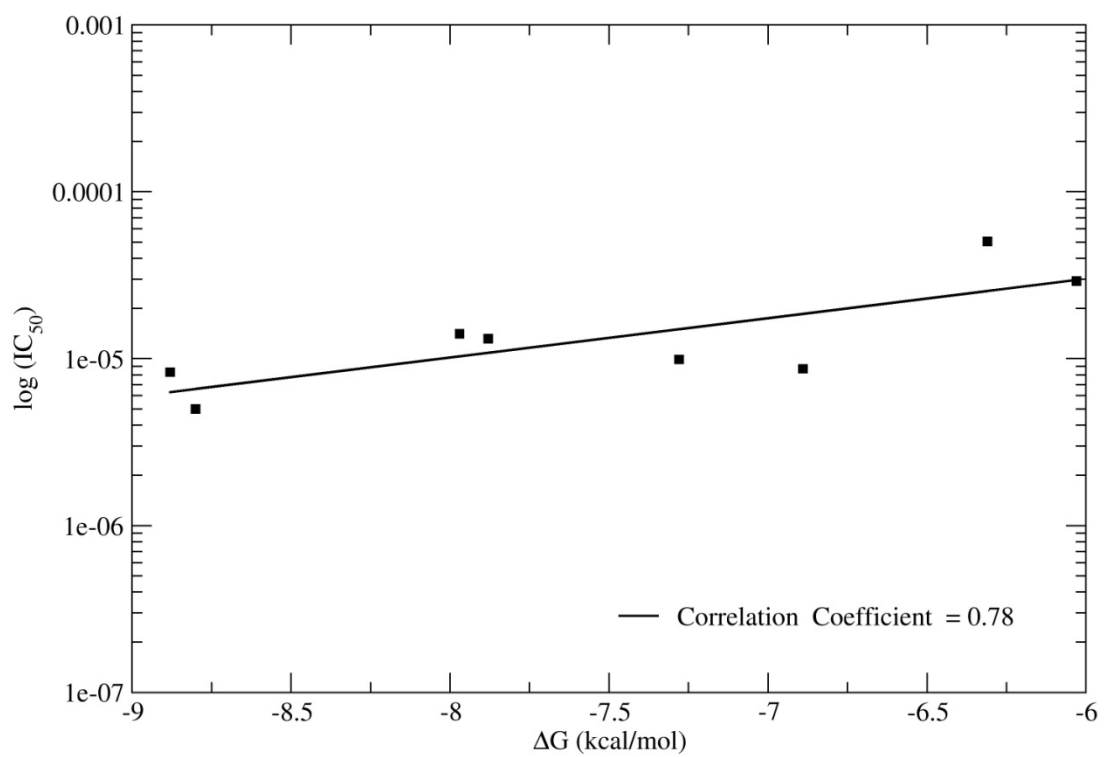


**Figure 3-6.** Correlation between  $\log(\text{IC}_{50})$  and calculated Free energy of binding ( $\Delta G$ ).

### 3.F Discussion

Anthrax lethal factor is a zinc dependent endopeptidase that cleaves MAPKKs 1-4, 6, and 7 to inhibit downstream pathways that culminate in macrophage apoptosis. The  $\text{Zn}^{2+}$  ion in the lethal factor active site is tetrahedrally coordinated by two histidine residues (His686 and His690), one glutamic acid residue (Glu735), and one water molecule. The bound water molecule which occurs in several different zinc metalloproteases, is responsible for substrate cleavage.<sup>29</sup> Our goal is to exploit the presence of a metal ion and develop LFi that can chelate and inactivate the catalytic  $\text{Zn}^{2+}$  ion while optimizing the noncovalent interactions of the backbone component with the protein active site. Most LFi and metalloprotein inhibitors in general utilize a hydroxamic acid as the ZBG; the poor pharmacokinetics of hydroxamates however has made the search for alternative chelators a prudent topic of interest.<sup>14,17</sup>

Of the previously reported ZBGs, hydroxypyrothiones were determined to be the most potent against LF and thus were incorporated into the LFi **11b** as shown in Figure 3-1.<sup>15</sup> **11b** inspired the design of additional hydroxypyrothione inhibitors as shown in Figure 3-2, along with their hydroxypyronone precursors, to develop a structure-activity-relationship (SAR). The overall goal was to design and synthesize inhibitors with variations in three key components (the ZBG, linker, and backbone) and to analyze the contribution of each component toward potency against LF.

Figure 3-2 shows the compounds that were synthesized for this study which also include MMPi (**1a** and **9a**) that were previously reported.<sup>22</sup> As shown in Figure 3-2, four different ZBGs (hydroxypyronone, hydroxypyrothione, *N*-hydroxypyridinone, *N*-hydroxypyridinethione), two different linkers (amide and thioamide), and eight



different backbones were assembled in different combinations to generate 28 compounds. Table 3-1 lists the IC<sub>50</sub> values of each compound against LF. As previously noted, the *N*-hydroxypyridinone- (both *O,O,O* and *O,S,O*) and the hydroxypyrrone-based (*O,O,O*) compounds are poor inhibitors of LF. In contrast, the (*O,S,O*) hydroxypyrothione ZBG clearly improves inhibition of LF, consistent with the earlier studies on **11b**.<sup>15</sup>

A calculated structure of the bound complex formed between **11b** and anthrax LF showed the biphenyl backbone of **11b** targeting a specific pocket in the LF active site.<sup>15</sup> To optimize the backbone interactions in LF, different substituted and unsubstituted aromatic backbones were appended to the ZBGs via an amide or thioamide linker. The hydroxypyrothiones coupled via an amide bond (*O,S,O*) showed moderate potency (consistent with **11b**) with some variations depending on the backbone group. However, the use of a thioamide linker with a hydroxypyrothione ZBG (*O,S,S*) showed consistently improved potency against LF, regardless of the backbone used. These results suggested that the potency of the (*O,S,S*) compounds was primarily a result of the ZBG and linker alone. To improve potency by enhancing backbone interactions, we targeted the S1' pocket of LF with the design of inhibitor series **4a-c**. The “bifurcated” biphenyl backbone of **4c** was designed to interact with the same pocket as found for **11b** while also targeting the S1' pocket. Compound **4c** showed a slight but not pronounced improvement in inhibition compared to the other LFi reported here. To confirm the dominance of the ZBG and linker over the backbone in this series of LFi, compounds with a simple ethyl backbone were prepared (**8a-c**). Indeed, the potency of **8c** showed that the backbone groups play a minimal role in

these compounds, and further design is required to fully exploit additional protein-specific interactions.

To probe the specific interactions of the ZBG, linker, and backbone in the active site, computational models for the binding mode of several of the inhibitors were generated using the previously calculated **11b** model as a starting point.<sup>15</sup> QM/MM minimization procedures were employed on each model in order to take into account electronic effects in the interaction between  $\text{Zn}^{2+}$ , the active site residues, and the ZBG. The models show a good agreement, at least qualitatively, with the experimentally observed  $\text{IC}_{50}$  values. The optimized structures reveal that different backbone fragments have little effect on the orientation of the ZBG in the active site. The main structural difference found in our models was in the orientation of the amide/ thioamide linker relative to the ZBG. The models show that twisting about the bond between the ZBG and the amide group (e.g., breaking planarity of the amide group and aromatic pyrone rings) allows for formation of specific interactions between residues Lys392, Gly393, and the oxygen/sulfur amide atoms of the inhibitors. Dihedral angles between the amide/thioamide groups and pyrone rings in **1b**, **1c**, **3b**, **3c**, **4b**, and **4c** were found to be  $71^\circ$ ,  $62^\circ$ ,  $28^\circ$ ,  $98^\circ$ ,  $61^\circ$ , and  $57^\circ$ , respectively. The hydrogen bonding is most pronounced in the inhibitor with bulky backbones (**1b,c** and **4b,c**), where the hydrogen-bonded amide/ thioamide linkers sit in essentially the same configuration (Figure 3-4). The smaller angle in **3b** is consistent with the lack of hydrogen bonding (Figure 3-4) with the protein active site compared to the other LFi. It is important to note that QM minimizations of the inhibitors, in the absence of protein and solvation, converge to a planar thioamide-pyrone ring conjugated system.

This was validated by minimizing the conformation of **5c**, which converged to the structure found by crystallographic analysis (Figure 3-3). The hydrogen bond formed by the thioamide LFi was somewhat surprising, as thioamides are known to be weaker hydrogen bond acceptors compared to their amide analogues.<sup>30,31</sup> However, Allen and co-workers have shown that thioamides possess a resonance induced hydrogen bonding potential that arises from the lone pair of electrons on the neighboring nitrogen atom of the amino group.<sup>30</sup> This leads to a net increase in electronegativity of the thioamide sulfur and a lengthening of the C=S bond, which likely facilitates hydrogen bonding in these molecules.

Despite the difference in potency among the (O,S,O) and (O,S,S) compounds, the LE values of both sets of hydroxypyrothiones fall in a reasonably efficient, small window of 0.28-0.54 kcal mol<sup>-1</sup> per heavy atom.<sup>20,21,25</sup> As discussed earlier LE is used to normalize the potency of various ligands with respect to their molecular weight.<sup>20,21,25,32</sup> In this way, LE is an important metric in controlling the size of a druggable lead while maintaining potency. The LE of the hydroxypyrothione ZBG (i.e., thiomaltol) is 0.58 kcal mol<sup>-1</sup> per heavy atom and with the addition of a thioamide ethyl linkage (**8c**) is 0.54 kcal mol<sup>-1</sup> per heavy atom. The remaining hydroxypyrothione LFi with aromatic backbones have an average LE of 0.33 kcal mol<sup>-1</sup> per heavy atom. The potency gained by the thioamide bond is further reflected in the similar LE values obtained for thiomaltol and **8c** and remains relatively consistent throughout the LFi series compared to their amide analogues. As discussed above, the potency of the thioamide-linked compounds may be attributed to the longer C=S bond

and twisting of the ZBG, which helps to introduce hydrogen bonding with the protein active site.<sup>30,33</sup>

There is some concern about the clinical use of thioamides, as in some cases they have been associated with hepatotoxic effects.<sup>34,35</sup> However, other studies have shown thioamides to improve the stability of compounds against certain proteases.<sup>33,36,37</sup> In this study, in addition to being more potent, the thioamide LFi meet certain drug discovery criteria, with molecular weights of less than 500 Da, possessing less than 5 hydrogen-bond donors and less than 10 hydrogen-bond acceptors with adequate ligand efficiencies.<sup>32</sup> To further develop the hydroxypyrothione ZBGs with a thioamide linker, we plan to utilize our computational models to probe the active site and further elaborate the (O,S,S) scaffold with more specific, protein-interacting backbones.

### 3.G Conclusions

In this study we have successfully shown the effect of the ZBG and linker on the potency of a series of metal-chelating LFi. Some of the compounds include potent, isoform-specific MMPi (**1a** and **9a**) that showed negligible potency against LF. The active inhibitors identified here elicit the effect by tight binding of the ZBG and strong hydrogen bonding to the protein via a thioamide linking group. Even though at present we have not identified an optimal backbone component, we have succeeded in identifying a potent ZBG-linker scaffold from which an optimized backbone can be grafted to obtain a new class of highly potent LFi.

### 3.H Experimental

Unless otherwise noted, all chemicals were purchased from commercial suppliers (Aldrich and Fisher) and used as received. Flash silica gel chromatography was performed using Merck silica gel 40-63  $\mu\text{m}$  mesh. Inert reactions were carried out under a dinitrogen atmosphere.  $^1\text{H}/^{13}\text{C}$  NMR spectra were recorded at ambient temperature on a 300 or 400 MHz Varian FT-NMR instrument, property of the Department of Chemistry and Biochemistry, University of California, San Diego. Mass spectra were obtained at the Small Molecule Mass Spectrometry Facility in the Department of Chemistry and Biochemistry at the University of California, San Diego. Elemental analysis was performed by NuMega Resonance Laboratories, San Diego, CA.

#### 3.H.i Synthesis of LF inhibitors (1a,b,c-8a,b,c and 9a,b-10a,b)

##### *N*-(Biphenyl-4-ylmethyl)-3-hydroxy-4-oxo-4*H*-pyran-2-carboxamide (**1a**).

This compound was prepared as previously reported.<sup>22</sup> Anal. calcd for  $\text{C}_{19}\text{H}_{15}\text{NO}_4$ : C, 71.02; H, 4.71; N, 4.36. Found: C, 71.15; H, 5.04; N, 4.43.

##### *N*-(Biphenyl-4-ylmethyl)-3-hydroxy-4-thioxo-4*H*-pyran-2-carboxamide

(**1b**). To a solution of **1a** (200 mg, 0.62 mmol) in benzene (20 mL) was added  $\text{P}_4\text{S}_{10}$  (0.366 equiv, 102 mg, 0.23 mmol) and HMDO (3.339 equiv, 336 mg, 442  $\mu\text{L}$ , 2.07 mmol), and the mixture was heated to reflux at 105  $^\circ\text{C}$  for 3 h. Solid byproducts were removed by vacuum filtration, and the filtrate was evaporated in vacuo to a crude brown solid. The crude product was purified via column chromatography (50% EtOAc/hexanes) to afford **1b** (33 mg, 0.10 mmol). Yield = 16%.  $^1\text{H}$  NMR (400 MHz,  $\text{CDCl}_3$ - $d_1$ , 25  $^\circ\text{C}$ ):  $\delta$  = 4.71 (d,  $J$  = 6.0 Hz,  $\text{NHCH}_2$ ), 7.34 (t,  $J$  = 7.2 Hz, 1H; ArH),

7.42 (m, 5H; ArH), 7.57 (m, 4H; ArH), 7.72 (d,  $J = 5.2$  Hz, 1H; ArH), 7.92 (brt, 1H; CONHCH<sub>2</sub>), 9.73 (brs, 1H; ArOH). <sup>13</sup>C NMR (100 MHz, CDCl<sub>3</sub>-*d*<sub>1</sub>, 25 °C):  $\delta = 43.6$  (CH<sub>2</sub>), 125.7 (ArC), 127.1 (ArC), 127.4 (ArC), 127.6 (ArC), 128.3 (ArC), 128.8 (ArC), 132.4 (ArC), 136.0 (ArC), 140.5 (ArC), 140.9 (ArC), 147.4 (ArC), 151.6 (ArC), 160.9 (C=O), 190.5 (ArC=S). APCI-MS(-)  $m/z$  336.11 [M-H]<sup>-</sup>. Anal. calcd for C<sub>19</sub>H<sub>15</sub>NO<sub>3</sub>S•H<sub>2</sub>O: C, 64.21; H, 4.82; N, 3.94; S, 10.80. Found: C, 64.51; H, 4.94; N, 3.89; S, 11.26.

***N*-(Biphenyl-4-ylmethyl)-3-hydroxy-4-thioxo-4*H*-pyran-2-carbothioamide**

**(1c).** **1c** was obtained from **1a** from the same reaction as that of **1b** (vide supra) as a dark-brown solid (94 mg, 0.27 mmol). Yield = 43%. <sup>1</sup>H NMR (400 MHz, CDCl<sub>3</sub>-*d*<sub>1</sub>, 25 °C):  $\delta = 5.01$  (d,  $J = 4.4$  Hz, NHCH<sub>2</sub>), 7.35 (t,  $J = 7.4$  Hz, 1H; ArH), 7.42 (m, 5H; ArH), 7.58 (m, 4H; ArH), 7.75 (d,  $J = 5.2$  Hz, 1H; ArH), 9.53 (brt, 1H; CONHCH<sub>2</sub>), 10.30 (brs, 1H; ArOH). <sup>13</sup>C NMR (100 MHz, CDCl<sub>3</sub>-*d*<sub>1</sub>, 25 °C):  $\delta = 50.0$  (CH<sub>2</sub>), 125.3 (ArC), 127.0 (ArC), 127.5 (ArC), 127.7 (ArC), 128.6 (ArC), 128.8 (ArC), 133.9 (ArC), 134.2 (ArC), 140.2 (ArC), 141.2 (ArC), 147.4 (ArC), 149.3 (ArC), 184.8 (C=S), 191.2 (ArC=S). APCI-MS(+)  $m/z$  353.98 [M+H]<sup>+</sup>. Anal. Calcd for C<sub>19</sub>H<sub>15</sub>NO<sub>2</sub>S<sub>2</sub>•0.65H<sub>2</sub>O: C, 62.49; H, 4.50; N, 3.84; S, 17.56. Found: C, 62.29; H, 4.45; N, 3.66; S, 17.40.

***N*-(4-Fluorobenzyl)-3-hydroxy-4-oxo-4*H*-pyran-2-carboxamide (2a).** To a solution of 3-(benzyloxy)-4-oxo-4*H*-pyran-2-carboxylic acid (**BPCA**)<sup>22</sup>, (500 mg, 2.0 mmol) in dichloromethane was added NHS (1.0 equiv, 230 mg, 2.0 mmol), EDCI (1.0 equiv, 383 mg, 2.0 mmol), and 4-fluorobenzylamine (1.0 equiv, 250 mg, 227  $\mu$ L, 2.0 mmol). The mixture was stirred overnight at room temperature under N<sub>2</sub> and then

poured into a separatory funnel and extracted with water and dichloromethane. The layers were separated, and the organic layers were combined, dried over anhydrous magnesium sulfate, filtered, and concentrated to an orange oil. The crude oil was purified via silica column chromatography (0-2% MeOH/CH<sub>2</sub>Cl<sub>2</sub>) to yield a yellow solid of the benzyl protected product. To the yellow product was added 10 mL of a 1:1 solution of concentrated HCl and glacial acetic acid. The reaction mixture was stirred for 5 d and then concentrated in vacuo to yield an off-white residue which was co-evaporated with MeOH and dried to yield an off-white solid (269 mg, 1.02 mmol). Yield = 93%. <sup>1</sup>H NMR (400 MHz, CDCl<sub>3</sub>-d<sub>1</sub>, 25 °C): δ = 4.46 (d, *J* = 6.0 Hz, NHCH<sub>2</sub>), 6.32 (d, *J* = 5.6 Hz, 1H; ArH), 6.90 (t, *J* = 8.4 Hz, 2H; ArH), 7.20 (dd, *J* = 3.6, 14 Hz, 2H; ArH), 7.67 (d, *J* = 5.2 Hz, 1H; ArH), 8.11 (brt, 1H; CONHCH<sub>2</sub>). <sup>13</sup>C NMR (100 MHz, CDCl<sub>3</sub>-d<sub>1</sub>, 25 °C): δ = 42.1 (CH<sub>2</sub>), 114.8 (ArC), 115.0 (ArC), 115.2 (ArC), 129.1 (ArC), 129.2 (ArC), 132.9 (ArC), 148.9 (ArC), 153.2 (ArC), 160.5 (ArC), 162.4 (ArC), 162.9 (C=O), 173.6 (ArC=O). ESI-MS(+) *m/z* 264.02 [M+H]<sup>+</sup>. Anal. calcd for C<sub>13</sub>H<sub>10</sub>FNO<sub>4</sub>: C, 59.32; H, 3.83; N, 5.32. Found: C, 58.97; H, 4.03; N, 5.47.

***N*-(4-Fluorobenzyl)-3-hydroxy-4-thioxo-4*H*-pyran-2-carboxamide (2b).**

This compound was prepared from **2a** according to the procedure outlined for **1b**. **2a** (150 mg, 0.57 mmol) was treated with P<sub>4</sub>S<sub>10</sub> and HMDO for 1 h to yield an orange-red solid of **2b** (48 mg, 0.17 mmol). Yield = 30%. <sup>1</sup>H NMR (400 MHz, CDCl<sub>3</sub>-d<sub>1</sub>, 25 °C): δ = 4.63 (d, *J* = 6.0 Hz, NHCH<sub>2</sub>), 7.02 (t, *J* = 9.4 Hz, 2H; ArH), 7.31 (m, 2H; ArH), 7.42 (dd, *J* = 3.6, 6.4 Hz, 1H; ArH), 7.72 (dd, *J* = 3.6, 6.4 Hz, 1H; ArH), 7.90 (brt, 1H; CONHCH<sub>2</sub>), 9.65 (brs, 1H; ArOH). <sup>13</sup>C NMR (100 MHz, CDCl<sub>3</sub>-d<sub>1</sub>, 25 °C): δ = 42.5



(CH<sub>2</sub>), 115.0 (ArC), 115.2 (ArC), 126.4 (ArC), 129.1 (ArC), 129.2 (ArC), 131.3 (ArC), 146.2 (ArC), 152.7 (ArC), 160.7 (ArC), 162.2 (ArC), 163.1 (C=O), 191.5 (ArC=S). APCI-MS(+)  $m/z$  280.06 [M+H]<sup>+</sup>. Anal. calcd for C<sub>13</sub>H<sub>10</sub>FNO<sub>3</sub>S: C, 55.91; H, 3.61; N, 5.02; S, 11.48. Found: C, 55.57; H, 4.00; N, 4.66; S, 10.73.

***N*-(4-Fluorobenzyl)-3-hydroxy-4-thioxo-4*H*-pyran-2-carbothioamide (2c).**

**2c** was obtained from **2a** from the same reaction as that of **2b** as a brown solid (47 mg, 0.16 mmol). Yield = 28%. <sup>1</sup>H NMR (400 MHz, CDCl<sub>3</sub>-*d*<sub>1</sub>, 25 °C):  $\delta$  = 4.94 (d,  $J$  = 4.8 Hz, NHCH<sub>2</sub>), 7.06 (t,  $J$  = 8.8 Hz, 2H; ArH), 7.35 (dd,  $J$  = 2.8, 13.6 Hz, 2H; ArH), 7.41 (d,  $J$  = 5.2 Hz, 1H; ArH), 7.76 (d,  $J$  = 4.8 Hz, 1H; ArH), 9.50 (brt, 1H; CONHCH<sub>2</sub>), 10.18 (brs, 1H; ArOH). <sup>13</sup>C NMR (100 MHz, CDCl<sub>3</sub>-*d*<sub>1</sub>, 25 °C):  $\delta$  = 49.4 (CH<sub>2</sub>), 115.8 (ArC), 116.0 (ArC), 125.2 (ArC), 129.8 (ArC), 130.0 (ArC), 133.8 (ArC), 147.4 (ArC), 149.1 (ArC), 161.2 (ArC), 163.7 (ArC), 184.8 (C=S), 191.1 (ArC=S). APCI-MS(+)  $m/z$  296.03 [M+H]<sup>+</sup>. Anal. calcd for C<sub>13</sub>H<sub>10</sub>FNO<sub>2</sub>S<sub>2</sub>: C, 52.87; H, 3.41; N, 4.74; S, 21.71. Found: C, 52.43; H, 3.50; N, 4.55; S, 21.32.

**3-Hydroxy-*N*-(4-methoxybenzyl)-4-oxo-4*H*-pyran-2-carboxamide (3a).** **3a**

was prepared according to the same procedure outlined for **2a** starting from **BPCA** (1.0 g, 4.1 mmol), EDCI (786 mg, 4.1 mmol), HOBT (554 mg, 4.1 mmol), and 4-methoxybenzylamine (562 mg, 536  $\mu$ L, 4.1 mmol) to yield an off-white solid of **3a** (600 mg, 2.2 mmol). Yield = 54%. <sup>1</sup>H NMR (400 MHz, CDCl<sub>3</sub>-*d*<sub>1</sub>, 25 °C):  $\delta$  = 3.81 (s, 3H; OCH<sub>3</sub>), 4.55 (d,  $J$  = 4.8 Hz, NHCH<sub>2</sub>), 6.44 (d,  $J$  = 6.0 Hz, 1H; ArH), 6.89 (d,  $J$  = 8.8 Hz, 2H; ArH), 7.02 (brt, 1H; CONHCH<sub>2</sub>), 7.26 (d,  $J$  = 9.6 Hz, 2H; ArH), 7.68 (d,  $J$  = 5.6 Hz, 1H; ArH). <sup>13</sup>C NMR (100 MHz, CDCl<sub>3</sub>-*d*<sub>1</sub>, 25 °C):  $\delta$  = 43.1 (CH<sub>2</sub>), 55.3 (OCH<sub>3</sub>), 114.3 (ArC), 115.5 (ArC), 128.5 (ArC), 129.4 (ArC), 135.9 (ArC), 149.6

(ArC), 153.0 (ArC), 159.4 (ArC), 163.1 (C=O), 173.6 (ArC=O). ESI-MS(+)  $m/z$  275.98 [M+H]<sup>+</sup>. Anal. calcd for C<sub>14</sub>H<sub>13</sub>NO<sub>5</sub>: C, 61.09; H, 4.76; N, 5.09. Found: C, 61.25; H, 4.54; N, 4.98.

**3-Hydroxy-*N*-(4-methoxybenzyl)-4-thioxo-4*H*-pyran-2-carboxamide (3b).**

This compound was prepared from **3a** according to the procedure outlined for **1b**. **3a** (150 mg, 0.54 mmol) was treated with P<sub>4</sub>S<sub>10</sub> and HMDO for 1 h to yield an orange-red solid of **3b** (65 mg, 0.22 mmol). Yield = 41%. <sup>1</sup>H NMR (400 MHz, CDCl<sub>3</sub>-*d*<sub>1</sub>, 25 °C):  $\delta$  = 3.77 (s, 3H; OCH<sub>3</sub>), 4.56 (d,  $J$  = 5.2 Hz, NHCH<sub>2</sub>), 6.85 (d,  $J$  = 8.0 Hz, 2H; ArH), 7.24 (d,  $J$  = 8.4 Hz, 2H; ArH), 7.36 (d,  $J$  = 4.8 Hz, 1H; ArH), 7.64 (d,  $J$  = 4.8 Hz, 1H; ArH), 7.80 (brt, 1H; CONHCH<sub>2</sub>), 9.95 (brs, 1H; ArOH). <sup>13</sup>C NMR (100 MHz, CDCl<sub>3</sub>-*d*<sub>1</sub>, 25 °C):  $\delta$  = 43.3 (CH<sub>2</sub>), 55.2 (OCH<sub>3</sub>), 114.1 (ArC), 125.9 (ArC), 128.8 (ArC), 129.1 (ArC), 132.0 (ArC), 146.9 (ArC), 151.6 (ArC), 159.1 (ArC), 160.8 (C=O), 190.6 (ArC=S). ESI-MS(-)  $m/z$  290.09 [M-H]<sup>-</sup>. Anal. calcd for C<sub>14</sub>H<sub>13</sub>NO<sub>4</sub>S•0.35H<sub>2</sub>O: C, 56.50; H, 4.64; N, 4.71; S, 10.77. Found: C, 56.90; H, 5.04; N, 4.49; S, 10.38.

**3-Hydroxy-*N*-(4-methoxybenzyl)-4-thioxo-4*H*-pyran-2-carbothioamide**

**(3c).** **3c** was obtained from **3a** from the same reaction as that of **3b** as a dark-brown solid (20 mg, 0.07 mmol). Yield = 7%. <sup>1</sup>H NMR (400 MHz, CDCl<sub>3</sub>-*d*<sub>1</sub>, 25 °C):  $\delta$  = 3.82 (s, 3H; OCH<sub>3</sub>), 4.87 (d,  $J$  = 5.6 Hz, NHCH<sub>2</sub>), 6.91 (d,  $J$  = 8.8 Hz, 2H; ArH), 7.31 (d,  $J$  = 8.4 Hz, 2H; ArH), 7.40 (d,  $J$  = 4.8 Hz, 1H; ArH), 7.73 (d,  $J$  = 5.2 Hz, 1H; ArH), 9.38 (brt, 1H; CONHCH<sub>2</sub>), 10.33 (brs, 1H; ArOH). <sup>13</sup>C NMR (100 MHz, CDCl<sub>3</sub>-*d*<sub>1</sub>, 25 °C):  $\delta$  = 49.8 (CH<sub>2</sub>), 55.2 (OCH<sub>3</sub>), 114.2 (ArC), 125.3 (ArC), 127.1 (ArC), 129.6 (ArC), 133.6 (ArC), 147.0 (ArC), 149.4 (ArC), 159.4 (ArC), 184.2

(C=S), 191.2 (ArC=S). APCI-MS(-)  $m/z$  306.06 [M-H]<sup>-</sup>. Anal. calcd for C<sub>14</sub>H<sub>13</sub>NO<sub>3</sub>S<sub>2</sub>: C, 54.70; H, 4.26; N, 4.56; S, 20.86. Found: C, 54.75; H, 4.59; N, 4.45; 20.62.

***N*-Benzhydryl-3-hydroxy-4-oxo-4*H*-pyran-2-carboxamide (4a).** This compound was prepared according to the same procedure outlined for **3a** starting from **BPCA** (1.0 g, 4.1 mmol), EDCI (1.2 equiv, 939 mg, 4.9 mmol), HOBT (1.2 equiv, 662 mg, 4.9 mmol), and diphenylmethanamine (1.2 equiv, 898 mg, 844  $\mu$ L, 4.9 mmol) to yield a tan solid of **4a** (732 mg, 2.3 mmol). Yield = 56%. <sup>1</sup>H NMR (400 MHz, CDCl<sub>3</sub>-*d*<sub>1</sub>, 25 °C):  $\delta$  = 6.37 (d,  $J$  = 8.0 Hz, NHCH), 6.45 (d,  $J$  = 5.2 Hz, 1H; ArH), 7.05 (brd,  $J$  = 7.6 Hz, CONHCH<sub>2</sub>), 7.28-7.43 (m, 10H; ArH), 7.72 (d,  $J$  = 6.0 Hz, 1H; ArH). <sup>13</sup>C NMR (100 MHz, DMSO-*d*<sub>6</sub>, 25 °C):  $\delta$  = 56.4 (CH<sub>2</sub>), 114.4 (ArC), 127.3 (ArC), 128.5 (ArC), 137.7 (ArC), 141.2 (ArC), 147.9 (ArC), 155.2 (ArC), 160.8 (C=O), 173.5 (ArC=O). ESI-MS(+)  $m/z$  321.85 [M+H]<sup>+</sup>. Anal. calcd for C<sub>19</sub>H<sub>15</sub>NO<sub>4</sub>•0.25H<sub>2</sub>O: C, 70.04; H, 4.79; N, 4.30. Found: C, 70.09; H, 5.16; N, 4.47.

***N*-Benzhydryl-3-hydroxy-4-thioxo-4*H*-pyran-2-carboxamide (4b).** This compound was prepared from **4a** according to the procedure outlined for **1b**. **4a** (600 mg, 1.9 mmol) was treated with P<sub>4</sub>S<sub>10</sub> and HMDO for 3 h to yield a light-brown solid of **4b** (90 mg, 0.27 mmol). Yield = 14%. <sup>1</sup>H NMR (400 MHz, CDCl<sub>3</sub>-*d*<sub>1</sub>, 25 °C):  $\delta$  = 6.44 (d,  $J$  = 8.0 Hz, NHCH), 7.30-7.38 (m, 10H; ArH), 7.41 (d,  $J$  = 5.2 Hz, 1H; ArH), 7.70 (d,  $J$  = 4.8 Hz, 1H; ArH), 8.27 (brd,  $J$  = 7.2 Hz, CONHCH<sub>2</sub>), 9.72 (brs, 1H; ArOH). <sup>13</sup>C NMR (100 MHz, DMSO-*d*<sub>6</sub>, 25 °C):  $\delta$  = 56.5 (ArC), 127.4 (ArC), 127.5 (ArC), 128.5 (ArC), 132.5 (ArC), 140.9 (ArC), 147.0 (ArC), 153.5 (ArC), 161.9 (C=O), 191.9 (ArC=S). APCI-MS(+)  $m/z$  338.18 [M+H]<sup>+</sup>. Anal. calcd for

C<sub>19</sub>H<sub>15</sub>NO<sub>3</sub>S•0.6H<sub>2</sub>O: C, 65.54; H, 4.69; N, 4.02; S, 9.21. Found: C, 65.60; H, 5.05; N, 4.02; S, 10.33.

***N*-Benzhydryl-3-hydroxy-4-thioxo-4*H*-pyran-2-carbothioamide (4c).** **4c** was obtained from **4a** from the same reaction as that of **4b** as a dark-brown solid (216 mg, 0.61 mmol). Yield = 32%. <sup>1</sup>H NMR (400 MHz, CDCl<sub>3</sub>-*d*<sub>1</sub>, 25 °C): δ = 6.93 (d, *J* = 7.2 Hz, NHCH), 7.30-7.40 (m, 10H; ArH), 7.42 (d, *J* = 5.2 Hz, 1H; ArH), 7.76 (d, *J* = 5.2 Hz, 1H; ArH), 9.92 (brd, CONHCH<sub>2</sub>), 10.15 (brs, 1H; ArOH). <sup>13</sup>C NMR (100 MHz, DMSO-*d*<sub>6</sub>, 25 °C): δ = 61.7 (CH<sub>2</sub>), 125.5 (ArC), 127.6 (ArC), 127.7 (ArC), 28.6 (ArC), 139.2 (ArC), 139.7 (ArC), 147.7 (ArC), 184.4 (C=S), 191.1 (ArC=S). APCI-MS(+) *m/z* 353.85 [M+H]<sup>+</sup>. Anal. calcd for C<sub>19</sub>H<sub>15</sub>NO<sub>2</sub>S<sub>2</sub>•0.4H<sub>2</sub>O: C, 63.27; H, 4.42; N, 3.88; S, 17.78. Found: C, 63.47; H, 4.86; N, 3.90; S, 18.16.

**3-Hydroxy-*N*-(2-methoxybenzyl)-4-oxo-4*H*-pyran-2-carboxamide (5a).** This compound was prepared according to the same procedure outlined for **3a** starting from **BPCA** (500 mg, 2.0 mmol), EDCI (1.2 equiv, 713 mg, 2.4 mmol), HOBt (1.2 equiv, 324 mg, 2.4 mmol), and 2-methoxybenzylamine (1.2 equiv, 329 mg, 310 μL, 2.4 mmol), to yield an off-white solid of **5a** (355 mg, 1.3 mmol). Yield = 65%. <sup>1</sup>H NMR (400 MHz, CDCl<sub>3</sub>-*d*<sub>1</sub>, 25 °C): δ = 3.86 (s, 3H; OCH<sub>3</sub>), 4.57 (d, *J* = 3.6 Hz, HCH<sub>2</sub>), 6.39 (d, *J* = 5.2 Hz, 1H; ArH), 6.87 (q, *J* = 7.2 Hz, 2H; ArH), 7.25 (m, 2H; ArH), 7.57 (brt, 1H; CONHCH<sub>2</sub>), 7.71 (d, *J* = 6.0 Hz, 1H; ArH). <sup>13</sup>C NMR (100 MHz, CDCl<sub>3</sub>-*d*<sub>1</sub>, 25 °C): δ = 39.6 (CH<sub>2</sub>), 55.4 (OCH<sub>3</sub>), 110.5 (ArC), 115.5 (ArC), 120.8 (ArC), 124.5 (ArC), 129.6 (ArC), 130.1 (ArC), 136.1 (ArC), 149.7 (ArC), 152.8 (ArC), 57.6 (ArC), 163.0 (C=O), 173.7 (ArC=O). APCI-MS(+) *m/z* 275.88 [M+H]<sup>+</sup>. Anal. calcd for C<sub>14</sub>H<sub>13</sub>NO<sub>5</sub>: C, 61.09; H, 4.76; N, 5.09. Found: C, 60.88; H, 4.86; N, 4.97.

**3-Hydroxy-*N*-(2-methoxybenzyl)-4-thioxo-4*H*-pyran-2-carboxamide (5b).**

This compound was prepared from **5a** according to the procedure outlined for **1b**. **5a** (400 mg, 1.4 mmol) was treated with P<sub>4</sub>S<sub>10</sub> and HMDO for 2.5 h to yield a reddish brown solid of **5b** (290 mg, 1.0 mmol). Yield = 76%. <sup>1</sup>H NMR (300 MHz, CDCl<sub>3</sub>-*d*<sub>1</sub>, 25 °C): δ = 3.90 (s, 3H; OCH<sub>3</sub>), 4.65 (d, *J* = 5.7 Hz, NHCH<sub>2</sub>), 6.90 (q, *J* = 7.8 Hz, 2H; ArH), 7.28-7.35 (m, 2H; ArH), 7.40 (d, *J* = 4.8 Hz, 1H; ArH), 7.68 (d, *J* = 5.7 Hz, 1H; ArH), 8.08 (brt, 1H; CONHCH<sub>2</sub>), 9.88 (brs, 1H; ArOH). <sup>13</sup>C NMR (75 MHz, CDCl<sub>3</sub>-*d*<sub>1</sub>, 25 °C): δ = 39.9 (CH<sub>2</sub>), 55.4 (OCH<sub>3</sub>), 110.4 (ArC), 120.7 (ArC), 125.0 (ArC), 125.8 (ArC), 129.4 (ArC), 129.9 (ArC), 133.4 (ArC), 147.0 (ArC), 152.1 (ArC), 157.6 (ArC), 161.4 (C=O), 191.7 (ArC=O). ESI-MS(+) *m/z* 292.00 [M+H]<sup>+</sup>. HRMS calcd for C<sub>14</sub>H<sub>13</sub>NO<sub>4</sub>S: 291.0560. Found: 291.0563.

**3-Hydroxy-*N*-(2-methoxybenzyl)-4-thioxo-4*H*-pyran-2-carbothioamide**

**(5c).** **5c** was obtained from **5a** from the same reaction as that of **5b** as a dark-brown solid (90 mg, 0.29 mmol). Yield = 21%. <sup>1</sup>H NMR (400 MHz, CDCl<sub>3</sub>-*d*<sub>1</sub>, 25 °C): δ = 3.90 (s, 3H; OCH<sub>3</sub>), 4.99 (d, *J* = 5.2 Hz, NHCH<sub>2</sub>), 6.93 (q, *J* = 7.2 Hz, 2H; ArH), 7.33 (q, *J* = 8.0 Hz, 2H; ArH), 7.40 (d, *J* = 5.2 Hz, 1H; ArH), 7.73 (d, *J* = 5.2 Hz, 1H; ArH), 9.70 (brt, 1H; CONHCH<sub>2</sub>), 10.43 (brs, 1H; ArOH). <sup>13</sup>C NMR (100 MHz, CDCl<sub>3</sub>-*d*<sub>1</sub>, 25 °C): δ = 45.4 (CH<sub>2</sub>), 55.1 (OCH<sub>3</sub>), 110.3 (ArC), 120.4 (ArC), 122.9 (ArC), 125.7 (ArC), 129.5 (ArC), 130.2 (ArC), 133.6 (ArC), 146.4 (ArC), 150.1 (ArC), 157.4 (ArC), 183.6 (C=S), 191.8 (ArC=S). APCI-MS(+) *m/z* 307.91 [M+H]<sup>+</sup>. Anal. calcd for C<sub>14</sub>H<sub>13</sub>NO<sub>3</sub>S<sub>2</sub>•0.5H<sub>2</sub>O: C, 53.15; H, 4.46; N, 4.43; S, 20.27. Found: C, 52.90; H, 4.49; N, 4.12; S, 20.44.

**3-Hydroxy-*N*-(3-methoxybenzyl)-4-oxo-4*H*-pyran-2-carboxamide (6a).**

This compound was prepared according to the same procedure outlined for **3a** starting from **BPCA** (500 mg, 2.0 mmol), EDCI (1.2 equiv, 713 mg, 2.4 mmol), HOBT (1.2 equiv, 324 mg, 2.4 mmol), and 3-methoxybenzylamine (1.2 equiv, 329 mg, 310  $\mu$ L, 2.4 mmol) to yield a tan solid of **6a** (330 mg, 1.2 mmol). Yield = 60%.  $^1\text{H}$  NMR (400 MHz,  $\text{CDCl}_3-d_1$ , 25  $^\circ\text{C}$ ):  $\delta$  = 3.79 (s, 3H;  $\text{OCH}_3$ ), 4.57 (d,  $J$  = 4.8 Hz,  $\text{NHCH}_2$ ), 6.52 (d,  $J$  = 6.0 Hz, 1H; ArH), 6.82-6.92 (m, 3H; ArH), 7.24 (t,  $J$  = 7.8 Hz, 1H; ArH), 7.60 (brt, 1H;  $\text{CONHCH}_2$ ), 7.81 (d,  $J$  = 5.2 Hz, 1H; ArH).  $^{13}\text{C}$  NMR (100 MHz,  $\text{CDCl}_3-d_1$ , 25  $^\circ\text{C}$ ):  $\delta$  = 43.5 ( $\text{CH}_2$ ), 55.3 ( $\text{OCH}_3$ ), 113.2 (ArC), 113.4 (ArC), 113.7 (ArC), 120.1 (ArC), 130.0 (ArC), 136.0 (ArC), 138.1 (ArC), 149.6 (ArC), 153.1 (ArC), 159.9 (ArC), 163.1 (C=O), 173.6 (ArC=O). APCI-MS(+)  $m/z$  275.96  $[\text{M}+\text{H}]^+$ . Anal. calcd for  $\text{C}_{14}\text{H}_{13}\text{NO}_5$ : C, 61.09; H, 4.76; N, 5.09. Found: C, 60.75; H, 4.87; N, 5.16.

**3-Hydroxy-*N*-(3-methoxybenzyl)-4-thioxo-4*H*-pyran-2-carboxamide (6b).**

This compound was prepared from **6a** according to the procedure outlined for **1b**. **6a** (40 mg, 0.15 mmol) was treated with  $\text{P}_4\text{S}_{10}$  and HMDO for 40 min to yield a brown solid of **6b** (40 mg, 0.14 mmol). Yield = 95%.  $^1\text{H}$  NMR (300 MHz,  $\text{CDCl}_3-d_1$ , 25  $^\circ\text{C}$ ):  $\delta$  = 3.81 (s, 3H;  $\text{OCH}_3$ ), 4.64 (d,  $J$  = 6.0 Hz,  $\text{NHCH}_2$ ), 6.83-6.89 (m, 2H; ArH), 6.92 (d,  $J$  = 7.8 Hz, 1H; ArH), 7.28 (d,  $J$  = 7.8 Hz, 1H; ArH), 7.41 (d,  $J$  = 5.4 Hz, 1H; ArH), 7.70 (d,  $J$  = 4.8 Hz, 1H; ArH), 7.86 (brt, 1H;  $\text{CONHCH}_2$ ), 9.74 (brs, 1H; ArOH).  $^{13}\text{C}$  NMR (75 MHz,  $\text{DMSO}-d_6$ , 25  $^\circ\text{C}$ ):  $\delta$  = 42.4 ( $\text{CH}_2$ ), 55.0 ( $\text{OCH}_3$ ), 112.5 (ArC), 113.2 (ArC), 119.5 (ArC), 127.8 (ArC), 129.5 (ArC), 131.7 (ArC), 139.6 (ArC), 154.1 (ArC), 159.3 (ArC), 161.9 (ArC), 163.4 (C=O), 192.4 (ArC=S). ESI-MS(+)  $m/z$  292.05  $[\text{M}+\text{H}]^+$ . HRMS calcd for  $\text{C}_{14}\text{H}_{13}\text{NO}_3\text{S}$ : 291.0560. Found: 291.0556.

**3-Hydroxy-N-(3-methoxybenzyl)-4-thioxo-4H-pyran-2-carbothioamide**

**(6c)**. This compound was prepared from **6a** according to the procedure outlined for **1c**. **6a** (450 mg, 1.6 mmol) was treated for 2 h to yield a dark-greenish-brown solid of **6c** (126 mg, 0.43 mmol). Yield = 27%. <sup>1</sup>H NMR (400 MHz, CDCl<sub>3</sub>-d<sub>1</sub>, 25 °C): δ = 3.83 (s, 3H; OCH<sub>3</sub>), 4.93 (d, *J* = 5.2 Hz, NHCH<sub>2</sub>), 6.89-6.92 (m, 2H; ArH), 6.96 (d, *J* = 8.0 Hz, 1H; ArH), 7.30 (t, *J* = 8.0 Hz, 1H; ArH), 7.42 (d, *J* = 5.2 Hz, 1H; ArH), 7.76 (d, *J* = 5.2 Hz, 1H; ArH), 9.47 (brt, 1H; CONHCH<sub>2</sub>), 10.26 (brs, 1H; ArOH). <sup>13</sup>C NMR (75 MHz, CDCl<sub>3</sub>-d<sub>1</sub>, 25 °C): δ = 50.4 (CH<sub>2</sub>), 55.3 (OCH<sub>3</sub>), 113.6 (ArC), 113.9 (ArC), 120.4 (ArC), 125.2 (ArC), 129.2 (ArC), 130.2 (ArC), 133.9 (ArC), 136.8 (ArC), 147.5 (ArC), 160.0 (ArC), 185.3 (C=S), 197.0 (ArC=S). APCI-MS(+) *m/z* 307.96 [M+H]<sup>+</sup>. Anal. calcd for C<sub>14</sub>H<sub>13</sub>NO<sub>3</sub>S<sub>2</sub>•0.55H<sub>2</sub>O: C, 52.99; H, 4.48; N, 4.41; S, 20.21. Found: C, 52.83; H, 4.57; N, 4.40; S, 21.52.

**N-Benzyl-3-hydroxy-4-oxo-4H-pyran-2-carboxamide (7a)**. This compound was prepared according to the same procedure outlined for **3a** starting from **BPCA** (575 mg, 2.3 mmol), EDCI (1.0 equiv, 441 mg, 2.3 mmol), HOBT (1.0 equiv, 311 mg, 2.3 mmol), and benzylamine (1.0 equiv, 246 mg, 251 μL, 2.3 mmol) to yield a tan solid of **7a** (294 mg, 1.2 mmol). Yield = 52%. <sup>1</sup>H NMR (400 MHz, CDCl<sub>3</sub>, 25 °C): δ = 4.63 (d, *J* = 6.0 Hz, NHCH<sub>2</sub>), 6.46 (d, *J* = 5.2 Hz, 1H; ArH), 7.04 (brt, 1H; CONHCH<sub>2</sub>), 7.34-7.41 (m, 5H; ArH), 7.69 (d, *J* = 6 Hz, 1H; ArH). <sup>13</sup>C NMR (100 MHz, CDCl<sub>3</sub>-d<sub>1</sub>, 25 °C): δ = 43.6 (CH<sub>2</sub>), 115.5 (ArC), 128.0 (ArC), 128.1 (ArC), 129.0 (ArC), 135.9 (ArC), 136.5 (ArC), 149.6 (ArC), 153.0 (ArC), 163.1 (C=O), 173.5 (ArC=O). APCI-MS(+) *m/z* 246.00 [M+H]<sup>+</sup>. Anal. calcd for C<sub>13</sub>H<sub>11</sub>NO<sub>4</sub>: C, 63.67; H, 4.52; N, 5.71. Found: C, 63.28; H, 4.74; N, 5.87.

***N*-Benzyl-3-hydroxy-4-thioxo-4*H*-pyran-2-carboxamide (7b).** This compound was prepared from **7a** according to the procedure outlined for **1b**. **7a** (250 mg, 1.0 mmol) was treated for 1.5 h to yield a mustard-brown solid of **7b** (85 mg, 0.32 mmol). Yield = 32%. <sup>1</sup>H NMR (300 MHz, CDCl<sub>3</sub>-*d*<sub>1</sub>, 25 °C): δ = 4.51 (d, *J* = 6.0 Hz, NHCH<sub>2</sub>), 7.15-7.20 (m, 1H; ArH), 7.23 (s, 3H; ArH), 7.24 (s, 1H; ArH), 7.27 (d, *J* = 4.4 Hz, 1H; ArH), 7.58 (d, 7.04, *J* = 4.4 Hz, 1H; ArH), 8.29 (brt, 1H; CONHCH<sub>2</sub>), 9.80 (brs, 1H; ArOH). <sup>13</sup>C NMR (75 MHz, DMSO-*d*<sub>6</sub>, 25 °C): δ = 43.3 (CH<sub>2</sub>), 126.3 (ArC), 127.4 (ArC), 127.5 (ArC), 128.5 (ArC), 131.5 (ArC), 136.7 (ArC), 146.4 (ArC), 152.2 (ArC), 161.7 (C=S), 191.1 (ArC=S). APCI-MS(+) *m/z* 262.05 [M+H]<sup>+</sup>. HRMS calcd for C<sub>13</sub>H<sub>11</sub>NO<sub>3</sub>S: 261.0454. Found: 291.0455.

***N*-Benzyl-3-hydroxy-4-thioxo-4*H*-pyran-2-carbothioamide (7c).** This compound was prepared from **7a** according to the procedure outlined for **1c**. **7a** (180 mg, 0.73 mmol) was treated with P<sub>4</sub>S<sub>10</sub> and HMDO for 2.5 h to yield a dark-red solid of **7c** (24 mg, 0.09 mmol). Yield = 12%. <sup>1</sup>H NMR (400 MHz, CDCl<sub>3</sub>-*d*<sub>1</sub>, 25 °C): δ = 4.96 (d, *J* = 5.2 Hz, NHCH<sub>2</sub>), 7.35-7.39 (m, 5H; ArH), 7.41 (d, *J* = 5.2 Hz, 1H; ArH), 7.74 (d, *J* = 5.2 Hz, 1H; ArH), 9.47 (brt, 1H; CONHCH<sub>2</sub>), 10.30 (brs, 1H; ArOH). <sup>13</sup>C NMR (100 MHz, CDCl<sub>3</sub>-*d*<sub>1</sub>, 25 °C): δ = 50.0 (CH<sub>2</sub>), 125.4 (ArC), 128.0 (ArC), 128.1 (ArC), 128.8 (ArC), 133.6 (ArC), 135.1 (ArC), 146.8 (ArC), 149.6 (ArC), 184.5 (C=S), 191.3 (ArC=S). APCI-MS(+) *m/z* 278.08 [M+H]<sup>+</sup>. Anal. calcd for C<sub>13</sub>H<sub>11</sub>NO<sub>2</sub>S<sub>2</sub>•0.5H<sub>2</sub>O: C, 54.52; H, 4.22; N, 5.71; S, 22.39. Found: C, 54.69; H, 4.62; N, 4.89; S, 21.89.

***N*-Ethyl-3-hydroxy-4-oxo-4*H*-pyran-2-carboxamide (8a).** This compound was prepared according to the same procedure outlined for **3a** starting from **BPCA**



(500 mg, 2.0 mmol), EDCI (1.2 equiv, 713 mg, 2.4 mmol), HOBT (1.2 equiv, 324 mg, 2.4 mmol), and 2 M ethylamine in THF (1.2 equiv, 1.2 mL, 2.4 mmol) to yield an off-white solid of **8a** (210 mg, 1.2 mmol). Yield = 64%.  $^1\text{H}$  NMR (400 MHz,  $\text{CDCl}_3-d_1$ , 25 °C):  $\delta$  = 1.26 (t,  $J$  = 7.4 Hz, 2H;  $\text{CH}_2\text{CH}_3$ ), 3.47 (p,  $J$  = 7.2 Hz, 2H;  $\text{NHCH}_2\text{CH}_3$ ), 6.46 (d,  $J$  = 5.2 Hz, 1H; ArH), 6.75 (brt, 1H;  $\text{CONHCH}_2$ ), 7.71 (d,  $J$  = 5.6 Hz, 1H; ArH).  $^{13}\text{C}$  NMR (100 MHz,  $\text{CDCl}_3-d_1$ , 25 °C):  $\delta$  = 14.6 ( $\text{CH}_2\text{CH}_3$ ), 34.6 ( $\text{CH}_2\text{CH}_3$ ), 115.5 (ArC), 136.0 (ArC), 149.5 (ArC), 152.9 (ArC), 163.2 (C=O), 173.7 (ArC=O). ESI-MS(+)  $m/z$  184.09  $[\text{M}+\text{H}]^+$ . HRMS calcd for  $\text{C}_8\text{H}_9\text{NO}_4$ : 183.0526. Found: 183.0525.

***N*-Ethyl-3-hydroxy-4-thioxo-4*H*-pyran-2-carboxamide (8b).** This compound was prepared from **8a** according to the procedure outlined for **1b**. **8a** (107 mg, 0.6 mmol) was treated with  $\text{P}_4\text{S}_{10}$  and HMDO for 25 min to yield a reddish-brown solid of **8b** (30 mg, 0.15 mmol). Yield = 25%.  $^1\text{H}$  NMR (300 MHz,  $\text{CDCl}_3-d_1$ , 25 °C):  $\delta$  = 1.26 (t,  $J$  = 7.4 Hz, 2H;  $\text{CH}_2\text{CH}_3$ ), 3.50 (p,  $J$  = 7.0 Hz, 2H;  $\text{CH}_2\text{CH}_3$ ), 7.42 (d,  $J$  = 5.2 Hz, 1H; ArH), 7.71 (brt, 1H;  $\text{CONHCH}_2$ ), 7.70 (d,  $J$  = 5.2 Hz, 1H; ArH), 9.86 (brs, 1H; ArOH). ESI-MS(+)  $m/z$  222.02  $[\text{M}+\text{Na}]^+$ . HRMS calcd for  $\text{C}_8\text{H}_9\text{NO}_3\text{SNa}$ : 222.0195. Found: 222.0193.

***N*-Ethyl-3-hydroxy-4-thioxo-4*H*-pyran-2-carbothioamide (8c).** This compound was prepared from **8a** according to the procedure outlined for **1c**. **8a** (165 mg, 0.90 mmol) was treated for 2.5 h to yield a dark-brown solid of **8c** (77 mg, 0.36 mmol). Yield = 40%.  $^1\text{H}$  NMR (400 MHz,  $\text{CDCl}_3-d_1$ , 25 °C):  $\delta$  = 1.38 (t,  $J$  = 7.4 Hz, 2H;  $\text{CH}_2\text{CH}_3$ ), 3.81-3.88 (m, 2H;  $\text{CH}_2\text{CH}_3$ ), 7.41 (d,  $J$  = 5.2 Hz, 1H; ArH), 7.74 (d,  $J$  = 4.8 Hz, 1H; ArH), 9.21 (brt, 1H;  $\text{CONHCH}_2$ ), 10.44 (brs, 1H; ArOH).  $^{13}\text{C}$  NMR

(100 MHz, CDCl<sub>3</sub>-*d*<sub>1</sub>, 25 °C):  $\delta$  = 12.9 (CH<sub>2</sub>CH<sub>3</sub>), 41.1 (CH<sub>2</sub>CH<sub>3</sub>), 125.3 (ArC), 133.7 (ArC), 147.1 (ArC), 149.3 (ArC), 184.6 (C=S), 191.4 (ArC=S). APCI-MS(+) *m/z* 216.01 [M+H]<sup>+</sup>. Anal. calcd for C<sub>8</sub>H<sub>9</sub>NO<sub>2</sub>S<sub>2</sub>: C, 44.63; H, 4.21; N, 6.51; S, 29.79. Found: C, 44.89; H, 4.70; N, 6.51; S, 30.34.

***N*-(Biphenyl-4-ylmethyl)-1-hydroxy-6-oxo-1,6-dihydropyridine-2-carboxamide (9a)**. This compound was used as previously synthesized.<sup>22</sup>

***N*-(4-Fluorobenzyl)-1-hydroxy-6-oxo-1,6-dihydropyridine-2-carboxamide (10a)**. To a solution of 1-(benzyloxy)-6-oxo-1,6-dihydropyridine-2-carboxylic acid (**BDCA**)<sup>22</sup> (200 mg, 0.82 mmol) in dichloromethane was added EDCI (1.0 equiv, 157 mg, 0.82 mmol), HOBt (1.0 equiv, 111 mg, 0.82 mmol), and 4-fluorobenzylamine (1.0 equiv, 93  $\mu$ L, 0.82 mmol). The mixture was stirred overnight at room temperature under N<sub>2</sub> and then poured into a separatory funnel and extracted with water and dichloromethane. The organic layers were combined, dried over anhydrous magnesium sulfate, filtered, and concentrated to give the benzyl-protected intermediate. The intermediate was dissolved in 10 mL of a 1:1 solution of concentrated HCl and glacial acetic acid. The reaction mixture was stirred for 5 d and then concentrated in vacuo, coevaporated with MeOH, and dried to yield an off-white solid (55 mg, 0.21 mmol). Yield = 26%. <sup>1</sup>H NMR (400 MHz, CDCl<sub>3</sub>-*d*<sub>1</sub>, 25 °C):  $\delta$  = 4.51 (d, *J* = 5.6 Hz, 2H; NHCH<sub>2</sub>), 6.88 (q, *J* = 9.0 Hz, 2H; ArH), 7.23 (m, 4H; ArH), 7.41 (t, *J* = 8.0 Hz, 1H; ArH), 9.66 (br t, 1H; CONHCH<sub>2</sub>). APCI-MS(+) *m/z* 263.01 [M+H]<sup>+</sup>.

**2-Bromopyridine-6-carboxylic Acid 1-Oxide (BCAO)**. The synthesis is based on a modified literature procedure.<sup>24</sup> To 6-bromopicolinic acid (**6-BPA**) (2.0 g,

9.9 mmol) was added a solution of 26 mL of trifluoroacetic acid and 4 mL of 30% hydrogen peroxide in water. The reaction mixture was heated to reflux at 80 °C for 7 h under N<sub>2</sub>. The solution was concentrated in vacuo and the concentrate was added to 200 mL of water, which resulted in the immediate formation of a precipitate. The precipitate was vacuum-filtered and dried to afford an off-white solid (2.03 g, 9.3 mmol). Yield = 94%. <sup>1</sup>H NMR (400 MHz, DMSO-*d*<sub>6</sub>, 25 °C): δ = 7.69 (t, *J* = 8.0 Hz, 1H; ArH), 8.24 dd, *J* = 6.0, 10.4 Hz, 1H; ArH), 8.30 (dd, *J* = 5.6, 10.4 Hz, 1H; ArH). ESI-MS(-): *m/z* 215.86 [M-H]<sup>-</sup>.

**1-Hydroxy-6-thioxo-1,6-dihydropyridine-2-carboxylic Acid (HTDCA).**

The synthesis is based on a modified literature procedure.<sup>23</sup> **BCAO** (3.0 g, 14.0 mmol) was dissolved in a 50 mL solution of Na<sub>2</sub>S•9H<sub>2</sub>O (3.3 g, 14 mmol) at 70 °C. To this yellow solution was added 14 mmol of NaHS in 50 mL of water, and the pH was adjusted to 10. The resulting reaction mixture was heated to reflux at 95 °C for 6 h under N<sub>2</sub> and acidified while still hot with concentrated HCl to pH 2. The solution was concentrated in vacuo and the resulting precipitate was vacuum-filtered to yield a crude yellow crystalline solid. The crude acid was partially dissolved in dichloromethane and extracted 2× with 5 M NaOH. The aqueous phase was acidified to pH 1 with concentrated HCl and was further extracted 3× with dichloromethane. The organic phase was dried over anhydrous magnesium sulfate that was then vacuum-filtered off. The filtrate was concentrated to yield a pure bright-yellow solid (2.1 g, 12.3 mmol). Yield = 88%. <sup>1</sup>H NMR (400 MHz, CDCl<sub>3</sub>-*d*<sub>1</sub>, 25 °C): δ = 7.48 (t, *J* = 8.0 Hz, 1H; ArH), 7.67 (dd, *J* = 5.6, 10.4 Hz, 1H; ArH), 8.18 (dd, *J* = 6.0, 9.6 Hz, 1H; ArH). APCI-MS(+): *m/z* 172.12 [M+H]<sup>+</sup>. HR-EI-MS calcd for C<sub>6</sub>H<sub>5</sub>NO<sub>3</sub>S

170.9984. Expected 170.9985. Anal. calcd for C<sub>6</sub>H<sub>5</sub>NO<sub>3</sub>S: C, 42.10; H, 2.94; N, 8.18. Found: C, 42.10; H, 2.86; N, 8.05.

***N*-(Biphenyl-4-ylmethyl)-1-hydroxy-6-thioxo-1,6-dihydropyridine-2-carboxamide (9b)**. To a solution of **HTDCA** (105 mg, 0.6 mmol) in 20 mL of dichloromethane was added NHS (1.0 equiv, 70 mg, 0.6 mmol), EDCI (1.0 equiv, 117 mg, 0.6 mmol), and 4-phenylbenzylamine (1.0 equiv, 112 mg, 0.6 mmol). The mixture was stirred overnight at room temperature under N<sub>2</sub> and then poured into a separatory funnel and extracted with saturated NaHCO<sub>3</sub> in water and dichloromethane. The organic layers were combined, dried over anhydrous magnesium sulfate, filtered, and concentrated to a yellow residue. The crude residue was purified via silica column chromatography (1% MeOH/CHCl<sub>3</sub>). Maltol (3-hydroxy-2-methyl-4Hpyran-4-one) was first run through the column to remove any metal impurities in the silica. The compound **9b** was isolated as a yellow solid after removal of solvent (94 mg, 0.3 mmol). Yield = 46%. <sup>1</sup>H NMR (400 MHz, CDCl<sub>3</sub>-*d*<sub>1</sub>, 25 °C): δ = 4.73 (d, *J* = 6.0 Hz, 2H; NHCH<sub>2</sub>), 7.33 (t, *J* = 6.4 Hz, 1H; ArH), 7.42-7.59 (m, 9H; ArH), 7.67 (dd, *J* = 6.4, 10.0 Hz, 1H; ArH), 8.32 (dd, *J* = 6.0, 10.0 Hz, 1H; ArH), 11.17 (t, *J* = 5.8 Hz, 1H; NHCH<sub>2</sub>). APCI-MS(-): *m/z* 335.04 [M-H]<sup>-</sup>. Anal. calcd for C<sub>19</sub>H<sub>16</sub>N<sub>2</sub>O<sub>2</sub>: C, 67.84; H, 4.79; N, 8.33; S, 9.53. Found: C, 67.36; H, 5.06; N, 8.13; S, 9.32.

***N*-(4-Fluorobenzyl)-1-hydroxy-6-thioxo-1,6-dihydropyridine-2-carboxamide (10b)**. The synthesis of **10b** was performed as described for **9b**, starting from **HTDCA** (50 mg, 0.3 mmol), EDCI (1.0 equiv, 56 mg, 0.3 mmol), HOBt (1.0 equiv, 39 mg, 0.3 mmol), and 4-fluorobenzylamine (1.0 equiv, 36 mg, 33 μL, 0.3 mmol). Yield = 95%. <sup>1</sup>H NMR (400 MHz, CDCl<sub>3</sub>-*d*<sub>1</sub>, 25 °C): δ = 4.65 (d, *J* = 6.0 Hz,

2H;  $\text{NHCH}_2$ ), 7.01 (t,  $J = 8.8$  Hz, 2H; ArH), 7.34 (qd,  $J = 3.2, 4.8$  Hz, 2H; ArH), 7.43 (t,  $J = 8.4$  Hz, 1H; ArH), 7.66 (dd,  $J = 6.4, 10.4$  Hz, 1H; ArH), 8.30 (dd,  $J = 6.8, 9.6$  Hz, 1H; ArH), 11.13 (t,  $J = 5.6$  Hz, 1H;  $\text{NHCH}_2$ ). APCI-MS(-):  $m/z$  276.96  $[\text{M-H}]^-$ .

### 3.H.ii Fluorescence-Based Recombinant Lethal Factor Assay

The compounds were dissolved in dimethyl sulfoxide (DMSO) at a concentration of 50 mM. Serial dilutions of the inhibitor were made from this stock and were diluted 500 $\times$  in LF buffer (20 mM HEPES, 1 mM  $\text{CaCl}_2$ , 0.1 mg/mL bovine serum albumin (BSA), 0.01% Tween-20, pH 7). The assay was carried out in 96-well plates. Each well contained a total volume of 100  $\mu\text{L}$ : 25  $\mu\text{L}$  buffer, 10 nM (30  $\mu\text{L}$ ) recombinant LF (List Biological Laboratories), 20  $\mu\text{L}$  LFi, and after incubation for 35 min at 25 $^\circ\text{C}$ , the reaction was initiated by the addition of 3  $\mu\text{M}$  (25  $\mu\text{L}$ ) fluorogenic LF substrate. Upon cleavage of the fluorogenic substrate, (Cou)-*N*-Nle-Lys-Lys-Lys-Lys-Val-Leu-Pro-Ile-Gln-Leu-Asn-Ala-Ala-Thr-Asp-Lys-(QSY-35)-Gly-Gly-NH<sub>2</sub> ; Cou = 7-hydroxy-4-methyl-3-acetylcoumarinyl; QSY-35 = N-(4-((7-nitro-2,1,3-benzoxzdiazol-4-yl)amino)phenyl)acetyl) from Calbiochem at the Pro-Ile bond, the Cou fluorescence ( $\lambda_{\text{ex}} = 390$  nm,  $\lambda_{\text{em}} = 450$  nm) was measured every min for 15 min. Experiments were repeated at least three times. IC<sub>50</sub> values were calculated as described in Chapter 2, which is the inhibitor concentration at which the enzyme is at 50% control activity (i.e. with no inhibitor present).

### 3.H.iii Single-Crystal X-ray Diffraction

A single crystal of **5c** suitable for X-ray diffraction structural determination was mounted on a nylon loop with Paratone oil and placed under a nitrogen cold stream (100 K). Data were collected on a Bruker P4 diffractometer using Mo K $\alpha$  radiation ( $\lambda = 0.71073 \text{ \AA}$ ) controlled using the APEX 2.0 software package. A semiempirical method utilizing equivalents was employed to correct for absorption.<sup>38</sup> The structure was solved and refined using SHELXTL suite. All hydrogen atoms were fixed at calculated positions with isotropic thermal parameters, while all non-hydrogen atoms were refined anisotropically.

### 3.H.iv.a Construction of an Inhibitor/Anthrax LF Complex Model

Our starting structure was the complex from Lewis et al.,<sup>15</sup> in which **11b** is in the anthrax lethal factor (LF) active site. The 6-methyl group of **11b** was replaced with a hydrogen atom to construct inhibitor **1b**. The inhibitor **1c** was obtained by replacing the carbonyl oxygen atom of **1b** with a sulfur atom. The atomic charges for both **1b** and **1c** were derived by fitting to HF/6-31G\* electrostatic potentials (ESP) using the RESP module. Other force parameters for the two inhibitors were adapted from the standard force field by following the general parametrization procedures outlined in AMBER manual.<sup>39,40</sup> After the added atoms in the gas phase were relaxed, each structure was immersed in a cubic TIP3P water box and neutralized by addition of Na<sup>+</sup> counterions using the AMBER Leap module. This led to the [**1b** • LF] (or [**1c** • LF]) simulation system of 55,268 atoms. MD simulations were conducted in the NPT ensemble at 300 K and 1 atm. The SHAKE algorithm<sup>41</sup> was used to constrain all bond

lengths involving hydrogens. A 10.0 Å cutoff was used for non-bonded interactions, and the neighbor pair list was updated every 10 steps. The long-range electrostatic interactions were treated with the particle mesh Ewald method.<sup>42</sup> The two prepared systems were first equilibrated with a series of minimizations interspersed by short MD simulations, and then two snapshots from two models were selected for the following QM/MM investigations. These selected structures were first minimized using the MM method and then optimized with the B3LYP(6-31G\*) QM/MM calculations using an iterative minimization approach.<sup>43</sup>

### **3.H.iv.b QM/MM Minimization Calculations.**

The pseudobond ab initio QM/MM approach<sup>44,45</sup> has achieved great success in accurate modeling of the chemistry at an enzyme active site while properly including the effects of the enzymatic environment. It has been applied to various enzyme reactions, including enolase,<sup>46</sup> acetylcholinesterase,<sup>47</sup> 4-oxalocrotonate tautomerase,<sup>48</sup> kinase,<sup>49</sup> and methyl transferase.<sup>50</sup> The QM/MM approach divides the whole enzyme-substrate system into a QM and a MM subsystem. The active site of the enzyme was described by a QM Hamiltonian, and the influence of the remainder of the protein and the solvent was included via a coupled MM potential. The code combining the modified Gaussian 98<sup>50</sup> and Tinker 3.6<sup>51</sup> was utilized for all the calculations. An efficient iterative optimization procedure<sup>43</sup> was repeatedly applied to minimize the enzyme-substrate system into a local minimum. For each minimization cycle, the large MM subsystem was relaxed with the truncated Newton method in Cartesian coordinates while the small QM subsystem was treated using the quasi-Newton minimizer at the B3LYP/6-31G\* level in redundant internal coordinates. For the

QM/MM calculations on the [**1b** • LF] and [**1c** • LF] models, the QM subsystem consists of the side chain of His422, His426, Glu471, Zn<sup>2+</sup>, and **1b** (or **1c**), resulting in a total of 70 QM atoms. Geometry optimizations for both the QM subgroups were at the B3LYP(6-31G\*) level, with the boundary between the QM and MM subsystems treated using the pseudobond approach.<sup>45</sup> The scheme used in our QM/MM calculations corresponds to a good compromise between accuracy and computational cost. While being economical for the large system size, B3LYP is quite reliable for geometry optimizations including those of Zn(II) complexes, which is the primary issue in this work. More accurate schemes are available where computational requirements may be more demanding.<sup>52</sup> All other atoms are described by the classical MM force fields. Similarly, we constructed the [**2b** • LF] and [**2c** • LF], [**3b** • LF] and [**3c** • LF], and [**7b** • LF] and [**7c** • LF] QM/MM models.



### 3.I Appendix

**Table 3-2.** Crystallographic data collection and structural parameters of crystal structure of (O,S,S) inhibitor **5c**.

|  |   |
|--|---|
| Name   | Compound <b>5c</b>                          |
| Formula  | $C_{14}H_{13}NO_3S_2$                       |
| Morphology   | Plates                                      |
| Color  | Red   |
| Size (mm)  | 0.45<br>0.30<br>0.07                        |
| Crystal System   | Orthorhombic                                |
| Space Group  | $Pca2_1$                                    |
| <i>a</i>   | 13.516(6)Å                                  |
| <i>b</i>   | 9.108(4)Å                                   |
| <i>c</i>   | 22.558(9)Å                                  |
| $\alpha = \beta = \gamma$  | 90°   |
| Volume (Å <sup>3</sup> )   | 2777(2)                                     |
| <i>T</i> , K   | 100(2)K                                     |
| Reflections measured   | 17598                                       |
| Data/restraints/parameters   | 5139/1/379                                  |
| Final <i>R</i> indices<br>[ $I > 2\sigma(I)$ ] <sub>a</sub>                | <i>R</i> 1 = 0.0422<br><i>wR</i> 2 = 0.1054 |
| <i>R</i> indices (all data, <i>F</i> <sup>2</sup> refinement) <sub>a</sub> | <i>R</i> 1 = 0.0467<br><i>wR</i> 2 = 0.1096 |
| GOF on <i>F</i> <sup>2</sup>   | 1.032                                       |
| Largest diff. peak and hole, e/Å <sup>3</sup>                              | 0.525 and -0.318e/Å <sup>3</sup>            |

### 3.J Acknowledgements

Text, schemes, and figures in this chapter, in part, are reprints of the materials published in the following paper: Agrawal, Arpita; De Oliveira, Ceasar A.F.; Cheng, Yuhui; Jacobsen, Jennifer A.; McCammon, Andrew J.; Cohen, Seth M., “Thioamide Hydroxypyrones Supersede Amide Hydroxypyrothiones in Potency against Anthrax Lethal Factor” *J. Med. Chem.* **2009**, *52*, 1063-1074. The dissertation author was the primary researcher for the data presented and was the primary author on the paper included. The co-authors listed in the publication also participated in the research. The author would like to thank Kristine K. Tanabe for solving the crystal structure of **5c**. The permission to reproduce this paper was granted by the American Chemical Society, copyright 2009.

### 3.K References

- (1) Agrawal, A.; Pulendran, B. *Cell. Mol. Life Sci.* **2004**, *61*, 2859.
- (2) Chopra, A. P.; Boone, S. A.; Liang, X.; Duesbery, N. S. *J. Biol. Chem.* **2003**, *278*, 9402.
- (3) Puhar, A.; Montecucco, C. *TRENDS in Microbiol.* **2007**, *15*, 477.
- (4) Tonello, F.; Ascenzi, P.; Montecucco, C. *J. Biol. Chem.* **2003**, *278*, 40075.
- (5) Ascenzi, P.; Visca, P.; Ippolito, G.; Spallarossa, A.; Bolognesi, M.; Montecucco, C. *FEBS Lett.* **2002**, *531*, 384.
- (6) Hanna, P. C.; Acosta, D.; Collier, R. J. *Proc. Natl. Acad. Sci., USA* **1993**, *90*, 10198.
- (7) Pezard, C.; Berche, P.; Mock, M. *Infect. Immun.* **1991**, *59*, 3472.
- (8) Forino, M.; Johnson, S. L.; Wong, T. Y.; Rozanov, D. V.; Savinov, A. Y.; Li, W.; Fattorusso, R.; Becattini, B.; Orry, A. J.; Jung, D.; Abagyan, R. A.; Smith, J. W.; Alibek, K.; Liddington, R. C.; Strongin, A. Y.; Pellecchia, M. *Proc. Natl. Acad. Sci., USA* **2005**, *2005*, 9499.
- (9) Gaddis, B. D.; Avramova, L. V.; Chmielewski, J. *Bioorg. Med. Chem. Lett.* **2007**, *17*, 4575.
- (10) Konstantinopoulos, P. A.; Karamouzis, M. V.; Papatsoris, A. G.; Papavassiliou, A. G. *Int. J. Biochem. Cell Biol.* **2008**, *40*, 1156.
- (11) Levitt, N. C.; Eskens, F. A. L. M.; O'Byrne, K. J.; Propper, D. J.; Denis, L. J.; Owen, S. J.; Choi, L.; Foekens, J. A.; Wilner, S.; Wood, J. M.; Nakajima, M.; Talbot, D. C.; Steward, W. P.; Harris, A. L.; Verweij, J. *Clin. Cancer Res.* **2001**, *7*, 1912.
- (12) Andrianov, V.; Gailite, V.; Lola, D.; Loza, E.; Semenikhina, V.; Kalvinsh, I.; Finn, P.; Petersen, K. D.; Ritchie, J. W. A.; Khan, N.; Tumber, A.; Collins, L. S.; Vadlamudi, S. M.; Bjorkling, F.; Sehested, M. *Eur. J. Med. Chem.* **2008**, *44*, 1067.
- (13) Hajduk, P. J.; Sheppard, G.; Nettesheim, D. G.; Olejniczak, E. T.; Shuker, S. B.; Meadows, R. P.; Steinman, D. H.; Carrera Jr, G. M.; Marcotte, P. A.; Severin, J.; Walter, K.; Smith, H.; Gubbins, E.; Simmer, R.; Holzman, T. F.; Morgan, D. W.; Davidsen, S. K.; Summers, J. B.; Fesik, S. W. *J. Am. Chem. Soc.* **1997**, *119*, 5818.

- (14) Jacobsen, F. E.; Lewis, J. A.; Cohen, S. M. *J. Am. Chem. Soc.* **2006**, *10*, 3156.
- (15) Lewis, J. A.; Mongan, J.; McCammon, J. A.; Cohen, S. M. *ChemMedChem* **2006**, *7*, 694.
- (16) Lewis, J. A.; Tran, B. L.; Puerta, D. T.; Rumberger, E. M.; Hendrickson, D. N.; Cohen, S. M. *Dalton Trans.* **2005**, *15*, 2588.
- (17) Puerta, D. T.; Griffin, M. O.; Lewis, J. A.; Romero-Perez, D.; Garcia, R.; Villarreal, F. J.; Cohen, S. M. *J. Biol. Inorg. Chem.* **2006**, *11*, 131.
- (18) Puerta, D. T.; Lewis, J. A.; Cohen, S. M. *J. Am. Chem. Soc.* **2004**, *126*, 8388.
- (19) Cummings, R. T.; Salowe, S. P.; Cunningham, B. R.; Wiltsie, J.; Park, Y. W.; Sonatore, L. M.; Wisniewski, D.; Douglas, C. M.; Hermes, J. D.; Scolnick, E. M. *Proc. Natl. Acad. Sci., USA* **2002**, *99*, 6603.
- (20) Reynolds, C. H.; Bembenek, S. D.; Tounge, B. A. *Bioorg. Med. Chem. Lett.* **2007**, *17*, 4258.
- (21) Reynolds, C. H.; Tounge, B. A.; Bembenek, S. D. *J. Med. Chem.* **2008**, *51*, 2432.
- (22) Agrawal, A.; Romero-Perez, D.; Jacobsen, J. A.; Villarreal, F. J.; Cohen, S. M. *ChemMedChem* **2008**, *3*, 812.
- (23) Abu-Dari, K.; Raymond, K. N. *Inorg. Chem.* **1991**, *30*, 519.
- (24) Scarrow, R. C.; Riley, P. E.; Abu-Dari, K.; White, D. L.; Raymond, K. N. *Inorg. Chem.* **1985**, *24*, 954.
- (25) Hopkins, A. L.; Groom, C. R.; A., A. *Drug Disc. Today* **2004**, *9*, 430.
- (26) Shoop, W. L.; Xiong, Y.; Wiltsie, J.; Woods, A.; Guo, J.; Pivnichny, J. V.; Felcetto, T.; Michael, B. F.; Bansal, A.; Cummings, R. T.; Cunningham, B. R.; Friedlander, A. M.; Douglas, C. M.; Patel, S. B.; Wisniewski, D.; Scapin, G.; Salowe, S. P.; Zaller, D. M.; Chapman, K. T.; Scolnick, E. M.; Schmatz, D. M.; Bartizal, K.; MacCoss, M. *Proc. Natl. Acad. Sci., USA* **2005**, *102*, 7958.
- (27) Turk, B. E.; Wong, T. Y.; Schwarzenbacher, R.; Jarrell, E. T.; Leppla, S. H.; Collier, R. J.; Liddington, R. C.; Cantley, L. C. *Nat. Struct. Mol. Biol.* **2004**, *11*, 60.
- (28) Morris, G. M.; Goodsell, D. S.; Halliday, R. S.; Huey, R.; Hart, W. E.; Belew, R. K.; Olson, A. J. *J. Comp. Chem.* **1998**, *19*, 1639.

- (29) Parkin, G. *Chem. Comm.* **2000**, 2000, 1971.
- (30) Allen, F. H.; Bird, C. M.; Rowland, R. S.; Raithby, P. R. *Acta. Cryst.* **1997**, B53, 680.
- (31) Hori, T.; Otani, Y.; Kawahata, M.; Yamaguchi, K.; Ohwada, T. *J. Org. Chem.* **2008**, 73, 9102.
- (32) Pellecchia, M.; Bertini, I.; Cowburn, D.; Dalvit, C.; Giralt, E.; Jahnke, W.; James, T. L.; Homans, S. W.; Kessler, H.; Luchinat, C.; Meyer, B.; Oschkinat, H.; Peng, J.; Schwalbe, H.; Siegal, G. *Nat. Rev. Drug Discov.* **2008**, 7, 738.
- (33) Venkatesan, N.; Kim, B. H. *Curr. Med. Chem.* **2002**, 9, 2243.
- (34) Hanzlik, R. P.; Vyas, K. P.; Traiger, G. J. *Toxicol. Applied Pharmacol.* **1978**, 46, 685.
- (35) Ikehata, K.; Duzhak, T. G.; Galeva, N. A.; Ji, T.; Koen, Y. M.; Hanzlik, R. P. *Chem. Res. Toxicol.* **2008**, 21, 1432.
- (36) Jeschke, P.; Harder, A.; Etzel, W.; Gau, W.; Thielking, G.; Bonse, G.; Iinuma, K. *Pest. Manag. Sci.* **2001**, 57, 1000.
- (37) Pfund, E.; Lequeux, T.; Masson, S.; Vazeux, M.; Cordi, A.; Pierre, A.; Serre, V.; Herve, G. *Bioorg. Med. Chem.* **2005**, 13, 4921.
- (38) Sheldrick, G. M. S. *Acta. Crystallogr.* **1995**, A51, 33.
- (39) Case, D. A.; Perlman, D. A.; Caldwell, J. W.; Chetham III, T. E.; Ross, W. S.; Simmerling, C. L.; Darden, T. A.; Merz, K. M.; Stanton, R. V.; Cheng, A. L.; Vincent, J. J.; Crowley, M.; Tsui, V.; Gohlke, H.; Radmer, R. J.; Duan, Y.; Pitera, J.; Massova, I.; Seibel, G. L.; Singh, U. C.; Weiner, P. K.; Kollman, P. A. **2002**.
- (40) Cornell, W. D.; Cieplak, P.; Bayly, C. I.; Gould, I. R.; Merz, K. M.; Ferguson, D. M.; Spellmeyer, D. C.; Fox, T.; Caldwell, J. W.; Kollman, P. A. *J. Am. Chem. Soc.* **1995**, 117, 5179.
- (41) Ryckaert, J. P.; Ciccotti, G.; Berendsen, H. J. C. *J. Comp. Phys.* **1977**, 23, 327.
- (42) Darden, T.; York, D.; Pedersen, L. *J. Chem. Phys.* **1993**, 98, 10089.
- (43) Zhang, Y. K.; Liu, H. Y.; Yang, W. T. *J. Chem. Phys.* **2000**, 112, 3483.
- (44) Liu, H. Y.; Zhang, Y. K.; Yang, W. T. *J. Am. Chem. Soc.* **2000**, 122, 6560.

- (45) Zhang, Y. K.; Lee, T. S.; Yang, W. T. *J. Chem. Phys.* **1999**, *110*, 46.
- (46) Zhang, Y. K.; Kua, J.; McCammon, J. A. *J. Am. Chem. Soc.* **2002**, *124*, 10572.
- (47) Cisneros, G. A.; Wang, M.; Silinski, P.; Fitzgerald, M. C.; Yang, W. T. *Biochemistry* **2004**, *43*, 6885.
- (48) Cheng, Y. H.; Zhang, Y. K.; McCammon, J. A. *J. Am. Chem. Soc.* **2005**, *127*, 1553.
- (49) Hu, P.; Zhang, Y. K. *J. Am. Chem. Soc.* **2006**, *128*, 1272.
- (50) Frisch, M. J.; Trucks, G. W.; Schlegel, H. B.; Scuseria, G. E.; Robb, M. A.; Cheeseman, J. R.; Zakrzewski, V. G.; Montgomery Jr., J. A.; Stratmann, R. E.; J.C., B.; Dapprich, S.; Millam, J. M.; Daniels, A. D.; Kudin, K. N.; Strain, M. C.; Farkas, O.; Tomasi, J.; Barone, V.; Cossi, M.; Cammi, R.; Mennucci, B.; Pomelli, C.; Adamo, C.; Clifford, S.; Ochterski, J.; Petersson, G. A.; Ayala, P. Y.; Cui, Q.; Morokuma, K.; Malick, D. K.; Rabuck, A. D.; Raghavachari, K.; Foresman, J. B.; Cioslowski, J.; Ortiz, J. V.; Baboul, A. G.; Stefanov, B. B.; Liu, G.; Liashenko, A.; Piskorz, P.; Komaromi, I.; Gomperts, R.; Martin, R. L.; Fox, D. J.; Keith, T.; Al-Laham, M. A.; Peng, C. Y.; Nanayakkara, A.; Gonzalez, C.; Challacombe, M.; Gill, P. M. W.; Johnson, B. G.; Chen, W.; Wong, M. W.; Andres, J. L.; Head-Gordon, M.; Replogle, E. S.; Pople, J. A. **1998**.
- (51) Ponder, J. W. *TINKER, Software Tools for Molecular Design, Version 3.6* **1998**.
- (52) Amin, E. A.; Truhlar, D. G. *J. Chem. Theory Comput.* **2008**, *4*, 75.

## **Chapter 4. Chelator Fragment Libraries for Targeting Metalloproteinases**

#### 4.A Introduction

Fragment-based lead design (FBLD), or recently coined as “fragonomics“ by Zartler and Shapiro,<sup>1</sup> has gained widespread attention in the past decade as an attractive tool for drug design in both the academic and pharmaceutical community.<sup>1,2</sup> FBLD, which is also referred to as fragment-based drug discovery (FBDD), is an increasingly important strategy for the discovery of biologically active compounds.<sup>3</sup>

FBLD generally utilizes small molecular fragments (MW <300 amu) that can be screened against targets of interest.<sup>2</sup> These small fragments lack multiple functional groups observed on most hits from traditional high-throughput screening (HTS) methods; with typical binding affinities in the millimolar to high micromolar range.<sup>4</sup> Accordingly, more sensitive screening methods that include biophysical screening tools such as NMR, X ray crystallography and surface plasmon resonance (SPR) are particularly suitable;<sup>5-8</sup> even though traditional biomolecular assays for rapid screening are also used. The advantage of the more biophysical methods affords a better structural understanding of protein-ligand interactions which is crucial in prioritizing fragment hits for their subsequent development into leads.

Compared to HTS libraries of thousands of molecules, fragment screening generally utilizes libraries consisting of modest collections (100-1000 compounds) of low molecular weight fragments (Figure 4-1). Although such fragments do not bind as tightly ( $K_d$  values in the micro- to milli-molar range) as larger molecules (e.g. natural products) often used in HTS approaches, fragments can provide ‘hits’ that serve as efficient starting scaffolds for the development of potent inhibitors. Additionally, FBLD retains the binding property of the original fragment in the drug lead, compared



to HTS, in which the original binding properties of the lead compounds are often lost when developed into a drug, due to the large molecules present in HTS libraries. The binding efficiency of fragments can be measured in terms of their binding energies per unit molecular mass; otherwise referred to as Ligand Efficiency (LE) which was previously defined in Chapter 3.<sup>9,10</sup>

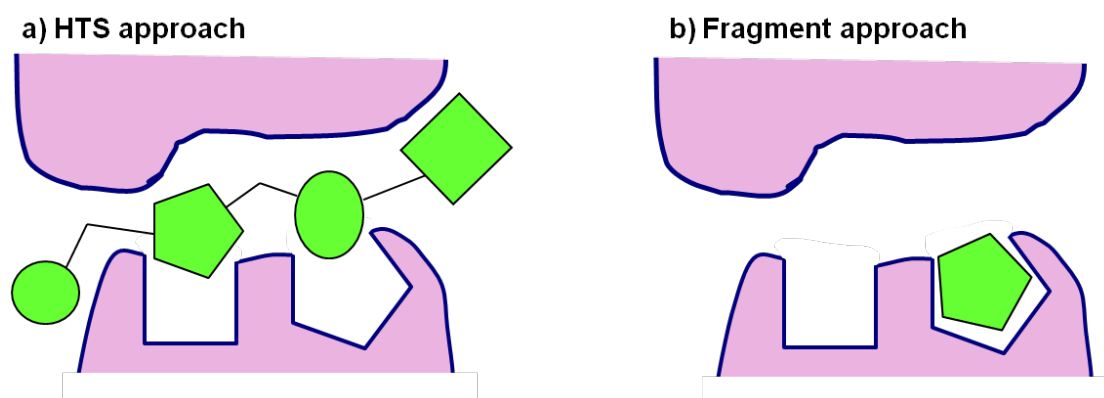


**Figure 4-1. Schematic representation of HTS vs fragment hit.** a) The HTS hit is large and makes surface contacts with the receptor without forming high quality interactions in key pockets. The affinity is spread throughout the entire molecule b) The fragment is much smaller and makes high-quality contacts with the receptor despite the weak affinity.

At present, even though there are several guidelines for defining drug-like properties which are used to maximize an oral drug candidate,<sup>11-13</sup> they are not as relevant for assessing the optimum properties of a fragment lead. Instead, a ‘Rule of 3’ for fragment-based lead discovery has been proposed, whereby the fragment should conform to several parameters, including: a molecular weight  $\leq 300$  Da, the number of hydrogen bond donors (HBD) should be  $\leq 3$ , the number of hydrogen bond acceptors (HBA) should be  $\leq 3$ , the ClogP  $\leq 3$  ( $\log P_{\text{oct/water}}$ , i.e. the partition co-efficient for the solubility of a fragment in octanol over water), and the number of rotatable bonds (NROT) should be  $\leq 3$ .<sup>14</sup>

In adhering to these rules, FBLD screening identifies fragments that bind to a target, after which one of two approaches is generally pursued: a) a single fragment can be elaborated in order to obtain a tight binder (fragment evolution or fragment growing, Figure 4-2), or b) multiple fragments binding at adjacent and distinct sites can be connected by an appropriate linker to obtain a potent inhibitor (fragment linking, Figure 4-3). Compared to HTS, FBLD is purported to have several advantages, which include a more efficient exploration of chemical diversity space (Figure 4-1) and higher ligand efficiencies.

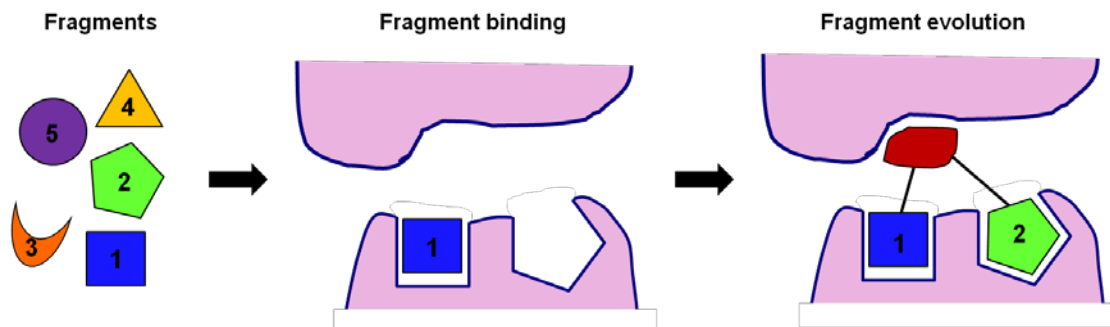


**Figure 4-2.** Fragment 1 binds to the receptor at one site and the lead molecule is evolved by building away from the starting fragment and making good contact with the upper surface and then by growing into a second pocket.

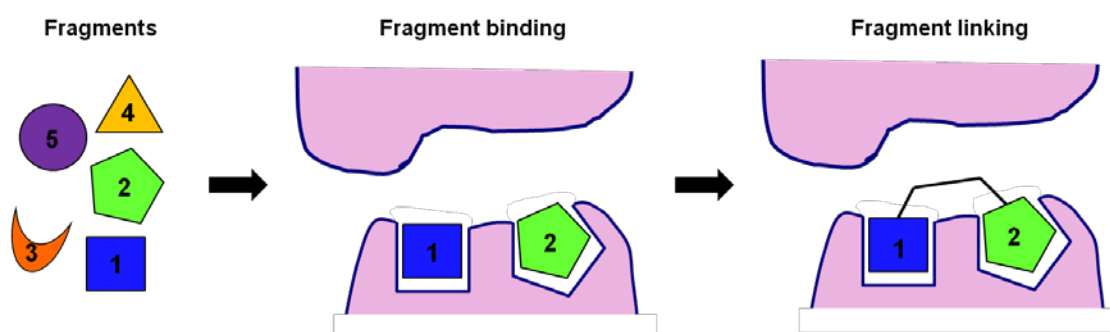


**Figure 4-3.** Fragments 1 and 2 bind to the receptor at different sites from the various fragments screened, and are joined together by a linking group that allows the lead molecule to span both sites.

The application of FBLD towards metalloproteins was first introduced by Fesik and co-workers where they used SAR-by-NMR to identify potent fragments against stromelysin-1 (MMP-3, Chapters 1 and 2).<sup>15</sup> As shown in Figure 4-4, they used fragment linking to combine two modestly potent fragments (hydroxamic acid and a substituted aryl backbone) into a potent, nanomolar inhibitor of MMP-3; that targets both the metal active site (catalytic  $Zn^{2+}$ ) and the deep S1 pocket of MMP -3 (Chapters 1 and 2). Although the application of FBLD to metalloprotein targets of medicinal interest has been previously introduced,<sup>15,16</sup> the design, synthesis, and use of general fragment libraries based on metal chelators for FBLD applications has not

been widely reported.<sup>17-20</sup> This is surprising in light of the fact that several small molecule chelators have been shown to effectively inhibit metalloproteins.<sup>21,22</sup> Furthermore, FBLD using metal-chelating moieties should be particularly well-suited for inhibitor discovery against metalloproteins because: a) chelators demonstrate binding affinities suitable for FBLD screening; b) chelators provide a diverse range of molecular platforms from which to develop lead compounds; and c) the propensity for chelators to bind metal ions allows for better prediction of their probable binding position within a protein active site in the absence of experimental structural data of the complex.

The study presented in this chapter describes the preparation of an expanded chelator fragment library (eCFL) derived from a chelator fragment library (CFL) and shows the usefulness of these libraries in identifying novel leads, using biochemical assays for metalloprotein inhibitors, including inhibitors of matrix metalloproteinases (MMPs) and anthrax lethal factor (LF), both of which were previously discussed in Chapters 2 and 3.

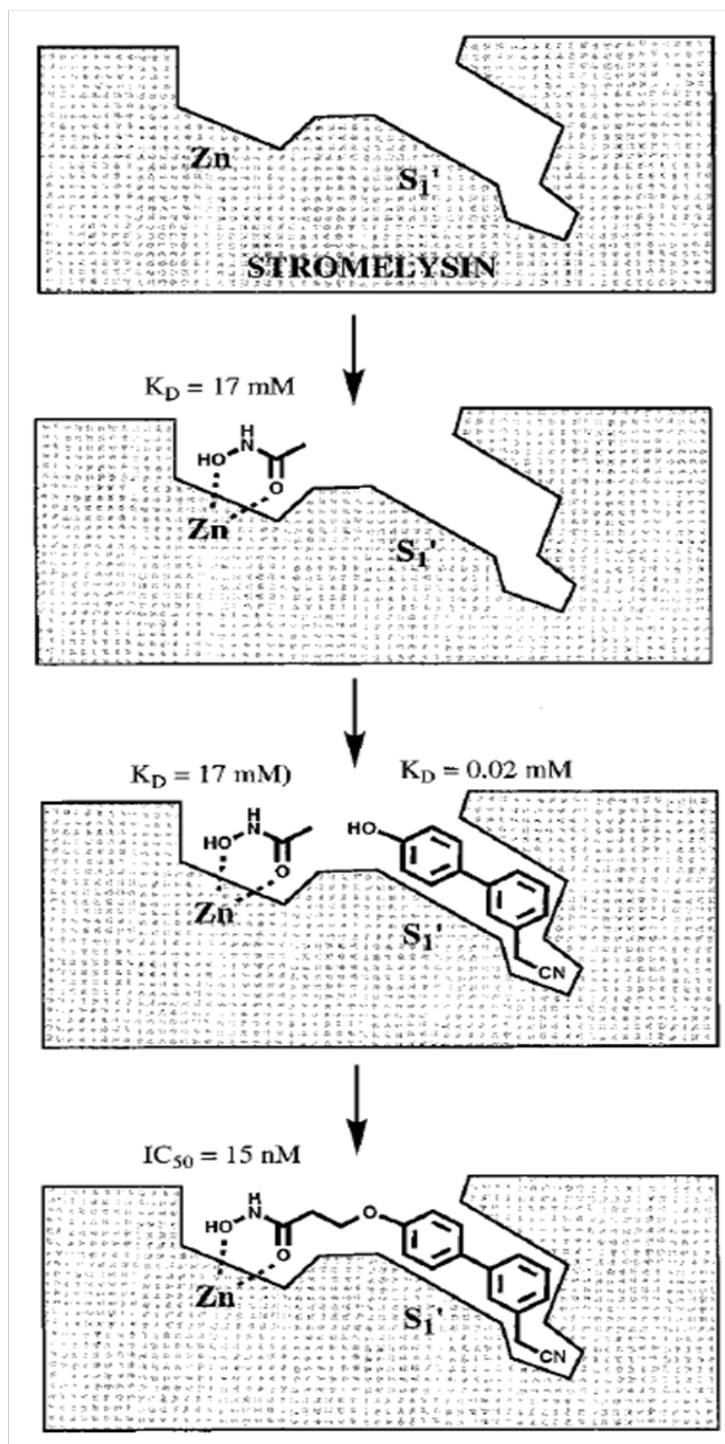


**Figure 4-4.** A summary of the SAR by NMR fragment based method as applied to discovery of stromelysin inhibitors.<sup>15</sup>

## 4.B Chelator Fragment Library (CFL-1)

As discussed above, matrix metalloproteinases (MMPs) represent one of the most well established targets in the realm of metalloproteins. These  $Zn^{2+}$ -dependent enzymes have been extensively studied and the development of MMP inhibitors (MMPi) has played an important role in the discovery of inhibitors for other  $Zn^{2+}$ -dependent metalloproteins such as anthrax lethal factor (LF), histone deacetylases (HDACs), and others.<sup>23</sup> Indeed, the earliest application of FBLD to a metalloprotein target was directed at MMP-3 as discussed above.<sup>15</sup> Therefore, we focused our preliminary library screening efforts on MMPs, as a representative system for identifying fragments that would bind  $Zn^{2+}$  metalloproteins.

Based on widely-reported criteria for fragment libraries,<sup>2</sup> an initial chelator fragment library (CFL-1) was assembled (Figure 4-5).<sup>24</sup> As seen in Figure 4-5, CFL-1 contains 96 chelators that possess two to four donor atoms for binding metal ions. In addition, fragments were selected for their commercial availability and/or ease of synthesis, and adequate solubility for screening at millimolar concentrations. The chelating groups include picolinic acids, hydroxyquinolones, pyrimidines, hydroxypyrones, hydroxypyridinones, and salicylic acids in addition to other compounds that are well-established components of metalloprotein inhibitors, such as hydroxamic acids and sulfonamides.

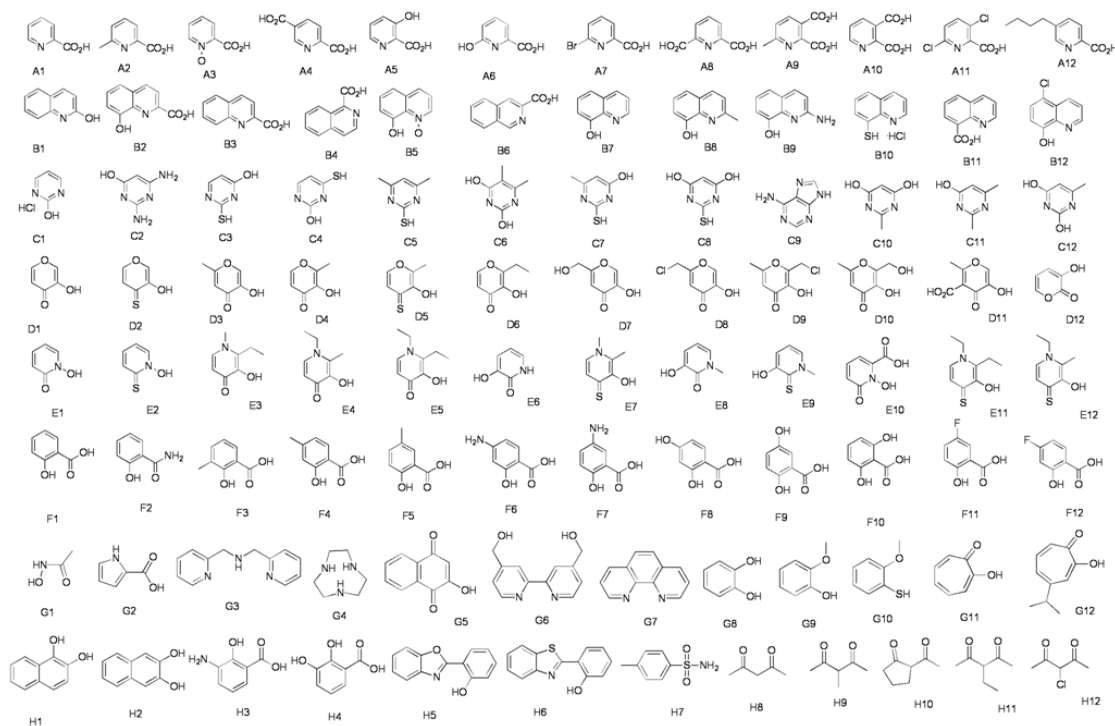


**Figure 4-5.** Chelator fragment library (CFL-1). The library consists of 96 compounds grouped into several classes including picolinic acids, hydroxyquinolones, pyrimidines, hydroxypyrones, hydroxypyridinones, salicylic acids, hydroxamic acids and sulphonamides.

CFL-1 library was screened against MMP-2 at a fragment concentration of 1 mM, using a fluorescent based assay as previously described.<sup>25</sup> A fragment that displayed a >50% inhibition at 1 mM was considered a “hit”. From the initial screening of the library, 31 compounds were found to be weak “hits”; and this high hit rate is consistent with the fact that all fragments are known metal chelators. Several of the hits were known from previous studies,<sup>21,22</sup> thus validating the screening approach as positive controls. Importantly, several fragments were identified that had not been widely reported for use in metalloprotein inhibitors.

The screening results of CFL-1 against MMP-2 are shown in Figure 4-6 as a percent inhibition thermoplot. The thermoplot table in Figure 4-6 is a 96-well plate

layout of the CFL-1 library in Figure 4-5. The fragments were screened at a concentration of 1 mM in a 96-well NUNC plate and percent inhibition of each fragment was calculated using the procedure described in the Experimental Section of this chapter. Briefly, Figure 4-6 shows that fragments that generated a 0-25% inhibition are represented by maroon squares; those that generated a 26-50% inhibition are represented by red squares; those that generated a percent inhibition generally above  $IC_{50}$  values from 51-75% are represented by orange squares, and those that were the most potent with percent inhibition values between 76-100% are shown as yellow squares. The black squares denote fragments that interfered with the assay due to solubility and/or fluorescence.

As seen in Figure 4-6, the hydroxyquinolines (**B2**, **B7**, **B9**), the hydroxypyrothiones (**D2**, **D5**), hydroxypyridinethiones (**E2**, **E7**, **E9**, **E11**, **E12**) and some miscellaneous fragments (**G3**, **G4**, **G5**, **G6**, **G7**, **G11**, **G12**) were the most potent (76-100% inhibition). Of these various classes, the hydroxyquinolines are already being studied in the lab, and the hydroxypyridinethiones are easily synthesized from their hydroxypyrothione precursors (for example, **E7** is synthesized from **D5**). The promising results obtained from the MMP-2 screening of CFL-1 therefore prompted the development of an expanded chelator fragment library (eCFL-1) geared toward the inhibition of specific  $Zn^{2+}$  metalloproteins. The components of eCFL-1 are based on the chelator hit **E7** (3-hydroxy-1,2-dimethylpyridine-4(1*H*)-thione) from CFL-1 which had a percent inhibition in the 76-100% range against MMP-2 (as discussed above).



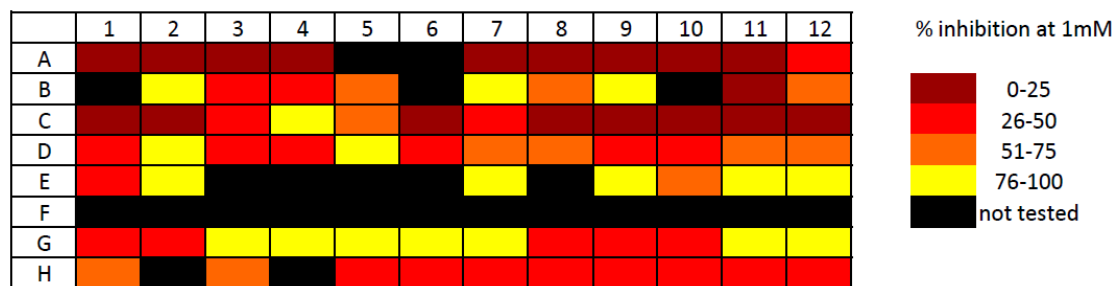
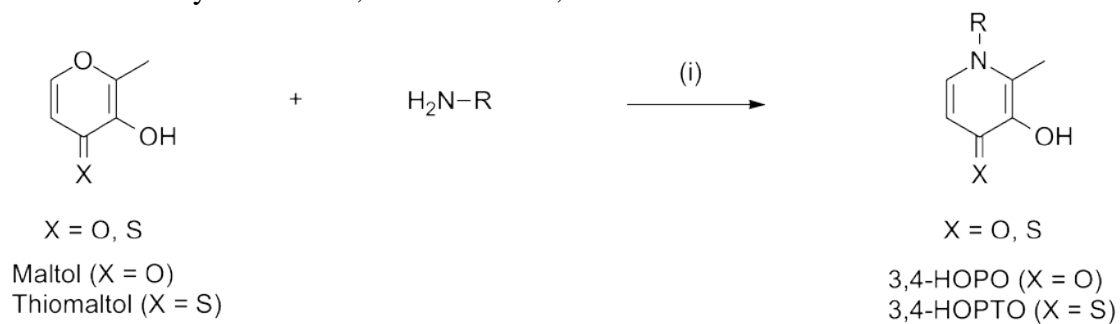


**Figure 4-6.** Thermoplot representing the percent inhibition of MMP-2 by the various fragments of the chelator fragment library (CFL-1). Those in black were not tested due to interference with the assay readout and/or solubility issues. Structures of each 96-well plate label are shown in Figure 4-5.

#### 4.C Expanded chelator fragment library (eCFL-1)

The expanded library was used to demonstrate that hits from the parent library (CFL-1) could be further elaborated to more advanced leads, just as in a traditional hit maturation approach. Derivatives of 3-hydroxy-1,2-dimethylpyridine-4(1*H*)-thione (3,4-HOPTO), which consists of an O,S atom donor set, and its O,O analog 3-hydroxy-1,2-dimethylpyridine-4(1*H*)-one (3,4-HOPO), were utilized for the generation of eCFL-1 (Figure 4-7). In order to prepare a reasonable number of 3,4-HOPO and 3,4-HOPTO derivatives, a robust microwave-assisted synthetic procedure was developed (Scheme 4-1).<sup>26</sup> Using reaction conditions adapted from Orvig et al.,<sup>27</sup> ~2.2 equiv of amine and 1 equiv of hydroxypyrrone (or hydroxypyrothione) heterocycle were combined in 0.38 M HCl and irradiated in a microwave synthesizer, generating the desired products in <2 min. These conditions were used to produce 63 3,4-HOPO fragments and 24 3,4-HOPTO fragments (Figure 4-7). Isolated yields for these reactions ranged between 3-50%. The 3,4-HOPO fragments outnumber those obtained for 3,4-HOPTO owing to their ease of isolation, as the 3,4-HOPO fragments generally precipitated from the reaction mixture upon cooling. In contrast, the 3,4-HOPTO reactions resulted in mixtures (as determined by TLC) and in most cases required flash silica column chromatography to isolate. Nevertheless, the resulting small fragment library (87 components) was suitable for screening in a 96-well plate format. The fragments in eCFL-1 possessed chemical properties (MW between 139 and 353 amu with only 8 fragments >300 amu; number of hydrogen bond donors and acceptors between 0 and 2) that are consistent with reported FBLD libraries.<sup>2</sup>

**Scheme 4-1.** Synthesis of 3,4-HOPO and 3,4-HOPTO derivatives of eCFL-1<sup>a</sup>



<sup>a</sup>Reagents and conditions: (i) 0.38 M HCl, MW, 165 °C, 1.5 min, 1-2 cycles, 0-50%.



**Figure 4-7.** 3,4-HOPO and 3,4-HOPTO components (87 total) of extended chelator fragment library (eCFL-1).

#### 4.D In vitro screening of eCFL-1 against MMPs and LF

The eCFL-1 library was screened, by using commercially-available fluorescence based assays, against four Zn<sup>2+</sup>-dependent metalloprotein targets: gelatinase-1 (MMP-2), gelatinase-2 (MMP-9), stromelysin-1 (MMP-3), and anthrax lethal factor (LF). All fragments were tested at a concentration of 50 μM; compounds that showed >50% inhibition of metalloenzyme activity were classified as a hit against that enzyme (Figure 4-8). The 87-fragment library generated a total of 17 hits against MMP-2, 18 hits against MMP-9, 5 hits against MMP-3, and 10 hits against LF (Table 4-1). Considering the overall modest number of compounds screened (87 in eCFL-1), this result is quite remarkable. Hits with similar affinities have generally been obtained with much greater effort by testing libraries consisting of >10,000 compounds in HTS campaigns.<sup>28,29</sup> Between the two different fragment groups in eCFL-1, the 63 3,4-HOPO fragments produced only one hit against MMP-2 (**94G12**), two hits against MMP-9 (**94G6**, **94G12**) and three hits against LF (**94B11**, **94D8**, **94F10**). There were no 3,4-HOPO hits identified against MMP-3. Of the 24 3,4-HOPO fragments screened, 16 hits were found against MMP-2, 16 hits against MMP-9, 5 hits against MMP-3, and 7 hits against LF. The significant difference in the number of hits generated from the smaller 3,4-HOPO set of fragments against these metalloenzymes highlights the importance the chelating group plays in these libraries. The *O,S*-chelator of the 3,4-HOPO fragments produced at least five or more hits against each enzyme, despite comprising the minor portion (~28%) of eCFL-1.

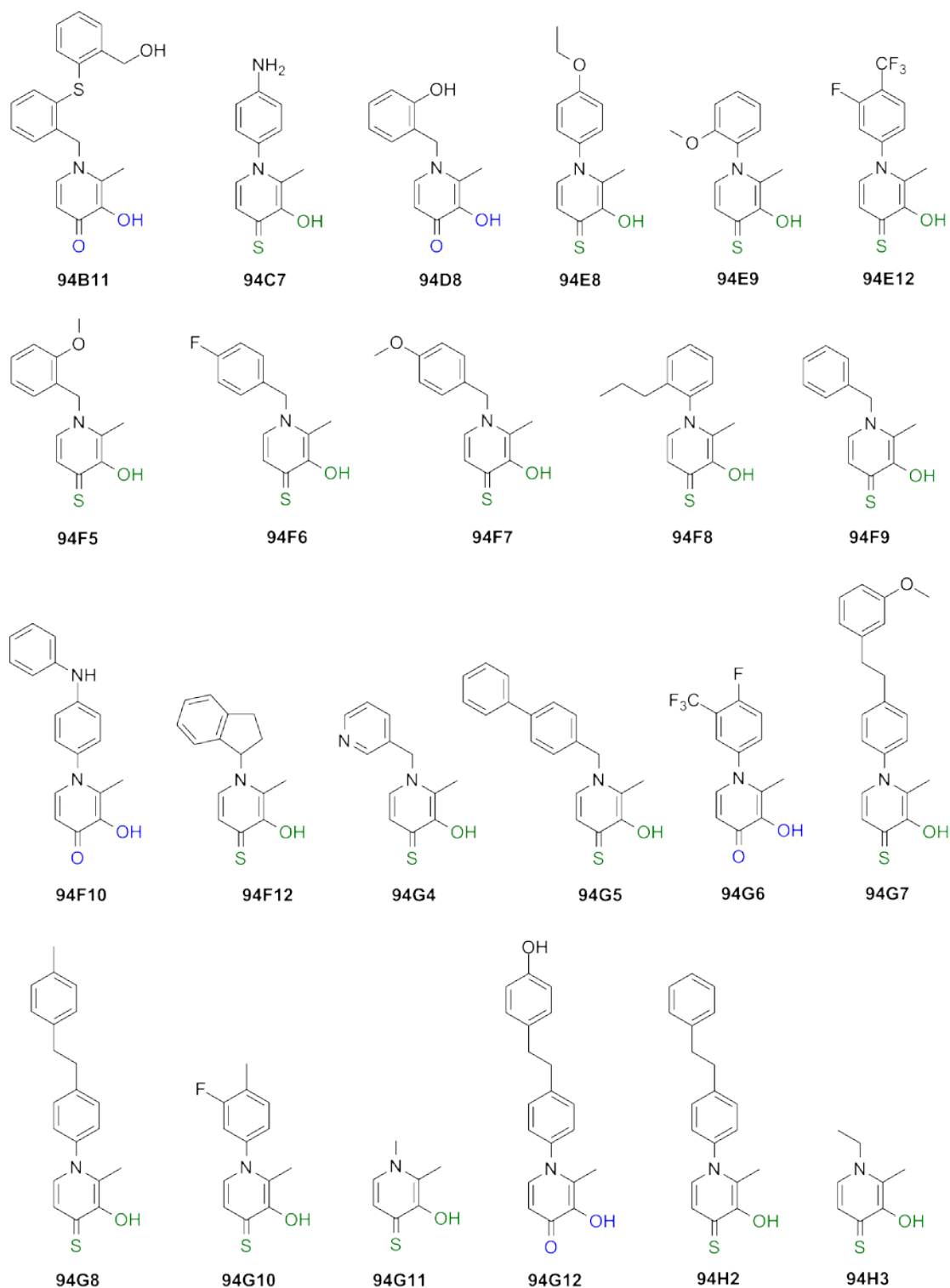


**Figure 4-8.** Lead hits identified against  $\text{Zn}^{2+}$ -dependent metalloenzymes from an expanded library (eCFL-1) of 3,4-HOPO (blue chelating groups) and 3,4-HOPTO (green chelating groups) fragments.

With only one exception (**94C7**), all of the hits against MMP-2 were also found to be hits against the other gelatinase MMP-9. The common hits identified for MMP-2 and -9 is consistent with the high degree of structural homology between the catalytic domains of these enzymes. A review of the literature shows that most MMP-9 inhibitors are also potent against MMP-2, but the reverse is not necessarily true due to the slightly larger S1' pocket present in MMP-2.<sup>30</sup> Only five fragments, all based on the 3,4-HOPTO chelator, were shared hits across the three MMPs. Among these, only one 3,4-HOPTO fragment (**94G5**) was a hit against all four metalloenzymes tested. Four fragments were found to be unique hits against LF (**94B11**, **94D8**, **94E9**, **94F10**).

**Table 4-1.** IC<sub>50</sub> values (μM) of lead fragments against metalloenzyme targets. IC<sub>50</sub> values of non-hits (>50 μM) are designated with an ×. Standard deviations from triplicate measurements for all values listed are <10%. <sup>a</sup>Ligand efficiency for some fragments are provided against MMP-9 only

| Compound | LF | MMP-2 | MMP-3 | MMP-9 | LE<br>(kcal/mol) <sup>a</sup> |
|----------|----|-------|-------|-------|-------------------------------|
| 94B11    | 34 | ×     | ×     | ×     | -                             |
| 94C7     | ×  | 34    | ×     | ×     | -                             |
| 94D8     | 17 | ×     | ×     | ×     | -                             |
| 94E8     | ×  | 13    | 33    | 17    | 0.46                          |
| 94E9     | 41 | ×     | ×     | ×     | -                             |
| 94E12    | 34 | 33    | ×     | 33    | 0.33                          |
| 94F5     | ×  | 20    | ×     | 21    | 0.38                          |
| 94F6     | ×  | 12    | 28    | 12    | 0.42                          |
| 94F7     | ×  | 10    | 39    | 9     | 0.41                          |
| 94F8     | 13 | 24    | ×     | 20    | 0.38                          |
| 94F9     | ×  | 23    | ×     | 21    | 0.43                          |
| 94F10    | 23 | ×     | ×     | ×     | -                             |
| 94F12    | 32 | 4     | ×     | 8     | 0.41                          |
| 94G4     | ×  | 34    | ×     | 23    | 0.42                          |
| 94G5     | 3  | 1     | 4     | 2     | 0.37                          |
| 94G6     | ×  | ×     | ×     | 36    | 0.33                          |
| 94G7     | ×  | 17    | ×     | 18    | 0.37                          |
| 94G8     | 38 | 30    | 38    | 19    | 0.38                          |
| 94G10    | 21 | 35    | ×     | 31    | 0.39                          |
| 94G11    | ×  | 35    | ×     | 41    | 0.65                          |
| 94G12    | ×  | 29    | ×     | 30    | 0.37                          |
| 94H2     | ×  | ×     | ×     | 30    | 0.39                          |
| 94H3     | ×  | 36    | ×     | 34    | 0.60                          |

#### 4.E Discussion

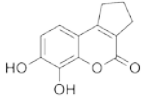
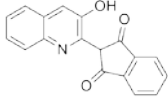
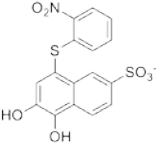
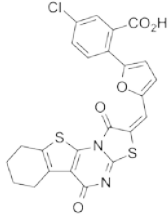
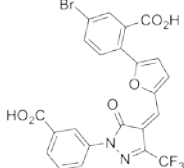
The most potent fragment identified against all the metalloenzymes was **94G5**, which is comprised of a 3,4-HOPTO chelator and a biphenyl moiety. This fragment showed a particularly notable IC<sub>50</sub> value of 3 μM against anthrax LF. Although a handful of very potent (<0.5 μM) LF inhibitors have been reported,<sup>31</sup> the activity of the **94G5** fragment against LF rivals many of the described inhibitors.<sup>17,28,29,32-35</sup> Interestingly, the biphenyl substituent found in **94G5** is common to other LF<sup>32,36</sup> and MMP inhibitors,<sup>16,37</sup> although it is quite possible that the biphenyl group in **94G5** does not occupy the same subsites as in these previously reported inhibitors. Nonetheless, this finding validates that the chelator fragment library approach can identify potent structures that are consistent with established chemical motifs for these metalloprotein targets.

LF has been a particularly difficult target for the development of effective inhibitors.<sup>38</sup> Comparing the results obtained here against LF with those obtained from traditional HTS approaches further highlights the significance of these chelator fragment libraries. Table 4-2 compares the five most potent LF hits obtained from eCFL-1 to top hits obtained from two previously reported HTS screens performed on libraries that each contained at least 10,000 compounds.<sup>28,29</sup> These results show that eCFL-1, with only 87 components, generated hits that are comparable or superior in potency, ligand efficiency, and drug-likeness to those obtained from labor and cost intensive HTS screens. Specifically, compared to the reported typical HTS campaigns, the proposed FBLD approach provided: i) a much higher hit frequency (11% for eCFL-1 versus <0.25% for the HTS libraries), ii) ligand efficiencies<sup>39</sup> equal



to or higher than those observed for the HTS hits were realized; iii) compounds that are generally more “drug-like” given their initial selection based on general drug-like criteria. In fact, the low molecular weight of the fragments identified in eCFL-1 are still amenable to further elaboration (<307 amu), unlike most of the HTS hits,<sup>28,29</sup> which are already near the conventional MW limits for a small molecule therapeutic (Table 4-2).<sup>11</sup> Overall, this comparison shows that chelator-based fragment libraries are a much more efficient and effective way to explore the relevant chemical space for metalloprotein targets.

**Table 4-2.** Comparison of leads identified by chelator-based FBLD (this work) versus large library ( $\geq 10,000$  compounds) HTS findings

| Compound <sup>[a]</sup>   | IC <sub>50</sub> /K <sub>i</sub><br>( $\mu\text{M}$ ) <sup>[b]</sup> | MW (amu) | $\Delta\text{G}$<br>(kcal/mol) | Ligand<br>Efficiency <sup>[b]</sup><br>(kcal/mol) |
|---|--|----------|--------------------------------|---|
| 94D8  | 17/4.3   | 231      | -7.4                           | 0.43  |
| 94F8  | 13/3.3   | 259      | -7.5                           | 0.42  |
| 94F10   | 23/5.9   | 292      | -7.2                           | 0.33  |
| 94G5  | 3/0.8  | 307      | -8.4                           | 0.38  |
| 94G10   | 21/5.4   | 249      | -7.2                           | 0.42  |
|    | 1.7/0.6  | 218      | -8.6                           | 0.53  |
|    | 3.9/3.8  | 289      | -7.4                           | 0.34  |
|  | 5.9/2.1  | 392      | -7.8                           | 0.30  |
|  | 0.8/0.8  | 510      | -8.4                           | 0.25  |
|  | 1.7/1.6  | 549      | -7.9                           | 0.23  |

[a] Compounds identified in this study shown by alphanumeric code, compounds identified in reference HTS studies shown by structure [b] Determination of K<sub>i</sub> values and L.E. values is in Experimental Section

#### 4.F Fragment evolution

As shown in Figure 4-2, fragments that bind potently to a target can be further evolved with other protein-binding fragments to produce a more potent lead over the original hit. Due to its potency across the enzymes tested, **94G5** was also chosen as a lead compound for fragment evolution in order to gain more insight into lead design. We hypothesized that by attaching different substituents onto the biphenyl ring of **94G5**, we could transform a universal hit into a specific hit, i.e modestly tune the selectivity toward the different enzymes by adding different chemical groups. The choice of chemical modifications to the biphenyl ring was arbitrary and new substitutions were chosen based on their synthetic accessibility. Due to the lack of commercially available substituted phenylbenzylamines, new biphenyl amines were synthesized using Suzuki-Miyaura coupling conditions (discussed in Chapter 2). In general, various aryl boronic acids were combined with BOC protected 4-iodobenzylamine (**BOC-IBA**) and a palladium catalyst in the presence of a base to produce a number of BOC protected biphenyl amines (Scheme 2-4, Chapter 2). The BOC protecting groups were then removed with TFA and  $\text{CH}_2\text{Cl}_2$  to yield the various biphenyl substituted amines shown in Scheme 2-4, Chapter 2. Preliminary attempts of inserting the synthesized amines in 3-hydroxy-2-methyl-4H-pyran-4-thione (thiomaltol) to replace the oxygen with an amine in the pyrone ring system, using the procedure outlined in Scheme 4-1 were unsuccessful. After close examination of the mechanism of this reaction (Figure 4-9), a new procedure was developed (Scheme 4-2).

According to the mechanism published for this reaction,<sup>40</sup> the pyrone ring undergoes a ring opening followed by dehydration. Ring closure by the amine yields the final product. Because thiomaltol has a pKa of 8.3, the pH of the reaction was maintained at 8.0 to facilitate the nucleophilic attack of various amines at the C-2 position of thiomaltol (shown in Figure 4-9). A higher pH would result in deprotonation of the hydroxyl group of the pyrothione ring system and increase the electron density at C-3. This would hinder the formation of the C-2 pyrothione resonance hybrid which is necessary for nucleophilic attack by the primary amine. The reaction outlined in Scheme 4-2 was thereby designed from the mechanism shown in Figure 4-9 to generate at most five derivatives of **94G5** (Figure 4-10).

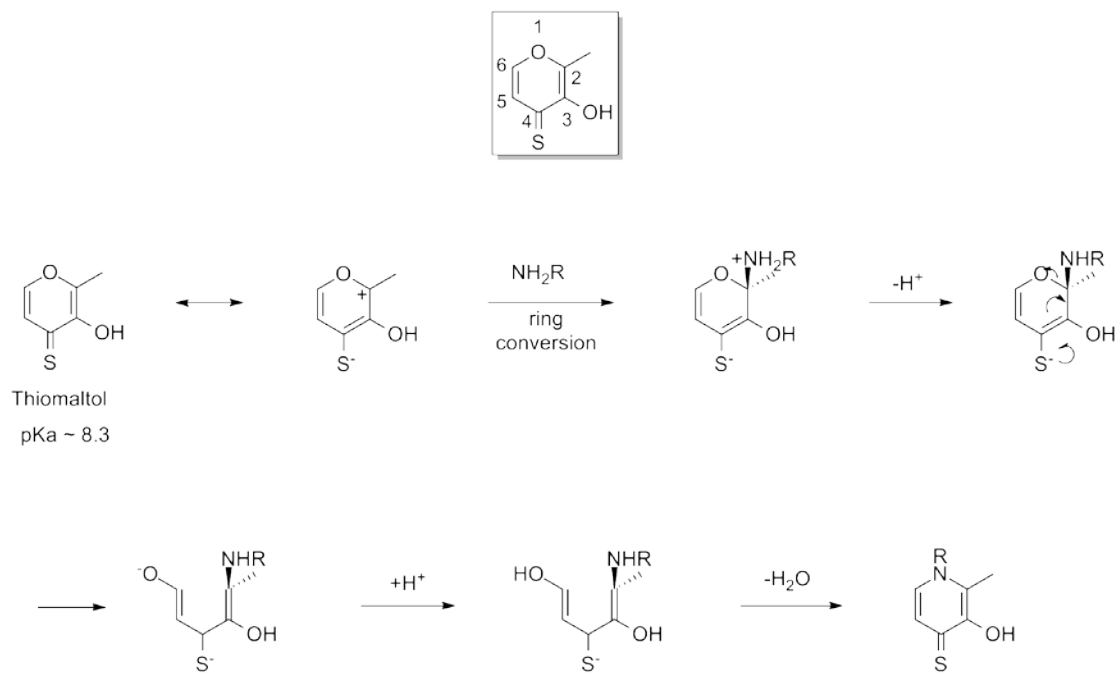
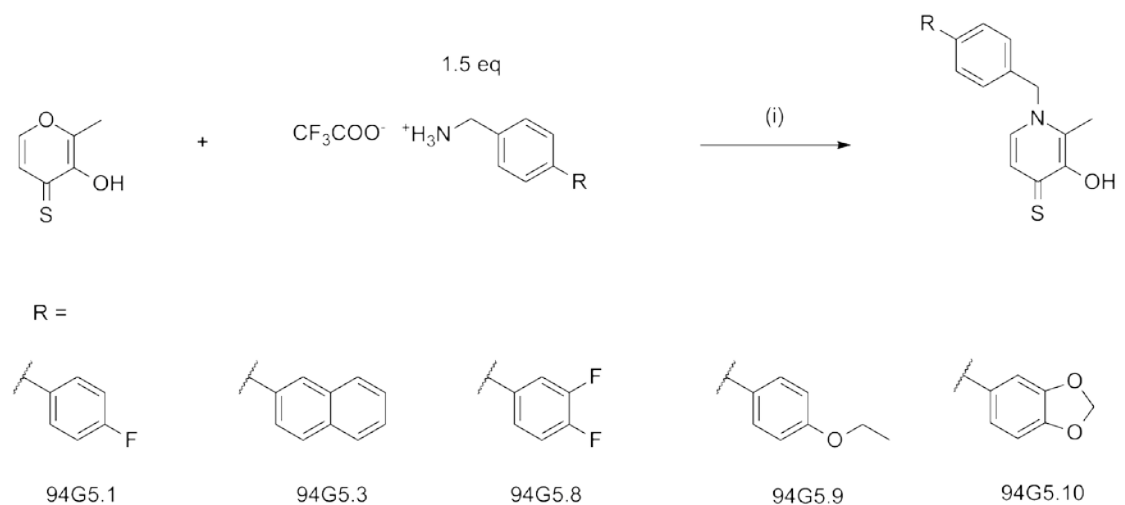


**Figure 4-9.** Mechanism of amine insertion in a pyrone/pyrothione ring system.<sup>40</sup> The numbering scheme used for the pyrone ring system is shown above.

**Scheme 4-2.** Synthesis of fragments evolved from **94G5**<sup>b</sup>



<sup>b</sup>Reagents and conditions: (i) 0.38 M HCl, MW, 165 °C, 1.5 min, 1-2 cycles, 0-50%.

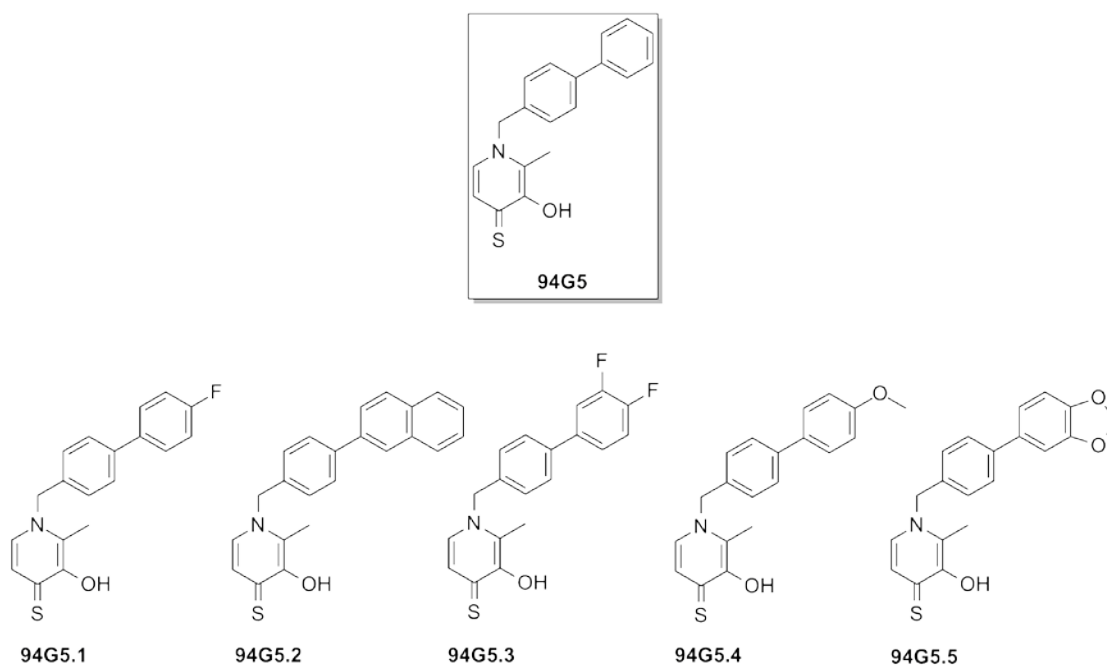


**Figure 4-10.** Structures of the five different fragments (**94G5.1-94G5.5**) evolved from **94G5** (shown boxed above)

#### 4.F.i In vitro potency of fragment evolution

IC<sub>50</sub> values of **94G5** against MMP-2, -3, -9 and LF are 1.2, 4.4, 2.3, and 2.8 μM respectively. The five derivatives of **94G5** that were synthesized (Figure 4-10) were screened against the various Zn<sup>2+</sup> endopeptidases studied for eCFL-1. The percent inhibition for each derivative was calculated at concentrations of 50 μM, 5 μM, and 0.5 μM as described under the Experimental Section. Since, the IC<sub>50</sub> value of **94G5** < 5 μM against the aforementioned enzymes, only derivatives that generated > 50% inhibition at 5 μM were further considered for IC<sub>50</sub> calculations. The results of the screen are listed in Table 4-3; unfortunately, none of the additional substituents on the biphenyl ring led to any improved potency compared to that of **94G5**. This is not surprising, as the substituents added were based on synthetic accessibility and not on structure guided design.

The results therefore obtained by fragment evolution further stresses the importance of biophysical tools in structure guided design toward fragment based lead design. This helps to understand key interactions between the fragment hit/lead and the specific protein “hot-pocket”; and additionally study vicinal hot-pockets as targets for fragment evolutions. The choice of substituents toward fragment evolution on **94G5** could be enhanced by the use of computational docking studies in MMPs (which are now performed in the Cohen lab) and LF to guide the placement of different substituents toward a more potent lead.

**Table 4-3.** IC<sub>50</sub> values (in  $\mu\text{M}$ ) of **94G5** derivatives synthesized above. (n.d. = not determined)

| Fragment | MMP-2 | MMP-3 | MMP-9 | LF    |
|----------|-------|-------|-------|-------|
| 94G5     | 1.2   | 4.4   | 2.3   | 2.8   |
| 94G5.1   | 3.9   | > 5.0 | > 5.0 | > 5.0 |
| 94G5.3   | 4.0   | > 5.0 | > 5.0 | > 5.0 |
| 94G5.8   | 3.5   | > 5.0 | 5.2   | > 5.0 |
| 94G5.9   | > 5.0 | > 5.0 | > 5.0 | > 5.0 |
| 94G5.10  | n.d.  | > 5.0 | > 5.0 | > 5.0 |

#### 4.G Conclusions

In summary, we have presented a new approach to fragment libraries based on known small-molecule chelators and derivatives of these metal-binding molecules. The chelator fragment library (CFL-1) produced several hits when screened against a matrix metalloproteinase. Two chelators from this library were used to prepare a modest expanded library of hydroxypyridinone and hydroxypyridinethione fragments that were screened against four  $\text{Zn}^{2+}$  dependent metalloprotein targets. This screen revealed a strong preference for hydroxypyridinethione fragments and generated leads with good activity against all the metalloenzymes, including anthrax LF. The results obtained show that these chelator libraries are particularly well suited for the application of FBLD against metalloprotein targets. Indeed, our findings demonstrate that this approach produces, with a relatively modest screening effort, high quality hits that are superior to those obtained from traditional HTS campaigns where random libraries of tens of thousands of compounds are tested. These findings clearly demonstrate the potential of chelator-based libraries for targeting metalloproteins. Such libraries should be useful for identifying lead structures against a variety of metalloenzymes, well beyond the  $\text{Zn}^{2+}$  dependent targets reported here.



## 4.H Experimental

Unless otherwise noted, all chemicals were purchased from commercial suppliers and used as received. Flash silica gel chromatography was performed using Merck silica gel 40-63  $\mu\text{m}$  mesh. Inert reactions were carried out under a dinitrogen atmosphere.  $^1\text{H}/^{13}\text{C}$  NMR spectra were recorded at ambient temperature on a 300, 400 or 500 MHz Varian FT-NMR or a 500 MHz Jeol ECA NMR instrument at the Department of Chemistry and Biochemistry, University of California San Diego. Mass spectra were obtained at the Small Molecule Mass Spectrometry Facility in the Department of Chemistry and Biochemistry at the University of California, San Diego. Elemental Analysis was performed by NuMega Resonance Labs, San Diego.

### 4.H.i Synthesis of eCFL-1

*3,4-HOPO derivatives.* To 200 mg (1.58 mmol) of 3-hydroxy-2-methyl-4*H*-pyran-4-one (maltol) in 2 mL of 0.38 M HCl was added 3.5 mmol (2.2 equiv) of the amine in a 10 mL microwave reaction vessel. The heterogenous reaction mixture was sealed and stirred at 65 °C for 5 min prior to one microwave cycle of 1.5 min at 165 °C, 250 psi (max *P*), and 300 W. The product was precipitated from solution at 4 °C overnight, isolated by vacuum filtration, and dried in vacuo.

*3,4-HOPTO derivatives.* To 200 mg (1.41 mmol) of 3-hydroxy-2-methyl-4*H*-pyran-4-thione (thiomaltol) in 2 mL of 0.38 M HCl was added 3.1 mmol (2.2 equiv) of the amine in a 10 mL microwave reaction vessel. The heterogenous reaction mixture was sealed and stirred at 65 °C for 5 min prior to one microwave cycle of 1.5 min at 165

°C, 250 psi (max *P*), and 300 W. The reaction typically produced a yellow solution with a black, oily residue at the bottom of the tube. The reaction mixture was extracted 2× with CH<sub>2</sub>Cl<sub>2</sub>. The organic phase was dried over MgSO<sub>4</sub>, vacuum filtered, and evaporated in vacuo to a dark residue. The product was purified via silica column chromatography in CH<sub>2</sub>Cl<sub>2</sub> or 0-2% MeOH in CH<sub>2</sub>Cl<sub>2</sub>. Pure fractions were pooled and evaporated to yield the desired product.

**94A1 (3-Hydroxy-1,2-dimethylpyridin-4(1*H*)-one):** <sup>1</sup>H NMR (400 MHz, CDCl<sub>3</sub>-*d*<sub>1</sub>, 25 °C): δ = 2.38 (s, CH<sub>3</sub>), 3.64 (s, CH<sub>3</sub>), 6.35 (d, *J* = 7.2 Hz, 1H; ArH), 7.20 (d, *J* = 7.6 Hz, 1H; ArH). ESI-MS(+) *m/z* 140.13 [M+H]<sup>+</sup>.

**94A2 (3-Hydroxy-2-methyl-1-phenylpyridin-4(1*H*)-one):** <sup>1</sup>H NMR (300 MHz, CDCl<sub>3</sub>-*d*<sub>1</sub>, 25 °C): δ = 2.13 (s, CH<sub>3</sub>), 6.45 (d, *J* = 7.5 Hz, 1H; ArH), 7.28-7.30 (m, 3H; ArH), 7.54-7.57 (m, 3H; ArH). ESI-MS(+) *m/z* 202.09 [M+H]<sup>+</sup>.

**94A3 (3-Hydroxy-1-(4-methoxybenzyl)-2-methylpyridin-4(1*H*)-one):** <sup>1</sup>H NMR (400 MHz, CDCl<sub>3</sub>-*d*<sub>1</sub>, 25 °C): δ = 2.26 (s, CH<sub>3</sub>), 3.75 (s, CH<sub>3</sub>), 5.01 (s, CH<sub>2</sub>), 6.40 (d, *J* = 6.8 Hz, 1H; ArH), 6.84 (d, *J* = 8.8 Hz, 2H; ArH), 7.91 (d, *J* = 8.8 Hz, 2H; ArH), 7.32 (d, *J* = 7.2 Hz, 1H; ArH). ESI-MS(+) *m/z* 245.90 [M+H]<sup>+</sup>.

**94A4 (1-Benzyl-3-hydroxy-2-methylpyridin-4(1*H*)-one):** <sup>1</sup>H NMR (300 MHz, CDCl<sub>3</sub>-*d*<sub>1</sub>, 25 °C): δ = 2.28 (s, CH<sub>3</sub>), 5.09 (s, CH<sub>2</sub>), 6.43 (d, *J* = 7.2 Hz, 1H; ArH), 7.00 (d, *J* = 7.2 Hz, 2H; ArH), 7.31 (m, 4H; ArH). APCI-MS(+) *m/z* 216.07 [M+H]<sup>+</sup>.

**94A5 (1-(2,3-Dihydrobenzo[*b*][1,4]dioxin-6-yl)-3-hydroxy-2-methylpyridin-4(1*H*)-one):** <sup>1</sup>H NMR (300 MHz, CDCl<sub>3</sub>-*d*<sub>1</sub>, 25 °C): δ = 2.40 (s,

$CH_3$ ), 4.10-4.40 (m, 4H), 6.45 (d,  $J = 5.0$  Hz, 1H; ArH), 6.66-6.86 (m, 2H; ArH), 7.00 (d,  $J = 8.0$  Hz, 1H; ArH), 7.41 (d,  $J = 7.2$  Hz, 1H; ArH), 7.71 (d,  $J = 5.0$  Hz, 1H; ArH). ESI-MS(+)  $m/z$  260.09 [M+H]<sup>+</sup>.

**94A6 (1-(Biphenyl-4-ylmethyl)-3-hydroxy-2-methylpyridin-4(1H)-one):** <sup>1</sup>H NMR (300 MHz, CDCl<sub>3</sub>-*d*<sub>1</sub>, 25 °C):  $\delta = 2.60$  (s,  $CH_3$ ), 5.50 (s,  $CH_2$ ), 7.13 (d,  $J = 7.7$  Hz, 1H; ArH), 7.23 (d,  $J = 6.7$  Hz, 1H; ArH), 7.36 – 7.59 (m, 4H; ArH), 7.58 (d,  $J = 8.0$  Hz, 2H; ArH), 7.66 (d,  $J = 8.0$  Hz, 2H; ArH), 7.75 (d,  $J = 6.7$  Hz, 1H; ArH). ESI-MS(+)  $m/z$  292.13 [M+H]<sup>+</sup>.

**94A7 (1-(Furan-2-ylmethyl)-3-hydroxy-2-methylpyridin-4(1H)-one):** <sup>1</sup>H NMR (300 MHz, CDCl<sub>3</sub>-*d*<sub>1</sub>, 25 °C):  $\delta = 2.45$  (s,  $CH_3$ ), 5.00 (s,  $CH_2$ ), 6.28 - 6.32 (dd,  $J = 0.8, 3.2$  Hz, 1H; ArH), 6.36 - 6.39 (dd,  $J = 1.9, 3.2$  Hz, 1H; ArH), 6.40 (d,  $J = 7.5$  Hz, 1H; ArH), 7.33 (d,  $J = 7.5$  Hz, 1H; ArH), 7.40 – 7.42 (dd,  $J = 0.8, 1.9$  Hz, 1H; ArH). ESI-MS(+)  $m/z$  206.08 [M+H]<sup>+</sup>.

**94A8 (1-((1H-indazol-3-yl)methyl)-3-hydroxy-2-methylpyridin-4(1H)-one):** <sup>1</sup>H NMR (300 MHz, CDCl<sub>3</sub>-*d*<sub>1</sub>, 25 °C):  $\delta = 2.34$  (s,  $CH_3$ ), 6.39 (d,  $J = 5.4$  Hz, 1H; ArH), 6.88 (bs, 1H; ArH), 7.11 (bs, 1H; ArH), 7.65 (d,  $J = 5.4$  Hz, 1H; ArH), 7.87 (bs, 1H; ArH). ESI-MS(+)  $m/z$  240.23 [M+H]<sup>+</sup>.

**94A9 (3-Hydroxy-2-methyl-1-phenethylpyridin-4(1H)-one):** <sup>1</sup>H NMR (300 MHz, CDCl<sub>3</sub>-*d*<sub>1</sub>, 25 °C):  $\delta = 2.28$  (s,  $CH_3$ ), 2.78 (t,  $J = 3.3$  Hz,  $CH_2$ ), 4.17 (t,  $J = 3.3$  Hz,  $CH_2$ ), 6.21 (d,  $J = 3.6$  Hz, 1H; ArH), 6.90 – 7.00 (m, 5H; ArH), 7.64 (d,  $J = 3.6$  Hz, 1H; ArH). ESI-MS(+)  $m/z$  230.12 [M+H]<sup>+</sup>.

**94A10 (1-(4-Ethylphenyl)-3-hydroxy-2-methylpyridin-4(1H)-one):** <sup>1</sup>H NMR (300 MHz, CDCl<sub>3</sub>-*d*<sub>1</sub>, 25 °C):  $\delta = 1.28$  (t,  $J = 7.8$  Hz,  $CH_3$ ), 2.21 (s,  $CH_3$ ), 2.78

(q,  $J = 7.8$  Hz,  $CH_2$ ), 6.68 (d,  $J = 6.9$  Hz, 1H; ArH), 7.14 (bs, 1H; ArH), 7.29 – 7.49 (m, 2H; ArH), 7.63 (d,  $J = 6.9$  Hz, 1H; ArH). ESI-MS(+)  $m/z$  230.32  $[M+H]^+$ .

**94A11 (3-Hydroxy-2-methyl-1-((5-methylisoxazol-3-yl)methyl)pyridin-4(1H)-one):**  $^1H$  NMR (300 MHz,  $CDCl_3-d_1$ , 25 °C):  $\delta = 2.38$  (s, 6H;  $CH_3$ ), 5.56 (s, 1H; ArH), 6.44 (d,  $J = 5.7$  Hz, 2H; ArH), 7.72 (d,  $J = 5.7$  Hz, 1H; ArH). ESI-MS(+)  $m/z$  207.08  $[M+H]^+$ .

**94A12 (3-Hydroxy-1-(4-methoxybenzyl)-2-methylpyridin-4(1H)-one):**  $^1H$  NMR (300 MHz,  $CDCl_3-d_1$ , 25 °C):  $\delta = 2.34$  (s,  $CH_3$ ), 3.89 (s,  $OCH_3$ ), 5.05 (s,  $CH_2$ ), 6.44 (d,  $J = 7.2$  Hz, 1H; ArH), 6.89 (d,  $J = 8.1$  Hz, 2H; ArH), 6.96 (d,  $J = 8.8$  Hz, 2H; ArH), 7.31 (d,  $J = 7.2$  Hz, 1H; ArH). APCI-MS(+)  $m/z$  216.07  $[M+H]^+$ .

**94B1 (3-Hydroxy-2-methyl-1-(2-(trifluoromethyl)benzyl)pyridin-4(1H)-one):**  $^1H$  NMR (300 MHz,  $CDCl_3-d_1$ , 25 °C):  $\delta = 2.37$  (s,  $CH_3$ ), 5.06 (s,  $CH_2$ ), 6.42 (d,  $J = 5.4$  Hz, 1H; ArH), 7.40 (m, 1H; ArH), 7.64 – 7.73 (m, 3H; ArH), 8.30 (d,  $J = 7.7$  Hz, 1H; ArH). ESI-MS(+)  $m/z$  284.09  $[M+H]^+$ .

**94B2 (1-(4-Aminophenyl)-3-hydroxy-2-methylpyridin-4(1H)-one):**  $^1H$  NMR (500 MHz,  $CDCl_3-d_1$ , 25 °C):  $\delta = 2.12$  (s,  $CH_3$ ), 6.44 (d,  $J = 7.2$  Hz, 1H; ArH), 6.76 (d,  $J = 8.8$  Hz, 2H; ArH), 7.028 (d,  $J = 8.8$  Hz, 2H; ArH), 7.54 (d,  $J = 7.6$  Hz, 1H; ArH). APCI-MS(+)  $m/z$  217.29  $[M+H]^+$ .

**94B3 (3-Hydroxy-1-(2-methoxybenzyl)-2-methylpyridin-4(1H)-one):**  $^1H$  NMR (300 MHz,  $CDCl_3-d_1$ , 25 °C):  $\delta = 2.34$  (s,  $CH_3$ ), 3.89 (s,  $OCH_3$ ), 5.08 (s,  $CH_2$ ), 6.43 (d,  $J = 7.2$  Hz, 1H; ArH), 6.70 (d,  $J = 7.2$  Hz, 1H; ArH), 6.85 – 6.96 (m, 2H; ArH), 7.27 – 7.36 (m, 2H; ArH). ESI-MS(+)  $m/z$  246.08  $[M+H]^+$ .

**94B4 (1-(3-Fluoro-5-(trifluoromethyl)benzyl)-3-hydroxy-2-methylpyridin-4(1H)-one):**  $^1\text{H}$  NMR (300 MHz,  $\text{CDCl}_3-d_1$ , 25 °C):  $\delta = 2.21$  (s,  $\text{CH}_3$ ), 5.10 (s,  $\text{CH}_2$ ), 6.45 (d,  $J = 3.6$  Hz, 1H; ArH), 7.08 (s, 1H; ArH), 7.27 (dist. t,  $J = 3.6, 4.0$  Hz, 3H; ArH). ESI-MS(+)  $m/z$  302.19  $[\text{M}+\text{H}]^+$ .

**94B5 (3-Hydroxy-2-methyl-1-(4-(trifluoromethoxy)benzyl)pyridin-4(1H)-one):**  $^1\text{H}$  NMR (300 MHz,  $\text{CDCl}_3-d_1$ , 25 °C):  $\delta = 2.25$  (s,  $\text{CH}_3$ ), 5.10 (s,  $\text{CH}_2$ ), 6.54 (d,  $J = 3.3$  Hz, 1H; ArH), 6.99 (d,  $J = 4.0$  Hz, 2H; ArH), 7.17 (d,  $J = 4.0$  Hz, 2H; ArH), 7.32 (d,  $J = 3.3$  Hz, 1H; ArH). ESI-MS(+)  $m/z$  300.08  $[\text{M}+\text{H}]^+$ .

**94B6 (1-(3,5-Bis(trifluoromethyl)benzyl)-3-hydroxy-2-methylpyridin-4(1H)-one):**  $^1\text{H}$  NMR (300 MHz,  $\text{CDCl}_3-d_1$ , 25 °C):  $\delta = 2.30$  (s,  $\text{CH}_3$ ), 5.24 (s,  $\text{CH}_2$ ), 6.53 (d,  $J = 7.2$  Hz, 1H; ArH), 7.35 (d,  $J = 7.2$  Hz, 1H; ArH), 7.49 (s, 2H; ArH), 7.90 (s, 1H; ArH). ESI-MS(+)  $m/z$  352.20  $[\text{M}+\text{H}]^+$ .

**94B7 (3-Hydroxy-2-methyl-1-(5-methylthiazol-2-yl)pyridin-4(1H)-one):**  $^1\text{H}$  NMR (300 MHz,  $\text{CDCl}_3-d_1$ , 25 °C):  $\delta = 2.26$  (s,  $\text{CH}_3$ ), 2.37 (s,  $\text{CH}_3$ ), 6.41 (d,  $J = 5.7$  Hz, 1H; ArH), 6.70 (s, 1H; ArH), 7.69 (d,  $J = 5.4$  Hz, 1H; ArH). ESI-MS(+)  $m/z$  223.19  $[\text{M}+\text{H}]^+$ .

**94B8 (1-(Benzo[d][1,3]dioxol-5-yl)-3-hydroxy-2-methylpyridin-4(1H)-one):**  $^1\text{H}$  NMR (300 MHz,  $\text{CDCl}_3-d_1$ , 25 °C):  $\delta = 2.30$  (s,  $\text{CH}_3$ ), 6.13 (s,  $\text{CH}_2$ ), 6.48 (d,  $J = 7.2$  Hz, 1H; ArH), 6.76-6.72 (m, 2H; ArH), 6.90 (d,  $J = 8.5$  Hz, 1H; ArH), 7.30 (d,  $J = 7.2$  Hz, 1H; ArH). ESI-MS(+)  $m/z$  246.29  $[\text{M}+\text{H}]^+$ .

**94B9 (3-Hydroxy-2-methyl-1-(4-(trifluoromethyl)benzyl)pyridin-4(1H)-one):**  $^1\text{H}$  NMR (300 MHz,  $\text{CDCl}_3-d_1$ , 25 °C):  $\delta = 2.30$  (s,  $\text{CH}_3$ ), 5.24 (s,  $\text{CH}_2$ ), 6.53

(d,  $J = 7.2$  Hz, 1H; ArH), 7.38 (bs, 2H; ArH), 7.49 (d,  $J = 7.2$  Hz, 1H; ArH), 7.68 (bs, 1H; ArH). ESI-MS(+)  $m/z$  284.09 [M+H]<sup>+</sup>.

**94B10 (1-(5,6-Dimethyl-1H-benzo[d]imidazol-2-yl)-3-hydroxy-2-methylpyridin-4(1H)-one):** <sup>1</sup>H NMR (300 MHz, CDCl<sub>3</sub>-*d*<sub>1</sub>, 25 °C):  $\delta = 2.09$  (s, 6H; CH<sub>3</sub>), 2.39 (s, CH<sub>3</sub>), 6.41 (d,  $J = 5.4$  Hz, 1H; ArH), 6.82 (bs, 2H; ArH), 7.68 (d,  $J = 5.3$  Hz, 1H; ArH), 7.68 (bs, 1H; ArH). ESI-MS(+)  $m/z$  270.12 [M+H]<sup>+</sup>.

**94B11 (3-Hydroxy-1-(2-(2-(hydroxymethyl)phenylthio)benzyl)-2-methylpyridin-4(1H)-one):** <sup>1</sup>H NMR (300 MHz, CDCl<sub>3</sub>-*d*<sub>1</sub>, 25 °C):  $\delta = 2.39$  (s, CH<sub>3</sub>), 3.99 (s, CH<sub>2</sub>), 4.69 (s, CH<sub>2</sub>), 6.45 (d,  $J = 7.2$  Hz, 1H; ArH), 7.15-7.60 (m, 8H; ArH), 7.66 (d,  $J = 7.2$  Hz, 1H; ArH), 7.68 (bs, 1H; ArH). ESI-MS(+)  $m/z$  354.08 [M+H]<sup>+</sup>.

**94B12 (3-Hydroxy-2-methyl-1-(thiazol-2-yl)pyridin-4(1H)-one):** <sup>1</sup>H NMR (300 MHz, CDCl<sub>3</sub>-*d*<sub>1</sub>, 25 °C):  $\delta = 2.39$  (s, CH<sub>3</sub>), 6.44 (d,  $J = 5.1$  Hz, 1H; ArH), 6.57 (d,  $J = 3.6$  Hz, 1H; ArH), 7.11 (d,  $J = 3.6$  Hz, 1H; ArH), 7.73 (d,  $J = 5.1$  Hz, 1H; ArH). ESI-MS(+)  $m/z$  209.20 [M+H]<sup>+</sup>.

**94C1 (1-(Biphenyl-4-yl)-3-hydroxy-2-methylpyridin-4(1H)-one):** <sup>1</sup>H NMR (600 MHz, CDCl<sub>3</sub>-*d*<sub>1</sub>, 25 °C):  $\delta = 2.20$  (s, CH<sub>3</sub>), 6.44 (d,  $J = 5.1$  Hz, 1H; ArH), 6.53-7.71 (m, 10H; ArH). ESI-MS(+)  $m/z$  278.36 [M+H]<sup>+</sup>.

**94C2 (1-(4-Ethoxyphenyl)-3-hydroxy-2-methylpyridin-4(1H)-one):** <sup>1</sup>H NMR (600 MHz, CDCl<sub>3</sub>-*d*<sub>1</sub>, 25 °C):  $\delta = 1.49$  (t,  $J = 4.2$  Hz; CH<sub>3</sub>), 2.13 (s, CH<sub>3</sub>), 4.12 (q,  $J = 4.2$  Hz; CH<sub>2</sub>), 6.46 (d,  $J = 4.2$  Hz, 1H; ArH), 7.00 (d,  $J = 5.1$  Hz, 2H; ArH), 7.19 (d,  $J = 5.1$  Hz, 2H; ArH), 7.73 (d,  $J = 4.2$  Hz, 1H; ArH). ESI-MS(+)  $m/z$  246.22 [M+H]<sup>+</sup>.

**94C3 (3-Hydroxy-1-(2-methoxyphenyl)-2-methylpyridin-4(1H)-one):**  $^1\text{H}$  NMR (600 MHz,  $\text{CDCl}_3-d_1$ , 25 °C):  $\delta = 2.13$  (s,  $\text{CH}_3$ ), 3.85 (s,  $\text{OCH}_3$ ), 6.46 (d,  $J = 4.2$  Hz, 1H; ArH), 6.75 (t,  $J = 5.1$  Hz, 2H; ArH), 7.22 (t,  $J = 3.6$  Hz, 2H; ArH), 7.73 (d,  $J = 3.0$  Hz, 1H; ArH). ESI-MS(+)  $m/z$  232.26  $[\text{M}+\text{H}]^+$ .

**94C4 (3-Hydroxy-2-methyl-1-o-tolylpyridin-4(1H)-one):**  $^1\text{H}$  NMR (300 MHz,  $\text{CDCl}_3-d_1$ , 25 °C):  $\delta = 2.02$  (s,  $\text{CH}_3$ ), 2.09 (s,  $\text{CH}_3$ ), 6.51 (d,  $J = 6.9$  Hz, 1H; ArH), 7.20-7.23 (m, 2H; ArH), 7.35-7.48 (m, 3H; ArH). ESI-MS(+)  $m/z$  216.31  $[\text{M}+\text{H}]^+$ .

**94C5 (1-(3,5-Dimethoxyphenyl)-3-hydroxy-2-methylpyridin-4(1H)-one):**  $^1\text{H}$  NMR (500 MHz,  $\text{CDCl}_3-d_1$ , 25 °C):  $\delta = 2.39$  (s,  $\text{CH}_3$ ), 3.77 (s,  $\text{OCH}_3$ ), 5.91 (s, 2H; ArH), 5.95 (s, 1H; ArH), 6.44 (d,  $J = 7.2$  Hz, 1H; ArH), 7.73 (d,  $J = 6.8$  Hz, 1H; ArH). ESI-MS(+)  $m/z$  262.26  $[\text{M}+\text{H}]^+$ .

**94C6 (1-(4-Tert-butylphenyl)-3-hydroxy-2-methylpyridin-4(1H)-one):**  $^1\text{H}$  NMR (300 MHz,  $\text{CDCl}_3-d_1$ , 25 °C):  $\delta = 1.39$  (s, 9H;  $\text{CH}_3$ ), 2.13 (s,  $\text{CH}_3$ ), 6.47 (d,  $J = 7.2$  Hz, 1H; ArH), 7.20 (d,  $J = 8.1$  Hz, 2H; ArH), 7.31 (d,  $J = 7.2$  Hz, 1H; ArH), 7.54 (d,  $J = 8.1$  Hz, 2H; ArH). ESI-MS(+)  $m/z$  258.30  $[\text{M}+\text{H}]^+$ .

**94C7 (1-(4-Aminophenyl)-3-hydroxy-2-methylpyridine-4(1H)-thione):**  $^1\text{H}$  NMR (500 MHz,  $\text{CD}_3\text{OD}-d_4$ , 25 °C):  $\delta = 2.21$  (s,  $\text{CH}_3$ ), 6.76 (d,  $J = 8.6$  Hz, 2H; ArH), 7.06 (d,  $J = 9.1$  Hz, 2H; ArH), 7.42 (d,  $J = 6.8$  Hz, 2H; ArH). APCI-MS(+)  $m/z$  233.16  $[\text{M}+\text{H}]^+$ .

**94C8 (3-Hydroxy-2-methyl-1-(3-(trifluoromethyl)phenyl)pyridin-4(1H)-one):**  $^1\text{H}$  NMR (300 MHz,  $\text{CDCl}_3-d_1$ , 25 °C):  $\delta = 2.14$  (s,  $\text{CH}_3$ ), 6.52 (d,  $J = 6.0$  Hz,

1H; ArH), 7.32 (brd,  $J = 10.5$  Hz, 1H; ArH), 7.55 (brs, 1H; ArH), 7.61 (s, 1H; ArH), 7.74 (bs, 1H; ArH), 7.83 (d,  $J = 7.2$  Hz, 1H; ArH). ESI-MS(+)  $m/z$  270.30 [M+H]<sup>+</sup>.

**94C9 (1-(3-Fluorophenyl)-3-hydroxy-2-methylpyridin-4(1H)-one):** <sup>1</sup>H NMR (300 MHz, CDCl<sub>3</sub>-*d*<sub>1</sub>, 25 °C):  $\delta = 2.41$  (s, CH<sub>3</sub>), 6.49 (d,  $J = 5.7$  Hz, 1H; ArH), 6.74 (brd,  $J = 8.4$  Hz, 2H; ArH), 7.15 (t,  $J = 8.1$  Hz, 1H; ArH), 7.76 (d,  $J = 5.7$  Hz, 2H; ArH), 8.87 (d,  $J = 8.4$  Hz, 1H; ArH). ESI-MS(+)  $m/z$  220.30 [M+H]<sup>+</sup>.

**94C10 (1-(3-Ethylphenyl)-3-hydroxy-2-methylpyridin-4(1H)-one):** <sup>1</sup>H NMR (300 MHz, CDCl<sub>3</sub>-*d*<sub>1</sub>, 25 °C):  $\delta = 1.31$  (t,  $J = 7.8$  Hz, 3H; CH<sub>3</sub>), 2.15 (s, CH<sub>3</sub>), 2.76 (q,  $J = 7.8$  Hz, 2H; CH<sub>2</sub>), 6.49 (d,  $J = 6.9$  Hz, 1H; ArH), 7.11 (bs, 2H; ArH), 7.29-7.49 (m, 3H; ArH). ESI-MS(+)  $m/z$  230.33 [M+H]<sup>+</sup>.

**94C11 (1-(4-Ethylphenyl)-3-hydroxy-2-methylpyridin-4(1H)-one):** <sup>1</sup>H NMR (300 MHz, CDCl<sub>3</sub>-*d*<sub>1</sub>, 25 °C):  $\delta = 1.31$  (t,  $J = 7.5$  Hz, 3H; CH<sub>3</sub>), 2.12 (s, CH<sub>3</sub>), 2.76 (q,  $J = 7.5$  Hz, 2H; CH<sub>2</sub>), 6.47 (d,  $J = 7.0$  Hz, 1H; ArH), 7.19 (d,  $J = 8.0$  Hz, 2H; ArH), 7.20-7.40 (m, 3H; ArH). ESI-MS(+)  $m/z$  230.33 [M+H]<sup>+</sup>.

**94C12 (3-Hydroxy-1-(3-hydroxy-4-methoxyphenyl)-2-methylpyridin-4(1H)-one):** <sup>1</sup>H NMR (600 MHz, CDCl<sub>3</sub>-*d*<sub>1</sub>, 25 °C):  $\delta = 2.41$  (s, CH<sub>3</sub>), 3.90 (s, OCH<sub>3</sub>), 6.44 (d,  $J = 3.0$  Hz, 1H; ArH), 6.52 (d,  $J = 5.1$  Hz, 1H; ArH), 6.68 (s, 1H; ArH), 6.79 (d,  $J = 5.1$  Hz, 1H; ArH), 7.74 (d,  $J = 3.0$  Hz, 1H; ArH). ESI-MS(+)  $m/z$  248.29 [M+H]<sup>+</sup>.

**94D1 (3-Hydroxy-1-(4-methoxyphenyl)-2-methylpyridin-4(1H)-one):** <sup>1</sup>H NMR (300 MHz, CDCl<sub>3</sub>-*d*<sub>1</sub>, 25 °C):  $\delta = 2.12$  (s, CH<sub>3</sub>), 3.90 (s, OCH<sub>3</sub>), 6.47 (d,  $J = 6.3$  Hz, 1H; ArH), 7.03 (d,  $J = 8.0$  Hz, 2H; ArH), 7.20 (d,  $J = 8.1$  Hz, 2H; ArH), 6.31



(dist. d,  $J = 8.0$  Hz, 1H; ArH), 7.74 (d,  $J = 3.0$  Hz, 1H; ArH). ESI-MS(+)  $m/z$  232.29 [M+H]<sup>+</sup>.

**94D2 (1-(2-Fluorobenzyl)-3-hydroxy-2-methylpyridin-4(1H)-one):** <sup>1</sup>H NMR (300 MHz, CDCl<sub>3</sub>-*d*<sub>1</sub>, 25 °C):  $\delta = 2.34$  (s, CH<sub>3</sub>), 5.15 (s, CH<sub>2</sub>), 6.48 (d,  $J = 6.9$  Hz, 1H; ArH), 6.83 (t,  $J = 7.8$  Hz, 1H; ArH), 7.12-7.19 (m, 2H; ArH), 7.34-7.42 (m, 2H; ArH). ESI-MS(+)  $m/z$  234.14 [M+H]<sup>+</sup>.

**94D3 (1-(2,6-Dichlorobenzyl)-3-hydroxy-2-methylpyridin-4(1H)-one):** <sup>1</sup>H NMR (300 MHz, CDCl<sub>3</sub>-*d*<sub>1</sub>, 25 °C):  $\delta = 2.60$  (s, CH<sub>3</sub>), 5.32 (s, CH<sub>2</sub>), 6.32 (d,  $J = 4.2$  Hz, 1H; ArH), 6.84 (d,  $J = 4.5$  Hz, 1H; ArH), 7.40 (t,  $J = 4.5$  Hz, 1H; ArH), 7.48 (dist. d,  $J = 4.8$  Hz, 2H; ArH). ESI-MS(+)  $m/z$  284.08 [M+H]<sup>+</sup>.

**94D4 (3-Hydroxy-2-methyl-1-(3-(2-methylthiazol-4-yl)phenyl)pyridin-4(1H)-one):** <sup>1</sup>H NMR (300 MHz, CDCl<sub>3</sub>-*d*<sub>1</sub>, 25 °C):  $\delta = 2.15$  (s, CH<sub>3</sub>), 2.77 (s, CH<sub>3</sub>), 6.48 (d,  $J = 6.9$  Hz, 1H; ArH), 7.21 (d,  $J = 7.5$  Hz, 1H; ArH), 7.36 (d,  $J = 6.9$  Hz, 1H; ArH), 7.46 (s, 1H; ArH), 7.56 (t,  $J = 7.5$  Hz, 1H; ArH), 7.88 (s, 1H; ArH), 7.98 (t,  $J = 7.2$  Hz, 1H; ArH), . ESI-MS(+)  $m/z$  299.27 [M+H]<sup>+</sup>.

**94D5 (1-(2,3-Dichlorobenzyl)-3-hydroxy-2-methylpyridin-4(1H)-one):** <sup>1</sup>H NMR (600 MHz, CDCl<sub>3</sub>-*d*<sub>1</sub>, 25 °C):  $\delta = 2.33$  (s, CH<sub>3</sub>), 5.18 (s, CH<sub>2</sub>), 6.51 (dist. t,  $J = 4.0$  Hz, 1H; ArH), 7.23 (t,  $J = 4.8$  Hz, 1H; ArH), 7.29 (bs, 2H; ArH), 7.50 (d,  $J = 4.8$  Hz, 1H; ArH). ESI-MS(+)  $m/z$  284.09 [M+H]<sup>+</sup>.

**94D6 (1-(4-Chlorobenzyl)-3-hydroxy-2-methylpyridin-4(1H)-one):** <sup>1</sup>H NMR (500 MHz, CDCl<sub>3</sub>-*d*<sub>1</sub>, 25 °C):  $\delta = 2.29$  (s, CH<sub>3</sub>), 5.09 (s, 2H; CH<sub>2</sub>), 6.47 (d,  $J = 7.0$  Hz, 1H; ArH), 6.98 (d,  $J = 7.0$  Hz, 2H; ArH), 7.32 (d,  $J = 8.0$  Hz, 1H; ArH), 7.37 (d,  $J = 7.0$  Hz, 2H; ArH). ESI-MS(+)  $m/z$  250.11 [M+H]<sup>+</sup>.

**94D7 (1-(2,5-Dimethylphenethyl)-3-hydroxy-2-methylpyridin-4(1H)-one):**

$^1\text{H}$  NMR (300 MHz,  $\text{CDCl}_3-d_1$ , 25 °C):  $\delta$  = 2.21 (s,  $\text{CH}_3$ ), 2.29 (s,  $\text{CH}_3$ ), 2.39 (s,  $\text{CH}_3$ ), 3.00 (t,  $J$  = 6.0 Hz, 2H;  $\text{CH}_2$ ), 4.06 (t,  $J$  = 6.0 Hz, 2H;  $\text{CH}_2$ ), 6.33 (d,  $J$  = 6.6 Hz, 1H; ArH), 6.80 (s, 1H; ArH), 6.99-7.10 (m, 3H; ArH). ESI-MS(+)  $m/z$  258.16  $[\text{M}+\text{H}]^+$ .

**94D8 (3-Hydroxy-1-(2-hydroxybenzyl)-2-methylpyridin-4(1H)-one):**

$^1\text{H}$  NMR (300 MHz,  $\text{CDCl}_3-d_1$ , 25 °C):  $\delta$  = 2.40 (s,  $\text{CH}_3$ ), 5.32 (s,  $\text{CH}_2$ ), 6.44 (d,  $J$  = 5.7 Hz, 1H; ArH), 6.79-7.00 (m, 4H; ArH), 7.74 (d,  $J$  = 5.7 Hz, 1H; ArH). ESI-MS(+)  $m/z$  232.10  $[\text{M}+\text{H}]^+$ .

**94D9 (1-(2,4-Dichlorobenzyl)-3-hydroxy-2-methylpyridin-4(1H)-one):**

$^1\text{H}$  NMR (600 MHz,  $\text{CDCl}_3-d_1$ , 25 °C):  $\delta$  = 2.28 (s,  $\text{CH}_3$ ), 5.14 (s,  $\text{CH}_2$ ), 6.50 (d,  $J$  = 4.2 Hz, 1H; ArH), 6.58 (d,  $J$  = 5.1 Hz, 1H; ArH), 7.27 (bs, 2H; ArH), 7.51 (bs, 1H; ArH). ESI-MS(+)  $m/z$  284.08  $[\text{M}+\text{H}]^+$ .

**94D10 (1-(3,5-Dichlorobenzyl)-3-hydroxy-2-methylpyridin-4(1H)-one):**

$^1\text{H}$  NMR (600 MHz,  $\text{CDCl}_3-d_1$ , 25 °C):  $\delta$  = 2.34 (s,  $\text{CH}_3$ ), 5.15 (s,  $\text{CH}_2$ ), 6.64 (bs, 1H; ArH), 7.38 (bs, 1H; ArH), 7.42 (bs, 1H; ArH), 7.52 (bs, 2H; ArH). ESI-MS(+)  $m/z$  284.15  $[\text{M}+\text{H}]^+$ .

**94D11 (1-(3,4-Dichlorobenzyl)-3-hydroxy-2-methylpyridin-4(1H)-one):**

$^1\text{H}$  NMR (600 MHz,  $\text{CDCl}_3-d_1$ , 25 °C):  $\delta$  = 2.30 (s,  $\text{CH}_3$ ), 5.07 (s,  $\text{CH}_2$ ), 6.49 (d,  $J$  = 4.2 Hz, 1H; ArH), 6.87 (d,  $J$  = 4.8 Hz, 1H; ArH), 7.32 (d,  $J$  = 4.2 Hz, 2H; ArH), 7.48 (d,  $J$  = 4.8 Hz, 1H; ArH). ESI-MS(+)  $m/z$  284.06  $[\text{M}+\text{H}]^+$ .

**94D12 (3-Hydroxy-1-(4-methoxyphenethyl)-2-methylpyridin-4(1H)-one):**

<sup>1</sup>H NMR (400 MHz, CDCl<sub>3</sub>-d<sub>1</sub>, 25 °C): δ = 2.33 (s, CH<sub>3</sub>), 2.92 (t, *J* = 7.0 Hz, CH<sub>2</sub>), 3.79 (s, O CH<sub>3</sub>), 4.03 (t, *J* = 7.0 Hz, CH<sub>2</sub>), 6.27 (d, *J* = 7.6 Hz, 1H; ArH), 6.81 (d, *J* = 8.8 Hz, 2H; ArH), 6.92 (m, 3H; ArH). ESI-MS(+) *m/z* 260.10 [M+H]<sup>+</sup>.

**94E1 (3-Hydroxy-2-methyl-1-(2-methylbenzyl)pyridin-4(1H)-one):** <sup>1</sup>H

NMR (500 MHz, CDCl<sub>3</sub>-d<sub>1</sub>, 25 °C): δ = 2.31 (s, CH<sub>3</sub>), 2.35 (s, CH<sub>3</sub>), 5.06 (s, CH<sub>2</sub>), 6.49 (d, *J* = 7.2 Hz, 1H; ArH), 6.63 (s, 1H; ArH), 7.21 (m, 5H; ArH). ESI-MS(+) *m/z* 230.10 [M+H]<sup>+</sup>.

**94E2 (1-(3-Chloro-4-fluorobenzyl)-3-hydroxy-2-methylpyridin-4(1H)-one):** <sup>1</sup>H NMR (300 MHz, CDCl<sub>3</sub>-d<sub>1</sub>, 25 °C): δ = 2.29 (s, CH<sub>3</sub>), 5.14 (s, CH<sub>2</sub>), 6.50

(d, *J* = 7.5 Hz, 1H; ArH), 6.62 (d, *J* = 7.8 Hz, 1H; ArH), 7.24-7.35 (m, 2H; ArH), 7.66 (d, *J* = 7.8 Hz, 1H; ArH). ESI-MS(+) *m/z* 268.05 [M+H]<sup>+</sup>.

**94E3 (1-(3,4-Dichlorophenethyl)-3-hydroxy-2-methylpyridin-4(1H)-one):**

<sup>1</sup>H NMR (300 MHz, CDCl<sub>3</sub>-d<sub>1</sub>, 25 °C): δ = 2.42 (s, CH<sub>3</sub>), 3.01 (t, *J* = 6.9 Hz, CH<sub>2</sub>), 4.12 (t, *J* = 6.9 Hz, CH<sub>2</sub>), 6.46 (dd, *J* = 3.0, 5.4 Hz, 1H; ArH), 6.90 (d, *J* = 8.0 Hz, 1H; ArH), 7.03 (dd, *J* = 3.3, 7.2 Hz, 1H; ArH), 7.43 (dd, *J* = 3.0, 8.1 Hz, 1H; ArH), 7.76 (dd, *J* = 3.0, 5.1 Hz, 1H; ArH). ESI-MS(+) *m/z* 298.16 [M+H]<sup>+</sup>.

**94E4 (3-Hydroxy-2-methyl-1-(2-(trifluoromethoxy)benzyl)pyridin-4(1H)-one):** <sup>1</sup>H NMR (300 MHz, CDCl<sub>3</sub>-d<sub>1</sub>, 25 °C): δ = 2.12 (s, CH<sub>3</sub>), 5.10 (s, CH<sub>2</sub>), 6.44

(d, *J* = 3.0 Hz, 1H; ArH), 7.25-7.30 (m, 4H; ArH), 7.34 (d, *J* = 3.0 Hz, 1H; ArH). ESI-MS(+) *m/z* 300.04 [M+H]<sup>+</sup>.

**94E5 (1-(3-Bromo-4-methoxyphenethyl)-3-hydroxy-2-methylpyridin-4(1H)-one):**  $^1\text{H}$  NMR (300 MHz,  $\text{CDCl}_3-d_1$ , 25 °C):  $\delta = 2.27$  (s,  $\text{CH}_3$ ), 2.79 (t,  $J = 3.6$  Hz,  $\text{CH}_2$ ), 4.02 (t,  $J = 3.6$  Hz,  $\text{CH}_2$ ), 6.34 (d,  $J = 3.0$  Hz, 1H; ArH), 6.72 (d,  $J = 4.2$  Hz, 2H; ArH), 7.36 (s, 1H; ArH), 7.32 (d,  $J = 3.0$  Hz, 1H; ArH). ESI-MS(+)  $m/z$  338.07  $[\text{M}+\text{H}]^+$ .

**94E6 (3-Hydroxy-2-methyl-1-(4-methyl-3-(trifluoromethyl)phenyl)pyridin-4(1H)-one):**  $^1\text{H}$  NMR (300 MHz,  $\text{CDCl}_3-d_1$ , 25 °C):  $\delta = 2.13$  (s,  $\text{CH}_3$ ), 2.38 (s,  $\text{CH}_3$ ), 6.43 (d,  $J = 6.3$  Hz, 1H; ArH), 6.53 (d,  $J = 8.1$  Hz, 1H; ArH), 7.36 (d,  $J = 8.1$  Hz, 1H; ArH), 7.49 (d,  $J = 7.8$  Hz, 1H; ArH), 7.72 (d,  $J = 6.3$  Hz, 1H; ArH). ESI-MS(+)  $m/z$  284.29  $[\text{M}+\text{H}]^+$ .

**94E7 (3-Hydroxy-2-methyl-1-(3-(trifluoromethyl)phenyl)pyridin-4(1H)-one):**  $^1\text{H}$  NMR (300 MHz,  $\text{CDCl}_3-d_1$ , 25 °C):  $\delta = 2.13$  (s,  $\text{CH}_3$ ), 2.38 (s,  $\text{CH}_3$ ), 6.54 (d,  $J = 8.1$  Hz, 1H; ArH), 7.31 (bs, 1H; ArH), 7.36 (d,  $J = 8.1$  Hz, 1H; ArH), 7.58 (bs, 1H; ArH), 7.72 (d,  $J = 5.7$  Hz, 2H; ArH). ESI-MS(+)  $m/z$  270.30  $[\text{M}+\text{H}]^+$ .

**94E8 (1-(4-Ethoxyphenyl)-3-hydroxy-2-methylpyridine-4(1H)-thione):**  $^1\text{H}$  NMR (400 MHz,  $\text{CDCl}_3-d_1$ , 25 °C):  $\delta = 1.45$  (t,  $J = 6.8$  Hz, 3H;  $\text{CH}_3$ ), 2.20 (s,  $\text{CH}_3$ ), 4.07 (q,  $J = 6.9$  Hz, 2H;  $\text{CH}_2$ ), 7.00 (d,  $J = 8.8$  Hz, 2H; ArH), 7.16-7.18 (m, 3H; ArH), 7.52 (d,  $J = 6.4$  Hz, 1H; ArH), 8.77 (brs, 1H; OH). ESI-MS(+)  $m/z$  262.24  $[\text{M}+\text{H}]^+$ .  
Anal. calcd for  $\text{C}_{14}\text{H}_{15}\text{NO}_2\text{S}$ : C, 64.34; H, 5.79; N, 5.36; S, 12.27. Found: C, 64.37; H, 6.17; N, 5.26; S, 12.23.

**94E9 (3-Hydroxy-1-(2-methoxyphenyl)-2-methylpyridine-4(1H)-thione):**  $^1\text{H}$  NMR (400 MHz,  $\text{CDCl}_3-d_1$ , 25 °C):  $\delta = 2.25$  (bs,  $\text{CH}_3$ ), 3.81 (s,  $\text{CH}_3$ ), 7.10-7.22

(m, 4H; ArH), 7.54 (bs, 1H; ArH), 8.79 (bs, 1H; ArH). ESI-MS(+)  $m/z$  248.07 [M+H]<sup>+</sup>.

**94E10 (3-Hydroxy-1-(3-methoxyphenyl)-2-methylpyridin-4(1H)-one):** <sup>1</sup>H NMR (400 MHz, CDCl<sub>3</sub>-*d*<sub>1</sub>, 25 °C):  $\delta$  = 2.12 (s, CH<sub>3</sub>), 3.85 (s, OCH<sub>3</sub>), 6.44 (d,  $J$  = 7.2 Hz, 1H; ArH), 6.77 (s, 1H; ArH), 6.83 (d,  $J$  = 8.0 Hz, 1H; ArH), 7.02 (d,  $J$  = 10.4 Hz, 1H; ArH), 7.29 (d,  $J$  = 7.2 Hz, 1H; ArH), 7.39 (t,  $J$  = 8.0 Hz, 1H; ArH). ESI-MS(+)  $m/z$  232.27 [M+H]<sup>+</sup>.

**94E11 (3-Hydroxy-1-(3-methoxybenzyl)-2-methylpyridine-4(1H)-thione):** <sup>1</sup>H NMR (400 MHz, CDCl<sub>3</sub>-*d*<sub>1</sub>, 25 °C):  $\delta$  = 2.39 (s, CH<sub>3</sub>), 3.78 (s, OCH<sub>3</sub>), 5.17 (s, CH<sub>2</sub>), 6.55 (m, 2H; ArH), 6.86 (dd,  $J$  = 2.4, 8.8 Hz, 1H; ArH), 7.18 (d,  $J$  = 7.6 Hz, 1H; ArH), 7.28 (t,  $J$  = 7.6 Hz, 1H; ArH), 7.52 (d,  $J$  = 6.4 Hz, 1H; ArH), 8.77 (brs, 1H; OH). ESI-MS(+)  $m/z$  262.04 [M+H]<sup>+</sup>.

**94E12 (1-(4-Fluoro-3-(trifluoromethyl)phenyl)-3-hydroxy-2-methylpyridine-4(1H)-thione):** <sup>1</sup>H NMR (400 MHz, CDCl<sub>3</sub>-*d*<sub>1</sub>, 25 °C):  $\delta$  = 2.21 (s, CH<sub>3</sub>), 7.12 (d,  $J$  = 7.6 Hz, 1H; ArH), 7.44 (t,  $J$  = 9.0 Hz, 1H; ArH), 7.51 (d,  $J$  = 6.8 Hz, 1H; ArH), 7.56-7.60 (m, 1H; ArH), 7.62 (dd,  $J$  = 2.8, 6.0 Hz, 1H; ArH), 8.73 (brs, 1H; OH). ESI-MS(+)  $m/z$  304.35 [M+H]<sup>+</sup>. HRMS calcd for C<sub>13</sub>H<sub>9</sub>F<sub>4</sub>NOS: 304.0414. Found: 304.0416.

**94F1 (1-(3,5-Bis(trifluoromethyl)phenyl)-3-hydroxy-2-methylpyridine-4(1H)-thione):** <sup>1</sup>H NMR (400 MHz, CDCl<sub>3</sub>-*d*<sub>1</sub>, 25 °C):  $\delta$  = 2.39 (s, CH<sub>3</sub>), 6.98 (s, 2H; ArH), 7.16 (s, 1H; ArH), 7.27 (d,  $J$  = 4.8 Hz, 1H; ArH), 7.53 (d,  $J$  = 4.8 Hz, 1H; ArH), 7.79 (brs, 1H; OH). ESI-MS(-)  $m/z$  352.18 [M-H]<sup>-</sup>.

**94F2 (3-Hydroxy-2-methyl-1-(4-methylthiazol-2-yl)pyridin-4(1H)-one):**  $^1\text{H}$  NMR (400 MHz,  $\text{CDCl}_3-d_1$ , 25 °C):  $\delta = 2.17$  (s,  $\text{CH}_3$ ), 2.33 (s,  $\text{CH}_3$ ), 5.97 (s, 1H; ArH), 6.38 (d,  $J = 5.2$  Hz, 1H; ArH), 7.66 (d,  $J = 5.2$  Hz, 1H; ArH). APCI-MS(+)  $m/z$  223.10  $[\text{M}+\text{H}]^+$ .

**94F3 (1-(3-Fluoro-4-methylphenyl)-3-hydroxy-2-methylpyridin-4(1H)-one):**  $^1\text{H}$  NMR (400 MHz,  $\text{CDCl}_3-d_1$ , 25 °C):  $\delta = 2.11$  (s,  $\text{CH}_3$ ), 2.35 (s,  $\text{CH}_3$ ), 6.43 (d,  $J = 6.8$  Hz, 1H; ArH), 6.95 (m, 2H; ArH), 7.27 (s, 1H; ArH), 7.31 (t,  $J = 8.0$  Hz, 1H; ArH). ESI-MS(+)  $m/z$  234.30  $[\text{M}+\text{H}]^+$ .

**94F4 (1-(4-Fluorophenethyl)-3-hydroxy-2-methylpyridin-4(1H)-one):**  $^1\text{H}$  NMR (400 MHz,  $\text{CDCl}_3-d_1$ , 25 °C):  $\delta = 2.33$  (s,  $\text{CH}_3$ ), 2.96 (t,  $J = 7.0$  Hz, 2H;  $\text{CH}_2$ ), 4.04 (t,  $J = 7.0$  Hz, 2H;  $\text{CH}_2$ ), 6.28 (d,  $J = 7.6$  Hz, 1H; ArH), 6.94 (d,  $J = 7.2$  Hz, 1H; ArH), 6.98 (d,  $J = 7.2$  Hz, 4H; ArH). ESI-MS(+)  $m/z$  248.28  $[\text{M}+\text{H}]^+$ .

**94F5 (3-Hydroxy-1-(2-methoxybenzyl)-2-methylpyridine-4(1H)-thione):**  $^1\text{H}$  NMR (400 MHz,  $\text{CDCl}_3-d_1$ , 25 °C):  $\delta = 2.45$  (s,  $\text{CH}_3$ ), 3.85 (s,  $\text{OCH}_3$ ), 5.16 (s,  $\text{CH}_2$ ), 6.75 (d,  $J = 6.4$  Hz, 1H; ArH), 6.92 (t,  $J = 7.8$  Hz, 2H; ArH), 7.15 (d,  $J = 6.8$  Hz, 1H; ArH), 7.34 (t,  $J = 8.0$  Hz, 1H; ArH), 7.49 (d,  $J = 6.8$  Hz, 1H; ArH), 8.76 (brs, 1H; OH). ESI-MS(+)  $m/z$  262.08  $[\text{M}+\text{H}]^+$ . Anal. calcd for  $\text{C}_{14}\text{H}_{15}\text{NO}_2\text{S}$ : C, 64.34; H, 5.79; N, 5.36; S, 12.27. Found: C, 64.63; H, 6.14; N, 5.59; S, 11.88.

**94F6 (1-(4-Fluorobenzyl)-3-hydroxy-2-methylpyridine-4(1H)-thione):**  $^1\text{H}$  NMR (400 MHz,  $\text{CDCl}_3-d_1$ , 25 °C):  $\delta = 2.37$  (s,  $\text{CH}_3$ ), 5.19 (s,  $\text{CH}_2$ ), 7.00 (m, 4H; ArH), 7.17 (d,  $J = 6.4$  Hz, 1H; ArH), 7.44 (t,  $J = 7.0$  Hz, 1H; ArH), 8.73 (brs, 1H; OH). ESI-MS(+)  $m/z$  250.04  $[\text{M}+\text{H}]^+$ . Anal. calcd for  $\text{C}_{13}\text{H}_{12}\text{FNOS}$ : C, 62.63; H, 4.85; N, 5.62; S, 12.86. Found: C, 62.32; H, 5.25; N, 5.65; S, 12.50.

**94F7 (3-Hydroxy-1-(4-methoxybenzyl)-2-methylpyridine-4(1H)-thione):**

$^1\text{H}$  NMR (400 MHz,  $\text{CDCl}_3-d_1$ , 25 °C):  $\delta$  = 2.40 (s,  $\text{CH}_3$ ), 3.80 (s,  $\text{OCH}_3$ ), 5.13 (s,  $\text{CH}_2$ ), 6.88 (d,  $J$  = 8.8 Hz, 2H; ArH), 6.96 (d,  $J$  = 8.8 Hz, 2H; ArH), 7.16 (d,  $J$  = 6.8 Hz, 1H; ArH), 7.48 (d,  $J$  = 6.8 Hz, 1H; ArH), 8.74 (brs, 1H; OH). ESI-MS(+)  $m/z$  261.96  $[\text{M}+\text{H}]^+$ . Anal. calcd for  $\text{C}_{14}\text{H}_{15}\text{NO}_2\text{S}$ : C, 64.34; H, 5.79; N, 5.36; S, 12.27.

Found: C,

64.60; H, 6.15; N, 5.28; S, 11.88.

**94F8 (3-Hydroxy-2-methyl-1-(2-propylphenyl)pyridine-4(1H)-thione):**

$^1\text{H}$  NMR (400 MHz,  $\text{CDCl}_3-d_1$ , 25 °C):  $\delta$  = 1.01 (t,  $J$  = 7.2 Hz,  $\text{CH}_3$ ), 1.63 (h,  $J$  = 7.6 Hz,  $\text{CH}_2$ ), 2.45 (s,  $\text{CH}_3$ ), 2.47 (t,  $J$  = 7.8 Hz,  $\text{CH}_2$ ), 6.68 (d,  $J$  = 7.2 Hz, 2H; ArH), 6.74 (t,  $J$  = 7.6 Hz, 2H; ArH), 7.31 (d,  $J$  = 4.8 Hz, 1H; ArH), 7.55 (d,  $J$  = 5.2 Hz, 1H; ArH), 7.84 (brs, 1H; OH). ESI-MS(+)  $m/z$  260.26  $[\text{M}+\text{H}]^+$ .

**94F9 (1-Benzyl-3-hydroxy-2-methylpyridine-4(1H)-thione):**

$^1\text{H}$  NMR (400 MHz,  $\text{CDCl}_3-d_1$ , 25 °C):  $\delta$  = 2.36 (s,  $\text{CH}_3$ ), 5.22 (s,  $\text{CH}_2$ ), 7.01 (d,  $J$  = 7.2 Hz, 2H; ArH), 7.20 (d,  $J$  = 6.4 Hz, 1H; ArH), 7.36 (m, 3H; ArH), 7.54 (d,  $J$  = 6.8 Hz, 1H; ArH), 8.79 (brs, 1H; OH). ESI-MS(+)  $m/z$  232.13  $[\text{M}+\text{H}]^+$ . Anal. calcd for  $\text{C}_{13}\text{H}_{13}\text{NOS}$ : C, 67.50; H, 5.66; N, 6.06; S, 13.86. Found: C, 67.26; H, 5.96; N, 6.19; S, 13.49.

**94F10 (3-Hydroxy-2-methyl-1-(4-(phenylamino)phenyl)pyridin-4(1H)-one):**

$^1\text{H}$  NMR (400 MHz,  $\text{CDCl}_3-d_1$ , 25 °C):  $\delta$  = 2.37 (s,  $\text{CH}_3$ ), 6.98 (t,  $J$  = 7.4 Hz, 1H; ArH), 7.18-7.21 (m, 5H; ArH), 7.28 (d,  $J$  = 4.4 Hz, 2H; ArH), 7.31 (d,  $J$  = 8.4 Hz, 2H; ArH), 8.09 (d,  $J$  = 7.2 Hz, 2H; ArH), ESI-MS(+)  $m/z$  293.23  $[\text{M}+\text{H}]^+$ .

**94F11 (1-(4-Fluorophenyl)-3-hydroxy-2-methylpyridine-4(1H)-thione):**  $^1\text{H}$  NMR (400 MHz,  $\text{CDCl}_3-d_1$ , 25 °C):  $\delta = 2.18$  (s,  $\text{CH}_3$ ), 7.15 (d,  $J = 6.8$  Hz, 1H; ArH), 7.23 (m, 2H; ArH), 7.30 (m, 2H; ArH), 7.48 (d,  $J = 6.8$  Hz, 1H; ArH), 8.72 (brs, 1H; OH). ESI-MS(+)  $m/z$  236.31  $[\text{M}+\text{H}]^+$ .

**94F12 (1-(2,3-Dihydro-1H-inden-1-yl)-3-hydroxy-2-methylpyridine-4(1H)-thione):**  $^1\text{H}$  NMR (400 MHz,  $\text{CDCl}_3-d_1$ , 25 °C):  $\delta = 2.06$  (m, 1H,  $\text{CH}_2$ ), 2.68 (s,  $\text{CH}_3$ ), 2.76 (m, 1H,  $\text{CH}_2$ ), 3.00 (m, 1H,  $\text{CH}_2$ ), 3.13 (m, 1H,  $\text{CH}_2$ ), 5.87 (dd,  $J = 2.0, 14.0$  Hz, 1H, CH), 6.78 (d,  $J = 6.8$  Hz, 1H; ArH), 7.10 (d,  $J = 7.2$  Hz, 1H; ArH), 7.29 (m, 1H; ArH), 7.37 (m, 3H; ArH), 8.80 (brs, 1H; OH). ESI-MS(+)  $m/z$  257.96  $[\text{M}+\text{H}]^+$ .

**94G1 (3-Hydroxy-2-methyl-1-(4-morpholinophenyl)pyridin-4(1H)-one):**  $^1\text{H}$  NMR (400 MHz,  $\text{CDCl}_3-d_1$ , 25 °C):  $\delta = 2.35$  (s,  $\text{CH}_3$ ), 2.99 (t,  $J = 4.6$  Hz, 4H,  $\text{CH}_2$ ), 3.82 (t,  $J = 4.6$  Hz, 4H,  $\text{CH}_2$ ), 6.40 (d,  $J = 5.6$  Hz, 1H; ArH), 6.64 (d,  $J = 8.8$  Hz, 2H; ArH), 6.77 (d,  $J = 8.8$  Hz, 2H; ArH), 7.68 (d,  $J = 6.0$  Hz, 1H; ArH). APCI-MS(+)  $m/z$  287.28  $[\text{M}+\text{H}]^+$ .

**94G2 (1-(3,4-Dimethoxyphenyl)-3-hydroxy-2-methylpyridine-4(1H)-thione):**  $^1\text{H}$  NMR (400 MHz,  $\text{CDCl}_3-d_1$ , 25 °C):  $\delta = 2.23$  (s,  $\text{CH}_3$ ), 3.90 (s,  $\text{OCH}_3$ ), 3.96 (s,  $\text{OCH}_3$ ), 6.69 (m, 1H; ArH), 6.83 (dd,  $J = 2.6, 8.0$  Hz, 1H; ArH), 6.96 (d,  $J = 8.4$  Hz, 1H; ArH), 7.19 (d,  $J = 6.4$  Hz, 1H; ArH), 7.53 (d,  $J = 6.8$  Hz, 1H; ArH). ESI-MS(+)  $m/z$  278.31  $[\text{M}+\text{H}]^+$ .

**94G3 (1-(3,5-Bis(trifluoromethyl)phenyl)-3-hydroxy-2-methylpyridin-4(1H)-one):**  $^1\text{H}$  NMR (400 MHz,  $\text{CDCl}_3-d_1$ , 25 °C):  $\delta = 2.36$  (s,  $\text{CH}_3$ ), 6.41 (d,  $J = 5.2$  Hz, 1H; ArH), 7.19 (s, 3H; ArH), 7.69 (d,  $J = 5.6$  Hz, 1H; ArH). ESI-MS(+)  $m/z$  338.30  $[\text{M}+\text{H}]^+$ .



**94G4 (3-Hydroxy-2-methyl-1-(pyridin-3-ylmethyl)pyridine-4(1H)-thione):**

$^1\text{H}$  NMR (400 MHz,  $\text{CDCl}_3-d_1$ , 25 °C):  $\delta$  = 2.40 (s,  $\text{CH}_3$ ), 5.25 (s,  $\text{CH}_2$ ), 7.19 (d,  $J$  = 6.4 Hz, 1H; ArH), 7.28 (m, 2H; ArH), 7.51 (d,  $J$  = 6.4 Hz, 1H; ArH), 8.47 (d,  $J$  = 2.0 Hz, 1H; ArH), 8.63 (d,  $J$  = 4.4 Hz, 1H; ArH), 8.76 (brs, 1H; OH). ESI-MS(+)  $m/z$  233.12  $[\text{M}+\text{H}]^+$ . Anal. for calcd  $\text{C}_{12}\text{H}_{12}\text{N}_2\text{OS}$ : C, 62.04; H, 5.21; N, 12.06; S, 13.80. Found: C, 62.22; H, 5.60; N, 12.23; S, 13.45.

**94G5 (1-(Biphenyl-4-ylmethyl)-3-hydroxy-2-methylpyridine-4(1H)-**

**thione):**  $^1\text{H}$  NMR (400 MHz,  $\text{CDCl}_3-d_1$ , 25 °C):  $\delta$  = 2.42 (s,  $\text{CH}_3$ ), 5.25 (s,  $\text{CH}_2$ ), 7.08 (d,  $J$  = 8.0 Hz, 2H; ArH), 7.23 (d,  $J$  = 5.6 Hz, 1H; ArH), 7.35 (t,  $J$  = 7.4 Hz, 1H; ArH), 7.43 (t,  $J$  = 7.4 Hz, 2H; ArH), 7.53 (m, 3H; ArH), 7.58 (d,  $J$  = 8.0 Hz, 2H; ArH), 8.77 (brs, 1H; OH). ESI-MS(+)  $m/z$  308.02  $[\text{M}+\text{H}]^+$ . Anal. calcd for  $\text{C}_{19}\text{H}_{17}\text{NOS}$ : C, 74.23; H, 5.57; N, 4.56; S, 10.43. Found: C, 73.56; H, 5.58; N, 4.46; S, 10.67.

**94G6 (1-(4-Fluoro-3-(trifluoromethyl)phenyl)-3-hydroxy-2-methylpyridin-**

**4(1H)-one):**  $^1\text{H}$  NMR (400 MHz,  $\text{CDCl}_3-d_1$ , 25 °C):  $\delta$  = 2.05 (s,  $\text{CH}_3$ ), 6.73 (d,  $J$  = 7.2 Hz, 1H; ArH), 7.75 (t,  $J$  = 9.4 Hz, 1H; ArH), 7.88 (d,  $J$  = 7.2 Hz, 1H; ArH), 7.96 (m, 1H; ArH), 8.11 (dd,  $J$  = 3.2, 6.8 Hz, 1H; ArH). ESI-MS(+)  $m/z$  288.37  $[\text{M}+\text{H}]^+$ . Anal. calcd for  $\text{C}_{13}\text{H}_9\text{F}_4\text{NO}_2\cdot\text{H}_2\text{O}$ : C, 51.16; H, 3.63; N, 4.59. Found: C, 51.57; H, 3.38; N, 4.75.

**94G7 (3-Hydroxy-1-(3-methoxyphenethyl)-2-methylpyridine-4(1H)-**

**thione):**  $^1\text{H}$  NMR (400 MHz,  $\text{CDCl}_3-d_1$ , 25 °C):  $\delta$  = 2.41 (s,  $\text{CH}_3$ ), 2.99 (t,  $J$  = 7.0 Hz,  $\text{CH}_2$ ), 3.74 (s,  $\text{OCH}_3$ ), 4.19 (t,  $J$  = 7.0 Hz,  $\text{CH}_2$ ), 6.55 (s, 1H; ArH), 6.58 (d,  $J$  = 7.6 Hz, 1H; ArH), 6.79 (dd,  $J$  = 2.0, 8.4 Hz, 1H; ArH), 6.85 (d,  $J$  = 6.4 Hz, 1H; ArH),

7.18 (t,  $J = 8.0$  Hz, 1H; ArH), 7.32 (d,  $J = 6.8$  Hz, 1H; ArH), 8.72 (brs, 1H; OH). ESI-MS(+)  $m/z$  276.14 [M+H]<sup>+</sup>. Anal. calcd for C<sub>15</sub>H<sub>17</sub>NO<sub>2</sub>S: C, 65.43; H, 6.22; N, 5.09; S, 11.64. Found: C, 65.83; H, 6.60; N, 5.37; S, 11.49.

**94G8 (3-Hydroxy-2-methyl-1-(4-methylphenethyl)pyridine-4(1H)-thione):**

<sup>1</sup>H NMR (400 MHz, CDCl<sub>3</sub>-*d*<sub>1</sub>, 25 °C):  $\delta = 2.32$  (s, CH<sub>3</sub>), 2.42 (s, CH<sub>3</sub>), 2.99 (t,  $J = 7.0$  Hz, CH<sub>2</sub>), 4.17 (t,  $J = 7.0$  Hz, CH<sub>2</sub>), 6.81 (d,  $J = 7.2$  Hz, 1H; ArH), 6.90 (d,  $J = 8.0$  Hz, 2H; ArH), 7.09 (d,  $J = 8.0$  Hz, 2H; ArH), 7.35 (d,  $J = 6.8$  Hz, 1H; ArH), 8.76 (brs, 1H; OH). ESI-MS(+)  $m/z$  260.19 [M+H]<sup>+</sup>. Anal. calcd for C<sub>15</sub>H<sub>17</sub>NOS: C, 69.46; H, 6.61; N, 5.40; S, 12.36. Found: C, 69.23; H, 6.97; N, 5.13; S, 12.56.

**94G9 (3-Hydroxy-1-(4-methoxyphenethyl)-2-methylpyridine-4(1H)-**

**thione):** <sup>1</sup>H NMR (400 MHz, CDCl<sub>3</sub>-*d*<sub>1</sub>, 25 °C):  $\delta = 2.39$  (s, CH<sub>3</sub>), 2.96 (t,  $J = 6.4$  Hz, CH<sub>2</sub>), 3.77 (s, OCH<sub>3</sub>), 4.15 (t,  $J = 7.0$  Hz, CH<sub>2</sub>), 6.79-6.82 (m, 3H; ArH), 6.90 (d,  $J = 8.8$  Hz, 1H; ArH), 7.29 (d,  $J = 6.4$  Hz, 1H; ArH). ESI-MS(+)  $m/z$  276.21 [M+H]<sup>+</sup>.

**94G10 (1-(3-Fluoro-4-methylphenyl)-3-hydroxy-2-methylpyridine-4(1H)-**

**thione):** <sup>1</sup>H NMR (400 MHz, CDCl<sub>3</sub>-*d*<sub>1</sub>, 25 °C):  $\delta = 2.22$  (s, CH<sub>3</sub>), 2.38 (s, CH<sub>3</sub>), 6.98 (m, 2H; ArH), 7.14 (d,  $J = 6.8$  Hz, 1H; ArH), 7.36 (d,  $J = 8.4$  Hz, 1H; ArH), 7.53 (d,  $J = 7.2$  Hz, 1H; ArH), 8.77 (brs, 1H; OH). ESI-MS(+)  $m/z$  250.34 [M+H]<sup>+</sup>. HRMS calcd for C<sub>13</sub>H<sub>12</sub>FNOS: 250.0696. Found: 250.0698.

**94G11 (3-Hydroxy-1,2-dimethylpyridine-4(1H)-thione):** <sup>1</sup>H NMR (400

MHz, CDCl<sub>3</sub>-*d*<sub>1</sub>, 25 °C):  $\delta = 2.49$  (s, CH<sub>3</sub>), 3.77 (s, CH<sub>3</sub>), 7.09 (d,  $J = 6.8$  Hz, 1H; ArH), 7.44 (d,  $J = 6.8$  Hz, 1H; ArH), 8.75 (brs, 1H; OH). ESI-MS(+)  $m/z$  156.15 [M+H]<sup>+</sup>. Anal. calcd for C<sub>7</sub>H<sub>9</sub>NOS: C, 54.17; H, 5.84; N, 5.98; S, 20.66. Found: 54.18; H, 5.98; N, 9.06; S, 20.55.

**94G12 (3-Hydroxy-1-(4-hydroxyphenethyl)-2-methylpyridin-4(1H)-one):**

<sup>1</sup>H NMR (400 MHz, CDCl<sub>3</sub>-d<sub>1</sub>, 25 °C): δ = 2.37 (s, CH<sub>3</sub>), 2.88 (t, *J* = 7.4 Hz, CH<sub>2</sub>), 4.25 (t, *J* = 7.4 Hz, CH<sub>2</sub>), 6.64 (d, *J* = 7.6 Hz, 2H; ArH), 6.95 (d, *J* = 7.2 Hz, 2H; ArH), 7.21 (d, *J* = 6.8 Hz, 1H; ArH), 7.48 (d, *J* = 7.2 Hz, 1H; ArH), 9.29 (brs, 1H; OH). ESI-MS(+) *m/z* 262.03 [M+H]<sup>+</sup>.

**94H1 (3-Hydroxy-2-methyl-1-(4-methylthiazol-2-yl)pyridine-4(1H)-**

**thione):** <sup>1</sup>H NMR (400 MHz, CDCl<sub>3</sub>-d<sub>1</sub>, 25 °C): δ = 1.44 (t, *J* = 7.2 Hz, CH<sub>3</sub>), 2.50 (s, CH<sub>3</sub>), 4.03 (q, *J* = 7.4 Hz, CH<sub>3</sub>), 7.12 (d, *J* = 6.8 Hz, 1H; ArH), 7.47 (d, *J* = 6.8 Hz, 1H; ArH), 8.76 (brs, 1H; OH). APCI-MS(+) *m/z* 239.10 [M+H]<sup>+</sup>.

**94H2 (3-Hydroxy-2-methyl-1-phenethylpyridine-4(1H)-thione):** <sup>1</sup>H NMR

(400 MHz, CDCl<sub>3</sub>-d<sub>1</sub>, 25 °C): δ = 2.41 (s, CH<sub>3</sub>), 3.03 (t, *J* = 7.0 Hz, CH<sub>2</sub>), 4.20 (t, *J* = 7.0 Hz, CH<sub>2</sub>), 6.83 (d, *J* = 6.8 Hz, 1H; ArH), 7.02 (d, *J* = 7.6 Hz, 2H; ArH), 7.27 (m, 3H; ArH), 7.34 (d, *J* = 6.4 Hz, 1H; ArH), 8.79 (brs, 1H; OH). ESI-MS(+) *m/z* 246.27 [M+H]<sup>+</sup>. HRMS calcd for C<sub>14</sub>H<sub>15</sub>NOS: 246.0947. Found: 246.0949.

**94H3 (1-Ethyl-3-hydroxy-2-methylpyridine-4(1H)-thione):** <sup>1</sup>H NMR (400

MHz, CDCl<sub>3</sub>-d<sub>1</sub>, 25 °C): δ = 2.49 (s, CH<sub>3</sub>), 3.77 (s, CH<sub>3</sub>), 7.09 (d, *J* = 6.8 Hz, 1H; ArH), 7.44 (d, *J* = 6.8 Hz, 1H; ArH), 8.75 (brs, 1H; OH). ESI-MS(+) *m/z* 170.04 [M+H]<sup>+</sup>. Anal. calcd for C<sub>8</sub>H<sub>11</sub>NOS: C, 56.77; H, 6.55; N, 8.28; S, 18.95. Found: 56.76; H, 6.95; N, 8.38; S, 18.80.

**4.H.ii Synthesis of fragment evolution****1-((4'-Fluorobiphenyl-4-yl)methyl)-3-hydroxy-2-methylpyridine-4(1H)-**

**thione (94G5.1):** 75 mg (0.53 mmol) of thiomaltol, 252 mg (1.5 equiv., 0.80 mmol) of the triflate salt of **4b.iv** (Chapter 2) and 1.5 mmol (1.5 equiv.) of NaOH were reacted

in 4 mL of a 1:1 solution of EtOH and H<sub>2</sub>O at 95 °C. The reaction was stirred overnight under N<sub>2</sub>; and the precipitated solid was purified via flash silica column chromatography in 0-2% MeOH/CH<sub>2</sub>Cl<sub>2</sub> followed by 2% MeOH/49% EtOAc/49% CH<sub>2</sub>Cl<sub>2</sub>. Yield = 17%. <sup>1</sup>H NMR (500 MHz, CDCl<sub>3</sub>, 25 °C): δ = 2.42 (s, 3H), 5.25 (s, 2H), 7.08 (d, *J* = 8.0 Hz, 2H; ArH), 7.11 (t, *J* = 8.6 Hz, 2H; ArH), 7.22 (d, *J* = 6.8 Hz, 1H; ArH), 7.49 (dd, *J* = 9.1, 5.7 Hz, 1H; ArH), 7.52 (d, *J* = 8.0 Hz, 4H; ArH). ESI-MS(+) *m/z* 326.09 [M+H]<sup>+</sup>.

**3-Hydroxy-2-methyl-1-(4-(naphthalen-2-yl)benzyl)pyridine-4(1*H*)-thione**

**(94G5.2):** This compound was prepared similarly to **94G5.1**. 100 mg (0.70 mmol) of thiomaltol, 365 mg (1.5 equiv., 1.05 mmol) of the triflate salt of **4b.i** (Chapter 2) and 1.5 mmol (1.5 equiv.) of NaOH were reacted at 50 °C. After 2 h, an orange solid precipitated out which was vacuum filtered and dried to yield 157 mg (0.44 mmol) of product. Yield = 63%. <sup>1</sup>H NMR (500 MHz, CDCl<sub>3</sub>, 25 °C): δ = 2.45 (s, 3H), 5.27 (s, 2H), 7.13 (d, *J* = 8.0 Hz, 2H; ArH), 7.42 (m, 3H; ArH), 7.58 (d, *J* = 6.9 Hz, 1H; ArH), 7.68 (m, 2H; ArH), 7.73 (d, *J* = 8.0 Hz, 2H; ArH), 7.86 (m, 3H; ArH), 8.81 (brs, OH). ESI-MS(+) *m/z* 358.02 [M+H]<sup>+</sup>. NOTE: Product is still slightly crude.

**1-((3',4'-Difluorobiphenyl-4-yl)methyl)-3-hydroxy-2-methylpyridine-**

**4(1*H*)-thione (94G5.3):** This compound was prepared according to the procedure outlined for **94G5.1**. 75 mg (0.53 mmol) of thiomaltol, 267 mg (1.5 equiv., 0.80 mmol) of the triflate salt of **8b** and 0.8 mmol (1.5 equiv.) of NaOH were reacted; and purified via flash silica column chromatography in 0-2% MeOH/CH<sub>2</sub>Cl<sub>2</sub> to yield 54 mg (0.16 mmol) of a beige solid. Yield = 30%. <sup>1</sup>H NMR (300 MHz, CDCl<sub>3</sub>, 25 °C):

$\delta$  = 2.42 (s, 3H), 5.25 (s, 2H), 7.09 (d,  $J$  = 7.5 Hz, 2H; ArH), 7.22 (d,  $J$  = 7.2 Hz, 2H; ArH), 7.32 (m, 2H; ArH), 7.52 (d,  $J$  = 8.1 Hz, 2H; ArH), 7.57 (d,  $J$  = 6.6 Hz, 1H; ArH), 8.81 (brs, OH). APCI-MS(+)  $m/z$  344.06 [M+H]<sup>+</sup>.

**3-Hydroxy-1-((4'-methoxybiphenyl-4-yl)methyl)-2-methylpyridine-4(1H)-thione (94G5.4):** Still slightly crude. APCI-MS(+)  $m/z$  352.00 [M+H]<sup>+</sup>.

**1-(4-(Benzo[d][1,3]dioxol-5-yl)benzyl)-3-hydroxy-2-methylpyridine-4(1H)-thione (95G5.5):** This compound was prepared according to the procedure outlined for **94G5.1**. 100 mg (0.70 mmol) of thiomaltol, 360 mg (1.5 equiv., 1.05 mmol) of the triflate salt of **4b.ii** (Chapter 2) and 1.05 mmol (1.5 equiv.) of NaOH were reacted; and purified via flash silica column chromatography in 0-1% MeOH/CH<sub>2</sub>Cl<sub>2</sub> to yield 118 mg (0.34 mmol) of a yellow solid. Yield = 49%. <sup>1</sup>H NMR (500 MHz, CDCl<sub>3</sub>, 25 °C):  $\delta$  = 2.42 (s, 3H), 5.22 (s, 2H), 6.00 (s, 2H), 6.87 (d,  $J$  = 8.6 Hz, 1H; ArH), 7.01 (m, 2H; ArH), 7.50 (d,  $J$  = 8.6 Hz, 2H; ArH), 7.53 (d,  $J$  = 6.9, 2H; ArH), 8.78 (brs, OH). ESI-MS(+)  $m/z$  352.00 [M+H]<sup>+</sup>.

#### **4.H.iii Extended Chelator Fragment Library 1 (eCFL-1) – Screening against MMP-2, MMP-3, MMP-9, and anthrax LF**

The fragments were initially dissolved in dimethyl sulfoxide (DMSO) at a concentration of 50 mM in a 96-well plate. A 10-fold dilution in DMSO was performed to obtain a plate with 50  $\mu$ L of each fragment at a concentration of 5 mM. 1  $\mu$ L of each fragment from the 5 mM plate was plated for assays against each enzyme as described below. Initial screening against each enzyme was repeated a minimum of three times. IC<sub>50</sub> values of fragment hits were measured by preparing serial dilutions of DMSO stocks to obtain a final concentration of 500  $\mu$ M, 100  $\mu$ M, 50  $\mu$ M, 10  $\mu$ M, 5

$\mu\text{M}$ , 1  $\mu\text{M}$ , 0.5  $\mu\text{M}$ , 0.1  $\mu\text{M}$ , 0.05  $\mu\text{M}$  and 0.01  $\mu\text{M}$  for each hit in the assay. The  $\text{IC}_{50}$  value was calculated using GraphPad Prism 5 software as shown in Figure 4-11 below.  $\text{IC}_{50}$  values were determined in duplicate.

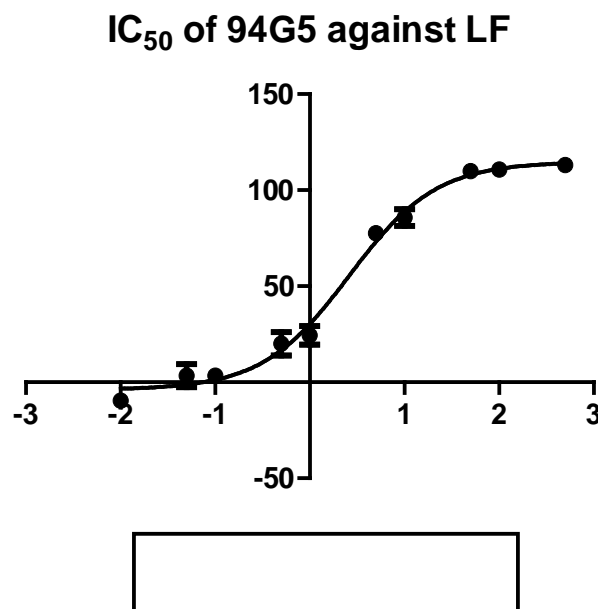


**Figure 4-11.** Non-linear dose response curve of the % inhibition versus the log of the inhibitor concentration using GraphPad Prism 5.

Curve is fitted to the equation below:

$$Y = \text{Bottom} + (\text{Top} - \text{Bottom}) / (1 + 10^{((\text{LogIC}_{50} - X) * \text{HillSlope}))})$$

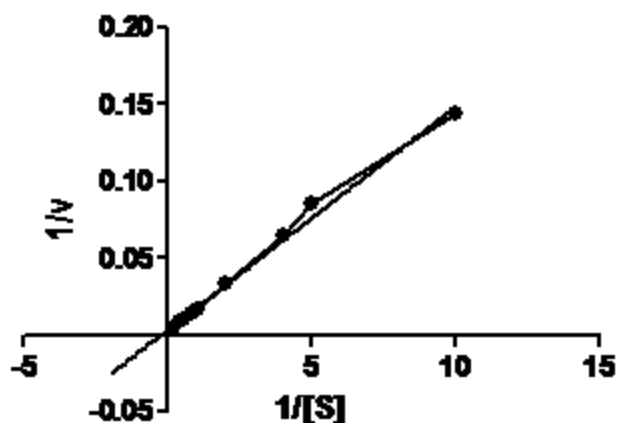
**4.H.iii.a MMP Inhibition Assays.** The assay was carried out in white NUNC 96-well plates as previously described with some modification (Puerta et al. *J. Biol. Inorg. Chem.* **2006**, *11*, 131–138). Each well contained a total volume of 100  $\mu\text{L}$ : 69  $\mu\text{L}$  of buffer (50 mM HEPES, 10 mM  $\text{CaCl}_2$ , 0.05% Brij-35, pH 7.5 for MMP-2, MMP-9 or 50 mM MES, 10 mM  $\text{CaCl}_2$ , 0.05% Brij-35, pH 6.0 for MMP-3), 20  $\mu\text{L}$  of human recombinant MMP-2, -3, or -9 (1.16 U, 2.0 U, or 0.9 U, respectively per well,

BIOMOL International, now Enzo Life Sciences), and 1  $\mu\text{L}$  of the fragment solution (50  $\mu\text{M}$  final concentration). After a 30 min incubation period at 37  $^{\circ}\text{C}$ , the reaction was initiated by the addition of 10  $\mu\text{L}$  fluorogenic MMP substrate (4  $\mu\text{M}$  final concentration, Mca-Pro-Leu-Gly-Leu-Dpa-Ala-Arg-NH<sub>2</sub>·AcOH, BIOMOL International, now Enzo Life Sciences). Kinetic measurements were recorded using a Bio-Tek Flx 800 fluorescence plate reader every minute for 20 min with excitation and emission wavelengths at 320 and 400 nm, respectively.

**4.H.iii.b LF Inhibition Assays.** The assay was carried out in white NUNC 96-well plates. Each well contained a total volume of 100  $\mu\text{L}$ : 69  $\mu\text{L}$  of LF buffer (20 mM HEPES, pH 7.4), 20  $\mu\text{L}$  of recombinant LF (10 nM final concentration, List Biological Laboratories), and 1  $\mu\text{L}$  of the fragment solution (50  $\mu\text{M}$  final concentration). After a 20 min incubation period at 25  $^{\circ}\text{C}$ , the reaction was initiated by the addition of 10  $\mu\text{L}$  fluorogenic LF substrate (2  $\mu\text{M}$  final concentration, MAPKKide DABCYL/FITC, List Biological Laboratories). Kinetic measurements were recorded using a Bio-Tek Flx 800 fluorescence plate reader every minute for 20 min with excitation and emission wavelengths at 485 and 528 nm, respectively.

**4.H.iii.c Enzyme Kinetic Assays.** Kinetic measurements were performed using the fluorescence-based assay kit to determine  $V_{max}$  and  $K_m$ . A representative Lineweaver-Burk plot for MMP-9 is shown in Figure 4-12, which is used to extrapolate  $V_{max}$  and  $K_m$ .  $K_i$  was calculated from the Michaelis-Menten equation below

### Lineweaver-Burk plot of MMP-9



|                        |                     |
|------------------------|---------------------|
| Y-intercept when X=0.0 | 0.003959 ± 0.001864 |
| X-intercept when Y=0.0 | -0.2729             |

|                 |        |
|-----------------|--------|
| Goodness of Fit |        |
| $r^2$           | 0.9930 |

**Figure 4-12.** Lineweaver-burk plot of MMP-9 to determine enzyme kinetic parameters

Y-intercept =  $1/V_{max}$   $\Rightarrow$   $V_{max} = 252.6$

X-intercept =  $-1/K_m$   $\Rightarrow$   $K_m = 3.6 \mu\text{M}$

$$K_i = \frac{[I]}{1 + [S]/K_m} \quad \text{equation (1)}$$

where [I] = inhibitor concentration at the  $IC_{50}$  value and [S] = initial substrate concentration used to determine  $IC_{50}$  value.



#### **4.I Acknowledgments**

Text, schemes, and figures in this chapter, in part, are reprints of materials published in the following paper: Agrawal, Arpita; Johnson, Sherida L.; Jacobsen, Jennifer A.; Miller, Melissa T; Pellecchia, Maurizio; Cohen, Seth M. “Chelator Fragment Libraries for Targeting Metalloproteinases” *ChemMedChem* **2010**, *5*, 195-199. The dissertation author was the primary researcher for the data presented and was the primary author on the paper included. The co-authors listed in these publications also participated in the research. The permission to reproduce this paper was granted by Wiley-VCH Verlag GmbH & Co. KGaA, Weinheim, copyright 2010.

**4.J References**

- (1) Zartler, E. R.; Shapiro, M. J. *Curr. Opin. Chem. Biol.* **2005**, *9*, 366.
- (2) Congreve, M.; Chessari, G.; Tisi, D.; Woodhead, A. J. *J. Med. Chem.* **2008**, *51*, 3661.
- (3) Hajduk, P. J. *J. Med. Chem.* **2006**, *49*, 6972.
- (4) Rees, D. C.; Congreve, M.; Murray, C. W.; Carr, R. *Nat. Rev. Drug Discov.* **2004**, *3*, 660.
- (5) Shuker, S. B.; Hajduk, P. J.; Meadows, R. P.; Fesik, S. W. *Science* **1996**, *274*, 1531.
- (6) Pellecchia, M.; Sem, D. S.; Wuthrich, K. *Nat. Rev. Drug Discov.* **2002**, *1*, 211.
- (7) Kuhn, P.; Wilson, K.; Patch, M. G.; Stevens, R. C. *Curr. Opin. Chem. Biol.* **2002**, *6*, 704.
- (8) Blundell, T. L.; Jhoti, H.; Abell, C. *Nat. Rev. Drug Discov.* **2002**, *1*, 45.
- (9) Reynolds, C. H.; Tounge, B. A.; Bembenek, S. D. *J. Med. Chem.* **2008**, *51*, 2432.
- (10) Reynolds, C. H.; Bembenek, S. D.; Tounge, B. A. *Bioorg. Med. Chem. Lett.* **2007**, *17*, 4258.
- (11) Lipinski, C. A. *J. Pharmacol. Toxicol. Methods* **2000**, *44*, 235.
- (12) Wenlock, M. C.; Austin, R. P.; Barton, P.; Davis, A. M.; Leeson, P. D. *J. Med. Chem.* **2003**, *46*, 1250.
- (13) Vieth, M.; Siegal, M. G.; Higgs, R. E.; Watson, I. A.; Robertson, D. H.; Savin, K. A.; Durst, G. L.; Hipskind, P. A. *J. Med. Chem.* **2004**, *47*, 224.
- (14) Congreve, M.; Carr, R. M., C.; Jhoti, H. A. *Drug Discov. Today* **2003**, *8*, 876.
- (15) Hajduk, P. J.; Sheppard, G.; Nettlesheim, D. G.; Olejniczak, E. T.; Shuker, S. B.; Meadows, R. P.; Steinman, D. H.; Carrera, J. G. M.; Marcotte, P. A.; Severin, J.; Walter, K.; Smith, H.; Gubbins, E.; Simmer, R.; Holzman, T. F.; Morgan, D. W.; Davidsen, S. K.; Summers, J. B.; Fesik, S. W. *J. Am. Chem. Soc.* **1997**, *119*, 5818.
- (16) Olejniczak, E. T.; Hajduk, P. J.; Marcotte, P. A.; Nettlesheim, D. G.; Meadows,

- R. P.; Edalji, R.; Holzman, T. F.; Fesik, S. W. *J. Am. Chem. Soc.* **1997**, *119*, 5828.
- (17) Patel, V.; Mazitschek, R.; Coleman, B.; Nguyen, C.; Urgaonkar, S.; Cortese, J.; Robert H. Barker, J.; Greenberg, E.; Tang, W.; Bradner, J. E.; Schreiber, S. L.; Duraisingh, M. T.; Wirth, D. F.; Clardy, J. *J. Med. Chem.* **2009**, *52*, 2185.
- (18) Sternson, S. M.; Wong, J. C.; Grozinger, C. M.; Schreiber, S. L. *Org. Lett.* **2001**, *3*, 4239.
- (19) Flipo, M.; Beghyn, T.; Charton, J.; Leroux, V. A.; Deprez, B. P.; Deprez-Poulain, R. F. *Bioorg. Med. Chem. Lett.* **2007**, *15*, 63.
- (20) Salvino, J. M.; Mathew, R.; Kiesow, T.; Narensingh, R.; Mason, H. J.; Dodd, A.; Robert Groneberg; Burns, C. J.; McGeehan, G.; Kline, J.; Orton, E.; Tang, S.-Y.; Morrisette, M.; Labaudiniere, R. *Bioorg. Med. Chem. Lett.* **2000**, *10*, 1637.
- (21) Jacobsen, F. E.; Lewis, J. A.; Cohen, S. M. *J. Am. Chem. Soc.* **2006**, *128*, 3156.
- (22) Puerta, D. T.; Lewis, J. A.; Cohen, S. M. *J. Am. Chem. Soc.* **2004**, *126*, 8388.
- (23) Jacobsen, F. E.; Lewis, J. A.; Cohen, S. M. *ChemMedChem* **2007**, *2*, 152.
- (24) Jacobsen, J. A.; Fullagar, J. L.; Miller, M. T.; Cohen, S. M. *J. Med. Chem.* **2011**, *54*, 591.
- (25) Puerta, D. T.; Griffin, M. O.; Lewis, J. A.; Romero-Perez, D.; Garcia, R.; Villarreal, F. J.; Cohen, S. M. *J. Biol. Inorg. Chem.* **2006**, *11*, 131.
- (26) Cablewski, T.; Faux, A. F.; Strauss, C. R. *J. Org. Chem.* **1994**, *59*, 3408.
- (27) Zhang, Z.; Rettig, S. J.; Orvig, C. *Inorg. Chem.* **1991**, *30*, 509.
- (28) Johnson, S. L.; Chen, L. H.; Pellicchia, M. *Bioorg. Chem.* **2007**, *35*, 306.
- (29) Schepetkin, I. A.; Khlebnikov, A. I.; Kirpotina, L. N.; Quinn, M. T. *J. Med. Chem.* **2006**, *49*, 5232.
- (30) Sang, Q.-X. A.; Jin, Y.; Newcomer, R. G.; Monroe, S. C.; Fang, X.; Hurst, D. R.; Lee, S.; Cao, Q.; Schwartz, M. A. *Curr. Top. Med. Chem.* **2006**, *6*, 289.
- (31) Forino, M.; Johnson, S. L.; Wong, T. Y.; Rozanov, D. V.; Savinov, A. Y.; Li, W.; Fattorusso, R.; Becattini, B.; Orry, A. J.; Jung, D.; Abagyan, R. A.; Smith,

- J. W.; Alibek, K.; Liddington, R. C.; Strongin, A. Y.; Pellecchia, M. *Proc. Natl. Acad. Sci., USA* **2005**, *2005*, 9499.
- (32) Agrawal, A.; de Oliveira, C. A. F.; Cheng, Y.; Jacobsen, J. A.; McCammon, J. A.; Cohen, S. M. *J. Med. Chem.* **2009**, *52*, 1063.
- (33) Johnson, S. L.; Jung, D.; Forino, M.; Chen, Y.; Satterhwait, A.; Rozanov, D. V.; Strongin, A. Y.; Pellecchia, M. *J. Med. Chem.* **2006**, *49*, 27.
- (34) Numa, M. M. D.; Lee, L. V.; Hsu, C. C.; Bower, K. E.; Wong, C. H. *ChemBioChem* **2005**, *2005*, 1002.
- (35) Panchal, R. G.; Hermone, A. R.; Nguyen, T. L.; Wong, T. Y.; Schwarzenbacher, R.; Schmidt, J.; Lane, D.; McGrath, C.; Turk, B. E.; Burnett, J.; Aman, M. J.; Little, S.; Sausville, E. A.; Zaharevitz, D. W.; Cantley, L. C.; Liddington, R. C.; Gussio, R.; Bavari, S. *Nat. Struct. Mol. Biol.* **2004**, *11*, 67.
- (36) Lewis, J. A.; Mongan, J.; McCammon, J. A.; Cohen, S. M. *ChemMedChem* **2006**, *1*, 694.
- (37) Agrawal, A.; Romero-Perez, D.; Jacobsen, J. A.; Villarreal, F. J.; Cohen, S. M. *ChemMedChem* **2008**, *3*, 812.
- (38) Johnson, S. L.; Pellecchia, M. *Curr. Top. Med. Chem.* **2006**, *6*, 317.
- (39) Hopkins, A. L.; Groom, C. R.; Alex, A. *Drug Discov. Today* **2004**, *9*, 430.
- (40) Monga, V. *Thesis*, 7.

## **Chapter 5. Beyond mononuclear Zn<sup>2+</sup> endopeptidases**

### 5.A.i HIV integrase (HIV-IN), a dinuclear endonuclease target

Twenty six years after the discovery of AIDS and twenty years after the first anti-AIDS drug hit the market; the first anti-HIV integrase inhibitor (Raltegravir) was FDA approved in 2007.<sup>1,2</sup> Raltegravir (RAL), which is the result of a decade long investigation by Merck, bears a striking resemblance to the inhibitors developed in our lab against MMPs and anthrax LF as discussed in Chapters 2 and 3 (Figure 5-1).<sup>3,4</sup> As opposed to the active site metal targeted approach taken by our lab to develop inhibitors against metalloenzymes; the discovery of Raltegravir was preceded by high-throughput screening efforts that identified diketo acids (DKAs) as the first class of strand transfer HIV-IN inhibitors.<sup>5-11</sup> DKAs were later discovered to inhibit HIV-IN by sequestering the active site metal ions.<sup>9</sup> Unlike the mononuclear  $Zn^{2+}$  endopeptidases - MMPs and LF, HIV-IN is a dinuclear  $Mg^{2+}$  endonuclease that is one of three enzymes transcribed by the viral genome of HIV.<sup>12</sup>

This chapter discusses the preliminary efforts taken by our lab to test “Raltegravir-like” in house MMP and LF inhibitors against HIV-IN. Additionally, the chapter is focused on the synthesis of new HIV-IN inhibitors with novel metal binding groups (MBGs). This will allow us to study the effects of different MBGs on the inhibition of HIV-IN and further expand upon novel and potent leads.

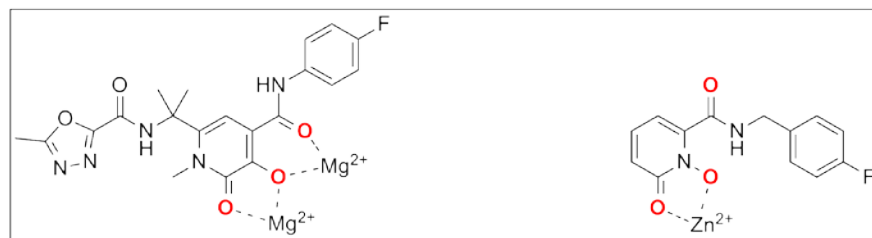
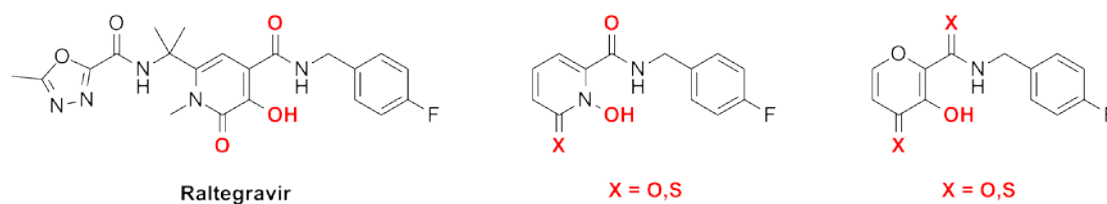


**Figure 5-1.** Raltegravir (left) shows a striking similarity to metalloenzyme inhibitors that have been reported in our lab.<sup>3,4</sup> The three compounds shown have the same *p*-fluorophenyl backbone, but employ different metal-binding groups (MBGs). From left to right (including RAL), the MBGs are a N-methylhydroxypyridinone, N-hydroxypyridin(one/thione), hydroxypyr(one/thione). The metal binding atoms are highlighted in bold red. Shown below in the box is the proposed metal binding of RAL to the dinuclear  $Mg^{2+}$  active site of HIV-IN, compared to the proposed binding of our inhibitors against mononuclear  $Zn^{2+}$  endopeptidases MMPs and LF.

### **5.A.ii HIV is the causative agent of AIDS**

Human immunodeficiency virus (HIV) is the lentivirus that causes AIDS (Acquired Immunodeficiency Syndrome); a disease in humans that leads to a compromised immune system and increased susceptibility to opportunistic infections.<sup>13,14</sup> The discovery of AIDS in the US dates back to 1981 where the first cases appeared in both New York and California; the discovery of HIV followed soon after.<sup>15</sup> Several viral isolates were initially detected in the blood of AIDS patients, but it was in 1984 that Robert Gallo and co-workers at the National Cancer Institute, and Luc Montagnier and colleagues at the Pasteur Institute in Paris identified HIV as the causative agent of AIDS.<sup>16</sup> AIDS develops as a result of the virus going undiagnosed for long periods of time between infection and the appearance of serious symptoms. This leads to inadvertent transmission of the virus and the spread of HIV/AIDS.<sup>17</sup> Since its discovery in 1981, AIDS continues to be an interminable pandemic. According to the 2009 UNAIDS epidemic report, 33.3 million people around the globe live with HIV and in the year 2009 itself, approximately 2.6 million people were infected with the virus, and 1.8 million people died from HIV.<sup>18</sup>

Like most viruses, HIV-1 surreptitiously controls cellular machinery of the host at multiple steps (Figure 5-2) to complete a productive cycle. As shown in Figure 5-2, the virus enters the cells by binding to immunologically important host cellular receptors (CD4 and CXCR4/CCR5) and fusing with the cellular membrane. The virus then delivers its genetic material to the cytoplasm, where the viral RNA genome is copied into DNA, transported to the nucleus and integrated into the host DNA. After



export from the nucleus, viral RNA is translated into viral proteins which assemble at the cell membrane to bud off into new particles of HIV-1.<sup>12,19</sup>

HIV-1 primarily infects CD4<sup>+</sup> T4 helper lymphocytes, macrophages and dendritic cells, which consequently leads to immuno-suppression. HIV infection lowers the CD4<sup>+</sup> T cell count via apoptosis and killing of infected CD4<sup>+</sup> T4 cells by CD8<sup>+</sup> cytotoxic lymphocytes that recognize infected cells.<sup>20</sup> When CD4<sup>+</sup> T cells are progressively depleted, cell-mediated immunity is lost, and the body becomes more susceptible to opportunistic infections. Therefore, most untreated HIV infections eventually develop into AIDS.<sup>19</sup>

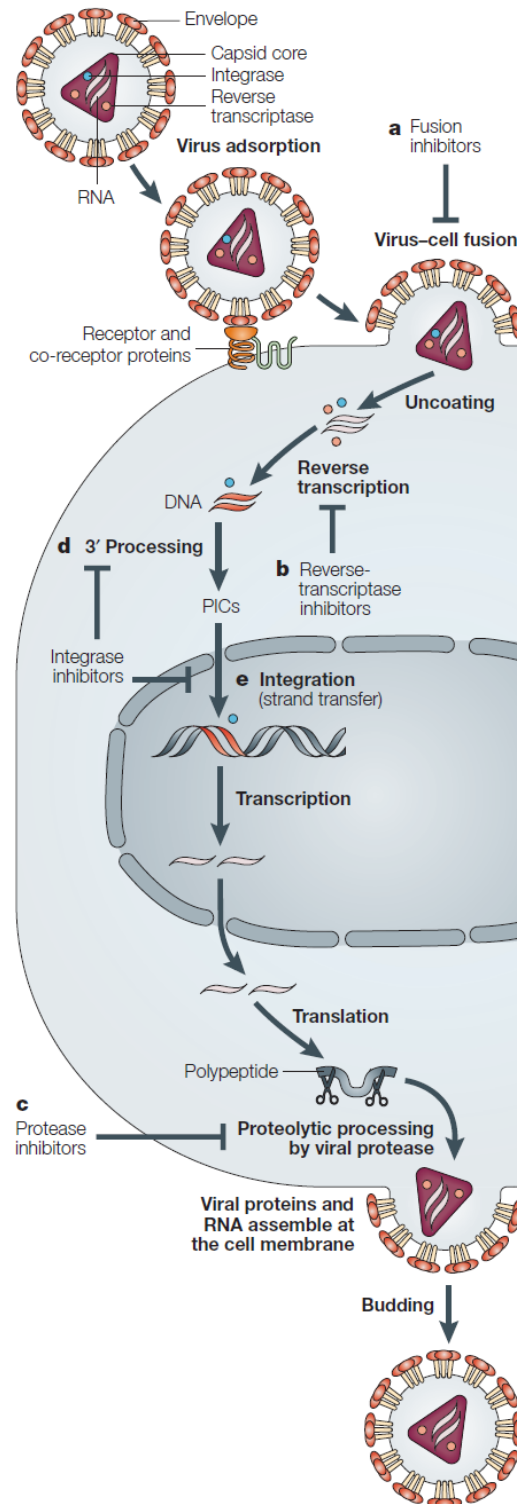


**Figure 5-2. Life cycle of HIV-1 replication.** (a-e) represents the different stages and/or proteins that can be targeted for inhibition in the replication cycle.<sup>12</sup>

### 5.B Anti-retroviral therapy

HIV infection and replication can be blocked at various stages in the HIV life cycle as shown in Figure 5-2. A comprehensive list of current FDA approved inhibitors targeting the various stages of HIV replication is represented in Table 5-1. Several of the inhibitors in Table 5-1 are taken in different combinations as Highly Active Anti-Retroviral Therapy (HAART). HAART is the most common therapy against HIV/AIDS, and has been shown to be the most effective against the progression of HIV.<sup>12,21</sup> Until July of 2009, HAART consisted of multi-drug combinations that only targeted two of the three viral enzymes – protease and reverse transcriptase.<sup>22</sup> HAART is most commonly comprised of a protease inhibitor (PI) or a non-nucleoside reverse transcriptase inhibitor (NNRTI) in combination with two nucleoside reverse transcriptase inhibitors (NRTIs).<sup>12</sup>

Since the advent of anti-retroviral therapy in 1987 (Table 5-1), the efficiency of HAART treatment continues to remain robust, which is also reflected in the current UNAIDS epidemic report.<sup>23</sup> According to the report, in 2009 there was an estimated 2.6 million people who were newly infected with the virus, compared to the estimated 3.2 million people infected in 1997 (the year in which annual infections peaked). Additionally, the number of annual AIDS-related deaths is steadily decreasing, from the peak of 2.1 million people in 2004 to an estimated 1.8 million in 2009. The success of HAART is further demonstrated by renowned basketball player Magic Johnson, who was diagnosed with the virus in 1991 and after treatment with HAART has been able to suppress the occurrence of AIDS.<sup>24</sup>

**Table 5-1.** A current and comprehensive list of FDA approved anti-AIDS drugs.<sup>1</sup>

| FDA Approval   | Brand Name | Generic Name                                  | Manufacturer                     |
|--|------------|---|----------------------------------|
| <i>Nucleosides Reverse Transcriptase Inhibitors (NRTIs)</i>      |            |   |                                  |
| 1987   | Retrovir   | zidovudine, azidothymidine, AZT, ZDV          | GlaxoSmithKline                  |
| 1991   | Videx      | didanosine, dideoxyinosine, ddI               | Bristol-Myers Squibb             |
| 1992   | Hivid      | zalcitabine, dideoxycytidine, ddC             | Roche Pharmaceuticals            |
| 1994   | Zerit      | stavudine, d4T                                | Bristol-Myers Squibb             |
| 1995   | Epivir     | lamivudine, 3TC                               | GlaxoSmithKline                  |
| 1997   | Combivir   | lamivudine + zidovudine                       | GlaxoSmithKline                  |
| 1998   | Ziagen     | abacavir sulfate, ABC                         | GlaxoSmithKline                  |
| 2000   | Trizivir   | abacavir+ lamivudine+ zidovudine              | GlaxoSmithKline                  |
| 2000   | Videx EC   | enteric coated didanosine, ddI EC             | Bristol-Myers Squibb             |
| 2001   | Viread     | tenofovir disoproxil fumarate, TDF            | Gilead Sciences                  |
| 2003   | Emtriva    | emtricitabine, FTC                            | Gilead Sciences                  |
| 2004   | Epzicom    | abacavir+ lamivudine                          | GlaxoSmithKline                  |
| 2004   | Truvada    | emtricitabine + tenofovir disoproxil fumarate | Gilead Sciences                  |
| <i>Non-Nucleosides Reverse Transcriptase Inhibitors (NNRTIs)</i> |            |   |                                  |
| 1996   | Viramune   | nevirapine, NVP                               | Boehringer Ingelheim             |
| 1997   | Rescriptor | delavirdine, DLV                              | Pfizer                           |
| 1998   | Sustiva    | efavirenz, EFV                                | Bristol-Myers Squibb             |
| 2008   | Intence    | etravirine                                    | Tibotec Therapeutics             |
| <i>Protease Inhibitors (PIs)</i>                                 |            |   |                                  |
| 1995   | Invirase   | saquinavir mesylate, SQV                      | Roche Pharmaceuticals            |
| 1996   | Norvir     | ritonavir, RTV                                | Abbott Laboratories              |
| 1996   | Crixivan   | indinavir, IDV                                | Merck                            |
| 1997   | Viracept   | nelfinavir mesylate, NFV                      | Pfizer                           |
| 1997   | Fortovase  | saquinavir (no longer marketed)               | Roche Pharmaceuticals            |
| 1999   | Agenerase  | amprenavir, APV                               | GlaxoSmithKline                  |
| 2000   | Kaletra    | lopinavir+ ritonavir, LPV/RTV                 | Abbott Laboratories              |
| 2003   | Reyataz    | atazanavir sulfate, ATV                       | Bristol-Myers Squibb             |
| 2003   | Lexiva     | fosamprenavir calcium, FOS-APV                | GlaxoSmithKline                  |
| 2005   | Aptivus    | tipranavir, TPV                               | Boehringer Ingelheim             |
| 2006   | Prezista   | darunavir                                     | Tibotec Therapeutics             |
| <i>Fusion Inhibitors</i>   |            |   |                                  |
| 2003   | Fuzeon     | Enfuvirtide, T-20                             | Roche Pharmaceuticals & Trimeris |
| <i>Entry Inhibitors</i>  |            |   |                                  |
| 2007   | Selzentry  | maraviroc                                     | Pfizer                           |
| <i>IN Inhibitors</i>   |            |   |                                  |
| 2007   | Isentress  | raltegravir                                   | Merck                            |

Despite the success of HAART in reducing plasma levels of viral RNA and increasing the CD4<sup>+</sup> cell count, HAART regimens lack the ability to completely eradicate the virus. HIV can establish viral reservoirs within latently infected and resting CD4<sup>+</sup> T cells and CD8<sup>+</sup> T cells, which are impervious to HAART treatments.<sup>25</sup> In the presence of HAART, the virus reproduces at a slower rate and in some cases suppresses the occurrence of AIDS (*vide supra*); but this requires discipline, is expensive, and can lead to multidrug resistance. Therefore, additional therapeutic approaches are warranted which can supplement HAART, such as the July 2009 addition of HIV-IN inhibitor raltegravir to the HAART regimens.<sup>22</sup>

Even though RAL was recently added to HAART treatments, the HIV-IN inhibitor stands alone under FDA approval, compared to the various approved protease and reverse transcriptase inhibitors (Table 5-1). Also, RAL resistant virus strains have emerged,<sup>22</sup> which calls for new inhibitors against the dinuclear enzyme, with a focus on the active site structure and mechanism of catalysis.

### 5.C.i HIV-1 integrase (HIV-IN) – belongs to the family of polynucleotidyl transferases

HIV-IN is an essential enzyme for viral replication, responsible for depositing the viral genome into a host cell. Integration is therefore “a point of no return” for the cell, which becomes a permanent carrier of the viral genome. Integration immediately follows the reverse transcriptase-mediated production of double-stranded viral cDNA from viral RNA. HIV-IN inserts viral cDNA into the host chromosomal DNA via two separate mechanisms (Figures 5-3 and 5-4):<sup>26,27</sup>

- 1) **3'-processing** (3'-P) occurs in the cytoplasm where a dimer of HIV-IN assembles onto double stranded viral cDNA to form a pre-integration complex (PIC) with other viral and cellular proteins. During this process, the  $Mg^{2+}$  coordinated water in the HIV-IN active site acts as a nucleophile to generate reactive CpA 3'-hydroxyl ends (cytosine–adenosine overhangs) by specifically cleaving two terminal nucleotides (GT) from the viral cDNA (Figures 5-3 and 5-4).<sup>27</sup>
- 2) **Strand transfer** (ST) proceeds the 3' recession of viral cDNA, and begins with a conformational change of the PIC and a multimerization of HIV-IN to a tetramer, before the entire complex is translocated to the nucleus. Within the nucleus, HIV-IN uses the 3'-hydroxyl ends of the viral cDNA to non-specifically activate and attack a phosphodiester bond of host DNA via a  $S_N2$ -like nucleophilic mechanism (Figures 5-3 and 5-4).<sup>27</sup>

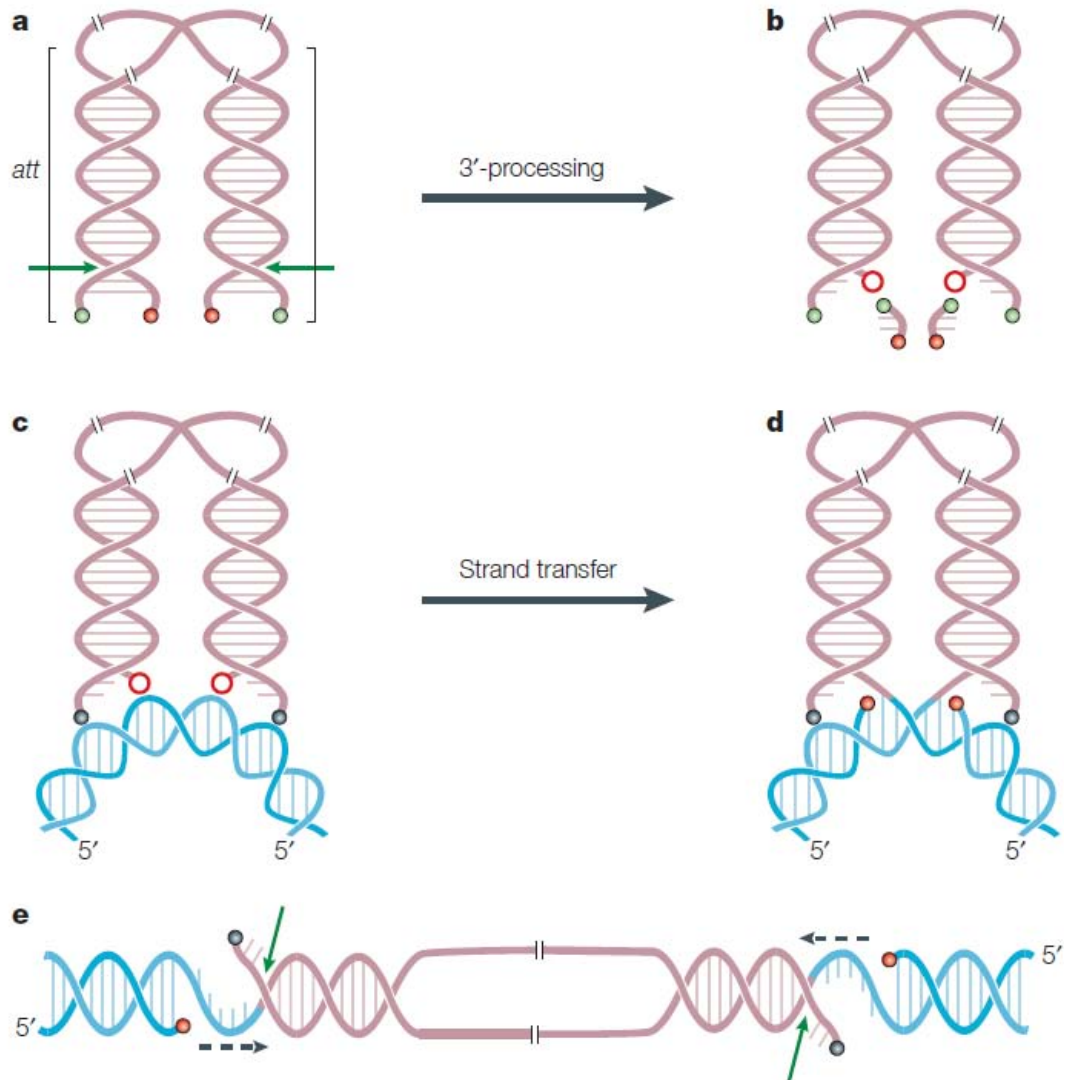


**Figure 5-3. Integrase catalytic reactions: 3'-processing and Strand transfer.** **a, b)** 3'-processing of conserved CAGT viral DNA ends by  $Mg^{2+}$  bound  $H_2O$  (green arrows) mediated endonucleolytic cleavage. Open circles represent recessed 3'-CpA-OH ends. **c, d)** Strand transfer of nicked, reactive 3'-OH ends of viral DNA into a host-cell chromosome. **e)** Gap filling of integrated viral DNA by cellular repair enzymes. Adapted from reference.<sup>12</sup>

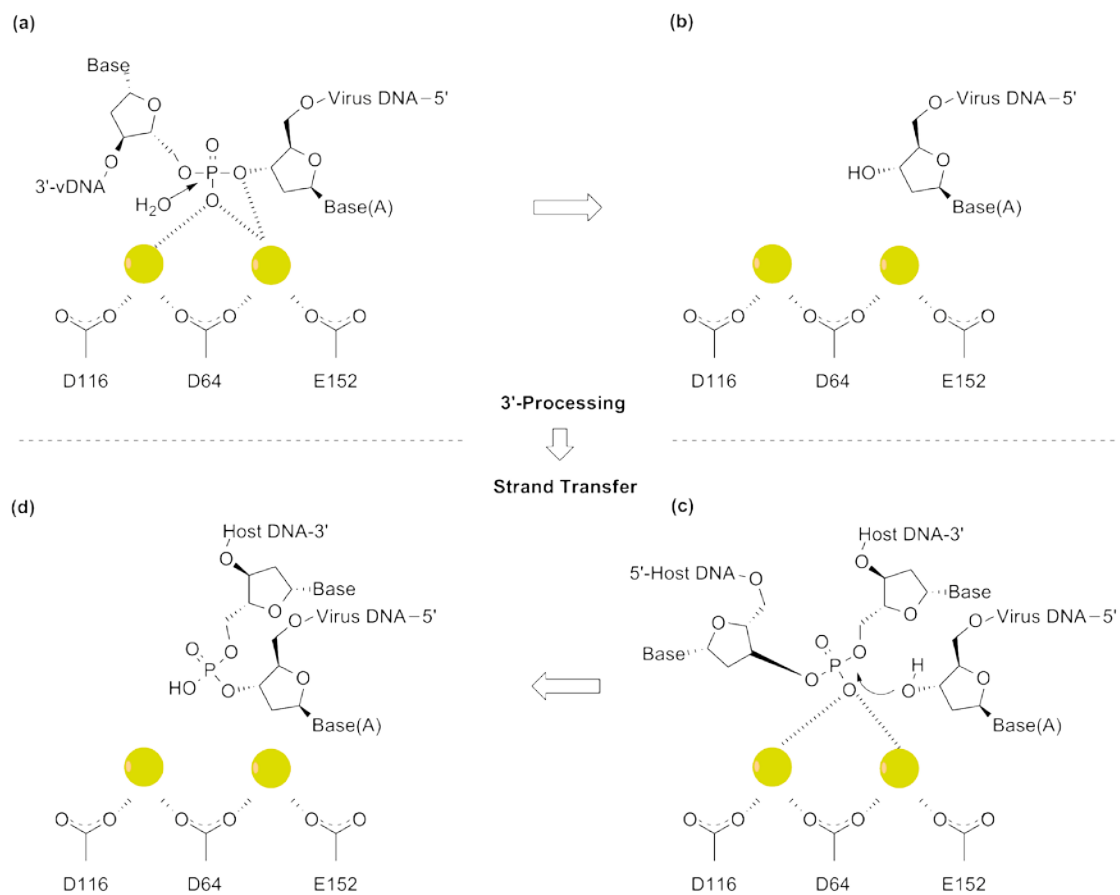


**Figure 5-4. The two-metal dependent catalytic mechanism.** Schematic representation of catalytic triad (DDE) involved in integration reactions. **a, b**) 3'-processing of viral DNA by attack of  $\text{Mg}^{2+}$  (yellow spheres) coordinated  $\text{H}_2\text{O}$  on phosphodiester bond. **c, d**) Strand transfer of viral DNA by nucleophilic attack of 3'-OH of viral DNA on phosphodiester bond of host DNA. Adapted from reference.<sup>28</sup>



### 5.C.ii Structural and Functional Domains of HIV-IN

HIV-IN is a 32 kDa protein encoded at the 3'-end of the HIV *pol* gene, which also encodes for protease and reverse transcriptase (Figure 5-5).<sup>29</sup> HIV-IN is a single polypeptide, multi-domain protein comprised of three structurally and functionally distinct domains (Figure 5-5) – the amino-terminal domain (NTD), the catalytic core domain (CCD) and the carboxy-terminal domain (CTD); all of which are involved in binding both viral and cellular DNA. The catalytic core domain is primarily responsible for the aforementioned endonuclease catalysis, in conjunction with the N- and C-terminal domains.<sup>29,30</sup>

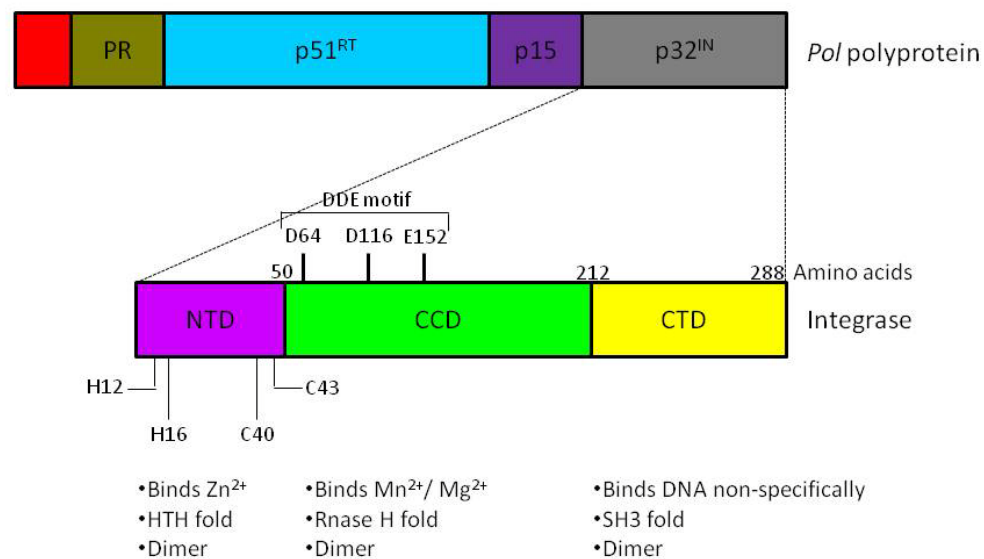


**Figure 5-5.** The various domains of HIV-IN with structural features highlighted in bullet points below each domain. Adapted from reference.<sup>12</sup>

- a. N-terminal domain (NTD): The N-terminal domain of HIV-IN is a helical structure comprised of residues 1-49 which contains a zinc finger like structural motif (Figure 5-6). This domain contains a structural zinc site coordinated by two histidine residues (His12, His16) and two cysteine residues (Cys40, Cys43), that

are highly conserved among integrases of all retroviruses. The HHCC structural zinc site is important for the oligomerization of IN. Even though this site resembles that of a zinc finger, the HHCC region differs from that of the prototypic zinc finger in the amino acid spacing, and hence three-dimensional arrangement of the four coordinating ligands. The NTD is important in 3'-processing and strand transfer, even though its exact function is not known.<sup>29</sup>

- b. Catalytic core domain (CCD): The catalytic core domain is comprised of residues 50-212 and contains the enzyme active site which is responsible for catalysis. Structurally, the CCD is comprised of five  $\beta$  sheets and six  $\alpha$  helices (Figure 5-6) and contains a catalytic triad motif of aspartic and glutamic acid - (D64, D116 and E152) commonly found in polynucleotidyl transferases.<sup>31</sup> This DDE motif coordinates divalent metal ions such as  $Mn^{2+}$  or  $Mg^{2+}$ . Even though  $Mg^{2+}$  is the preferred metal (based on cellular abundance), no conclusive arguments regarding metal preference can be made thus far. Substitution of any of the three catalytic residues in the CCD abolishes IN activity.<sup>29</sup>
- c. C-terminal domain: The C-terminal domain, comprised of residues 213 – 288, is the least conserved of the three domains. The CTD has an extended helical chain attached to a  $\beta$  barrel, formed from five strands that adopt a SH3-like fold (Figure 5-6). The CTD is known to bind donor DNA nonspecifically, and is also involved in multimerization of HIV-IN. Deletion of this domain abolishes 3'-processing and strand transfer activities.<sup>29,30</sup>

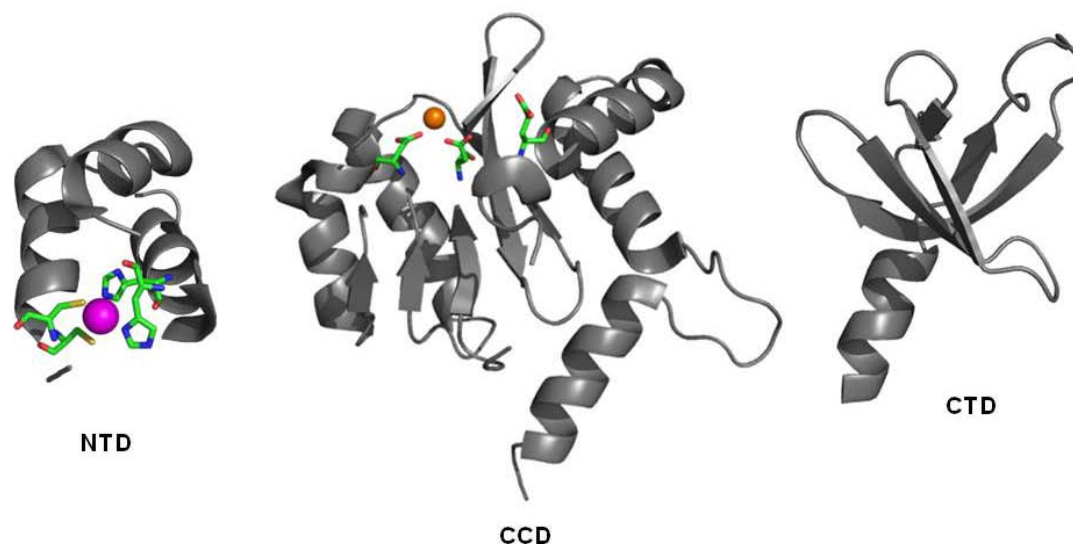


**Figure 5-6. The three domains of HIV-IN.** Shown above from left to right are the N-terminal domain (NTD) in ribbon representation, HHCC site in sticks and the  $Zn^{2+}$  ion as a magenta sphere, PDB code: 1K6Y;<sup>32</sup> Catalytic core domain (CCD) in ribbon representation with the catalytic triad DDE shown in sticks and one of two  $Mg^{2+}$  ions as an orange sphere, PDB code: 1QS4;<sup>33</sup> C-terminal domain (CTD) in ribbon representation highlighting the  $\beta$  barrel SH3 fold, PDB code: 1EX4.<sup>34</sup> (carbon = green, nitrogen = blue, oxygen = red, sulfur = yellow)

The three domains of HIV-IN (above) have been crystallized individually (Figure 5-6) and in combinations of two domains. All three domains form homo-dimers in solution.<sup>29,32-34</sup> However, the insolubility of the protein has made crystallization of full length HIV-IN very difficult. The lack of a crystal structure of the full enzyme can account for the twenty year gap between discovering the first FDA approved HIV-IN inhibitor and the first anti-retroviral drug (Table 5-1). Nevertheless, a combination of X-ray and NMR studies combined with computational methods has led incredible insight into the active site of this protein.<sup>35-37</sup> Moreover, the 2010 breakthrough of the crystal structure of integrase of the prototype foamy virus (PFV) in complex with cognate DNA has deemed extremely significant towards structure-based drug design of HIV-IN.<sup>38</sup> The structure of this complex was not only obtained with RAL (Figure 5-

7), but also with second generation HIV-IN inhibitor elvitegravir as discussed in the following section.

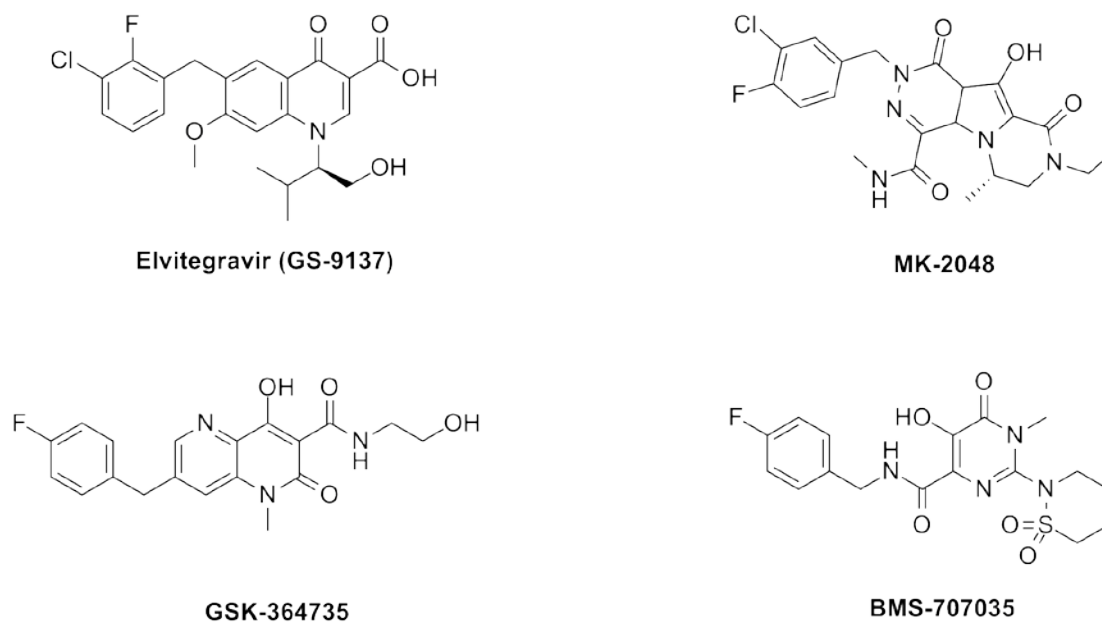
#### 5.D HIV-IN inhibitors: the historical synopsis

Several inhibitors of HIV-IN have been identified through traditional biochemical assays and pharmacokinetic profiles.<sup>1,39-41</sup> The discovery of raltegravir itself was preceded by more than a decade of integrase inhibitor research (Table 5-2). Some of the early work in discovering HIV-IN inhibitors began in 1992 by Cushman and Sherman, who tested various aurointricarboxylic acid (ATA) derivatives against HIV-IN.<sup>42</sup> Their interest in these compounds stemmed from the ability of ATAs to prevent cytopathic effects of HIV-1 in cell culture and inhibit other enzymes that processed nucleic acids.<sup>42</sup> The failure of ATA derivatives as potent HIV-IN inhibitors was followed by the success of hydroxylated natural products including dihydroxynaphthoquinones (DHNQ) and caffeic acid phenethyl esters (CAPE). CAPE was also the first natural product to show selectivity for the strand transfer step of the integration reaction over 3'-processing.<sup>21</sup>

Subsequently, coumarin derivatives were developed (Table 5-2), and a common motif observed in these early generation IN inhibitors was that of poly-hydroxylated metal chelating groups. The presence of metal chelating groups in HIV-IN inhibitors continued into the 21<sup>st</sup> century, which marked the emergence of the most important class of HIV-IN inhibitors, the diketo acids (DKAs). DKAs were the first strand transfer selective inhibitors to be developed with high specificity for HIV-IN, and showed competitive binding with target DNA substrate to the HIV-IN-viral DNA complex.<sup>1</sup> The DKA class of compounds are therefore referred to as strand transfer inhibitors (STi). Historically, the first reported DKAs were 5-CITEP developed by Shionogi & Co. Ltd<sup>33</sup> and the L-731,988 series developed by Merck<sup>8</sup>; both of which

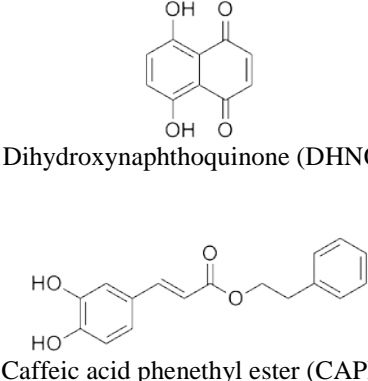
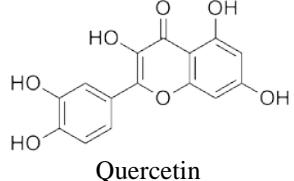
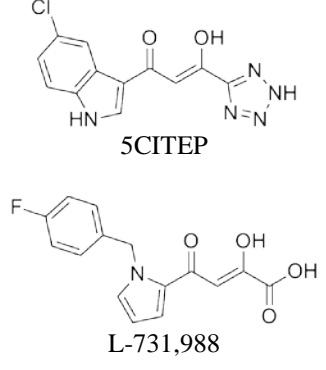
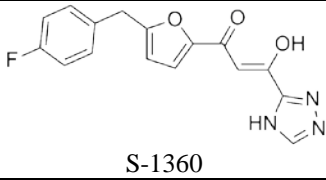
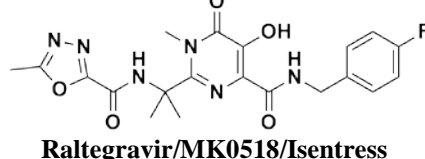
delivered blockbuster results. The L-731,988 series eventually led to the discovery of raltegravir and 5-CITEP made history as the only inhibitor to date to be crystallized with the CCD of HIV-IN. 5-CITEP was further developed into more potent leads and one such inhibitor, S-1360 became the first inhibitor to enter clinical trials. Despite the potency of S-1360 ( $IC_{50} = 20$  nM), it failed efficacy studies due to reduction in humans of the carbon linked to the triazole group and was later abandoned.<sup>21</sup>

Raltegravir on the other hand, was FDA approved in October 2007 and HAART supplemented in July 2009.<sup>22</sup> However, soon after raltegravir was approved, several mutations conferring RAL-resistant strains emerged. followed by the birth of several “me-too” inhibitors (Figure 5-7),<sup>21</sup> and the need for a new generation of IN inhibitors.



**Figure 5-7.** Structures of second generation and “me-too” HIV-IN inhibitors.

**Table 5-2.** Evolution of DKAs as metal binding groups towards the discovery of Raltegravir

| Year      | Structure  | History   | Ref    |
|-----------|--|---|--------|
| 1993      |  <p>Dihydroxynaphthoquinone (DHNQ)</p> <p>Caffeic acid phenethyl ester (CAPE)</p> | <p>Yves Pommier and co-workers tested various topoisomerase inhibitors to discover DHNQ and CAPE as IN inhibitors. Due to the presence of metal chelating groups on these compounds, they hypothesized that the compounds were chelating the HHCC coordinated Zn<sup>2+</sup> ion present in the NTD</p> <p>CAPE was the first natural product and inhibitor that showed selectivity for ST over 3'-P</p> | 43,44  |
| 1997      |  <p>Quercetin</p>  | <p>Coumarin derivatives were identified, thereby maintaining the requirement of a catechol moiety</p>   | 45     |
| 1999-2000 |  <p>5CITEP</p> <p>L-731,988</p>   | <p>Diketo acids (DKAs) were the first IN inhibitors reported to show selectivity for ST over 3'-P</p> <p>The two first DKA molecules reported are 5CITEP from Shionogi &amp; Co. Ltd and the L-731,988 series from Merck and Co.</p> <p>5CITEP has been the only DKA co-crystallized with the CCD of HIV-IN</p>   | 1,8,33 |
| 2003      |  <p>S-1360</p>  | <p>S-1360 was the first HIV-IN inhibitor to enter clinical trials and was later abandoned due to failed efficacy studies</p>  | 46     |
| 2007      |  <p>Raltegravir/MK0518/Isentress</p>  | <p>The first FDA approved HIV-IN inhibitor "RALTEGRAVIR" was discovered by Merck</p>  | 5      |

**5.E PFV-IN active site with cognate DNA and bound HIV-IN inhibitors**

The crystal structure of the PFV-IN active site has confirmed the expected two-metal binding mode of retroviral integrases and uncovered the positions of the metal ions within the assembled active site.<sup>38</sup> More importantly, the crystal structure obtained with HIV-IN inhibitors RAL and elvitegravir has confirmed the metal-dependent inhibition of these inhibitors through chelation of the metal co-factors. As expected, both inhibitors show binding of active site  $Mg^{2+}$  ions through a bis-bidentate mode of chelation as shown in Figure 5-8 and Figure 5-9 below.

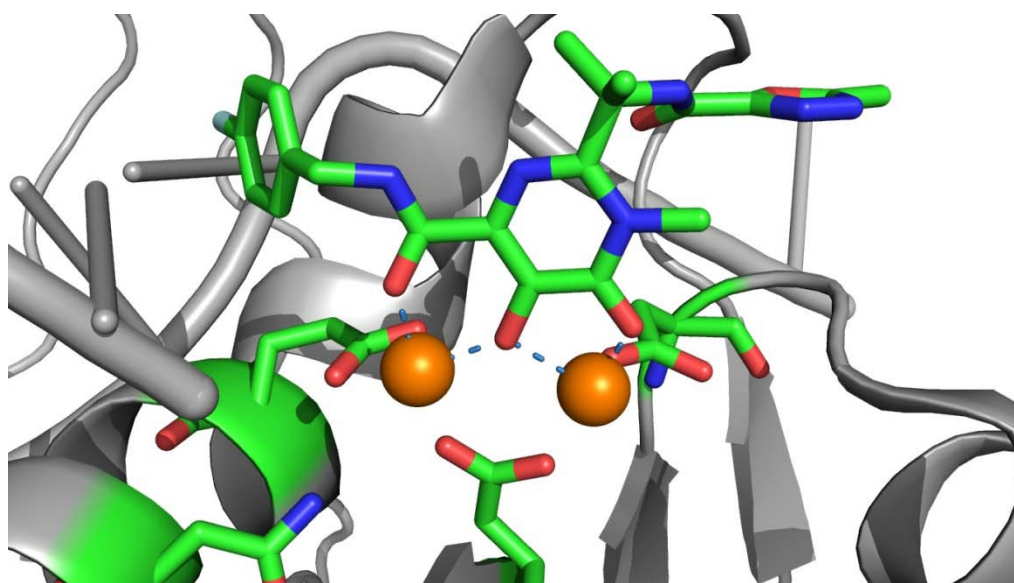


**Figure 5-8. Crystal structure of PFV-IN (PDB: 3OYA) with RAL.** The protein is represented by a gray ribbon, RAL and the active site coordinating residues are shown as sticks and are color-coded (carbon = green, nitrogen = blue, oxygen = red, fluorine = cyan) and the  $Mg^{2+}$  ions are represented by orange spheres.



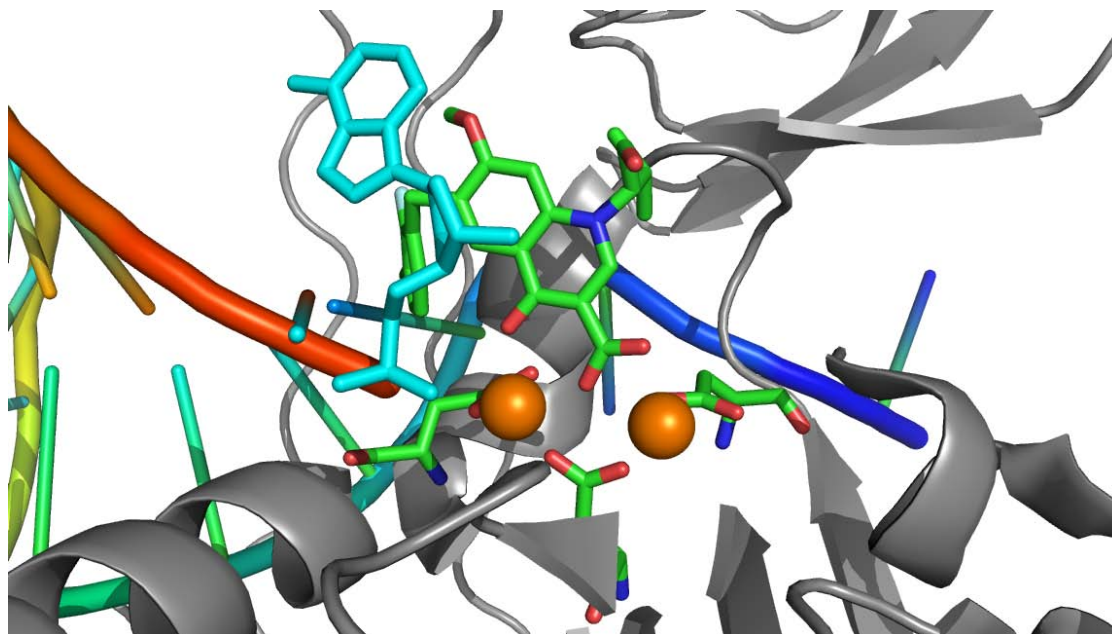


**Figure 5-9. Crystal structure of PFV-IN (PDB: 3L2U) with GS-3197 and viral DNA.** The protein is represented by a gray ribbon, GS-3197 and the active site coordinating residues are shown as sticks and color-coded (carbon = green, nitrogen = blue, oxygen = red, fluorine = cyan) and the  $Mg^{2+}$  ions are represented by orange spheres. The viral DNA is shown in rainbow colors and the invariant base A17 of the 3'-OH end of viral DNA is shown as sticks in cyan.

Both inhibitors bind via their planar (O,O,O) donor ligand set and the primary difference in metal-binding mode between these inhibitors lies in the different chelate rings (Figure 5-10) to the  $Mg^{2+}$  ions. RAL forms 6- and 5-membered chelate rings to the  $Mg^{2+}$  ions in the active site, whereas elvitegravir forms 6- and 4-membered chelate rings to the  $Mg^{2+}$  ions in the active site. Despite the differences in binding mode, both display good potencies (RAL,  $IC_{50} = 40$  nM, elvitegravir,  $IC_{50} = 7$  nM) and elvitegravir is now in Phase II clinical trials.

On the basis of the crystal structures, the two strand transfer inhibitors (STi) of HIV-IN also involve an induced fit mechanism upon metal binding. After their chelating oxygen residues orient towards the metal co-factors for coordination, the halogenated backbone residue places itself tightly in a pocket created by the

displacement of the invariant 3'-adenine residue (A17, Figure 5-9). The displacement of this nucleotide impairs the assembly of the intasome (minimal functional complex involving viral DNA and HIV-IN)<sup>38</sup> and compromises HIV-IN activity.

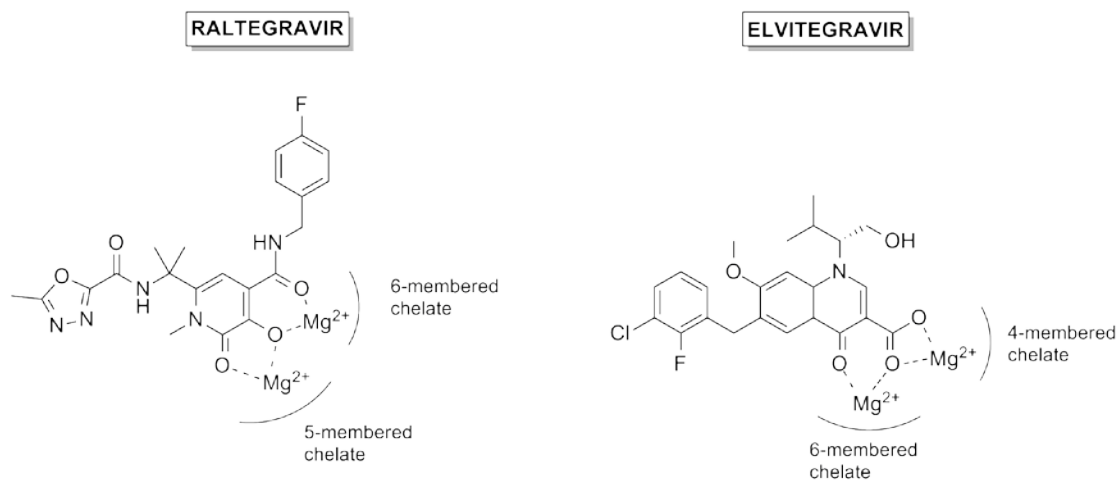
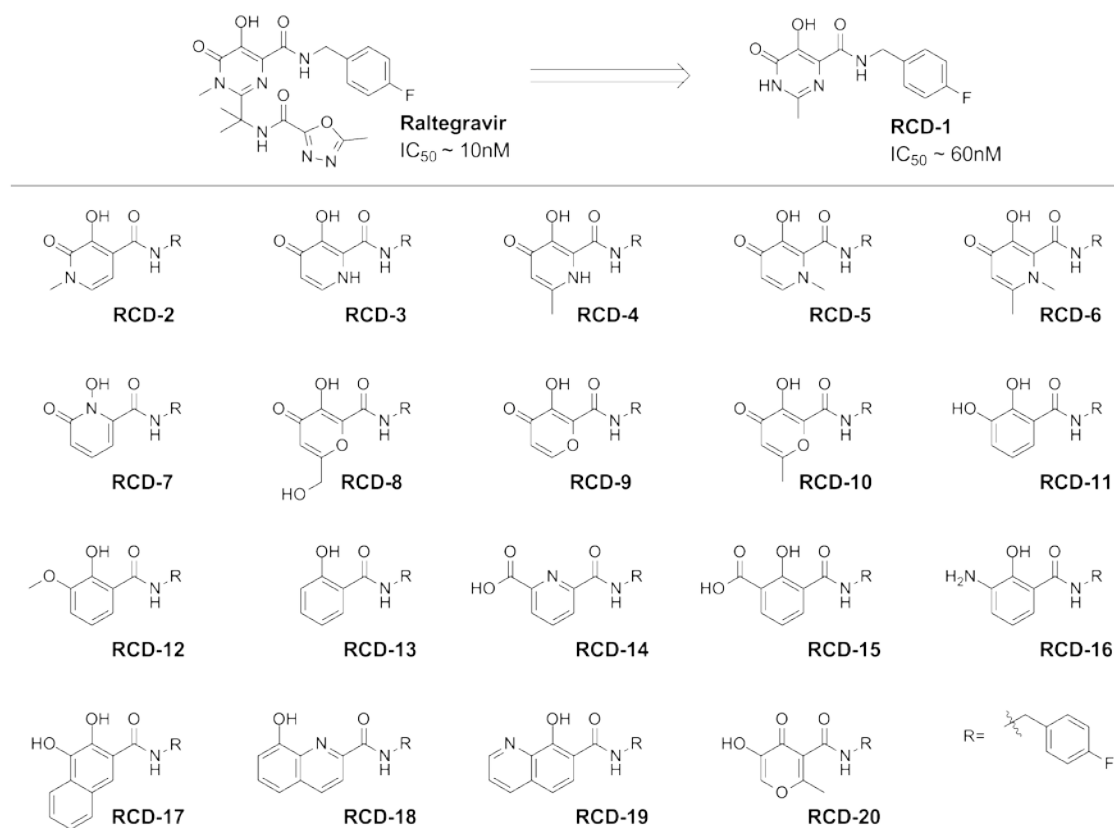


**Figure 5-10.** A representation of the metal-binding mode of Raltegravir (left) and Elvitegravir (right) in the active site of HIV-IN/PFV-IN.

## 5.F Synthesis of HIV-IN inhibitors

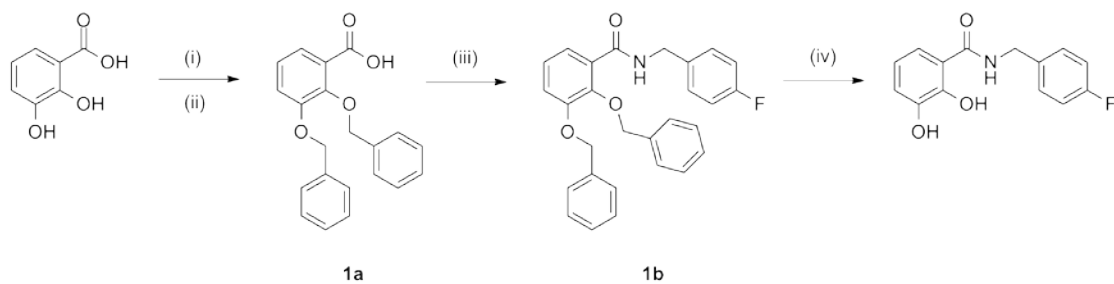
Chapters 2 and 3 discussed the design and synthesis of various inhibitors and metal-binding fragments against mononuclear  $Zn^{2+}$  endopeptidases that act via a metal-chelating inhibition mechanism. Some of these previously synthesized inhibitors bear a striking resemblance to RAL (Figure 5-1) and were therefore tested against HIV-IN. In order to expand the study to specifically target the dinuclear active site of HIV-IN, several inhibitors were synthesized with the same *p*-fluorobenzylamine backbone of RAL appended to different metal binding groups (MBGs). The various MBG containing inhibitors for this initial study are displayed in Figure 5-11. Since they are isostructural to RAL, we labeled these initial inhibitors as Raltegravir Chelator Derivatives (RCDs). As shown in Figure 5-11, all the compounds have the same backbone, but differ in the MBG of each compound.

As outlined in Schemes 5-1 to 5-4, the inhibitors were generally prepared by benzyl protection of the hydroxyl and carboxylic acid group of each MBG, hydrolysis of the benzyl-protected carboxylic acids and conversion to activated esters. The esters were then coupled to a *p*-fluorobenzylamine backbone. Removal of the benzyl protecting group using strongly acidic conditions yielded the compounds shown in Figure 5-11. The inhibitors in Figure 5-11 are relatively facile to prepare and allow for preparation on multigram scales. RCD-1 was synthesized as a positive control against which the potency of the other inhibitors could be compared. RCD-1 is easier to prepare than RAL, and it has been previously studied in the literature with a reported  $IC_{50}$  value of 60 nM against HIV-IN strand transfer.<sup>6</sup> Compounds RCD-5, -6, -7, -9, -9S, -9S2, -10 were prepared as previously reported.<sup>3,4</sup>

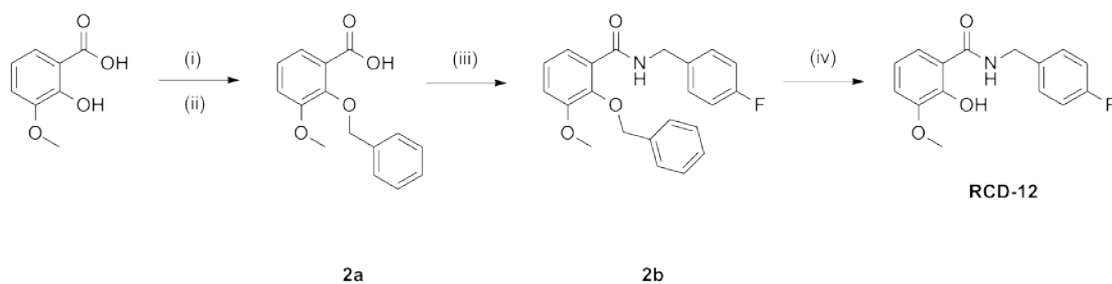


**Figure 5-11. Raltegravir-Chelator Derivatives (RCD).** Derivatives of RAL, based off the simplified scaffold RCD-1. Each RCD employs a different MBG to bind the active site metal ions.

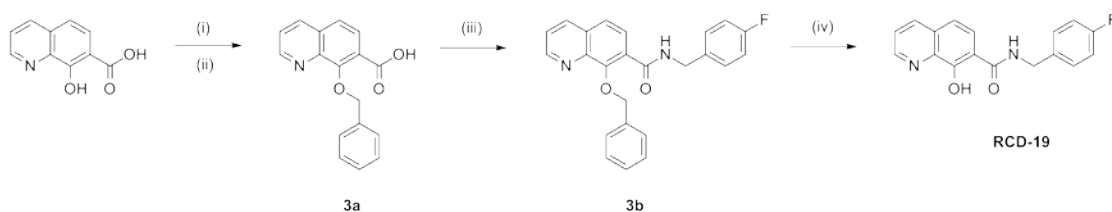
**Scheme 5-1. Synthesis of RCD-11<sup>a</sup>**



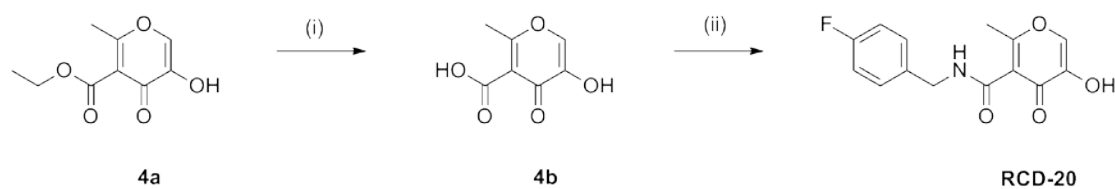
<sup>a</sup>Reagents and conditions: (i) benzyl chloride, K<sub>2</sub>CO<sub>3</sub>, DMF, 95 °C, N<sub>2</sub>, 96%. (ii) 6 M NaOH, MeOH, room temp, 100%. (iii) *p*-fluorobenzylamine, EDC iodide, HOBt, CH<sub>2</sub>Cl<sub>2</sub>, N<sub>2</sub>, 58%. (iv) 1:1 HCl: HOAc, room temp, 85%.

**Scheme 5-2. Synthesis of RCD-12<sup>b</sup>**

<sup>b</sup>Reagents and conditions: (i) benzyl chloride,  $K_2CO_3$ , DMF,  $95^\circ C$ ,  $N_2$ , 74%. (ii) 6 M NaOH, MeOH, room temp, 100%. (iii) *p*-fluorobenzylamine, EDC iodide, HOBT,  $CH_2Cl_2$ ,  $N_2$ , 48%. (iv) 1:1 HCl: HOAc, room temp, 72%.

**Scheme 5-3. Synthesis of RCD-19<sup>c</sup>**

<sup>c</sup>Reagents and conditions: (i) benzyl chloride,  $K_2CO_3$ , DMF,  $95^\circ C$ ,  $N_2$ , 60%. (ii) 6 M NaOH, MeOH, room temp, 100%. (iii) *p*-fluorobenzylamine, EDC iodide, HOBT,  $CH_2Cl_2$ ,  $N_2$ , 31%. (iv) 1:1 HCl: HOAc, room temp, 85%.

**Scheme 5-4. Synthesis of RCD-20<sup>d</sup>**

<sup>d</sup>Reagents and conditions: (i) 6 M NaOH,  $H_2O$ , room temp, 70%. (ii) *p*-fluorobenzylamine, EDC iodide, HOBT,  $CH_2Cl_2$ ,  $N_2$ , 29%.

### 5.G *In vitro* potency of HIV-IN inhibitors

As discussed above, HIV-IN performs two sequential functions for the integration of viral DNA into the host genome. In order to test the potency of our compounds against both functions of HIV-IN, *in vitro* assays were performed in collaboration with the laboratory of Dr. Yves Pommier at the National Institutes of Health. Briefly, the assay involves immobilization of viral DNA followed by the addition of HIV integrase, and a radioactive or fluorescent labeled oligonucleotide for strand transfer. The results of each assay with select RCD compounds (both 3'-P and ST) are listed in Table 5-3.

The RCD compounds belong to the DKA class of compounds, which were the first ST selective inhibitors to be developed. Therefore, it is not surprising that these compounds display very poor inhibition against the 3'-P function. In terms of the ST reaction, the  $IC_{50}$  value obtained for RCD-1 (Table 5-3) is similar to that reported in the literature (60 nM).<sup>6</sup> RCD-1 contains a hydroxypyrimidinone MBG and an (O,O,O) donor atom set. RCD-7 is a very potent MMP inhibitor, but only shows modest inhibition against HIV-IN ST. RCD-7 contains a 1-hydroxypyridinone MBG, also with a (O,O,O) donor atom set.

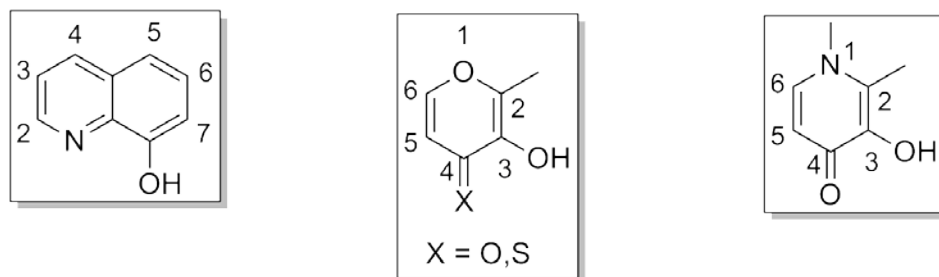


**Figure 5-12.** Numbering scheme of the hydroxyquinoline ring (left) and hydroxypyrone(thione) (center) and hydroxypyridinone (right).

RCD-9 and RCD-10 which contain a hydroxypyrrone MBG are the most potent against HIV-IN ST with  $IC_{50}$  values in the sub-micromolar range. RCD-9 and -10 only differ by the presence of an additional methyl substituent on C-6 of the pyrrone ring (Figure 5-12) of RCD-10. Hydroxypyrrone RCD-20 which is a structural isomer of RCD-10, has the backbone substituent attached to C-5 instead of C-2 (present in RCD-9 and RCD-10). Interestingly, RCD-20 is also 100-fold less potent than RCD-10. Despite identical MBGs and therefore chelating groups, changing the position of the amide backbone from C-2 to C-6 on the pyrrone MBG, completely abrogates potency against ST. Additionally, conversion of RCD-9 and RCD-10 to their sulfur hydroxypyrrone analogues diminishes the potency by a factor of 10, as observed for RCD-9S and RCD-9S2. This may be due to the fact that  $Mg^{2+}$  is a hard metal cation and prefers hard oxygen donor ligands over softer sulfur ligands.

RCD-5 and RCD-6, which contain hydroxypyridinone ZBGs are directly derived from RCD-9 and RCD-10, respectively (Experimental Section). The results obtained in Table 5-3 for RCD-5 and RCD-6 show that the conversion of the hydroxypyrrone MBG to the corresponding hydroxypyridinone MBG results in a complete loss of potency. The hydroxypyridinone MBGs of RCD-5 and RCD-6 also have an extra methyl substituent on C-1 of the hydroxypyridinone ring (Figure 5-12). The results observed thus far show that minor tweaking of the MBG within the hydroxypyrrone series of RCD derivatives leads to extreme differences in ST inhibition profiles.

Unlike the hydroxypyrrones, RCD-11, RCD-12 and RCD-13 contain an aromatic MBG with differences in the substituents on the C-3 position of the aromatic

ring. RCD-11 contains a hydroxyl group on C-3 making the MBG a catechol; RCD-12 contains a methoxy group on C-3, and RCD-13 lacks substitution on the C-3 position. Of the three compounds, RCD-11 is the only one with an (O,O,O) chelating donor atom ligand set which is observed in most ST inhibitors, and is also the only compound of the three that shows modest potency against HIV-IN ST. The third donor atom in RCD-12 is methyl protected, and RCD-13 lacks a third donor atom, both resulting in a loss of inhibition. This set of RCD compounds therefore highlights the importance of a tris-donor chelating MBG.

RCD-18 and RCD-19 contain identical hydroxyquinoline MBGs and are structural isomers of each other, yet they display very different inhibition profiles. RCD-18 has the amide backbone positioned on C-2 of the quinoline ring whereas RCD-19 has the backbone amide attached at the C-7 position of the ring (Figure 5-12). Yet, RCD-19 displays decent potency against HIV-IN ST whereas the inhibition imparted by RCD-18 is negligible. Similar to structural isomers, RCD-10 and RCD-20, the position of the amide backbone has a profound effect on the potency of the RCD compounds. This is not surprising since the amide oxygen is the third donor ligand of these compounds and must be appropriately positioned for effective chelation of both  $Mg^{2+}$  ions in the active site.



**Table 5-3.** Screening results of select RCD compounds from Figure 8 against both the 3'-processing (3'-P) reaction and the strand transfer (ST) reaction of HIV-IN.

| Compound Name | Structure | IC <sub>50</sub> (μM) 3'-P | IC <sub>50</sub> (μM) ST |
|---------------|-----------|----------------------------|--------------------------|
| RCD-1         |           | 112, 121                   | 1.0 ± 0.3                |
| RCD-5         |           | >111                       | >111                     |
| RCD-6         |           | >111                       | >111                     |
| RCD-7         |           | >111                       | 19.7 ± 1.6               |
| RCD-9         |           | 138, 123                   | 0.96 ± 0.27              |
| RCD-9S        |           | >111                       | 11.5 ± 0.86              |
| RCD-9S2       |           | 64 ± 6                     | 7.3 ± 0.6                |
| RCD-10        |           | 59.5 ± 1.4                 | 0.55 ± 0.1               |
| RCD-11        |           | >111                       | 39.4 ± 4.0               |
| RCD-12        |           | >111                       | >111                     |
| RCD-13        |           | >111                       | >111                     |
| RCD-18        |           | >111                       | >111                     |
| RCD-19        |           | 142, 156                   | 14.5 ± 2.2               |
| RCD-20        |           | >111                       | 56.0 ± 7                 |

## 5.H Discussion

Despite the success of RAL and some second generation inhibitors (including elvitegravir and GSK-364735, Figure 5-10),<sup>21</sup> there have been no studies to date that directly compare the metal binding moiety of different HIV-IN inhibitors. Even though several RAL-resistant strains have surfaced, these resistant mutants do not alter the metal binding motif of the wild type enzyme; and substitution of any of the metal-coordinating residues has been shown to abolish catalytic activity.<sup>22</sup> This stresses the importance of the  $Mg^{2+}$  ions and highlights their function in holding various components of the PIC in place, including viral DNA, HIV-IN and donor DNA (as seen in Figure 5-4), for endonucleolytic catalysis. The activity of HIV-IN can therefore be compromised by targeting the  $Mg^{2+}$  ions with strong MBGs.

In order to focus our study on the effect of varying the MBGs, we synthesized RAL derivatives from different MBGs that lack the oxadiazole backbone, but retain the *para*-fluorophenyl backbone (Figure 5-11). We chose to retain the *para*-fluorophenyl backbone for synthetic feasibility towards a small MBG-directed library (Figure 5-11). As seen in Figure 5-11, RCD-1 is a 'trimmed' version of raltegravir that was synthesized as a control, and the remaining compounds are derivatives of RCD-1 that change out the MBG. The inhibitors in this study are displayed in Figure 5-11 and the results of the in vitro 3'-processing and ST assays are listed in Table 5-3.

The various MBGs utilized in this study range from a hydroxypyrimidinone (RCD-1) to hydroxypyridinones (RCD-5, -6, -7), hydroxypyrones (RCD-9, -10, -20), hydroxypyrothiones (RCD-9S, -9S2), catechol (RCD-11), hydroxyquinolines (RCD-18, -19) and salicylic acids (RCD-12, -13). Of the RCD compounds presented in this

study, RCD-1, -5, -6, -7, -9, -10, -20 contain the same DKA (O,O,O) binding moiety that is present in RAL. RCD-9S and RCD-9S2 contain a sulfur analogue of this binding moiety with a (O,O,S) and (O,S,S) chelating motif respectively. RCD-11 contains a (O,O,O) donor atom set but is different from that present in the DKAs as it contains two hydroxyl groups instead of one carbonyl and one hydroxyl group. RCD-18 and RCD-19 contain a (O,N,O) chelating motif and RCD-12 and RCD-13 only contain a (O,O) binding moiety.

As discussed earlier in both RAL and elvitegravir crystal complexes with PFV-IN, the MBGs first orient themselves to chelate the  $Mg^{2+}$  ions in the active site. This metal binding is then pursued by the insertion of the fluorobackbone in a vicinal protein pocket. The *para*-fluorophenyl backbone remains invariant amongst all the RCD compounds studied here and hence the difference in potency observed amongst each RCD compound can be attributed to the MBG. The difference in the various metal-ligand interactions imparted by these RCD derivatives is indirectly reflected in the  $IC_{50}$  values in Table 5-3 and described in the previous section.

Hydroxypyrones RCD-9 and RCD-10 have ST  $IC_{50}$  values of 0.96  $\mu M$  and 0.55  $\mu M$  respectively. These values are comparable to the  $IC_{50}$  value obtained for RCD-1 (1.0  $\mu M$ ). RCD-1 is simply a “trimmed” version of RAL, and the loss in potency compared to RAL can be accounted for by the lack of the oxadiazole moiety which interacts with residue Tyr143 via a  $\pi$ - $\pi$  stacking interaction.<sup>22,38,47</sup> The MBG of RCD-1 otherwise orients itself identical to RAL in the HIV-IN active site which was confirmed by computational docking studies (Figure 5-13). The (O,O,O) donor atoms

of RCD-1 bind to both  $Mg^{2+}$  ions forming a 6-membered ring chelate adjacent to a 5-membered ring chelate as observed in RAL (Figure 5-10 and 5-13 a,b).

The same orientation of the MBG and backbone substituent was observed in both RCD-9 and RCD-10, which explains the similar inhibition profiles imparted by these derivatives compared to RCD-1. Conversely, the same positioning of the hydroxypyridinone analogues RCD-5 and RCD-6, of RCD-9 and RCD-10 respectively, was also observed. RCD-5 and RCD-6 have ST  $IC_{50}$  values  $> 100 \mu M$  and hence display negligible potency. This loss in potency may be attributed to several different factors (including differences in  $pK_a$  of the hydroxyl group compared to hydroxypyrones), but one factor determined via computational studies is the steric clash of the N-methyl substituent on the MBG ring with residue Pro214 in the active site of HIV-IN (Figure 5-13c). This residue is significant in that it has been shown to be one of the few conserved residues in the IN active site loop that is directly involved in separating the viral DNA strands.<sup>38</sup> In fact, both RAL and elvitegravir make intimate Van der Waals interactions with this residue.<sup>38</sup> Therefore it is not surprising that a steric hindrance with this residue would compromise the potency of RCD-5 and RCD-6. The potency of these compounds may be reversed by changing the substituent on the nitrogen of the MBG ring to interact with Pro214.

The sulfur analogues of RCD-9, RCD-9S and RCD-9S2, with donor atoms (O,S,O) and (O,S,S) respectively have compromised potencies compared to RCD-9. RCD-9S and RCD-9S2 have  $IC_{50}$  values of  $11.5 \mu M$  and  $7.3 \mu M$  respectively compared to the 10-fold more potent  $IC_{50}$  of RCD-9 ( $0.96 \mu M$ ). This result is not surprising as  $Mg^{2+}$  is a hard metal cation and prefers hard oxygen donor ligands over

softer sulfur ligands. Further, by replacing the oxygen with a sulfur atom results in a shift in orientation of the RCD-9S (not shown) and RCD-9S2 compounds (Figure 5-13f) in the active site of HIV-IN, compared to RCD-9 (Figure 5-13e). This results in a bidentate chelation to only one of the  $\text{Mg}^{2+}$  ions in the active site and a monodentate coordination to the other ion. Also, the idealized 6 and 5-membered chelate rings are completely lost with distances  $\sim 4.3\text{\AA}$  (not shown) between the sulfur of the hydroxyprothione MBG and the  $\text{Mg}^{2+}$  ion. The loss in active site  $\text{Mg}^{2+}$  ion chelation is most pronounced in RCD-18 (Figure 5-13g). Even though RCD-18 and RCD-19 are structural isomers with the same (O,N,O) donor atom set, the position of the amide backbone on C-2 of the hydroxyquinoline ring in RCD-18 instead of C-7 (RCD-19), prevents the nitrogen of the hydroxyquinoline from strongly interacting with the  $\text{Mg}^{2+}$  ions. The dashed lines shown in Figure 5-13g between the nitrogen and the  $\text{Mg}^{2+}$  ions are very weak interactions and therefore RCD-18 is mostly interacting with the ions via a monodentate coordination of the oxygen atoms of the compound. RCD-19 on the other hand displays a bidentate coordination of the metal active site with the 6- and 5-membered ring chelates but is still not as potent as RCD-9 and RCD-10. This may confirm the preference of the hard  $\text{Mg}^{2+}$  ions for the harder (O,O,O) containing ligands.

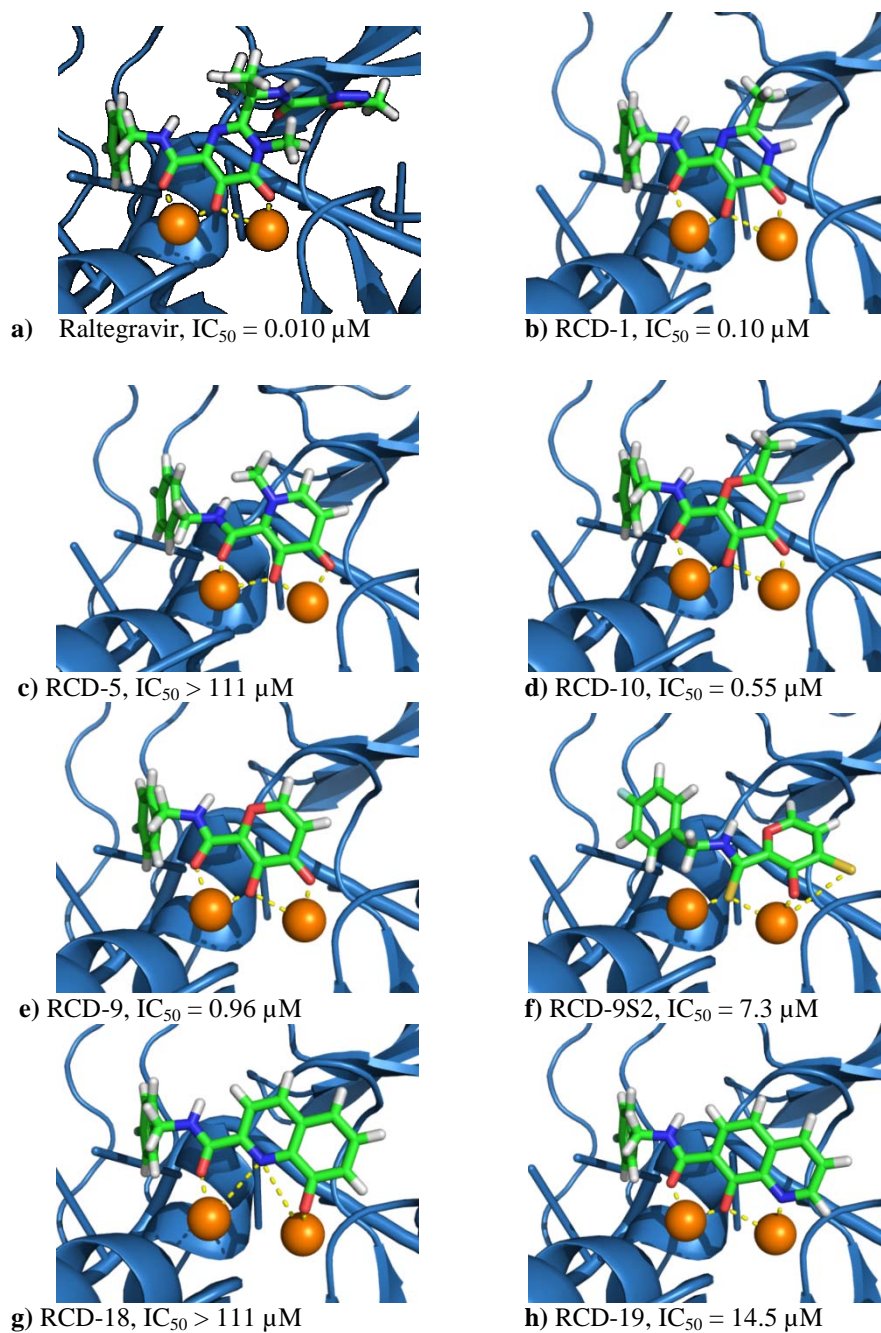


**Figure 5-13.** Docking studies of select RCD compounds in the active site of PFV-IN (PDB:3OYA). Selective RCD compounds are shown with their ST  $IC_{50}$  values.

## 5.I Conclusions

The study presented here is the first attempt to compare the effect of different MBGs on the activity of HIV-IN inhibitors. The study not only highlights the importance of a tris-donor ligand set in HIV-IN ST inhibitors, but also sheds light on the preference of the donor atoms for effective coordination of the active site  $\text{Mg}^{2+}$  ions. Overall, this study has introduced the significance that the metal binding groups (MBGs) play in inhibiting the dinuclear  $\text{Mg}^{2+}$  active site of HIV-IN and will hopefully lead to potent inhibitors that overcome drug-resistant viruses.

## 5.J Experimental

Unless otherwise noted, all chemicals were purchased from commercial suppliers and used as received. Flash silica gel chromatography was performed using Merck silica gel 40-63  $\mu\text{m}$  mesh. Inert reactions were carried out under a dinitrogen atmosphere.  $^1\text{H}/^{13}\text{C}$  NMR spectra were recorded at ambient temperature on a 300, 400 or 500 MHz Varian FT-NMR or a 500 MHz Jeol ECA NMR instrument at the Department of Chemistry and Biochemistry, University of California San Diego. Mass spectra were obtained at the Small Molecule Mass Spectrometry Facility in the Department of Chemistry and Biochemistry at the University of California, San Diego. Elemental Analysis was performed by NuMega Resonance Labs, San Diego.

***N*-(4-Fluorobenzyl)-3-hydroxy-1-methyl-4-oxo-1,4-dihydropyridine-2-carboxamide (RCD-5):** This compound was synthesized according to procedures previously reported in the lab.<sup>4</sup> 233 mg (0.64 mmol) of 3-(benzyloxy)-*N*-(4-fluorobenzyl)-1-methyl-4-oxo-1,4-dihydropyridine-2-carboxamide was acid deprotected in 10 mL of a 1:1 solution of HCl and HOAc to yield 176 mg (0.64 mmol) of the hydrochloride salt. Yield = 100%.  $^1\text{H}$  NMR (400 MHz, DMSO- $d_6$ , 25 °C):  $\delta$  = 3.85 (s,  $\text{CH}_3$ ), 4.47 (d, ,  $J$  = 5.2 Hz, 2H;  $\text{NHCH}_2$ ), 7.14 (dd,  $J$  = 8.8, 2.0 Hz, 2H; ArH), 7.22 (d,  $J$  = 6.8 Hz, 2H; ArH), 7.40 (t,  $J$  = 5.8 Hz, 2H; ArH), 8.15 (d,  $J$  = 6.4 Hz, 1H; ArH), 9.58 (t,  $J$  = 5.4 Hz, 1H;  $\text{CONHCH}_2$ ). APCI-MS(-)  $m/z$  275.02  $[\text{M}-\text{H}]^-$ . Anal. Calcd for  $\text{C}_{14}\text{H}_{13}\text{FN}_2\text{O}_3 \cdot 1.5 \text{HCl}$  : C, 50.81; H, 4.42; N, 8.46. Found: C, 50.90; H, 4.82; N, 8.40.

***N*-(4-Fluorobenzyl)-1-hydroxy-6-oxo-1,6-dihydropyridine-2-carboxamide (RCD-7):** This compound was prepared as previously reported.<sup>3</sup> 106 mg (0.45 mmol)



of 1-(benzyloxy)-*N*-(4-fluorobenzyl)-6-oxo-1,6-dihydropyridine-2-carboxamide was acid de-protected to obtain 106 mg (0.40 mmol) of clear crystalline needles. Yield = 90%. <sup>1</sup>H NMR (400 MHz, CDCl<sub>3</sub>-*d*<sub>1</sub>, 25 °C): δ = 4.65 (d, *J* = 5.2 Hz, NHCH<sub>2</sub>), 7.01 (t, *J* = 8.6 Hz, 2H; ArH), 7.08 (d, *J* = 8.8 Hz, 1H; ArH), 7.33 (dd, *J* = 8.8, 3.6 Hz, 2H; ArH), 7.48 (t, *J* = 8.0 Hz, 1H; ArH), 7.73 (d, *J* = 7.2 Hz, 1H; ArH), 10.22 (brs, 1H; CONHCH<sub>2</sub>). APCI-MS(+) *m/z* 263.04 [M-H]<sup>+</sup>. Anal. Calcd for C<sub>13</sub>H<sub>11</sub>FN<sub>2</sub>O<sub>3</sub> : C, 59.54; H, 4.23; N, 10.68. Found: C, 59.58; H, 4.54; N, 10.67.

***N*-(4-Fluorobenzyl)-3-hydroxy-4-oxo-4*H*-pyran-2-carboxamide (RCD-9):**

This compound was prepared as previously reported.<sup>3</sup> 150 mg (0.42 mmol) of 3-(benzyloxy)-*N*-(4-fluorobenzyl)-4-oxo-4*H*-pyran-2-carboxamide was acid de-protected to obtain 90 mg (0.34 mmol) of a pure white solid. Yield = 81%. <sup>1</sup>H NMR (400 MHz, CDCl<sub>3</sub>-*d*<sub>1</sub>, 25 °C): δ = 4.52 (s, 2H; NHCH<sub>2</sub>), 6.41 (d, *J* = 5.2 Hz, 1H; ArH), 6.97 (t, *J* = 8.8 Hz, 2H; ArH), 7.26 (dd, *J* = 8.8, 3.6 Hz, 2H; ArH), 7.76 (d, *J* = 5.6 Hz, 1H; ArH), 8.00 (brs, 1H; CONHCH<sub>2</sub>). APCI-MS(-) *m/z* 262.12 [M-H]<sup>-</sup>. Anal. Calcd for C<sub>13</sub>H<sub>10</sub>FNO<sub>4</sub> : C, 59.32; H, 3.83; N, 5.32. Found: C, 59.06; H, 4.20; N, 5.37.

***N*-(4-Fluorobenzyl)-3-hydroxy-4-thioxo-4*H*-pyran-2-carboxamide (RCD-**

**9S):** This compound was used as previously synthesized (Compound **2b** from Chapter 3).<sup>3</sup>

***N*-(4-Fluorobenzyl)-3-hydroxy-4-thioxo-4*H*-pyran-2-carbothioamide**

**(RCD-9S2):** This compound was used as previously synthesized (Compound **2c** from Chapter 3).<sup>3</sup>

**2,3-bis(Benzyloxy)benzoic acid (1a):** The synthesis of this compound is outlined in Scheme 5-1. To a solution of dihydroxybenzoic acid (500 mg, 3.24 mmol)

in 30 mL of DMF, was added benzyl chloride (1.33 mL, 11.6 mmol) and  $K_2CO_3$  (1.71 g, 12.4 mmol). The resulting reaction mixture was heated to reflux at 120°C under nitrogen and stirred overnight. The reaction was filtered and the filtrate was evaporated in vacuo to obtain a brown oil. The crude oil was purified via a silica plug in  $CH_2Cl_2$  and pure fractions were evaporated in vacuo to yield a clear oil (1.36 g, 3.12 mmol). Yield = 96%. To a solution of the oil (1.32 g, 3.11 mmol) in 10 mL of MeOH, was added 6 mL of a 6 M NaOH solution. The resulting reaction mixture was stirred overnight at room temperature under  $N_2$ . The reaction was evaporated in vacuo and the pure acid product **1a** was extracted with  $CH_2Cl_2$  and 6M HCl. The organic phase was dried over anhydrous  $MgSO_4$ , and evaporated in vacuo to yield a pure white solid (1.04 g, 3.11 mmol). Yield = 100%.  $^1H$  NMR (400 MHz,  $CDCl_3-d_1$ , 25 °C):  $\delta$  = 5.20 (s, 2H;  $CH_2$ ), 5.27 (s, 2H;  $CH_2$ ), 7.17 (t,  $J$  = 8.0 Hz, 1H; ArH), 7.27 - 7.50 (m, 10H; ArH), 7.73 (dd,  $J$  = 7.6, 1.6 Hz, 1H; ArH). ESI-MS(-)  $m/z$  332.92 [M-H].

**2,3-bis(Benzyloxy)-N-(4-fluorobenzyl)benzamide (1b)**: The synthesis of this compound is outlined in Scheme 5-1. To a solution of **1a** (500 mg, 1.49 mmol) in 15 mL of dry  $CH_2Cl_2$ , was added EDCI (343 mg, 1.79 mmol), HOBt (242 mg, 1.79 mmol) and *p*-fluorobenzylamine (204  $\mu$ L, 1.79 mmol). The mixture was stirred overnight at room temperature under  $N_2$  and extracted with 1 M HCl and  $CH_2Cl_2$ . The organic phase was dried over anhydrous  $MgSO_4$ , filtered, and concentrated to a brown oil. The crude oil was purified via silica column chromatography in (0-1% MeOH/ $CH_2Cl_2$ ) to yield a pure white solid of **1b** (381 mg, 0.86 mmol). Yield = 58%.  $^1H$  NMR (400 MHz,  $CDCl_3-d_1$ , 25 °C):  $\delta$  = 4.42 (d,  $J$  = 5.6 Hz, 2H;  $NHCH_2$ ), 4.99 (s, 2H;  $CH_2$ ), 5.09 (s, 2H;  $CH_2$ ), 6.93 (t,  $J$  = 8.6 Hz, 2H; ArH), 7.14 - 7.18 (m, 5H;

ArH), 7.23 (d,  $J = 7.0$  Hz, 2H; ArH), 7.27 (d,  $J = 7.6$  Hz, 1H; ArH), 7.31 (t,  $J = 7.4$  Hz, 2H; ArH), 7.37 – 7.43 (m, 2H; ArH), 7.47 (d,  $J = 7.6$  Hz, 2H; ArH), 7.81 (dd,  $J = 6.0, 3.2$  Hz, 1H; ArH), 8.42 (t,  $J = 5.4$  Hz, 1H; CONHCH<sub>2</sub>). ESI-MS(+)  $m/z$  441.91 [M+H]<sup>+</sup>, 464.01 [M+Na]<sup>+</sup>.

***N*-(4-Fluorobenzyl)-2,3-dihydroxybenzamide (RCD-11)**: This compound was synthesized as outlined in Scheme 5-1. Compound **1b** (372 mg, 0.84 mmol) was acid de-protected as previously reported, in 25 mL of a 1:1 solution of HCl:HOAc and to yield a pure white solid of **RCD-11** (186 mg, 0.71 mmol). Yield = 85%. <sup>1</sup>H NMR (400 MHz, DMSO-*d*<sub>6</sub>, 25 °C):  $\delta = 4.45$  (d,  $J = 6.0$  Hz, 2H; NHCH<sub>2</sub>), 6.65 (t,  $J = 8.0$  Hz, 1H; ArH), 6.89 (d,  $J = 7.6$  Hz, 1H; ArH), 7.12 (t,  $J = 8.8$  Hz, 2H; ArH), 7.29 (d,  $J = 8.4$  Hz, 1H; ArH), 7.33 (dd,  $J = 8.4, 2.8$  Hz, 2H; ArH), 9.31 (t,  $J = 6.0$  Hz, 1H; CONHCH<sub>2</sub>). APCI-MS(+)  $m/z$  262.11 [M+H]<sup>+</sup>. Anal. Calcd for C<sub>14</sub>H<sub>12</sub>FNO<sub>3</sub>•0.5 H<sub>2</sub>O: C, 62.22; H, 4.85; N, 5.18. Found: C, 62.36; H, 5.09; N, 5.23.

**2-(Benzyloxy)-3-methoxybenzoic acid (2a)**: The synthesis of this compound is outlined in Scheme 5-2. To a solution of 3-methoxysalicylic acid (500 mg, 2.97 mmol) in 10 mL of DMF, was added benzyl chloride (880  $\mu$ L, 7.63 mmol) and K<sub>2</sub>CO<sub>3</sub> (1.16 g, 8.41 mmol). The resulting reaction mixture was heated to reflux at 120 °C under nitrogen and stirred overnight. The reaction was vacuum filtered and the filtrate was concentrated to a dark brown oil. The crude oil was purified via a silica plug in CH<sub>2</sub>Cl<sub>2</sub> and pure fractions were evaporated in vacuo to yield an off-white oil (763 mg, 2.19 mmol). Yield = 74%. To a solution of the oil (763 mg, 2.19 mmol) in 5 mL of MeOH, was added 3 mL of a 6 M NaOH solution. The mixture was stirred overnight at room temperature under nitrogen. The reaction was evaporated in vacuo

and the acid product **3** was extracted with CH<sub>2</sub>Cl<sub>2</sub> and 6 M HCl. The organic phase was dried over anhydrous MgSO<sub>4</sub>, and concentrated to an off-white solid (566 mg, 2.19 mmol). Yield = 100%. <sup>1</sup>H NMR (300 MHz, CDCl<sub>3</sub>-d<sub>1</sub>, 25 °C): δ = 3.97 (s, 3H; OCH<sub>3</sub>), 5.27 (s, 2H; CH<sub>2</sub>), 7.19 (d, *J* = 3.6 Hz, 1H; ArH), 7.36 - 7.41 (m, 5H; ArH), 7.43 (d, *J* = 2.1 Hz, 1H; ArH), 7.68 (dd, *J* = 6.3, 3.0 Hz, 1H; ArH). ESI-MS(+) *m/z* 259.11 [M+H]<sup>+</sup>, 276.10 [M+NH<sub>4</sub>]<sup>+</sup>.

**2,3-bis(Benzyloxy)-N-(4-fluorobenzyl)benzamide (2b):** The synthesis of this compound is outlined in Scheme 5-2. To a solution of **2a** (566 mg, 2.19 mmol) in 15 mL of dry CH<sub>2</sub>Cl<sub>2</sub>, was added EDCI (504 mg, 2.63 mmol), HOBt (335 mg, 2.63 mmol) and *p*-fluorobenzylamine (301 μL, 2.63 mmol). The mixture was stirred overnight at room temperature under nitrogen and extracted with 1 M HCl and CH<sub>2</sub>Cl<sub>2</sub>. The organic phase was dried over anhydrous MgSO<sub>4</sub>, filtered, and concentrated to a yellow oil. The crude oil was purified via silica column chromatography (0-2% MeOH/CH<sub>2</sub>Cl<sub>2</sub>) and pure fractions were concentrated to an off-white solid of **4** (383 mg, 1.05 mmol). Yield = 48%. <sup>1</sup>H NMR (400 MHz, CDCl<sub>3</sub>-d<sub>1</sub>, 25 °C): δ = 3.92 (s, 3H; OCH<sub>3</sub>), 4.41 (d, *J* = 5.6 Hz, 2H; NHCH<sub>2</sub>), 4.99 (s, 2H; CH<sub>2</sub>), 6.91 (t, *J* = 8.8 Hz, 2H; ArH), 7.07 (dd, *J* = 8.0, 1.6 Hz, 1H; ArH), 7.11 (dd, *J* = 8.4, 5.2 Hz, 2H; ArH), 7.16 (t, *J* = 8.2 Hz, 1H; ArH), 7.22 (dd, *J* = 7.2, 1.6 Hz, 2H; ArH), 7.29 - 7.37 (m, 3H; ArH), 7.74 (dd, *J* = 7.6, 1.6, Hz, 1H; ArH), 8.31 (brs, 1H; CONHCH<sub>2</sub>). ESI-MS(+) *m/z* 366.27 [M+H]<sup>+</sup>, 388.25 [M+Na]<sup>+</sup>.

**N-(4-Fluorobenzyl)-2-hydroxy-3-methoxybenzamide (RCD-12):** This compound was synthesized as outlined in Scheme 5-2. Compound **2b** (300 mg, 0.82 mmol) was acid de-protected as previously reported, in 10 mL of a 1:1 solution of

HCl:HOAc and concentrated to a light yellow solid of **RCD-12** (163 mg, 0.59 mmol). Yield = 72%.  $^1\text{H}$  NMR (500 MHz, DMSO- $d_6$ , 25 °C):  $\delta$  = 3.74 (s, 3H; OCH<sub>3</sub>), 4.43 (d,  $J$  = 6.3 Hz, 2H; NHCH<sub>2</sub>), 6.78 (t,  $J$  = 8.0 Hz, 1H; ArH), 7.07 (d,  $J$  = 7.4 Hz, 1H; ArH), 7.11 (t,  $J$  = 8.9 Hz, 2H; ArH), 7.31 (dd,  $J$  = 8.6, 3.4 Hz, 2H; ArH), 7.41 (dd,  $J$  = 8.0, 1.1 Hz, 2H; ArH), 9.32 (t,  $J$  = 6.0 Hz, 1H; CONHCH<sub>2</sub>).  $^{13}\text{C}$  NMR (125 MHz, DMSO- $d_6$ , 25 °C): 42.1 (CH<sub>2</sub>), 56.2 (OCH<sub>3</sub>), 115.5 (ArC), 115.6 (ArC), 115.9 (ArC), 118.4 (ArC), 119.1 (ArC), 129.7 (ArC), 129.8 (ArC), 135.5 (ArC), 148.9 (ArC), 151.2 (ArC), 169.8 (C=O). ESI-MS(+)  $m/z$  276.20 [M+H]<sup>+</sup>. Anal. Calcd for C<sub>15</sub>H<sub>14</sub>FNO<sub>3</sub>: C, 65.45; H, 5.13; N, 5.09. Found: C, 65.76; H, 5.51; N, 5.12.

**8-(Benzyloxy)quinoline-7-carboxylic acid (3a):** The synthesis of this compound is outlined in Scheme 5-3. To a solution of 8-hydroxyquinoline-7-carboxylic acid (500 mg, 2.64 mmol) in 10 mL of DMF, was added benzyl chloride (782  $\mu\text{L}$ , 6.78 mmol) and K<sub>2</sub>CO<sub>3</sub> (1.03 g, 7.47 mmol). The resulting reaction mixture was heated to reflux at 120°C under nitrogen and stirred overnight. The reaction was vacuum filtered and the filtrate was concentrated to a reddish-brown oil. The crude oil was purified via a silica plug in CH<sub>2</sub>Cl<sub>2</sub> and pure fractions were evaporated in vacuo to yield an orange oil (585 mg, 1.58 mmol). Yield = 60%. To a solution of the oil (585 mg, 1.58 mmol) in 5 mL of MeOH, was added 3 mL of a 6M NaOH solution. The mixture was stirred overnight at room temperature under nitrogen. The reaction was evaporated in vacuo and the acid product **3a** was extracted with CH<sub>2</sub>Cl<sub>2</sub> and 6M HCl. The organic phase was dried over anhydrous MgSO<sub>4</sub>, and concentrated to a yellow solid (444 mg, 1.58 mmol). Yield = 100%.  $^1\text{H}$  NMR (400 MHz, DMSO- $d_6$ , 25 °C):  $\delta$  = 5.43 (s, 2H; CH<sub>2</sub>), 7.33 (d,  $J$  = 7.2 Hz, 2H; ArH), 7.37 (t,  $J$  = 7.2 Hz, 2H; ArH),

7.58 (d,  $J = 6.8$  Hz, 2H; ArH), 7.63 (dd,  $J = 8.4, 4.4$  Hz, 1H; ArH), 7.77 (d,  $J = 2.4$  Hz, 1H; ArH), 8.42 (dd,  $J = 8.4, 1.4$  Hz, 1H; ArH), 9.01 (dd,  $J = 4.4, 2.0$  Hz, 1H; ArH). ESI-MS(-)  $m/z$  278.32 [M-H]<sup>-</sup>.

**8-(Benzyloxy)-N-(4-fluorobenzyl)quinoline-7-carboxamide (3b):** The synthesis of this compound is outlined in Scheme 5-3. To a solution of **3a** (400 mg, 1.43 mmol) in 15 mL of dry CH<sub>2</sub>Cl<sub>2</sub>, was added EDCI (329 mg, 1.72 mmol), HOBt (232 mg, 1.72 mmol) and *p*-fluorobenzylamine (197 μL, 1.72 mmol). The mixture was stirred overnight at room temperature under nitrogen and extracted with 1 M HCl and CH<sub>2</sub>Cl<sub>2</sub>. The organic phase was dried over anhydrous MgSO<sub>4</sub>, filtered, and concentrated to a yellow oil. The crude oil was purified via silica column chromatography (0-2% MeOH/CH<sub>2</sub>Cl<sub>2</sub>) and pure fractions were concentrated to a yellow solid of **3b** (171 mg, 0.44 mmol). Yield = 31%. <sup>1</sup>H NMR (400 MHz, CDCl<sub>3</sub>-*d*<sub>1</sub>, 25 °C): δ = 4.43 (d,  $J = 5.6$  Hz, 2H; NHCH<sub>2</sub>), 5.51 (s, 2H; CH<sub>2</sub>), 6.92 (t,  $J = 8.8$  Hz, 2H; ArH), 7.13 (dd,  $J = 6.4, 3.0$  Hz, 2H; ArH), 7.32 (d,  $J = 5.2$  Hz, 5H; ArH), 7.48 (dd,  $J = 8.4, 4.0$  Hz, 1H; ArH), 7.64 (d,  $J = 8.4$  Hz, 1H; ArH), 8.18 (dd,  $J = 8.4, 2.0$ , Hz, 1H; ArH), 8.28 (d,  $J = 8.8$  Hz, 1H; ArH), 8.60 (brt, 1H; CONHCH<sub>2</sub>), 8.99 (dd,  $J = 4.0, 1.6$  Hz, 1H; ArH). ESI-MS(+)  $m/z$  387.11 [M+H]<sup>+</sup>.

**N-(4-Fluorobenzyl)-2,3-dihydroxybenzamide (RCD-19):** This compound was synthesized as outlined in Scheme 5-3. Compound **3b** (154 mg, 0.40 mmol) was acid de-protected as previously reported, in 10 mL of a 1:1 solution of HCl:HOAc and concentrated to a yellow solid of **RCD-19** (101 mg, 0.34 mmol). Yield = 85%. <sup>1</sup>H NMR (500 MHz, DMSO-*d*<sub>6</sub>, 25 °C): δ = 4.54 (d,  $J = 4.6$  Hz, 2H; NHCH<sub>2</sub>), 7.13 (t,  $J = 8.6$  Hz, 2H; ArH), 7.38 (t,  $J = 6.0$  Hz, 2H; ArH), 7.57 (d,  $J = 9.1$ , Hz, 1H; ArH),

7.85 (brt, 1H; ArH), 8.17 (d,  $J = 8.6$  Hz, 1H; ArH), 8.67 (d,  $J = 8.0$  Hz, 1H; ArH), 9.00 (brs, 1H; ArH), 9.75 (brt, 1H; CONHCH<sub>2</sub>). <sup>13</sup>C NMR (125 MHz, DMSO-*d*<sub>6</sub>, 25 °C): 42.4 (CH<sub>2</sub>), 113.6 (ArC), 115.5 (ArC), 115.7 (ArC), 117.7 (ArC), 124.4 (ArC), 126.1 (ArC), 130.0 (ArC), 131.4 (ArC), 135.4 (ArC), 148.2 (ArC), 155.9 (ArC), 160.7 (ArC), 162.7 (ArC), 168.8 (C=O). ESI-MS(+)  $m/z$  297.12 [M+H]<sup>+</sup>. Anal. Calcd for C<sub>17</sub>H<sub>13</sub>FN<sub>2</sub>O<sub>2</sub>•2.25 H<sub>2</sub>O: C, 60.62; H, 5.24; N, 8.32. Found: C, 60.53; H, 4.83; N, 8.33.

**Ethyl-5-hydroxy-2-methyl-4-oxo-4H-pyran-3-carboxylate (4a):** This compound was previously prepared in the lab and used as synthesized.<sup>48</sup>

**5-Hydroxy-2-methyl-4-oxo-4H-pyran-3-carboxylic acid (4b):** This compound was synthesized as outlined in Scheme 5-4. To a solution of **4a** (250 mg, 1.26 mmol) in 5 mL of H<sub>2</sub>O, was added 3 mL of a 6 M NaOH solution. The mixture was stirred for 3 hr at room temperature under nitrogen. The reaction was evaporated in vacuo and the acid product **4b** was extracted with CH<sub>2</sub>Cl<sub>2</sub> and 6 M HCl. The organic phase was dried over anhydrous MgSO<sub>4</sub>, and concentrated to a mustard yellow solid (150 mg, 0.88 mmol). Yield = 70%. <sup>1</sup>H NMR (400 MHz, DMSO-*d*<sub>6</sub>, 25 °C):  $\delta = 2.29$  (s, 2H; CH<sub>3</sub>), 8.05 (s, 1H; ArH), 9.36 (s, 1H; ArOH). ESI-MS(-)  $m/z$  169.22 [M-H]<sup>-</sup>.

**4-Fluorobenzyl-5-hydroxy-2-methyl-4-oxo-4H-pyran-3-carboxylate (RCD-20):** The synthesis of this compound is outlined in Scheme 5-4. To a solution of **4b** (60 mg, 0.35 mmol) in 10 mL of dry CH<sub>2</sub>Cl<sub>2</sub>, was added EDCI (81 mg, 0.42 mmol), HOBt (57 mg, 0.42 mmol) and *p*-fluorobenzylamine (48  $\mu$ L, 0.42 mmol). The mixture was stirred overnight at room temperature under nitrogen and extracted with 1 M HCl and CH<sub>2</sub>Cl<sub>2</sub>. The organic phase was dried over anhydrous MgSO<sub>4</sub>, filtered, and

concentrated to a yellow solid. The crude solid was purified via silica column chromatography (0-5% MeOH/CH<sub>2</sub>Cl<sub>2</sub>) and pure fractions were concentrated to a yellow solid of **RCD-20** (28 mg, 0.10 mmol). Yield = 29%. <sup>1</sup>H NMR (500 MHz, DMSO-*d*<sub>6</sub>, 25 °C): δ = 2.31 (s, 3H; CH<sub>3</sub>), 5.64 (d, *J* = 2.8 Hz, 2H; CH<sub>2</sub>), 7.08 (dd, *J* = 9.2, 2.8 Hz, 2H; ArH), 7.35 – 7.37 (m, 2H; ArH), 7.99 (s, 1H; ArH), 7.20 (brt, 1H; CONHCH<sub>2</sub>). ESI-MS(-) *m/z* 276.25 [M-H]<sup>-</sup>. Anal. Calcd for C<sub>14</sub>H<sub>12</sub>FNO<sub>4</sub>: C, 60.65; H, 4.36; N, 5.05. Found: C, 61.04; H, 4.76; N, 5.13.



## **5.K Acknowledgements**

The dissertation author was the primary researcher for the data presented. The author would like to thank Jamie L. Desoto for assistance in preparing RCD-1, -6, -10, -13, -18. The author would also like to thank both Dr. Matthieu Rouffet and Jamie L. Desoto in performing the docking studies in the integrase active site of PFV (PDB:3OYA).

**5.L References**

- (1) Marchand, C.; Maddali, K.; Metifiot, M.; Pommier, Y. *Curr. Top. Med. Chem.* **2009**, *9*, 1016.
- (2) Mehellou, Y.; Clercq, E. D. *J. Med. Chem.* **2010**, *53*, 521.
- (3) Agrawal, A.; De Oliveira, C. A. F.; Cheng, Y.; Jacobsen, J. A.; McCammon, J. A.; Cohen, S. M. *J. Med. Chem.* **2009**, *52*, 1063.
- (4) Agrawal, A.; Romero-Perez, D.; Jacobsen, J. A.; Villarreal, F. J.; Cohen, S. M. *ChemMedChem* **2008**, *3*, 812.
- (5) Summa, V.; Petrocchi, A.; Bonelli, F.; Crescenzi, B.; Donghi, M.; Ferrara, M.; Fiore, F.; Gardelli, C. P., O.G.; Hazuda, D. J.; Jones, P.; Kinzel, O.; Laufer, R.; Monteagudo, E.; Muraglia, E.; Nizi, E.; Orvieto, F.; Pace, P.; Pescatore, G.; Scarpelli, R.; Stillmock, K.; Witmer, M. V.; Rowley, M. *J. Med. Chem.* **2008**, *51*, 5843.
- (6) Pace, P.; Di Francesco, M. E.; Gardelli, C.; Harper, S.; Muraglia, E.; Nizi, E.; Orvieto, F.; Petrocchi, A.; Poma, M.; Rowley, M.; Scarpelli, R.; Laufer, R.; Paz, O. G.; Monteagudo, E.; Bonelli, F.; Hazuda, D. J.; Stillmock, K. A.; Summa, V. *J. Med. Chem.* **2007**, *50*, 2225.
- (7) Gardelli, C.; Nizi, E.; Muraglia, E.; Crescenzi, B.; Ferrara, M.; Orvieto, F.; Pace, P.; Pescatore, G.; Poma, M.; Rico Ferreira, M. D. R.; Scarpelli, R.; Homnick, C. F.; Ikemoto, N.; Alfieri, A.; Verdirame, M.; Bonelli, F.; Paz, O. G.; Taliani, M.; Monteagudo, E.; Pesci, S.; Laufer, R.; Felock, P.; Stillmock, K. A.; Hazuda, D. J.; Rowley, M.; Summa, V. *J. Med. Chem.* **2007**, *50*, 4953.
- (8) Hazuda, D. J.; Felock, P.; Witmer, M.; Wolfe, A.; Stillmock, K.; Grobler, J. A.; Espeseth, A.; Gabryelski, L.; Schleif, W.; Blau, C.; Miller, M. D. *Science* **2000**, *287*, 646.
- (9) Grobler, J. A.; Stillmock, K.; Hu, B.; Witmer, M.; Felock, P.; Espeseth, A. S.; Wolfe, A.; Egbertson, M.; Bourgeois, M.; Melamed, J.; Wai, J. S.; Young, S.; Vacca, J.; Hazuda, D. J. *Proc. Natl. Acad. Sci. USA* **2002**, *99*, 6661.
- (10) Espeseth, A.; Felock, P.; Wolfe, A.; Witmer, M.; Grobler, J.; Anthony, N.; Egbertson, M.; Melamed, J. Y.; Young, S.; Hamill, T.; Cole, J. L.; Hazuda, D. J. *Proc. Natl. Acad. Sci. USA* **2000**, *97*, 11244.
- (11) Hazuda, D. J.; Young, S. D.; Guare, J. P.; Anthony, N. J.; Gomez, R. P.; Wai, J. S.; Vacca, J. P.; Handt, L.; Motzel, S. L.; Klein, H. J.; Dornadula, G.; Danovich, R. M.; Witmer, M. V.; Wilson, K. A. A.; Tussey, L.; Schleif, W. A.;

- Gabryelski, L. S.; Jin, L.; Miller, M. D.; Casimiro, D. R.; Emini, E. A.; Shiver, J. W. *Science* **2004**, *305*, 528.
- (12) Pommier, Y.; Johnson, A. A.; Marchand, C. *Nat. Rev. Drug Discov.* **2005**, *4*, 236.
- (13) Barre-Sinoussi, F.; Chermann, J. C.; Rey, F.; Nugeyre, M. T.; Chamaret, S.; Gruest, J.; Dauguet, C.; Axler-Blin, C.; Vezinet-Brun, F.; Rouzioux, C.; Rozenbaum, W.; Montagnier, L. *Science* **1983**, *220*, 868.
- (14) Schupbach, J.; Popovic, M.; Gilden, R. V.; Gonda, M. A.; Sarngadharan, M. G.; Gallo, R. C. *Science* **1984**, *224*, 503.
- (15) Sepkowitz, K. A. *N. Engl. J. Med.* **2001**, *344*, 1764.
- (16) Gallo, R. C. *Science* **2002**, *298*, 1728.
- (17) Buchbinder, S. P.; Katz, M. H.; Hessel, N. A.; O'Malley, P. M.; Holmberg, S. D. *AIDS* **1994**, *8*, 1123.
- (18) UNAIDS: AIDS epidemic update. [Online Early Access]. Published Online: 2009.  
[http://www.unaids.org/documents/20101123\\_GlobalReport\\_Chap2\\_em.pdf](http://www.unaids.org/documents/20101123_GlobalReport_Chap2_em.pdf).
- (19) Lama, J.; Planelles, V. *Retrovirology* **2007**, *4*, 52.
- (20) Perelson, A. S.; Kirschner, D. E.; Boer, R. D. *Mathematical Biosciences* **1993**, *114*, 81.
- (21) Serrao, E.; Odde, S.; Ramkumar, K.; Neamati, N. *Retrovirology* **2009**, *6*, 25.
- (22) Metifiot, M.; Marchand, C.; Maddali, K.; Pommier, Y. *Viruses* **2010**, *2*, 1347.
- (23) Mitsuya, H.; Broder, S. *Nature* **1987**, *325*, 773.
- (24) Wikipedia.
- (25) Chun, T. W.; Fauci, A. S. *Proc. Natl. Acad. Sci. USA* **1999**, *96*, 10958.
- (26) Bushman, F. D.; Craigie, R. *Proc. Natl. Acad. Sci. USA* **1991**, *88*, 1339.
- (27) Engelman, A.; Mizuuchi, K.; Craigie, R. *Cell* **1991**, *67*, 1211.
- (28) Supuran, C. T.; Winum, J. Y. *Drug Design of Zinc-Enzyme Inhibitors*; John Wiley & Sons, Inc.: Hoboken, 2009.

- (29) Chiu, T. K.; Davies, D. R. *Curr. Top. Med. Chem.* **2004**, *4*, 965.
- (30) Bushman, F. D.; Engelman, A.; Palmer, I.; Wingfield, P.; Craigie, R. *Proc. Natl. Acad. Sci. USA* **1993**, *90*, 3428.
- (31) Venclovas, C.; Siksnyis, V. *Nat. Struct. Biol.* **1995**, *2*, 838.
- (32) Wang, J. Y.; Ling, H.; Yang, W.; Craigie, R. *EMBO J.* **2001**, *20*, 7333.
- (33) Goldgur, Y.; Craigie, R.; Cohen, G. H.; Fujiwara, T.; Yoshinaga, T.; Fujishita, T.; Sugimoto, H.; Endo, T.; Murai, H.; Davies, D. R. *Proc. Natl. Acad. Sci. USA* **1999**, *96*.
- (34) Chen, J. C.; Krucinski, J.; Miercke, L. J. W.; Finer-Moore, J. S.; Tang, A. H.; Leavitt, A. D.; Stroud, R. M. *Proc. Natl. Acad. Sci. USA* **2000**, *97*, 8233.
- (35) Perryman, A. L.; Forli, S.; Morris, G. M.; Burt, C.; Cheng, Y.; Palmer, M. J.; Whitby, K.; McCammon, J. A.; Phillips, C.; Olson, A. J. *J. Mol. Biol.* **2010**, *397*, 600.
- (36) Jaslolski, M.; Alexandratos, J. N.; Bujacz, G.; Wlodawer, A. *FEBS J.* **2009**, *276*, 2926.
- (37) Fitzkee, N. C.; Mase, J. E.; Shen, Y.; Davies, D. R.; Bax, A. *J. Biol. Chem.* **2010**, *285*, 18072.
- (38) Hare, S.; Gupta, S. S.; Valkov, E.; Engelman, A.; Cherepanov, P. *Nature* **2010**, *464*, 232.
- (39) Johnson, A. A.; Marchand, C.; Pommier, Y. *Curr. Top. Med. Chem.* **2004**, *4*, 1059.
- (40) Neamati, N. *Expert Opin. Ther. Patents* **2002**, *12*, 709.
- (41) Savarino, A. *Expert Opin. Ther. Patents* **2006**, *15*, 1507.
- (42) Cushman, M.; Sherman, P. *Biochem. Biophys. Res. Commun.* **1992**, *185*, 85.
- (43) Fesen, M. R.; Kohn, K. W.; Leteurtre, F.; Pommier, Y. *Proc. Natl. Acad. Sci. USA* **1993**, *90*.
- (44) Fesen, M. R.; Pommier, Y.; Leteurtre, F.; Hiroguchi, S.; Yung, J.; Kohn, K. W. *Biochem. Pharmacol.* **1994**, *48*, 595.

- (45) Zhao, H.; Neamati, N.; Hong, H.; Mazumder, A.; Wang, S.; Sunder, S.; Milne, G. W. A.; Pommier, Y.; Burke Jr., T. R. *J. Med. Chem.* **1997**, *40*, 242.
- (46) Rosemond, M. J.; St John-Williams, L.; Yamaguchi, T.; Fujishita, T.; Walsh, J. S. *Chem. Biol. Interact.* **2004**, *147*, 129.
- (47) Metifiot, M.; Maddali, K.; Naumova, A.; Zhang, X.; Marchand, C.; Pommier, Y. *Biochemistry* **2010**, *49*, 3715.
- (48) Yan, Y.; Miller, M. T.; Cao, Y.; Cohen, S. M. *Bioorg. Med. Chem. Lett.* **2009**, *19*, 1970.